2021 BES Separations Science Program Meeting

Virtual Meeting

August 10–12, 2021

The research grants and contracts described in this document are supported by the U.S. Department of Energy, Office of Science/Basic Energy Sciences, as part of the Separation Science Program within the Chemical Sciences, Geosciences and Biosciences Division.

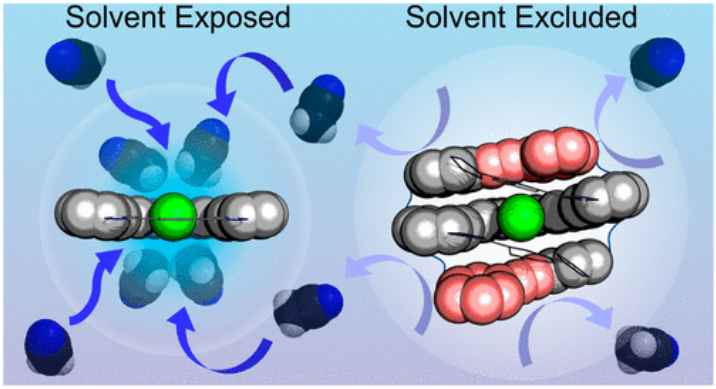

Liu et al. *J. Am. Chem. Soc.* **2021**, *143*, 3191–3204, https://doi.org/10.1021/jacs.0c12562

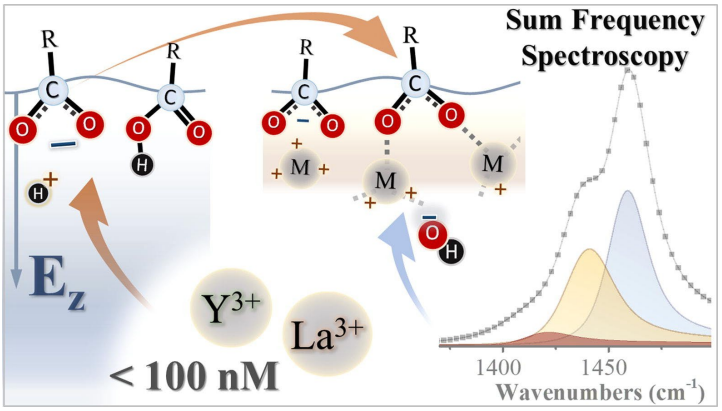

Sthoer et al. *Journal of Colloid And Interface Science*, Volume 608, Part 2, **2022,**2169–2180, 10.1016/j.jcis.2021.10.052

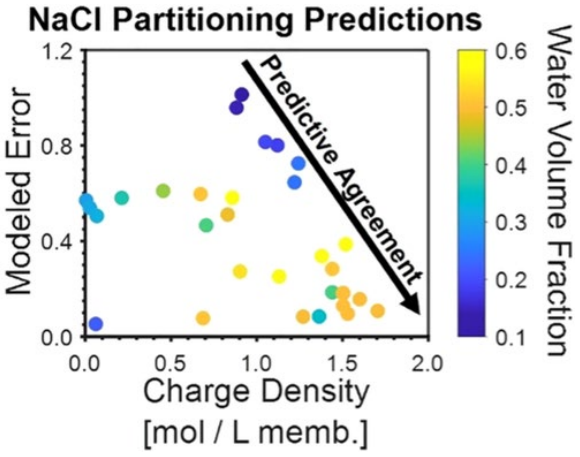

Kitto and Kamcev, *Journal of Polymer Science*, (2022) 1–45, https://doi.org/10.1002/pol.20210810

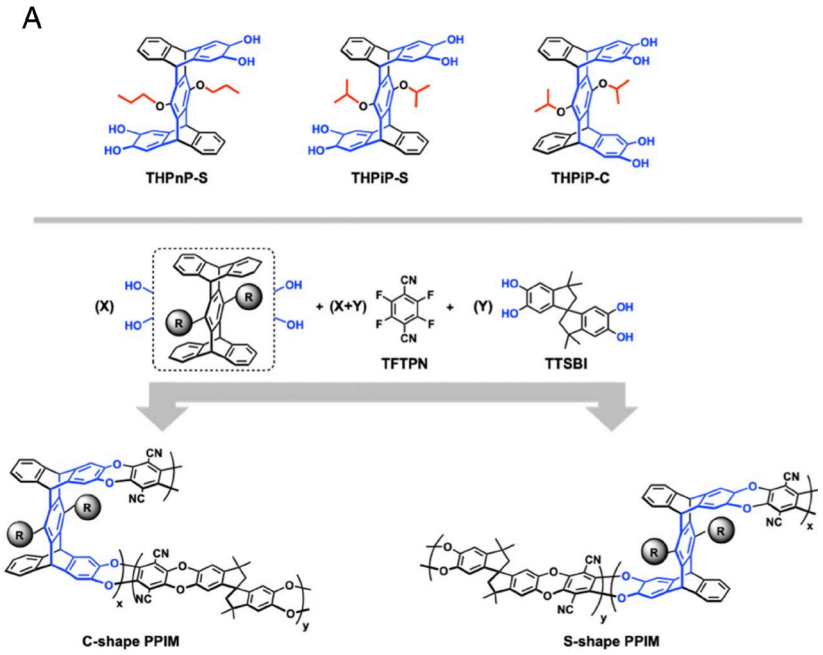

Corrado et al. PNAS, 2021, 118 (37) e2022204118, https://doi.org/10.1073/pnas.2022204118

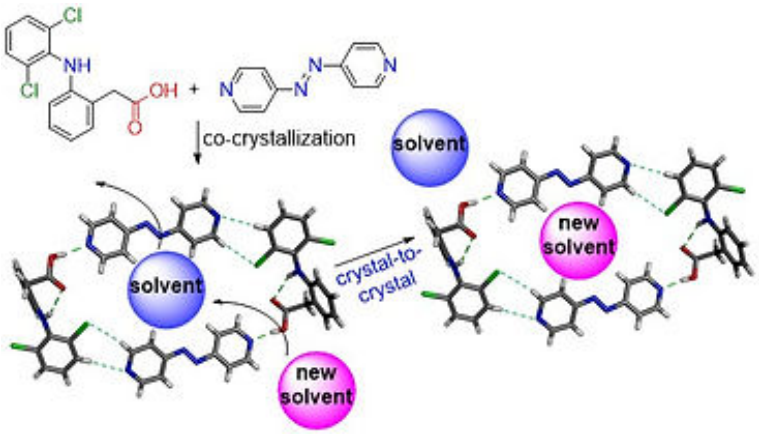

Materials for capture of contaminants or valuable resources, from K. M. Hutchins Group website, https://hutchinsgroup.wixsite.com/materials/research

Foreword

This abstract booklet provides a record of the 2021 U.S. Department of Energy (DOE) contractors' meeting in Separation Science. This meeting was held virtually on August 10-12, 2021, and was sponsored by the Chemical Sciences, Geosciences and Biosciences Division of the Office of Basic Energy Sciences (BES). The purpose of the meeting was to accelerate research progress through collegial interaction. The objectives of the meeting were to develop a common understanding of researchers' activities at the time of the meeting; to maximize potential for collaborative exchange among research groups; to identify the scientific needs of the research community; and to discuss areas for future research directions.

The agenda includes oral presentations delivered by a number of the principal investigators (PIs) and research staff, as well as a virtual poster session. The PIs and staff within the BES Separation Science Program presented their most recent work that was supported by the program. This meeting was focused on the exchange of information; rather than a formal review of researchers' achievements or a forum to deliberate and choose future directions for the program.

Thank you to all the PIs and researchers whose dedication and innovation have advanced separation science research and made this meeting possible and productive. Last, but not least, we thank Teresa Crockett (DOE BES), Connie Lansdon and Linda Severs (Oak Ridge Institute for Science and Education) for their technical and logistical support of this meeting.

With best regards,

Daniel Matuszak, PhD
Program Manager
Separation Science Program - Office of Basic Energy Sciences
U.S. Department of Energy

Vassiliki-Alexandra (Vanda) Glezakou, PhD
Pacific Northwest National Laboratory
Detailee to BES

Agenda

2021 Separation Science PI Meeting

August 10.–12, 2021
Virtual Meeting

(Times are in EST)

Tuesday, August 10

10:00am Welcome, News from DOE-BES Chemical Sciences, Geosciences, and Biosciences Division
Dan Matuszak and Bruce Garrett, DOE Office of Basic Energy Sciences

SESSION I
Trans-interfacial phenomena
Amar Flood, Chair

11:00am The Rare-Earth Project: Harnessing Differences in Electronic Structure for Multiscale, Multicomponent Separations
Rebecca Abergel, Lawrence Berkeley National Laboratory

11:30am Tailoring Photophysical Energy Transfer for Selective Separations of Critical Lanthanides
Andrew Ferguson, National Renewable Energy Laboratory

12:00am Synergistic Approaches to Advanced Minor Actinide Separations
Jessie Carrick, Tennessee Technological University

12:30am Break

SESSION II
Generative / Other phenomena
Heather Allen, Chair

1:30pm Making an inorganic analogue of a cell for direct air capture of CO2
Roger Rousseau, Pacific Northwest National Laboratory

2:00pm Probing Ianmodulin's Mechanisms of Rare-Earth Selectivity for Protein-Based Bioseparations
Joseph Cotruvo, The Pennsylvania State University

2:30pm Toward a photomagnetic mechanism for f-element separations

Joseph Zadrozny, Colorado State University

3:00pm Break, Breakout Sessions

4:00pm <u>Lightning Round 1</u>

Highly Permeable and Selective Model Network Membranes for Gas Separations
Ruilan Guo, University of Notre Dame

Understanding the extent of ionic dissociation and ionic conductivity in model thin film polymer electrolytes as a function of different side chain configurations
Christopher G. Arges

Design and Study of High-Performance Ionene Architectures for Membrane Separations
Jason E. Bara

Transport of Complex Mixtures in Ion-containing Polymer Membranes
Bryan S. Beckingham

Molecular Aspects of Transport in Thin Films of Controlled Architecture
Paul W. Bohn

Electrically Driven Ion Separations in Permeable Membranes
Merlin L. Bruening, University of Notre Dame

Porous Organic Cage Membranes for Molecular Gas Separations
Moises A. Carreon, Colorado School of Mines

Liquid/Liquid Interfaces that Modulate Solute Transport Mechanisms in Solvent Extraction
Aurora E. Clark, Washington State University

Exploiting Insertion Processes for Continuous Membrane-free Ion Separations
Richard M. Crooks, The University of Texas at Austin

Iminoguanidines: From Anion Recognition and Separation to Carbon Capture
Radu Custelcean, Oak Ridge National Laboratory

Fundamental Studies of Novel Separations
Sheng Dai, Oak Ridge National Laboratory

Probing the Mechanisms of Liquid Extraction at Buried Liquid/Liquid Interfaces
Benjamin Doughty, Oak Ridge National Laboratory

Binding Anions Selectively With Modular Triazolophanes and Releasing Them With Light
Amar Flood, Indiana University

Gas Transport Properties in Poly(benzimidazoles)
Benny D. Freeman, The University of Texas at Austin

Raman Microscopy for Investigating Separation Processes within Porous Materials
Joel M. Harris, University of Utah

Understanding and Control of Reactive Separations
David J. Heldebrant, Pacific Northwest National Laboratory

Dispersible Polymeric Systems for Selective Ion Separations
Marc Hillmyer, University of Minnesota-Twin Cities

Coordination-Chemistry-Derived Materials Featuring Nanoscale Porosity and Selective Chemical Separation Capabilities
Joseph T. Hupp, Northwestern University

4:45pm Emerging Projects

Transforming Critical Materials Separation using Precision Control
Santa Jansone-Popova, Oak Ridge National Laboratory

A Macromolecular Selection Platform for the Isolation of Lanthanide Ions
Abigail Knight, The University of North Carolina at Chapel Hill

5:15pm Poster Hall

6:15pm Adjourn

Wednesday, August 11

10:00am Plenary talk I
Jennifer Wilcox
Principal Deputy Assistant Secretary for Fossil Energy at DOE, Presidential Distinguished Professor of Chemical Engineering and Energy Policy at University of Pennsylvania

SESSION III
Phenomena on surfaces and within pores
Ruilan Guo, Chair

11:00am Permeation Properties of Disordered Metal-Organic Framework Membranes Made by Vapor Phase Ligand Treatment
Michael Tsapatsis, The Johns Hopkins University

11:30am Molecular-Level Investigation of Diffusion Behaviors within Cylindrical Nanoscale Pores

Takashi Ito, Dan Higgins, Kansas State University

12:00pm Combinatorial Membrane Synthesis: Fundamentals of Hybrid Metal-Organic Brush (MOB) Membranes for Organic Solvent Nanofiltration
Georges Belfort, Rensselaer Polytechnic Institute

12:30pm Break, Breakout Sessions

SESSION IV
Trans-interfacial phenomena
Jovan Kamcev, Chair

1:30pm Ionic Liquids and Deep Eutectic Solvents in Separation Science: An Understanding of Nanoscale Ordering
Jared Anderson, Ames Laboratory

2:00pm Creating Novel Gas Separation Constructs by Manipulating Free-Volume Distributions in Polymer-Grafted Nanoparticles
Sanat Kumar, Columbia University

2:30 Data-driven Separation Agent/Solvent Design - An Integrated Simulation Experiment Approach
Ping Yang, Los Alamos National Laboratory

3:00 Break, Breakouts

4:00pm <u>Lightning Round 2</u>

Design and Synthesis of Molecular and Macromolecular Sequestrants for Recovery of Rare Earth Elements via Electrodialysis
Kristin M Hutchins, Texas Tech University

Leveraging High-throughput Computation and Machine Learning to Discover and Understand Low-Temperature Fast Oxygen Conductors
Ryan Jacobs, University of Wisconsin-Madison

Ion Transport in Highly Charged Polymer Membranes with Subnanometer Free Volume Elements
Jovan Kamcev, University of Michigan

Fundamental Studies of Carbon Molecular Sieve Membranes for Energy Intensive Separations
William J. Koros, Georgia Institute of Technology

Molecular Interactions and Layer Stacking Dictate Covalent Organic Framework Effective Pore Size

Katie D. Li-Oakey, University of Wyoming

Understanding and controlling water-organic co-transport in amorphous microporous materials
Ryan P. Lively, Georgia Institute of Technology

Precise Control Over Molecular Structure in Polynorbornene-Based Membranes
Brian K. Long, University of Tennessee

Interrogating Selective Metal-Adsorbate Interactions in Metal–Organic Frameworks
Jeffrey R. Long, University of California, Berkeley

Selective Electrochemical Capture and Release of Uranyl in Solution
Gabriel Ménard, University of California–Santa Barbara

New Molecular Mechanisms for Greenhouse Gas Capture in Metal–Organic Frameworks: Carbon Dioxide and Beyond
Phillip J. Milner, Cornell University

Defect Repair of Polyelectrolyte Bilayers Using SDS: The Action of Micelles Versus Monomers
Steven L. Regen, Lehigh University

Accessing Kinetically Controlled Reactions for Efficient Rare Earth Separations
Eric J. Schelter, University of Pennsylvania

X-ray studies of molecular ordering at the liquid/liquid interface in solvent extraction
Mark L. Schlossman, University of Illinois at Chicago

Single-molecule Dynamics in Interface-rich Separations Environments
Daniel K. Schwartz, University of Colorado Boulder

Combining Molecular Simulations and Machine Learning to Comprehensively Explore Adsorption Space
David Sholl, Georgia Institute of Technology

A top-down and bottom-up strategy to generate free volume for membrane-based gas separations
Zachary P. Smith, Massachusetts Institute of Technology

Trivalent and Tetravalent Ion Adsorption at Graphene and Graphene Oxide Surfaces
Ahmet Uysal, Argonne National Laboratory

Computer Simulation of Complex Systems at the Extremes of pH
Gregory A. Voth, The University of Chicago

Field-enhanced Ion Selectivity and Transport Throughput: From Single Nanopores to Anodized Aluminum Oxide Membranes

Gangli Wang, Georgia State University

Data-science enabled investigation of the mechanisms for multiscale ion transport in functional electrolytes and for the radical generation in crystalline assemblies
Qi Wang, University of South Carolina

Tuning the Thermophysical Properties of Thermally Robust Ionic Liquids Through the Subtle Modification of Ion Structure
Kevin N. West, University of South Alabama

4:45pm Emerging Projects

Systematic study on the phase transition of confined fluid mixture up to the critical region
Hertanto Adidharma, University of Wyoming

Exploiting the Emergent Behavior in Ionic Liquids for Advanced Rare Earth Separations
George Goff, LANL

5:15pm Poster Hall

6:15pm Adjourn

Thursday, August 12

10:00am Plenary talk: Molecular dynamics studies of activated events.
Michele Parrinello
Istituto Italiano di Technologia, Genoa

SESSION V
Phenomena on surfaces and within pores
Kristin Hutchins, Chair

11:00am Interfacial Structure and Dynamics in Separations
Grant Johnson, Vanda Glezakou, **Manh-Thuong Nguyen,** and **Venky Prabhakaran**
PNNL

11:30am Supramolecular Control of Redox-Mediated Interactions for Ion-Selective Electroseparations
Xiao Su, University of Illinois, Urbana-Champaign

12:00pm From Captured CO_2 to Value-Added Chemicals: A Photochemical Approach
Ksenija Glusac, Argonne National Laboratory

12:30pm	Break, breakouts
1:30pm	Update on reactions and separations workshop **Joan Brennecke** (U Texas, Austin), Susannah Scott, (UCSB), Vanda Glezakou (PNNL)
2:00pm	Briefings by Session Chairs
2:30pm	Summary Comments and Updates **Dan Matuszak**, DOE Office of Basic Energy Sciences, **Vanda Glezakou**, DOE Detailee
3:00pm	PI Meeting Adjourns

Table of Contents

SESSION I: Trans-interfacial phenomena (Amar Flood, Chair)

From Small-Molecule Chelators to Macromolecular Assemblies: Combining Electronic Structure with Allosteric Effects for Enhanced Rare Earth Selectivity

Rebecca J. Abergel; Chemical Sciences Division, Lawrence Berkeley National Laboratory and Nuclear Engineering Department, University of California - Berkeley

Presentation Abstract

Selectivity in rare earth (RE) metal separations is largely governed by the ionic radii of the metal ions in the +3-oxidation state. Using covalent interactions to separate these metal ions based on their electronic properties has received less attention although this approach underlies the separation of Eu and Ce from the other REs by changing their oxidation states. Similarly, other factors such as entropic and allosteric effects could be leveraged, as in biological systems, which may achieve metal selectivity by relying on both affinity differences and conformational changes. Parts of this effort focus on the selective incorporation of ligands into large biopolymers to afford (i) control of chemical environment within the immediate vicinity of the RE and subsequent RE-ligand binding, and (ii) large entropic gain from reorganization upon binding. Such engineering can be modulated to amplify subtle differences in solubility, ligand binding affinity, and electronic properties, guiding separation *via* specificity in interaction. Results from the formation of non-natural biogenic protein platforms and their evaluation as selective RE binding-materials will be presented.

Grant Number: CH20CRIMAT
Grant Title: The Rare-Earth Project Harnessing Differences in Electronic Structure for Multiscale, Multicomponent Separations

(co)PIs: Rebecca J. Abergel, Polly L. Arnold, Ting Xu, Stefan G. Minasian, Wayne L. Lukens, Wibe A. de Jong, Ethan J. Crumlin, Alexei V. Fedorov, Michael D. Connolly, Emory M. Chan. Laura N. Lammers.
Postdoc(s): Roger M. Pallares, Amy Price, Rebecca Hamlyn, Patrick W. Smith
Student(s): Ivan Jayapurna

Overall research goals: The overall goal of this project is to delineate fundamental principles that will guide the incorporation of specific molecular systems into higher order materials, ultimately leading to breakthrough and innovation in rare earth extraction processes. The proposed scope of work include (i) the design, synthesis, and characterization of fundamentally new molecular architectures and biomimetic materials that enable electronic structure manipulation and selective charge- or size-based binding of rare earth metal ions; (ii) the discovery of new separation principles and materials that efficiently discriminate rare earth elements from complex mixtures, including possible cooperative, switch-like mechanisms, and allow for subsequent recovery and reuse of pure rare earth compounds with minimal energy input; and (iii) the use of in situ and in operando physical characterization techniques to directly probe the physical and chemical properties of rare earth systems and can be used to correlate behavior with electronic structure or monitor uptake and transport of rare earth metal ions. Computational methods, including machine learning approaches, are combined with high-throughput screening, to support and accelerate the design of new functional materials and molecules for rare earth separations, as well as the

interpretation of the physical characterization techniques required for accelerated discovery and design in this context.

Recent Progress:

Role of Covalency in Lanthanide Binding. Covalent contributions to lanthanide bonding may be understood using a Hubbard molecule model (HMM), where the contracted nature of the 4f orbitals makes strong mixing unlikely via spatial overlap but the ionic ground state (M^+ X^-) is stabilized by configuration interaction (CI) with a MLCT or LMCT state. We have illustrated the utility of the HMM cerocene, COT_2Ce, where COT is cyclooctatetraene (**Fig. 1**). This compound has a singlet ground state with a low-lying, triplet excited state. The stabilization of the ground state of COT_2Ce due to mixing between the ligand and 4f orbitals was determined to be 0.3 eV using the HMM and from the temperature independent magnetism of COT_2Ce. The previously determined singlet–triplet gap in COT''_2Ce was 0.45 eV. These values are similar to the stabilization determined computationally for COT_2Ce, which vary from 0.33 to 1.1 eV. However, these values do not consider stabilization resulting from to 5d-orbital mixing or electrostatic effects. We are now turning to X-ray absorption and X-ray and ultraviolet photoemission spectroscopies, to reveal the hybridization between the 4f orbitals and the valence band and deduce partial density of states.

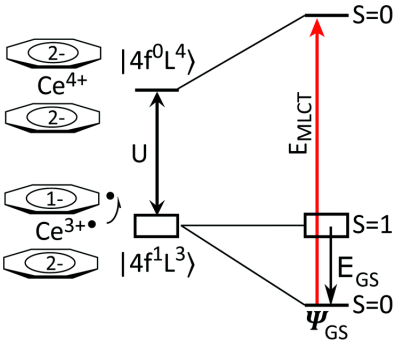

Figure 1. Bonding in COT_2Ce as described by the HMM. For clarity, the unpaired electron on the COT ligands is shown on a single ligand; it is actually delocalized over both COT ligands.

Tuning RE Oxidation State for Easier Separation. We have synthesized a series of new ligands with phosphine oxide $O{=}PAr_3$ and metal oxo complexes $O{=}ML_n$ reactive groups to stabilize more difficult to access redox states in RE metals through ligand photoexcitation, enabling a secondary, amplifying, redox trigger for high-purity separation of size-similar, neighboring REs to be incorporated into the general selectivity being carried out by polymer platforms (see below). The target critical REs are Nd, Dy, and Tb, with Eu > Nd = Dy > La > Ce > Tb being accessible by reduction, with easiest first, and Ce > Tb accessible by oxidation, with easiest first. Low-lying tetravalent states and complexes of these ions may be stabilized by mixing MLCT character into the ground state, which will be probed with newly-prepared substituted catecholamides, hydroxyl-pyridinones, and pyridine-substituted carboxylic acids.

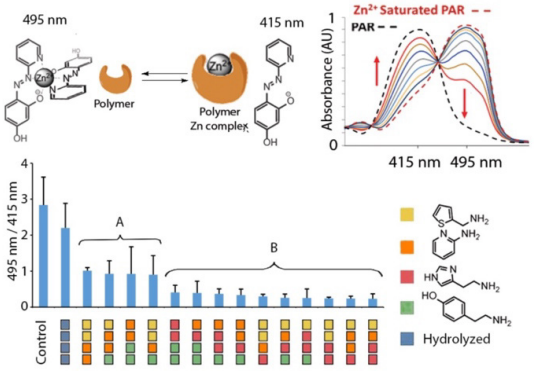

Figure 2. Polymer activity is assessed using the 4-(2 pyridylazo)resorcinol (PAR) competition assay against model metal, zinc. *Top:* Zn^{2+} partitions between the polymer and PAR facilitates colorimetric readout of polymer affinity. *Bottom:* relative Zn^{2+} affinity to neat polymer (control) and functionalized RHPs, as measured by PAR competition assay.

Discovery and Synthesis of Polymeric Macromolecular Platforms. We are investigating the selective incorporation of specific RE-binding moieties within several families of (bio)polymeric platforms: native proteins through selective amino-acid functionalization, the well-known styrene

maleic anhydride (StyMAnh, **Fig. 2**) copolymers, through post modification of side chains, and random methacrylate-based heteropolymers (RHPs) where monomer distribution can be statistically controlled. StyMAnh synthesis was guided by RHP sequence simulation, which determines the side chain distribution along polymer chains. We are transitioning the existing bench-scale workflow to a robotic, high-throughput (HTP) system, to accelerate the development of heteropolymer libraries for rapid binding screening. First, we have reproduced StyMAnh bench-scale Zinc binding results (**Fig. 2**) on the NIMBUS robotic system at the LBNL Molecular Foundry and are now expanding the scope of binding assays via HTP optical screening of RE metals.

Publications supported by this project - 2021

Lukens, W. W.; Booth, C. H.; Walter, M. D. "Experimental Evaluation of the Stabilization of the COT Orbitals by 4f Orbitals in COT_2Ce Using a Hubbard Model." *Dalton Trans*. **2021**, *50*, 2530-2535. DOI: 10.1039/D0DT03897K.

Pallares, R. M.; Carter, K. P.; Faulkner, D.; Abergel, R. J. "Macromolecular Crystallography for f-Element Complex Characterization." *Meth. Enzymol.* **2021**, *651*, 139-155. DOI: 10.1016/bs.mie.2021.01.014.

Arnedo-Sanchez, L.; Smith, K. F.; Deblonde, G. J.-P.; Carter, K. P.; Moreau, L. M.; Rees, J. A.; Tratnjek, T.; Booth, C. H.; Abergel, R. J. "Combining the Best of Two Chelating Titans: A Hydroxypyridinone-Decorated Macrocyclic Ligand for Efficient and Concomitant Complexation and Sensitized Luminescence of f-Elements." *ChemPlusChem.* **2021**, *86*, 483-491. DOI: 10.1002/cplu.202100083

Pallares, R. M.; Hebert, S.; Sturzbecher-Hoehne, M.; Abergel, R. J. "Chelator-Assisted High Performance Liquid Chromatographic Separation of Trivalent Lanthanides and Actinides". *New. J. Chem*. **2021**, *Accepted*.

Tailoring Photophysical Energy Transfer for Selective Separations of Critical Lanthanides

Andrew Ferguson,[1] *Christopher Chang,*[1] *Mark Jensen,*[2] *Alan Sellinger,*[2] *Eric Schelter*[3]*;* [1] *Materials, Chemical, and Computational Science Directorate, National Renewable Energy Laboratory;* [2] *Department of Chemistry, Colorado School of Mines;* [3] *Department of Chemistry, University of Pennsylvania*

PRESENTATION ABSTRACT

To overcome limitations of cation-size based separations of critical lanthanide elements,[1] or rare earths (REs), we aim to develop a novel approach that exploits the *unique and discontinuous electronic structures* of well-shielded 4*f* orbitals of the individual lanthanide ions,[2-3] via *dynamic and element specific photo-induced modifications of the chemical environment* surrounding the metal ions. This concept is built on synthesis of ligands with the desired chemical and physical motifs[4-7] that will ultimately enable demonstration of efficient solution-phase separations *via* control of (i) large, dynamic excited-state perturbations of the photophysical properties of the complexes or (ii) sensitization of ligand-centered photo-chemical reactions.[8-9] This work will expand our understanding and manipulation of excited-state energy flow in lanthanide complexes, to enable control of lanthanide complex solubility and separation, by:

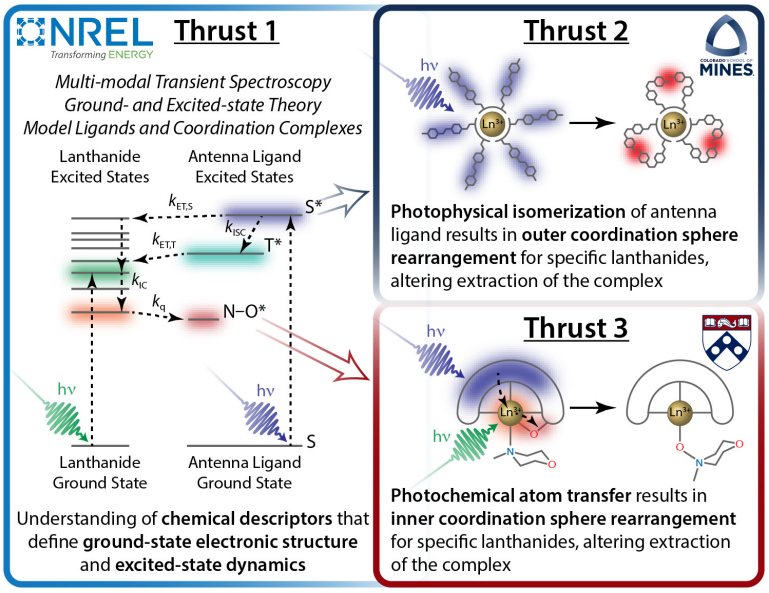

Fig. 1. Schematic illustrating the combined experimental-theoretical approach that will yield fundamental understanding to enable novel photophysical and photochemical lanthanide separations.

- Developing chemical descriptors of ground-state electronic structure & excited-state dynamics
- Probing energy transfer between lanthanide ions and surrounding coordination ligands
- Inducing lanthanide-selective photophysical/photochemical changes in the coordination sphere
- Evaluating changes in the strain and solubility within the coordination complexes

FWP: ERW1585
Co-PIs: Andrew Ferguson, Christopher Chang, Mark Jensen, Alan Sellinger, Eric Schelter
NREL Staff: Mark Steger
Graduate Students: Anastasia Kuvayskaya (CSM), Thomas Mallos (CSM), Kevin Ruoff (Penn.)

RECENT PROGRESS

Development of Organophosphorous Ligands and Complexes

Current rare earth separations exploit small systematic variations in the equilibrium constants of rare earth-organophosphorous ligand complexes, with selectivity arising from the interplay of the regular decrease in cation size and inter-ligand steric effects. The premise of our work is that direct or indirect photo-excitation of organophosphorous ligands in RE complexes can change intra-ligand and inter-ligand steric effects, thereby kinetically altering the solubility to enable dynamic selective separations. To accomplish this for mixtures of rare earths, the intrinsic thermodynamic size selectivity of the current generation of ground state organophosphorous ligand extractants used for the separation must be minimized before the selectivity for specific rare earths can be turned on in target excited state complexes. This is contrary to all previous work, which has focused on increasing the size-based selectivity of rare earths across the series.

We are computationallyl and experimentayl studying the intra-rare earth selectivity of extractants to understand how steric bulk and rigidity (and potentially even dipole) in the extracting ligands creates selectivity for specific rare earths. Our hypothesis is that increasing steric bulk and rigidity of an extractant's substituents systematically quenches rare earth size selectivity, while control of the asymmetry between the two phosphonic acid substituents (e.g., phenyl-vinyl and OR groups in Fig. 2) and the ligand dipole to alter the acidity[5] can counter those steric effects. To relate these effects, we have developed code that implements the continuous symmetry measures (CSM) approach to define the ligand molecular symmetry (Fig. 2). We are applying this methodology to acidic organophosphorus and diglycolamide extractants relevant to rare earth separations. The metrics from the CSM code can be coupled to computational estimates of intra-complex strain energies as well as experimental measurements of rare earth complex stability and selectivity. Benchmarking these symmetry measures against experimental studies of organophosphorus extractants, as represented by substituted phosphonic acid 2-ethylhexyl monoesters, suggest rare earth extractant strength is more strongly correlated to the strength of the phosphorus-oxygen dipoles and associated extractant acidity than the steric effects of the substituents. As we continue to probe the hypothesis that steric bulk and rigidity, along with ligand dipoles, determines extractant selectivity, the principles uncovered will be incorporated into designer photo-switchable ligands with variable inter-ligand interactions.

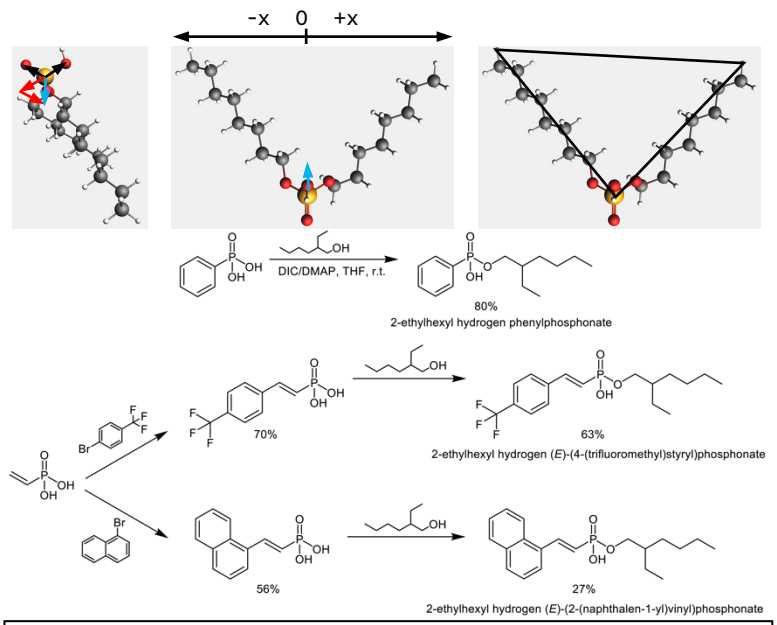

Fig. 2. (top) Coding continuous symmetry measures (CSM). $S(Cn)$: deviation from perfect polygons; $S(\sigma)$: deviation from perfect mirror symmetry. (1) Define internal axis using oxygen coordinates; (2) Sort arms based on sign of x value; (3) Define triangle based on longest vectors from phosphorus; (4) Output symmetry parameters and manipulated .xyz file.
(bottom) Synthetic scheme for target phenyl-vinylphosphonic acid ligands with tuned ground state dipoles.

Our efforts toward the synthesis of asymmetric monophosphonates (organophosphonic acids) have focused on the viability of two approaches: A) functionalization of vinyl phosphonic acid (VPA) followed by monoesterification and B) monoesterification of VPA followed by functionalization, with route A appearing to be optimum. Functionalization of VPA was achieved by a method that employs palladium catalyzed Heck coupling, and the product purity was verified by NMR. To determine the most suitable reaction conditions for producing the monophosphonate *via* Steiglich esterification, phenyl phosphonic acid was employed as the substrate in a model reaction with 2-ethylhexan-1-ol to produce 2-ethylhexyl hydrogen phenylphosphonate. We determined that high yield and efficient product separation was achieved using *N*,*N*′-diisopropylcarbodiimide (DIC) and 4-dimethylaminopyridine (DMAP), with THF as solvent. This approach was subsequently applied to the synthesis of 2-ethylhexyl hydrogen (E)-(4-(trifluoromethyl)styryl)phosphonate and 2-ethylhexyl hydrogen (E)-(2-(naphthalen-1-yl)vinyl)phosphonate (Fig. 2).

Development of Oxygen-atom Transfer Ligands and Complexes

The goal of this thrust is the discovery and development of light-driven photochemical separations of rare earth elements. We are pursuing air- and moisture-stable dysprosium (Dy) and (Y) yttrium complexes, to take advantage of Dy excited f-states to yield differences in photochemical reactivity from Y complexes, enabling their kinetic separation. One example is tris-hexafluoroacetyl-acetonate (hfac) complexes appended with nitroxide antenna sensitization ligands (Fig. 3a). Representative complexes using tert-butyl 2-pyridyl nitroxide (2pyNO),[10] RE(hfac)$_3$(2pyNO) RE = Y, Dy, have successfully been isolated as orange solids (Fig. 3b), characterized by ^{1}H & ^{19}F NMR spectroscopy, and analyzed by UV/Vis/NIR absorption (Fig. 3c) and luminescence spectroscopy. The spectra of both complexes display strong UV features (250-350 nm) owing to absorption by the hfac ligands, with weaker transitions at ca. 500 nm and 700 nm due to the 2pyNO ligand, and even weaker transitions due to the Dy(III) ion in the Dy complex. The luminescence spectra differ in the presence of characteristic f-f peaks for the Dy analogue around 475 & 575 nm. We have begun computational studies on an oxygen atom transfer reaction in the model Dy and Y RE(hfac)$_3$(2pyNO) complexes. Oxygen atom transfer to transform a nitroxide donor reactant to a pyridyl-N-oxide product complex is predicted to occur in the chemically reduced anionic form of these complexes. The anions serve as a convenient ground-state ligand proxy for targeted metal-ligand charge-transfer excited states. Preliminary DFT studies with relativistic core potentials show the anticipated difference in behavior between the Y analog (with no d or f electrons and simple SCF convergence) and the Dy complex (with a partially filled f shell and difficult SCF convergence). A transition state structure for the Y complex has not been found, lending support to the idea of a stepwise reaction mechanism. This

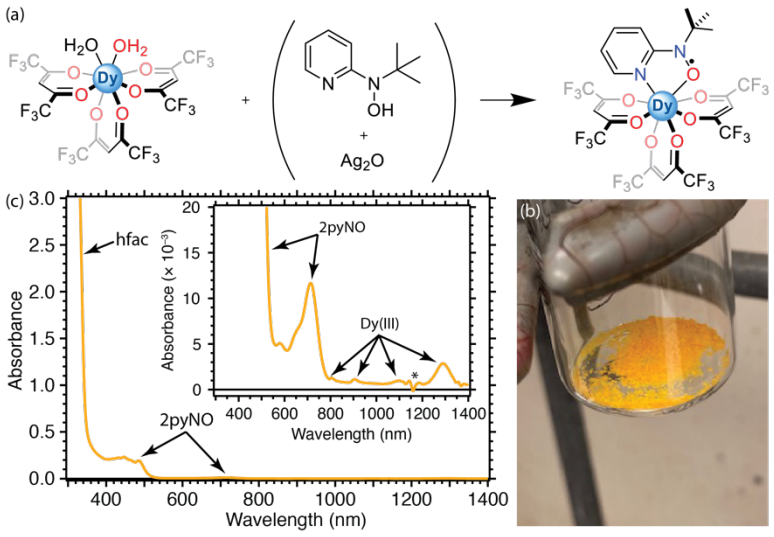

Fig. 3. (a) Synthetic scheme for Dy(hfac)$_3$(2pyNO) complex. (b) Digital photograph showing orange product. (c) Absorbance spectra highlighting the dominant ligand absorption bands. Inset shows the weak low-energy 2pyNO absorption bands and Dy(III) transitions. * indicates artifacts due to imperfect background subtraction.

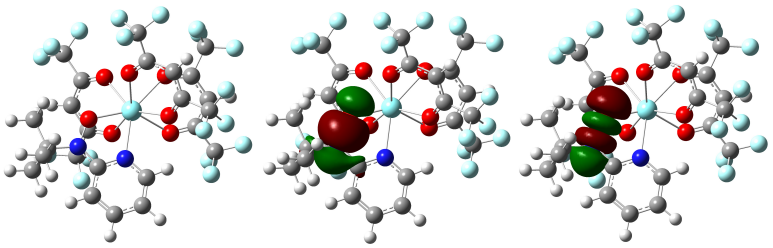

Fig. 4. Anionic $Y(hfac)_3(2pyNO)$ complex, showing nitroxide ligation (left), and N-O σ bonding (center) and anti-bonding (right) orbitals. Lack of frontier canonical MO contributions to orbitals suggests O-atom transfer to pyridinium nitrogen may follow an excited-state mechanism.

illustrates the complexity that may be found once studies move to the excited manifold of the target rare earth complexes. Continuing work will focus on excited state chemistry and dynamics, and examination of the electronic structure of the lanthanide complexes. Non-adiabaticity in the dynamics is expected, representing a challenge for upcoming years.

Notably, we discovered a heteroatom transfer reaction can occur between certain Dy/Y complexes and an organic receptor under light irradiation. These new complexes, upon light irradiation, react with the organic substrate and the resulting products coordinate to the metal ion, releasing a second organic product. The reaction occurs on the timescale of hours, with a notable, metal-dependent rate difference in the photochemical reactivity, but does not occur in the absence of light. While these reactions occur on pure solutions of the complexes, efforts to achieve a separation have, to date, been unsuccessful because of fast ligand exchange between Dy and Y complexes in mixtures. To translate these findings into a separations system, we propose to synthesize a multi-dentate ligand that resists ligand exchange and use it to study such reactions on mixtures of lanthanides.

References

(1) Xie, F.; Zhang, T.A.; Dreisinger, D.; Doyle, F., A critical review on solvent extraction of rare earths from aqueous solutions, *Miner. Eng.* **2014,** *56*, 10.

(2) Mancino, G.; Ferguson, A.J.; Beeby, A.; Long, N.J.; Jones, T.S., Dramatic Increases in the Lifetime of the Er3+ Ion in a Molecular Complex Using a Perfluorinated Imidodiphosphinate Sensitizing Ligand, *J. Am. Chem. Soc.* **2005,** *127*, 524.

(3) Liu, G.K.; Jensen, M.P.; Almond, P.M., Systematic Behavior of Charge-Transfer Transitions and Energy Level Variation in Soft Donor Complexes of the Trivalent Lanthanides, *J. Phys. Chem. A* **2006,** *110*, 2081.

(4) Jensen, M.P.; Chiarizia, R.; Ulicki, J.S.; Spindler, B.D.; Murphy, D.J.; Hossain, M.; Roca-Sabio, A.; de Blas, A.; Rodríguez-Blas, T., Solvent Extraction Separation of Trivalent Americium from Curium and the Lanthanides, *Solvent Extr. Ion Exch.* **2015,** *33*, 329.

(5) Koldemir, U.; Braid, J.L.; Morgenstern, A.; Eberhart, M.; Collins, R.T.; Olson, D.C.; Sellinger, A., Molecular Design for Tuning Work Functions of Transparent Conducting Electrodes, *J. Phys. Chem. Lett.* **2015,** *6*, 2269.

(6) Cole, B.E.; Falcones, I.B.; Cheisson, T.; Manor, B.C.; Carroll, P.J.; Schelter, E.J., A molecular basis to rare earth separations for recycling: tuning the TriNOx ligand properties for improved performance, *Chem. Commun.* **2018,** *54*, 10276.

(7) Cheisson, T.; Cole, B.E.; Manor, B.C.; Carroll, P.J.; Schelter, E.J., Phosphoryl-Ligand Adducts of Rare Earth-TriNOx Complexes: Systematic Studies and Implications for Separations Chemistry, *ACS Sustainable Chem. Eng.* **2019,** *7*, 4993.

(8) Qiao, Y.; Sergentu, D.-C.; Yin, H.; Zabula, A.V.; Cheisson, T.; McSkimming, A.; Manor, B.C.; Carroll, P.J.; Anna, J.M.; Autschbach, J.; Schelter, E.J., Understanding and Controlling the Emission Brightness and Color of Molecular Cerium Luminophores, *J. Am. Chem. Soc.* **2018,** *140*, 4588.

(9) Wang, N.; Wang, J.; Zhao, D.; Mellerup, S.K.; Peng, T.; Wang, H.; Wang, S., Lanthanide Complexes with Photochromic Organoboron Ligand: Synthesis and Luminescence Study, *Inorg. Chem.* **2018,** *57*, 10040.

(10) Bogart, J.A.; Lee, H.B.; Boreen, M.A.; Jun, M.; Schelter, E.J., Fine-Tuning the Oxidative Ability of Persistent Radicals: Electrochemical and Computational Studies of Substituted 2-Pyridylhydroxylamines, *J. Org. Chem.* **2013,** *78*, 6344.

Publications

Project initiated in September 2020, no publications to report.

Expanding the Operational Capacity of Soft-Donor Complexant Scaffolds for Minor Actinide Separations of Spent Nuclear Fuel through Strategic Functional Group Interconversion

Jesse D. Carrick[1], *Jenifer C. Shafer*[2], *David A. Dixon*[3; 1]*Tennessee Technological University,* [2]*Colorado School of Mines,* [3]*The University of Alabama*

Presentation Abstract

As the energy demands of the world continue to increase at a rate unsustainable for satisfaction by finite natural resources, nuclear energy will continue to be included as a vital component of the nation's energy portfolio. Carbon-neutral energy sources continue to gain momentum as a component of a comprehensive national energy strategy. Closure of the nuclear fuel cycle to allow for an efficient and cost-effective transmutation of residual fissile material in a non-proliferative manner can be further improved through liquid-liquid separations to decrease the volume, toxicity, and heat load of post-fission energy production. Addressing the burgeoning waste streams from decades of energy and weapons production is also of direct relevance to the future.

Previous results over the last two decades have disclosed the potential for multidentate, soft Lewis basic donors to effectively separate minor An^{3+} (Am, Cm, Np) from the neutron-poisoning Ln^{3+} from the post-PUREX raffinate via liquid-liquid separation. The challenges of a polar organic complexant surviving a strongly acidic, oxidative, and radiolytic environment, while maintaining solubility in a nonpolar diluent, and suitable efficiency for separations are immense.

The collaborative team's focus is on the synthetic design of novel molecular scaffolds based on the CHON principle for deployment in liquid-liquid separations of simulated spent nuclear fuel while combining the power of density functional theory to better understand minor-actinide/ligand interactions towards development of the next generation of complexants for selective separations of ions of interest. Recent results highlight three areas of progress: (1) The design, synthesis, and *in silico* evaluation of "frustrated" complexants for minor An^{3+} separations, (2) Improvement of the solubility of *bis*-1,2,4-triazinyl pyridine donors in process-relevant diluents via rational derivatization, and (3) Investigation of unsymmetric complexants in minor An^{3+} separations. Current synthetic, computational, and performance data will be disseminated.

DE-SC0018033: Modular Approaches to "Click" Complexants for Chemoselective Minor Actinide Separations

PI: Jesse D. Carrick[1], Jenifer C. Shafer[2] (Co-PI), and David A. Dixon[3] (Co-PI)

Research Scientists: Dr. Jessica J. Bachini[1]

Student(s): Fortune O. Dzeaku[1], Zachary Z. Gulledge[1], Connor C. Pinson[1], Alexander M. Stovall[1], and Mariah L. Tedder[1]

RECENT PROGRESS

"Frustrated" Soft-Donor Complexant Scaffolds One of the recent areas of inquiry by our team is to examine the role that Lewis acid/base frustration plays in effective separations. The aforementioned

required the synthesis of novel, tridentate indolyl pyridinyl [1,2,4] triazine complexants from MTP synthons using cross-coupling strategies (Scheme 1). Subsequently, a chemoselective Boc deprotection of the procomplexants (Publication 3) afforded substrates for evaluation in separations assays. Density functional theory was leveraged to understand the role that the N-H bond conferred to the arrangement of the complexant and metal center (Figure 1).

Scheme 1. Frustrated MTP Indole Procomplexants

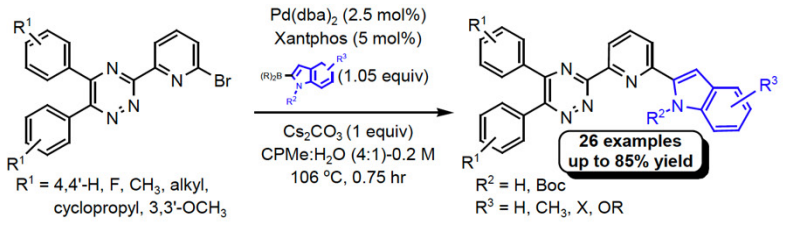

Formation of Frustrated Pyridinyl Indole Triazine Procomplexants
Carrick, *et. al. ACS Omega* **2019**, *4*, 18855-18866

Figure 1. Proposed Cm^{3+} / Ln Complex

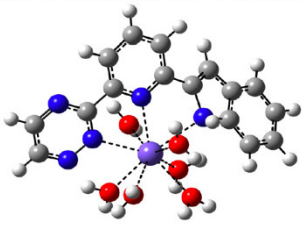

ΔG_{aq} = 2.3 kcal / mol ; ΔG_{nBuOH} = −10.5 kcal / mol
Dixon, *et. al. J. Phys. Chem. A.* **2021**, Accepted

Advancing BTP solubility beyond MOB-BTP One of the current over generalizations in the area of soft-*N*-donors is that BTP complexant solubility in process-relevant diluents will be minimal. Commercially available synthons limit access to functionalized BTPs with desired liquid-liquid separations performance characteristics. In 2017, we demonstrated that transposition of a methoxy group from the 4,4'-position to the 3,3'-position (MOB-BTP) afforded comparable D_{An} and SF to the benchmark complexant CA-BTP. Interested in improving solubility of this class of complexants further, a series of alkoxylated BTPs with substitution at the 4,4'- and 3,3'-positions has been realized (Scheme 2) affording access to seven complexants with distinctly non-crystalline morphologies and high solubility in nonpolar diluents (Figure 2).

Scheme 2. Preparation of Alkoxylated BTPs

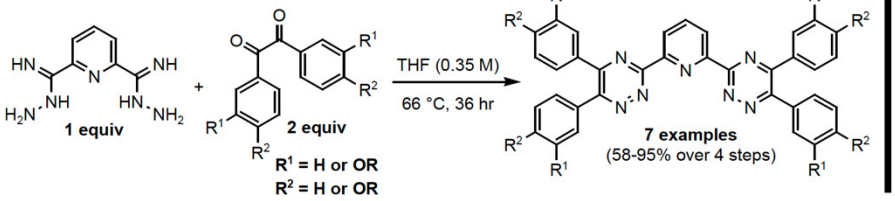

Carrick, *et. al.* **2021**, in prep.

Figure 2. Novel BTP Morphology

Unsymmetric Soft-Donor Complexants. Can One Atom Really Make a Difference?

If one casually peruses the current literature on soft-donor complexants, one repetitive theme easily emerges, that most complexants are symmetric with the same substitutents present on either side of a heteroaryl core. While symmetry can often play an important role in metal/complexant interactions and stabilization, one inherent detraction is also present, near planar topologies which

can preclude effective solvation. The assembled team has been evaluating the possibility of maintaining sufficient An^{3+} chelation while simultaneously improving the polar surfaces of the metal-ligand complex to enhance solubility and preclude the formation of a deleterious third phase during liquid-liquid separations. Pursuant to the aforementioned, a regioselective, transition metal, and azide-free, microwave-assisted synthesis of 1,2,3-triazolyl BTP derivatives (Scheme 3) has revealed significantly improved solubility in nonpolar diluents over the 1,2-pyrazole congener (Figure 3). Separations assays

are planned in the near future to evaluate the full extent of a one atom change from C to N in the case of the 1,2,3-triazole vs. the 1,2-pyrazole.

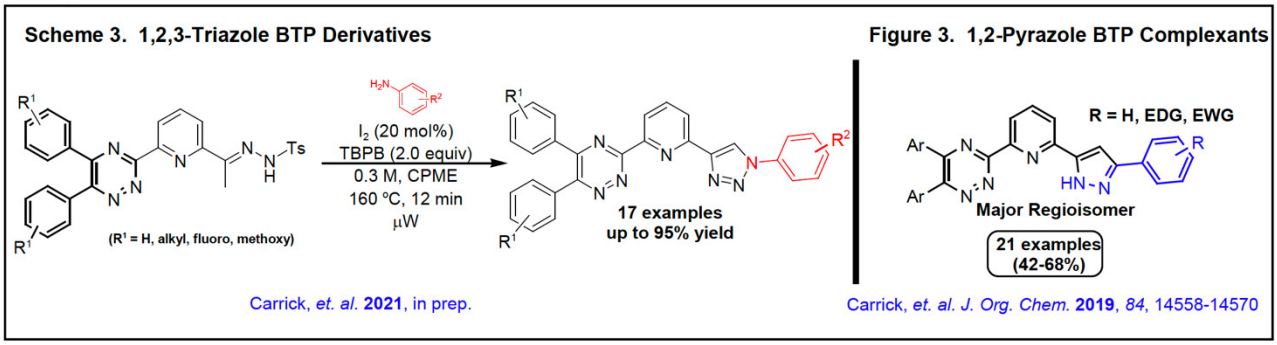

Publications Acknowledging this, and Immediate Preceding Grant 9/2017 – present

Publications Supported by DE-SC0018033

1) Mason, M. M.; Smith, C. M.; Vasiliu, M.; Carrick, J. D.; Dixon, D. A.* Density functional prediction of An(III)/Ln(III) separation by 1,2,4-triazinyl-pyridine derivatives. *Journal of Physical Chemistry A*, **2021, *WEB ASAP.*** DOI: 10.1021/acs.jpca.1c01854
2) Waters, G. D.; Carrick, J. D.* Convergent access to bis-1,2,4-triazinyl-2,2'-bipyridines (BTBPs) and 2,2'-bipyridines via a Pd-catalyzed Ullman-type reaction. *RSC Advances*, **2020**, *10*, 10807–10815, DOI: 10.1039/d0ra00673d
3) Gulledge, Z. Z.; Carrick, J. D. * Chemoselective BOC-deprotection of functionalized heteroarenes using an addition/elimination strategy. *European Journal of Organic Chemistry,* **2020**, *12*, 1817– 1822, DOI: 10.1002/ejoc.201901811
4) Gulledge, Z. Z.; Tedder, M. L.; Lyons, K. R.; Carrick, J. D. * Synthesis of tridentate indolyl pyridinyl [1,2,4] triazine Lewis basic complexants via Pd-catalyzed Suzuki-Miyaura cross-coupling. *ACS Omega*, **2019**, *4*, 18855–18866, DOI: 10.1021/acsomega.9b02891
5) Veerakanellore, G. B.; Smith, C. M.; Vasiliu, M.; Oliver, A. G.; Dixon, D. A.; Carrick, J. D. * Synthesis of 1H-pyrazol-5-yl-pyridin-2-yl-[1,2,4]triazinyl soft-Lewis basic complexants via metal and oxidant free [3+2] dipolar cycloaddition of terminal ethynyl pyridines with tosylhydrazides. *Journal of Organic Chemistry* **2019**, *84*, 14558–14570, DOI: 10.1021/acs.joc.9b02088
6) Chaudhuri, S.; Carrick, J. D.* Synthetic access to functionalized dipolarophiles of Lewis Basic Complexant Scaffolds through Sonogashira Cross-Coupling. *Journal of Organic Chemistry* **2018**, *83*, 10261−10271, DOI: 10.1021/acs.joc.8b01446
7) Downs, R. P.; Chin, A.-L.; Dean, K. M.; Carrick, J. D.* Synthesis of functionalized *hemi*-1,2,4-triazinyl-[2,2']-bipyridines via telescoped condensation of [2,2']-bipyridinyl-6-carbonitrile. *Journal of Heterocyclic Chemistry* **2017**, *54(6)*, 3008−3014. DOI: 10.1002/jhet.2908

Publications Partially Supported by DE-SC0018033

Servis, M. J.; Liu, Z.; Martinez-Baez, E.; Clark, A. E.; Su, J.; Batista, E. R.; Yang, P.; Wildman, A.; Stetina, T.; Li, X.; Newcomb, K.; Maginn, E. J.; Autschbach, J.; Dixon, D. Solvent Extraction through the Lens of Advanced Modeling and Simulation: in Ion Exchange and Solvent Extraction, Ed. B. Moyer, CRC Press, Boca Raton, FL, 2019, Chapter 5, pp. 147−218

SESSION II: Generative/Other Phenomena (Heather Allen, Chair)

Making an Inorganic Analogue of a Cell for Direct Air CO_2 Capture

Roger Rousseau[1], Jason Bara[2], David Heldebrant[1], Aaron Appel[1], Eric Wiedner[1], T. Alan Hatton[3], Xiao-Ying Yu[1], Eric Walter[1], David Hoyt[1], Asanga Padmaperuma[1], and Vassiliki-Alexandra Glezakou[1]; [1]Pacific Northwest National Laboratory, Richland WA; [2]University of Alabama, Tuscaloosa AL; [3]Massachusetts Institute of Technology, Boston MA

Presentation Abstract

We are exploring the direct air capture of CO_2 by mimicking crucial functions of single cell organisms that enable selective and kinetically efficient uptake under the small thermodynamic driving force created by low partial pressures of CO_2 in the atmosphere. We hypothesize that by tuning the bindign affinity of the amines of a CO_2 caputre solvent and functionalized electrodes, we can facilitate CO_2 delivery to a redox site where it can be bound and transiently stored under a bias and easily released by a pH swing or removal of bias. Our current project strives to achieve this by utilizing a CO_2 selective membrane (the ionone polymer membranes developed at U. Alabama to remove H_2O, O_2 and N_2), kinetically coupled to a CO_2 capture solvent (designed by PNNL) for enhanced uptake selectivity and favorable transport and an electrochemically generated transient site for strong binding and reversible conversion to carbonates/bicarbonates (Figure 1). We are taking a holistic approach to overcome the thermodynamic/kinetic limitations imposed by the low driving force for CO_2 uptake, successively increasing CO_2 sorption to create a free energy gradient to funnel CO_2 towards a strongly binding electrochemically generated active site. Conversely, the extensive energy penalties for CO_2 release can be mitigated by either electrochemical switching or a pH swing, the latter of which opens the potential for a high throughput flow system. In this presentation, an overview of the concept and our initial findings in the first year of funding will be presented.

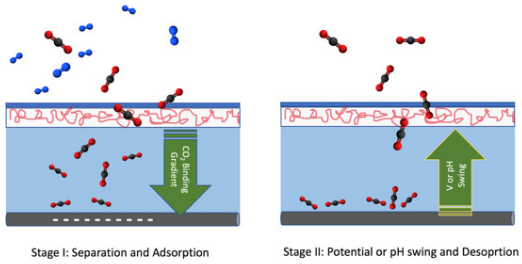

Figure 1. DAC using a capture solvent as a first stage adsorber and an electrode as a second-stage adsorber that can be switched off for facile CO_2 release.

FWR 76830 - Making an inorganic analogue of a cell for direct air capture of CO_2

PI: Roger Rousseau.

Co-PIs: Jason Bara, David Heldebrant, Aaron Appel, Eric Wiedner, T. Alan Hatton, Xiao-Ying Yu, Eric Walter, Daivd Hoyt, and Vassiliki-Alexandra Glezakou

Postdocs: (PNNL) Sarah Allec, Difan Zhang, Roberta Rodrigues, Jun Gao. (UA) Mousumi Rani Bepari, Sudhir Ravula. (MIT) Jin Soo Kang.

RECENT PROGRESS

In this our initial year of funding, we assembled the team and performed an initial evaluation of the components (membrane, solvent, electrochemical capture method) of our inorganic cell to evaluate which ones could operate together and how each piece would need to be modified to work most effectively together. The ultimate goal is to synchronize the kinetics across vapor/solid and solid/liquid interfaces into a cascade for rapid uptake and relative ease of release. We will need to characterize reactivity and kinetics at all interfaces and within the caputre solvent medium to indentify bottlenecks and propose mitigation strtegies

Membranes: Membranes form the analogue of the cell wall and serve to transport gases from the environment into the cell where they can be stored/transformed. The knowledge gap is to determine how we design and synthesize materials that are selective towards CO_2 yet will expel O_2 , H_2O, and airborne pollutants. These materials must enhance selectivity and rapidly conduct CO_2 from the air to the capture solvent medium. Our initial finding is that PEEK based ionone membranes when interfaced with PNNLs water lean capture solvent show a significantly enhanced CO_2 pumpability (~5 times higher) whilst permeability to N_2, O_2 and H_2O is an order of magnitude lower despite their higher concentration. We are currently evaluating the robustness through *in site* NMR and TOF-SIMS measurements of these membranes in contact with both amine and alcohol-based solvents to determine optimal parameters for membrane stability and selectivity. Potential impregnation of the membrane with capture solvent could aid in mass transport and selective uptake of CO_2.

The PNNL theory team has started modeling PEEK-based polymers to better understand thie membrane/solvent interface and how it impacts the CO_2 caputre. Monomers were built based on the experimental composition of neat [PEEK ionene polymers and OPLS-AA force field parameters have been assembled and for classical molecular dynamics simulations. We have generated a preliminary model for neat polymer, and current work focuses on geometric optimization of polymer models to match the experimental density of polymer as well as XRD diffraction patterns. Once finalized, we will initiate comparioson with *in-situ* NMR to understand wicking of the solvent and speciation observed upon interaction with CO_2.

Capture Solvent: The capture solvent is the analogue of the fluids in the cell that allow for the efficient transport of species. Our knowledge gaps reside in how to define and realize a window of CO_2 binding affinity strong enough to draw CO_2 from the air ar *ca*. ~0.1-1 mol% loading, yet not so strong that it could render the desorption process too costly or hinder transfer to the electrocatalysts. Our initial experimental and theoretical studies suggest pivoting away from amine-based solvents (used for post combustion capture) towards alkylguanidine based species due to) their higher CO_2 binding energy (-75 kJ/mol) and ionicity. We believe that these solvents will be best able to interface with both the membranes and electrochemical components and still provide rapid CO_2 uptake and transport.

Electrochemistry: The electrochemical active site serves as the analogue of the reactive part of the cell that provides the thermodynamic gradient in CO_2 binding needed to drive DAC. The challenge is to either bind CO_2 sufficiently strongly to the surface of the electrode (in the form of a carbonate) to drive the uptake process or convert it to a species like bicarbonate/carbonate which can be removed in a flow through process and released via a change in pH.

While the facile $2e^-/2H^+$ redox chemistry of quinones has enabled CO_2 capture from flue gas via an electrochemically-driven pH swing, application of this chemistry to direct air capture is challenging due to the slow kinetics of CO_2 delivery to the electrochemical active site. In addition, the quinones must bind CO_2 with a binding energy within an optimal range for each solvent in order to create the free energy gradient required to regenerate the solvent. Our prelinary quantum chemical calcualtions suggest that a wide array of quinones have sufficiently strong CO_2 binding energy (-90kJ/mol or stronger) to transfer CO_2 from the capture solvent to a quinone.

Furthermore, due to the sensitivity of quinones to oxygen, the formation of peroxide may be a competing reaction even in the presence of trace O_2 that permeates the membrane. Toward this last point, we have computed the reaction free energies for $H_2Q + O_2 \rightarrow Q + H_2O_2$ for quinones functionalized either with an electron-donating group (EDG) or an electron-withdrawing group (EWG). In Figure 2, we plot ΔG_{rxn} as a

function of the dielectric constant of the implicit solvent for hydroquinone functionalized with Cl (EWG) and NH_2 (EDG), observing that the reaction of O_2 with 2-chloro-H_2Q is the least exothermic. This indicated that quinones will be highly sensitive to the presence of O_2 even in minute quantities and that electron withdrawing substitutents may be the most viable.

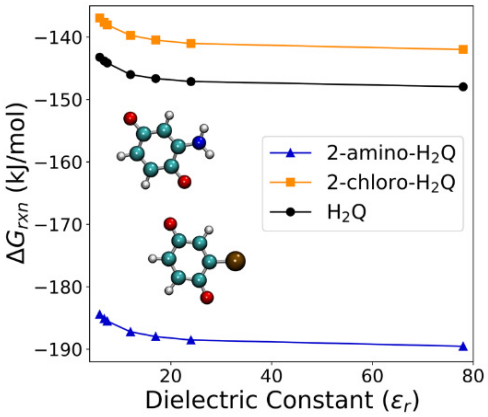

Figure 2 Reaction free energy (ΔG_{rxn}) for $H_2Q + O_2 \rightarrow Q + H_2O_2$ as a function of dielectric constant of implicit solvent for pure hydroquinone (H_2Q), hydroquinone functionalized with Cl (2-chloro-H_2Q), and hydroquinone functionalized with NH_2 (2-amino-H_2Q).

In our expemental efforts we have prepared and characterized both batch (H-Cell) and flow reactors for studying the electrochemical capture and made sure that kinetic/thermodynamic parameters obtained from MIT/PNNL are comparable. We have also tested a series of quinones for viability as either electro-swing CO_2 binding agents or pH-swing release agents. Oiur preliminary test demonstrated poor performance with the carbon capture fluid, although it is uncertain if this is due to kinetic or thermodyanamic barriers. *We are currently testing a method based on pH swing on TiO_2 based electrodes as our baseline system for comparison.*

Publications Acknowledging this Grant in 2018-2021

Intellectually led by this grant

1. O'Harra, K. E.; Kammakakam, I.; Tuan, Y.; Jackson, E. M.; Bara, J. E. PEEK-Ionenes: Ultra High-Performance Polymers Meet Ionic Liquids. *ACS Mater. Lett. Submitted*

Jointly funded by this grant and other grants with intellectual leadership by other funding sources

1. Sui, X.: Xu, B.; Yao, J.; Kostko, O.; Ahmed, M.; Yu X-Y. New insights into secondary organic aerosol formation at the air – liquid interface, *JPCL*, **2021**, *12*, 324-329.
2. Zhang, F.; Nguyen, M.T.; Fu, Y.; Yu X-Y. Interfacial dark aging is an overlooked source of aqueous secondary organic aerosol. *Chemosphere*, submitted in June 2021, currently in review.

Awards or leadership activities of all PIs during 2019-2021 calendar years

A*wards:*

1. **Vassiliki-Alexandra Glezakou,** co-recipient of R&D 100 award for self-healing cements in Mechanical/Materials category, as well as Silver medal for R&D 100 Green Tech category.
2. **Jason Bara:** Early Career Fellow – ACS Industrial & Engineering Chemistry Division (2021).

Invited Talks:

1. **Jason Bara**: Molecular Design of Imidazoles as a Route to New Monomers and Unprecedented Polymers for Separations and 3D printing. ACS Spring 2021 (Online) 4/5/2021 I&EC Division Early Career Fellow Symposium in Honor of Dr. Jason Bara
2. **Jason Bara**: Gas Separation Membranes and Functional Materials Derived from Ionic Liquids and High-Performance Polymers. West Virginia University (Online) 3/26/2021
3. **Roger Rousseau**: Direct Air Capture Kickoff Meeting, U.S. Department of Energy and National Energy Technology Laboratory. (Online) February, 2021.

4. **T. Alan Hatton**: University of Toronto Distinguished Lecture Series, *Electrochemically Modulated Mitigation of Acid Gas Emissions*, April 21, 2021
5. **T. Alan Hatton**: Monash University Platinum Seminar Series *Electrochemically Modulated Mitigation of Acid Gas Emissions*, April 14, 2021
6. **T. Alan Hatton**: CDI&E Conference (Opening Plenary) *Faradaically Modulated Electro-Swing Sorption for Mitigation of CO_2 Emissions*, May 10, 2021
7. **T. Alan Hatton**: EEES Conference (Keynote) *Electrochemically Modulated Mitigation of Acid Gas Emissions*, June 15, 2021
8. **T. Alan Hatton**: NAS Energy Subgroup, Panelist, June 28, 2021.
9. **T. Alan Hatton**: ECS Meeting Orlando *Electrochemically Modulated Mitigation of Acid Gas Emissions,* October 2021.
10. **T. Alan Hatton**: Gordon Research Conference on Chemical Separations, *Electrochemical Technologies for the Mitigation of Atmospheric Carbon Dioxide,* February 2022.
11. **Xiao-Ying Yu:** Multimodal imaging of solid-liquid interfaces, Catalysis and Chemical Engineering Conferences (CCE-2022), San Diego, CA, USA, online Feb. 22-24, 2022.
12. **Xiao-Ying Yu:** New Insights into Secondary Organic Aerosol Formation at the Air–Liquid Interface, 4th World Chemistry Conference and Exhibition (WCCE-2021), London, UK, online Oct. 04-06, 2021.
13. **Xiao-Ying Yu:** In situ imaging of particles in liquid, 2021 Virtual Material Conference (V-Mat2021), online Sept. 17-18, 2021.
14. **Xiao-Ying Yu:** Multimodal imaging of oil-in-water bilgewater emulsion and biofilms, the 11th International Conference Interfaces Against Pollution (IAP2021), Wuhan, China, online May 14th, 2021.
15. **Xiao-Ying Yu:** Molecular imaging of biological, material, and environmental interfaces, University of Illinois at Urbana Champaign, Urbana Champaign, IL, online May 4th, 2021.

Talks at conferences

1. Jun Gao, Yuchen Zhang, Jiyoung Son, David Heldebrant, Roger Rousseau, and **Xiao-Ying Yu.** Studying the compatibility of CO_2 capture solvents and membrane using ToF-SIMS, Pacific AVS , Virtual, September 2021.
2. Jun Gao, Jiyoung Son, Yuchen Zhang, Zihua Zhu, David Heldebrant, Roger Rousseau, and **Xiao-Ying Yu** Selecting a water-lean solvent for CO_2 capture using liquid ToF-SIMS, 67th AVS , Virtual, October 2021.

Towards bio-separations of rare earth elements using the natural protein, lanmodulin

Joseph A. Cotruvo, Jr., Joseph A. Mattocks, and Jonathan L. Tirsch; Department of Chemistry, The Pennsylvania State University

Presentation abstract

The discovery that certain bacteria utilize lanthanides for specific biological functions suggests that understanding their mechanisms of selective recognition of lanthanides could enable development of new methods for efficient, sustainable, aqueous separations of these important elements. Our group discovered the first selective, dedicated biological chelator for lanthanides, a protein that we named "lanmodulin." Lanmodulin exhibits hundreds of millions fold selectivity for rare earths over other metal ions, displays an unusual selectivity trend across the lanthanide series, and binds rare earths over a wide range of solution conditions. For example, we have shown that it quantitatively and selectively extracts rare earths from complex leachates down to pH ~2.5. During the last project period (the first of this award), we have investigated the relative importance of the three metal binding sites in the protein as well as methods of achieving selectivity within the lanthanide series. We have also explored the metal selectivities of lanmodulins from different organisms. These results suggest that lanmodulin proteins may serve as versatile platforms for f-element separations.

DE-SC0021007: Probing lanmodulin's mechanisms of rare earth selectivity for protein-based bioseparations

PI: Joseph Cotruvo, Jr.
Students: Joseph Mattocks, Jonathan Tirsch

Publications acknowledging this grant (since 2020)

(I) Exclusively funded by this grant:

Mattocks, J.A., Tirsch, J.L., Cotruvo, J.A., Jr. *Methods Enzymol.* **2021**, *651*, 23-61.

(II) Jointly funded by this grant and other grants with leading intellectual contribution from this grant: None yet

(III) Jointly funded by this grant and other grants with relatively minor intellectual contribution from this grant:

Deblonde, G.J.-P., Mattocks, J.A., Dong, Z., Wooddy, T., Cotruvo, J.A., Jr., Zavarin, M. *ChemRxiv*, doi:10.26434/chemrxiv.14763426.v1.

Encapsulating-Ligand Control of Magnetism Toward Photomagnetic Rare-Earth Separations

Joseph M. Zadrozny, *Amanda Gin, Siyoung Sung; Department of Chemistry, Colorado State University*

Presentation Abstract

Developing new mechanisms for controlling solubility is essential toward next generation separations schemes. Like many periodic trends across the rare-earth ions, solubility trends in a relatively gradual manner from left to right, thus, separations schemes that harness differences in these parameters need to be performed multiple times to engender high purity. Unlike many periodic trends, the magnetic properties of the rare-earth ions vary in a non-gradual manner from left to right. These differences, if harnessed to produce changes in solubility, will enable new types of separations based on electronic spin. To that end, we have been studying the synthesis and properties of molecular models that investigate the role of structure on magnetism, spin, and reactivity. Our first-generation models are based on encapsulated metal ions bound to functional groups that produce radical pairs (magnetic intermediates). Here, the radical pairs serve as local-magnetism-sensitive binding units between solubility-enhancing functional groups and metal ions. In principle, the local magnetism imparted by the rare-earth (which is rare-earth-dependent) will modify those linkages, ultimately producing a spin-based mechanism for controlling solubility with light. In this talk I will present recent results studying the magnetic influence of the encapsulating ligand shells as the first step toward the desired molecular models.

DE-SC0021259: Toward Photomagnetic Separations Mechanisms for Rare-Earth Metal Ions

PI: Joseph M. Zadrozny
Postdoc: Siyoung Sung
Undergraduate: Amanda Gin

Recent Progress

A Rigid Encapsulating Ligand For Solution-Phase Control of Magnetic Properties

One of the key ingredients in the target models is the encapsulated metal ion (**Fig. 1**). In particular, we seek the understanding to vary the encapsulating ligand to modulate the rare-earth magnetism and locate the effect on the radical pair group. We applied a set of ligands toward a proof-of-concept metal ion, Co(2+), to test how functional groups affect solution structure and variation between solid and solution-phase magnetic properties. Cobalt(2+) was selected in this case because it has an enormous sensitivity of its magnetic properties to coordination geometry. We

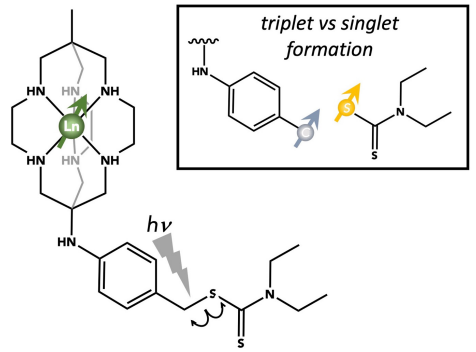

Fig. 1. Depiction of target molecular system for studying spin chemical effects.

prepared three encapsulating ligands based on cryptand-like scaffolds, getting structures as presented in **Fig. 2** upon reaction with $CoCl_2$. All three species contain six-coordinate Cobalt ions with imino-, amino-, and O-atom donors, respectively. Solid-state magnetic analyses (dc susceptibility and high-field electron paramagnetic resonance spectroscopy) on all three indicate a general trend in the zero-field splitting (an important magnetic parameter) from $[CoL1]^{2+}$ to $[CoL2]^{2+}$ to $[CoL3]^{2+}$. Comparison of the frozen-solution EPR spectrum with that from solid state (**Fig. 2**) samples reveals a strong match for the ligand L1, indicating near-identical structures for the Co ion in-solution and in the solid state. In contrast, large, broad spectra for L2 and L3 suggest large differences in solution. These results suggest that imino-donor groups in the ligand shell are essential to maintaining solution structure and enabling controlled tests of magnetic effects when extended to studies of rare-earth complexes.

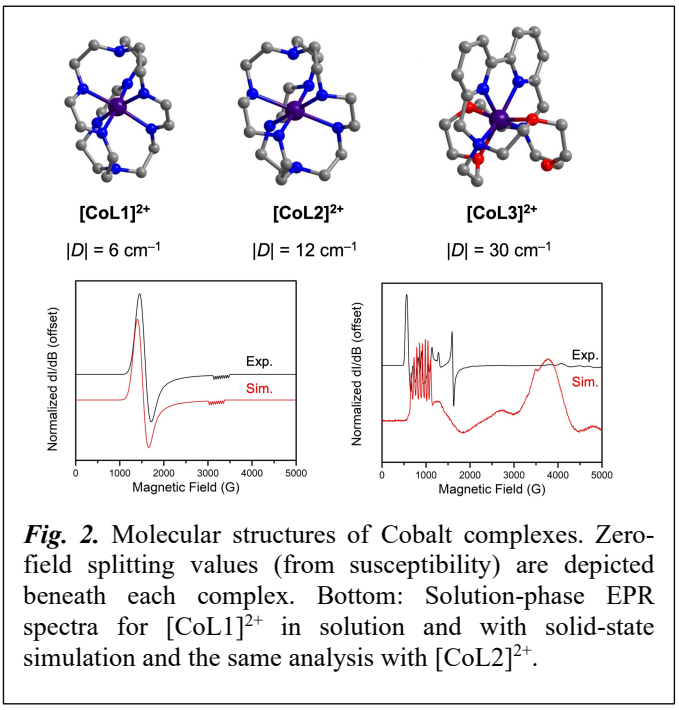

Fig. 2. Molecular structures of Cobalt complexes. Zero-field splitting values (from susceptibility) are depicted beneath each complex. Bottom: Solution-phase EPR spectra for $[CoL1]^{2+}$ in solution and with solid-state simulation and the same analysis with $[CoL2]^{2+}$.

Variable-Temperature Magnetic Properties in a Transition-Metal Mimic of Gd^{3+}.

Alongside investigations of rare-earth ions, we applied the ligands shown above to sets of Mn complexes. The ion Mn^{2+} resides in the center of the first-row of the transition metals, like Gd^{3+} does for the 4f elements. The Mn^{2+} ion has a half-filled 3d shell, like Gd^{3+} has a half-filled 4f shell. Both ions are predisposed to large-spin configurations, coordinative saturation, and weak magnetic anisotropy. In this way, Mn^{2+} is a chemical and magnetic mimic of Gd^{3+}. Design strategies for controlling the magnetic properties of ions like this are ill-explored, particularly for encapsulated geometries. Again, understanding the magnetic properties of the encapsulated units is essential for developing the model species targeted in this work. Particularly the variable-temperature magnetic properties, as understanding those will enable key

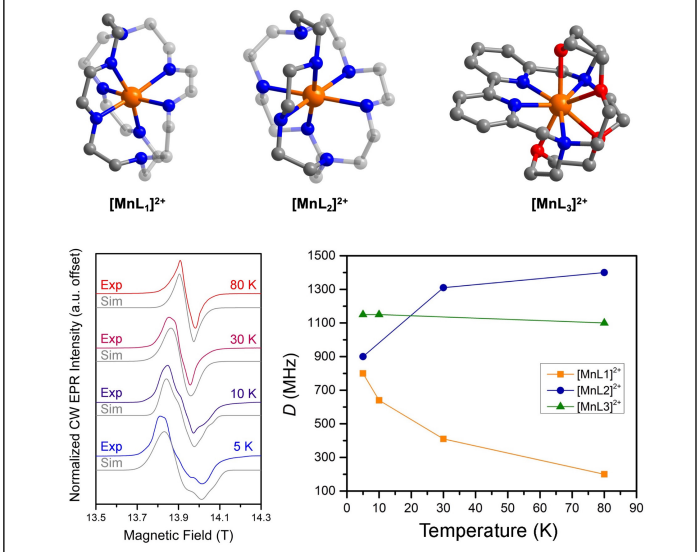

Fig. 3. Molecular structures of Mn complexes, example spectral broadening for $[MnL1]^{2+}$ as a function of temperature, and the trend in D for each complex.

understanding of temperature-dependence of any spin-based reactive properties.

We reacted the foregoing ligands with $MnCl_2$, producing a series of three Mn^{2+} complexes with the ligands L1, L2, and L3. All complexes exhibit the same, high-coordinate geometries like Co^{2+}. High-field/high-frequency EPR analyses were performed on frozen solutions of the complexes to reveal their zero-field splitting parameters. Routine inspection of the variable-temperature high-frequency EPR spectra revealed a nonroutine phenomenon: variable-temperature zero-field splitting. Perhaps more interestingly, the temperature dependence depends on the ligand shell: *D* increases for the Mn^{2+} ion encapsulated by ligand L1, decreases when bound to L2, and stays the same for L3. To the best of our knowledge, this is the first observation of this effect in Mn^{2+} complexes by EPR.

Encapsulating ligand-based modulation of magnetic properties in Gd^{3+}

Developing the proposed systems requires an in-depth understanding of how any of the above design strategies translate to rare-earth ions. Our preliminary investigations of this work involve Gd^{3+} owing to its half-integer spin state and correspondingly facile analysis by EPR. Frozen-solution investigations of the Gd^{3+} complexes of the ligands L1 and L2 reveal a substantial change in spectrum as a function of the two ligands, highlighting the impact of the ligand shells on the EPR properties. Just as excitingly, the crystal structure for one of the molecules revealed an incomplete encapsulation of the Gd^{3}+, leaving open two sites through which to bind potential radical-pair forming units (**Fig. 4**). This structural feature will be exploited to refine the initial synthetic design strategy for the magnetic models to study the possibility of spin-control of solubility.

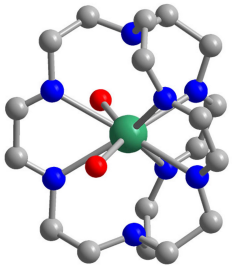

Fig. 4. Crystal structure of $[GdL1(H_2O)_2]^{3+}$ that depicts the open sites.

Lightning Round 1

Highly Permeable and Selective Model Network Membranes for Gas Separations

Ziwei Dai, Mengdi Liu, Si Li, Ruilan Guo; University of Notre Dame, Department of Chemical and Biomolecular Engineering

Abstract
Crosslinking is one of the most effective ways to improve polymer membranes' resistance toward plasticization caused by the exposure to condensable gases (e.g., CO2). However, existing random crosslinking methods inevitably lead to significantly reduced permeability with little selectivity gains. Moreover, randomly crosslinked polymers have complicated, uncontrollable structures resulting in unpredictable membrane properties that prevents the elucidation of fundamental structure-property relationships for crosslinked membranes. We are actively exploring a fundamentally new crosslinking strategy that involves a controlled end-linking approach to prepare crosslinked membranes with well-defined model network structures from telechelic oligomers with precisely-controlled chain length and chain length distribution. Via systematically varying the crosslink density (i.e., the average inter-crosslink chain length determined by the molecular weight of telechelic oligomers) and crosslink inhomogeneity (i.e., the uneven distribution of crosslink sites achieved by using telechelic oligomers with different molecular weights), we are able to achieve previously unattainable tunability in the microstructure and transport properties of crosslinked membranes. More importantly, the critical role of crosslink inhomogeneity, a previously unexplored structure parameter of crosslinked membranes, will be elucidated to provide fundamental guidance in the design of next-generation crosslinked membranes for challenging separations involving chemically and thermally challenging conditions.

DE-SC0019024: Regulating Gas Transport in Molecularly Engineered Polymer Membranes

Students: Ziwei Dai, Mengdi Liu, Si Li

RECENT PROGRESS

Overview

The overarching objective of this research project is to use specifically-designed model polymer networks with controlled architectural regularity and targeted synthetic motifs to determine the respective and synergetic effects of crosslink density and crosslink inhomogeneity (i.e., the uneven distribution of crosslink sites) on gas transport properties in crosslinked polymer membranes. Via end-linking of telechelic oligomers with controlled molecular weight, model networks, i.e., unimodal and bimodal networks (**Figure 1**), with well-define crosslinked structures that are systematically varied in terms of crosslink density and crosslink inhomogeneity can be prepared, enabling the development of fundamental structure-property relationships to guide the design of next-generation crosslinked membranes for chemical separations in chemically and/or thermally challenging environment.

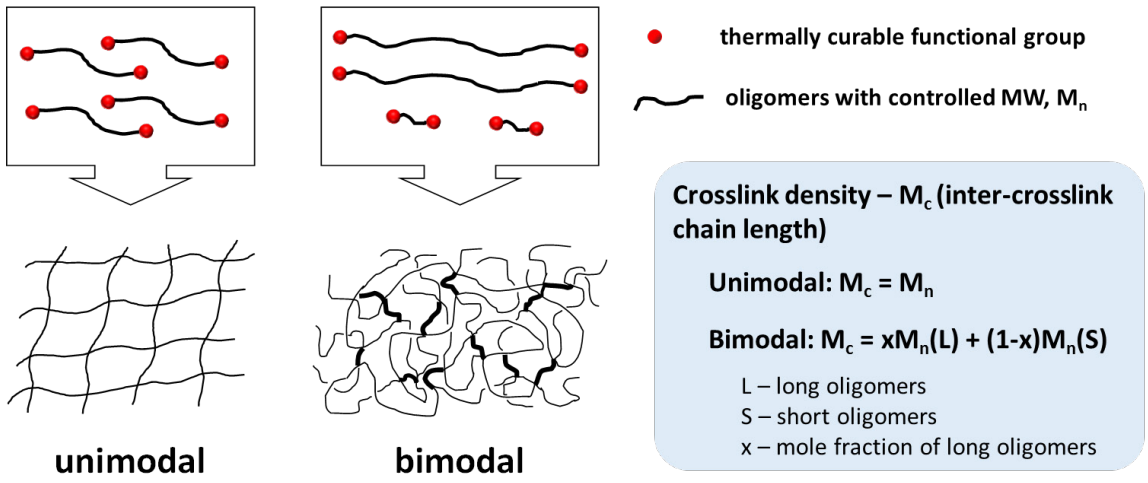

Figure 1. End-linking of telechelic oligomers to prepare model network membranes with well-defined crosslink density (M_c) and crosslink inhomogeneity (unimodal vs. bimodal)

Synthesis and Characterization of Telechelic Oligomers

Three series of telechelic oligomers, i.e., iptycene-based s-PBOs, iptycene-based TRable PHI/PAIs, and Matrimid®-like polyimide, containing thermally curable phenylethynyl (PEPA) end groups (**Figure 2**) have been prepared with molecular weight ranging from 3,000 to 15,000 g/mol. The diversity of oligomer structures along with a wide range of oligomer chain length enable systematic examination of the effect of crosslink density and crosslink inhomogeneity on gas transport properties in crosslinked membranes and investigation of the applicability of model network concept in a variety of polymer structures. Chemical structures of all telechelic oligomers were confirmed by ^{1}H NMR, where the intensity of characteristic peaks of end groups increases quantitatively with deceasing molecular weight suggesting precise molecular weight control.

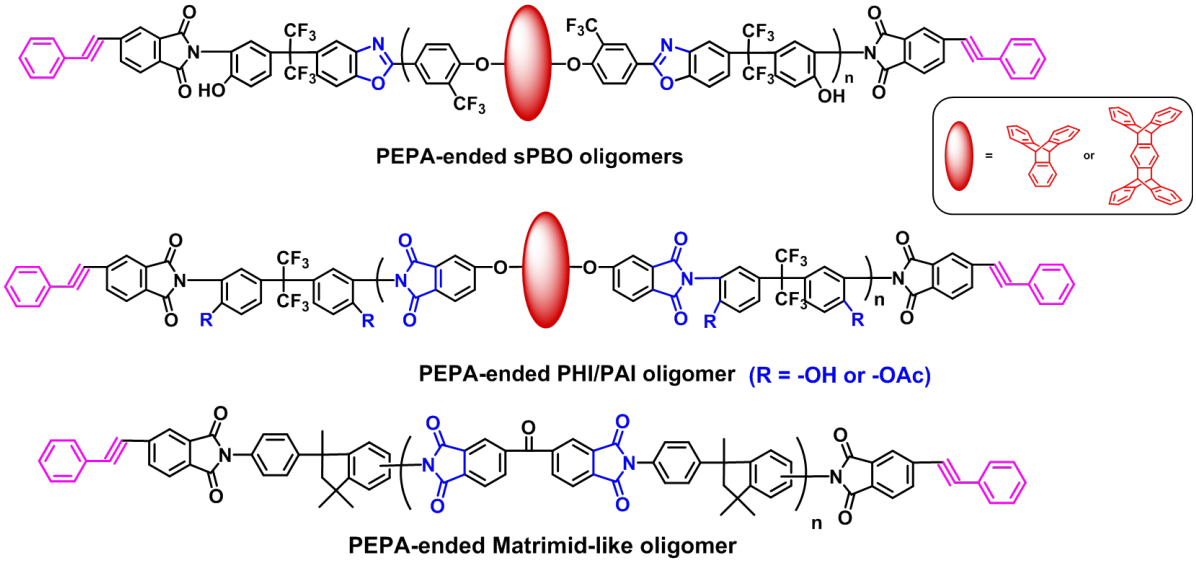

Figure 2. Phenylethynyl-terminated oligomers

Preparation and Characterization of Crosslinked Models Network Membranes

Crosslinked model network membranes were prepared via thermal end-linking of the oligomers. Thermal protocols (i.e., heating rate, intermediate temperature, final curing temperature, and curing time) is of critical importance to ensure the formation of defect- free films balanced with good mechanical properties and complete crosslinking. DSC and TGA analysis showed that Tg and decomposition temperature of the oligomers increased with increasing molecular weight as expected. A broad endothermic peak appeared in the DSC profiles for all the oligomers with a peak temperature at ~375 °C ascribed to the curing reaction of PEPA end groups. As such, the final curing temperature was chosen to be 400 °C to ensure complete crosslinking. To ensure concurrent thermal end- linking and film formation, a two-step heating protocol was adopted, which involved an intermediate isothermal stage to facilitate film formation and a final curing stage at 400 °C to complete the crosslinking. Comprehensive examination of the effects of the intermediate isothermal temperature and heating rate was performed. While all thermal protocols produced robust, fully crosslinked thin films (**Figure 3**), crosslinked microstructure and separation performance showed strong dependence on the intermediate isothermal temperature, i.e., higher than Tg isothermal treatment led to more open structure.

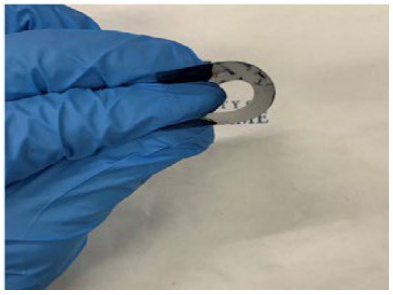

Figure 3. Picture of a crosslinked unimodal s- TPBO-3K film.

Crosslinked unimodal network membranes with systematically varied crosslink density were prepared using oligomers of varying molecular weight to examine the effect of crosslink density and phenylethynyl crosslinking chemistry. To investigate the effect of crosslink inhomogeneity, bimodal network membranes with the same average inter- crosslink chain length as in unimodal network ones were prepared using the mixture of long oligomer (e.g. 15K) and very short oligomer (e.g., 3K) in predetermined ratios (**Figure 1**). For example, a bimodal 10K membrane (B10K) could be prepared via end- linking a 3K oligomer and a 15K oligomer in a molar ratio of ~0.42, which has the same average inter-crosslink chain length of 10K as in a unimodal 10K membrane (U10K). It has been demonstrated that given the same crosslink density (i.e., the same Mc), bimodal networks generally showed improved overall separation performance.

Fundamental Structure-Property Relationship Study

Pure gas permeabilities for these new crosslinked membranes were measured with a feed pressure range of 30 – 230 psig at 35 °C. For all crosslinked membranes, gas permeabilities follow an order of P(H2) > P(CO2) > P(O2) > P(N2) > P(CH4), consistent with the kinetic diameters of the testing gases. Additionally, permeabilities for non-polar gases showed very weak dependence on feed pressure suggesting the dominant role of size sieving in these crosslinked model network membranes. In the case of CO2, compared to linear controls that showed continuous decrease in permeability with increasing feed pressure and exhibited plasticization pressure below 180 psig, the crosslinked membranes were much less sensitive to the feed pressure and did not show any sign of plasticization up to 230 psig feed pressure, the highest pressure for our current permeation testing system.

Thermal protocol effect: The examination of the thermal protocol effect focused on two parameters, i.e., intermediate isothermal temperature (Ti) and heating rate (R). Since end-linking reaction occur in solid state, oligomer Tg was chosen as a reference temperature for Ti, i.e., above or below Tg.

Table 1. Thermal end-linking protocols (**a-d**)

Thermal protocol	*Preheating (180 °C)*	*Isotherm temperature, Ti (°C, 2h)*	*Heating rate, R (°C/min)*	*Curing temperature (°C, 1h)*
a	1 h	< Tg, 300	50	400
b	none	none	10	400
c	none	> Tg	50	400
d	none	> Tg	10	400

The heating rate in the second step (from the intermediate isotherm treatment to the final curing at 400 °C) was applied at slow (10 °C/min) or fast (50 °C/min) rate to examine its effect on membrane properties. **Table 1** summarizes all four thermal protocols (a-d) that have been examined. **Figure 4** shows the effect of thermal protocols for s-PPBO series. As shown, regardless of the thermal protocol, all crosslinked membranes show highpermeability comparable to the linear control with much increased selectivity. Membranes with higher crosslink density (i.e., 13K series) are more sensitive to the thermal protocol than those with lower crosslink density (i.e., 20K series). The best-performing membranes (as judged by the distance of the data point to the upper bound lines) are those prepared using the above-T_g intermediate isotherm treatment combined with a fast heating rate, i.e., protocol **c**. These results demonstrate that thermal end-linking process involving phenylethynyl groups is highly effective in maintaining high gas permeablity in the crosslinked membranes; selectivity can be feasibly tuned in a wide range by varying the thermal protocols for various separation gas permeability needs.

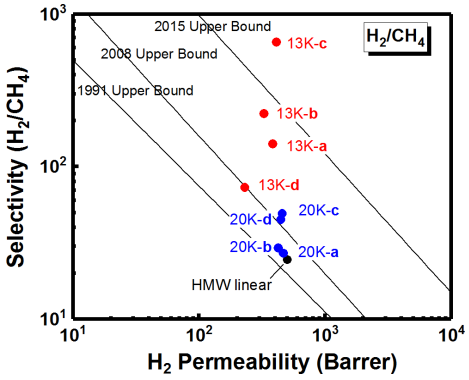

Figure 4. Effect of thermal protocol (a-d) for s-PPBO unimodal network series.

Crosslink density effect: In randomly crosslinked systems, crosslink density is the only adjustable structure parameter, which unfortunately cannot be readily quantified and frequently fails to develop reliable structure-property relationships. In our unimodal network membranes, crosslink density is precisely controlled by the molecular weight of the oligomer (i.e., Mc=Mn) as crosslinking reactions occur exclusively at the chain ends.

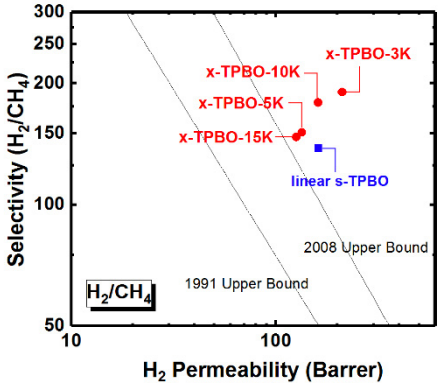

Figure 5. Effect of crosslink density for s-TPBO unimodal series.

For each series of oligomers, unimodal networks with

systematically varied crosslink density were prepared with Mc ranging from 3K to 15K. Unlike in randomly crosslinked membranes, the separation performance of unimodal network membranes shows a non-linear dependence on crosslink density where the most densely crosslinked film (unimodal 3K) shows the highest selectivity as well as the highest permeability. **Figure 5** provides an example of s-TPBO unimodal network series to illustrate the effect of crosslink density.

Similar trend was observed for TRable PHI/PAI series and Matrimid® like series. This unusual trend can be explained by the unique phenylethyl curing chemistry. The most densely crosslinked network has the smallest Mc. Therefore the highly bulky phenylethyl groups represent the largest fraction of the network structure which prevent dense packing of polymer chains leading to enhanced permeability. The superior selectivity is ascribed to the unimodal network structure where uniformly distributed crosslink sites result in narrow microcavity size distribution enabling high selectivity. These results clearly validate the concept of end-linked model network structure involving phenylethynyl crosslinking chemistry to improve the performance of crosslinked gas separation membranes.

Crosslink inhomogeneity effect: We examined for the first time the effect of crosslink inhomogeneity on transport properties of polymer gas separation membranes. Crosslink inhomogeneity describes the uneven spatial distribution of crosslink sites in the crosslinked membranes. The control of crosslink inhomogeneity can be feasibly achieved using the model network design that is unattainable in randomly crosslinked systems. Specifically, crosslinked membrane with two different types of crosslink inhomogeneity, i.e., unimodal and bimodal, were prepared. As illustrated in **Figure 1**, unimodal networks are prepared with oligomers of the same chain length, while bimodal networks are prepared from a combination of two types of oligomers of different chain length (i.e., very short and long ones) in predetermined ratio. **Figure 6** presents an example comparing s-PPBO unimodal networks with bimodal networks to illustrate the effect of crosslink density. Both types of networks were prepared at three levels of crosslink density to investigate the synergistic effects of crosslink density and crosslink inhomogeneity on gas transport: Mc= 6K, 8K and 11K. As shown, given the same crosslink density, increasing the crosslink inhomogeneity from unimodal to bimodal tends to increase the permeability while compromising the selectivity. These results validate our hypothesis that crosslink inhomogeneity plays an equally important role as crosslink density in regulating gas transport in the crosslinked membranes. This finding also greatly opens up the tunability of crosslinked membrane structure and separation performance window.

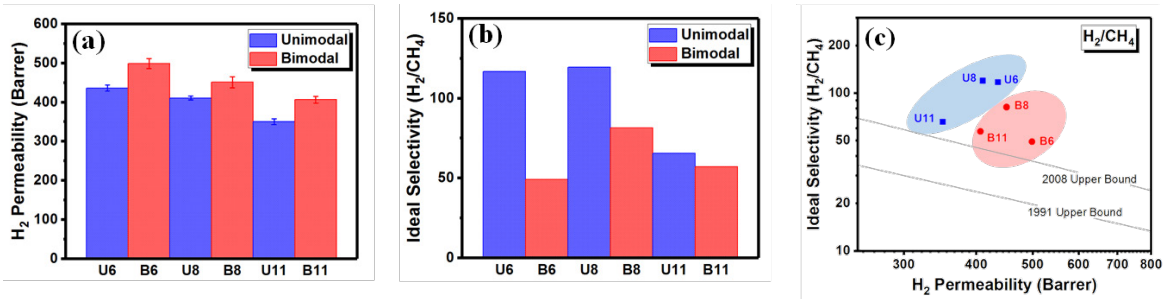

Figure 6. Effect of crosslink inhomogeneity on (a) H_2 permeability, (b) H_2/CH_4 selectivity, and (c) overall H_2/CH_4 separation performance comparing s-PPBO unimodal and bimodal network membranes.

Publications acknowledging this Grant in 2018 – present

Exclusively funded by this grant:

1. Loianno, V.; Zhang, Q.; Luo, S.; Guo, R.; Galizia, M., Modeling Gas and Vapor Sorption and Swelling in a Triptycene-based Polybenzoxazole: Evidence for Entropy-driven Sorption Behavior, *Macromolecules*, **2019**, *52, 4385−4395.*

2. Li, T.; Chen, Z. Q.; Huang, H.; Zhao, S.; Liu, J.; Guo, R.; Chen, Y., Microporous Polyimides Containing Bulky Tetra-o-isopropyl and Naphthalene Groups for Gas Separation Membranes, *Journal of Membrane Science*, **2019**, *585*, 282-288.

Jointly funded by this grant and other grants with leading intellectual contribution from this grant:

1. Deng, J.; Huang, Z.; Sundell, B.; Harrigan, D.; Zhang, K.; Guo, R.; Galizia, M., Polymer Membranes for Gas Separations in Chemically and Thermally Challenging Environments: A Review in Perspective, *Polymer*, **2021**, *229*, 123988.

2. Corrado, T.; Guo, R., Macromolecular Design Strategies Toward Tailoring Polymer Free Volume for High Performance Gas Separation Membranes, (invited paper for the Special Issue of "MSDE Emerging Investigators 2020"), *Molecular Systems Design & Engineering*, **2020**, *5*, 22-48.

3. Zhang, Q.; Li, S.; Wang, C.; Chang, H-C.; Guo, R., Carbon Nanotube-based Mixed- Matrix Membranes with Supramolecularly Engineered Interface for Enhanced Gas Separation Performance, *Journal of Membrane Science*, **2020**, *598*, 117794.

4. Zhang, Q.; Luo, S; Weidman, J.R.; Guo, R., Surface Modification of ZIF-90 with Triptycene for Enhanced Interfacial Interaction in Mixed-Matrix Membranes for Gas Separation, (Special Issue of "Polymeric membranes: chemistry, physics, and applications"), *Journal of Polymer Science*, **2020**, *58*, 2675-2637.

Jointly funded by this grant and other grants with relatively minor intellectual contribution from this grant;

1. Wang, T.; Li, T-Y.; Aboki, J.; Guo, R., Disulfonated Poly(arylene ether sulfone) Random Copolymers Containing Hierarchical Iptycene Units for Proton Exchange Membranes, (Special issue of "Women in Science: Chemistry"), *Frontiers in Chemistry (section of Green and Sustainable Chemistry)*, **2020**, *8*, 674.

2. Corrado, T.J.; Huang, Z.; Huang, D.; Wamble, N.; Luo, T.; Guo, R., Pentiptycene- based Ladder Polymers with Configurational Free Volume for High Gas Separation Performance and Physical Aging Resistance, *Proceedings of the National Academy of Sciences*, **2021**, *in press*.

Understanding the extent of ionic dissociation and ionic conductivity in model thin film polymer electrolytes as a function of different side chain configurations

Mario V. Ramos-Garcés,[a] Ishara Senadheera,[b] Revati Kumar,[b] Christopher G. Arges[a]; [a]Cain Department of Chemical Engineering and [b]Department of Chemistry, Louisiana State University, Baton Rouge, LA, 70803

Presentation Abstract

In this project, ionic activity coefficients and ionic conductivity of self-assembled block copolymer electrolytes (BCEs) were investigated as thin films using advanced metrology and with molecular dynamics (MD) simulations. The hypothesis of this work asserts that electron rich ether groups and sulfonate groups in alkoxy side chains and zwitterion sides, respectively, promote chloride anion dissociation (or other counteranion dissociation) from tethered pyridinium cations. Ionic activity coefficients are commensurate to ionic dissociation and govern ionic selectivity in electrically-driven deionization platforms. Ionic conductivity, on the other hand, dictates ohmic overpotentials across polymer ion-exchange separators and affects the energy efficiency in deionization. The preparation of model thin films commences with perpendicular alignment of self-assembled, lamellae forming poly(styrene-*block*-2-vinyl pyridine) (PS*b*P2VP) to the substrate surface. The conversion of the non-ionic block copolymer into a BCE occurred by alkylating the nitrogen in the P2VP domain with various halogenated reagents via a Menshutkin reaction. BCEs with systematically varied side-chains, such as alkoxy crosslinks, alkyl, and zwitterionic, to pyridinium were prepared post self-assembly without disrupting the self-assembled nanostructures using newly developed processing schemes. Atomic force microscopy (AFM) and x-ray photoelectron spectroscopy (XPS) substantiated retention of the structure after successful alkylation and the presence of the side-chain chemistry. Ionic conductivity was measured on interdigitated electrode (IDE) substrates with the various BCEs interfaced with DI water. MD simulations were performed on the model versions of the said BCE systems to complement experimental studies and to provide molecular level insights into the solvation structures and ion transport mechanisms that are difficult to probe experimentally. The simulation results reveal that ion-charge pair dissociation, such as chloride ion dissociation from the positively charged pyridinium, in all BCEs is governed by the extent of water available to coordinate with the ions. The amount of water in the first solvation shell around chloride ions in the zwitterionic system is lower compared to the BCEs containing alkyl and alkoxy side chains. When considering the first solvation shell around the pyridinium for BCEs with alkoxy side chains, it was observed that the pyridinium moiety coordinated to the ether group in the side chain. In the BCEs consisting of zwitterionic side chains, the oxygens of the sulfate group are coordinated to the pyridinium, while the first solvation around chloride has sodium ions present. These results explain the smaller number of water molecules coordinated to chloride ions in the zwitterionic system compared to the other two systems. Future scheduled work focuses on ion partitioning behavior between the BCEs and aqueous salt solutions, as well as ionic conductivity, using advanced metrology (e.g., QCM, GI-SAXS, and IDEs) and MD simulations.

DE-SC0018989: Understanding the extent of ionic dissociation and ionic conductivity in model thin film polymer electrolytes as a function of different side chain configurations
Postdoc(s): Dr. Mario V. Ramos-Garcés
Student(s): Ishara Senadheera

Preparation of BCEs with different side chains configurations

The preparation of the nanostructured BCEs in this work consisted of immersing the self-assembled PS*b*P2VP block copolymer in a solution containing either sodium 2-bromoethanesulfonate (2-BES), 1-bromododecane (1-BrC_{12}), or bromo-PEG3-bromide (PEG3). For 2-BES, PS*b*P2VP was submerged in a 0.1 M aqueous solution at 50 ºC for 48 hrs with constant stirring. The Menshutkin reaction that occurs between the pyridine moiety in the P2VP domain and the 2-BES forms a zwitterionic moiety (Figure 1a). For PEG3, a 5% v/v solution in ethanol was used and the reaction proceeded at room temperature for 24 hrs (Figure 1b). For, 1-BrC_{12}, a 10% v/v solution in a 50:50 hexane:ethanol solvent mixture was used, and the reaction proceeded at 50 ºC for 24 hrs with constant stirring (Figure 1c). Alkylation with the three side chains was confirmed with XPS in the nitrogen region. For all 3 reactions, a second N 1s peak appears at higher binding energies due to the formation of the pyridinium moieties (Figure1a-c). Peak fittings of the N 1s peaks shows the percentages of pyridine groups that were converted to pyridinium. For the 1-BrC_{12} and PEG3, both show a pyridinium conversion close to 40%, while the conversion for the zwitterionic side chain is 30%. AFM imaging, presented in Figure 2 was performed to confirm the retention of the BCE nanostructures after installing the various side chains. This is the first time alkoxy and zwitterionic moieties were installed in PS*b*P2VP to prepare BCEs with long-range order microstructures and with systematically varied side-chains. The goal of this study is to understand how side chain chemistry alters ionic activity, water uptake (a contributor to solvation and ionic dissociation) and ionic conductivity.

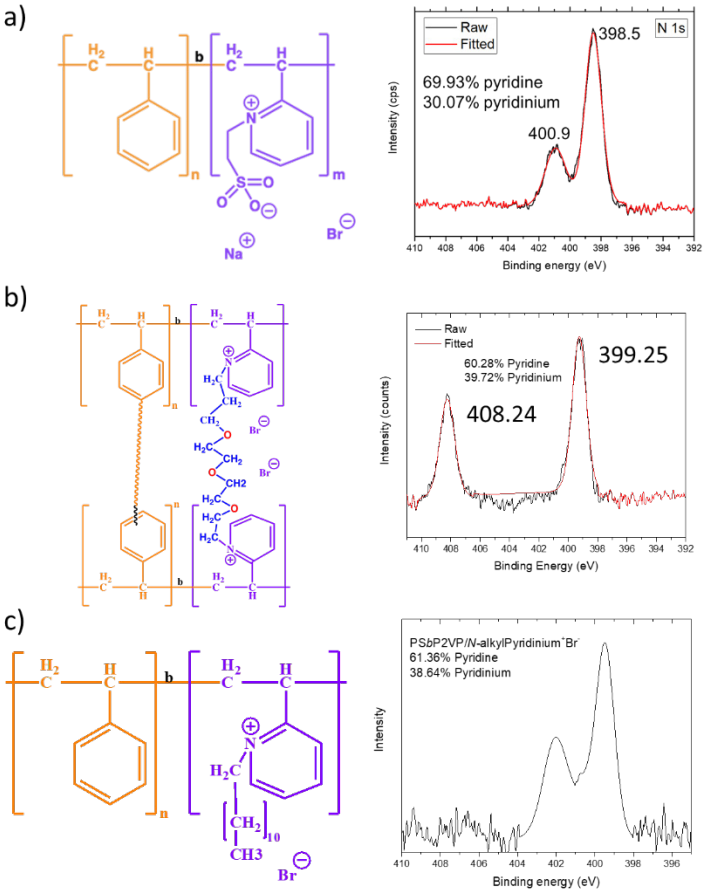

Figure 1. a) Schematic representation of the 2-BES reaction with PS*b*P2VP. b) Schematic representation of the PEG3 BCE. c) Schematic representation of the 1-BrC_{12} BCE. All panels show their respective N 1s XPS high resolution scans.

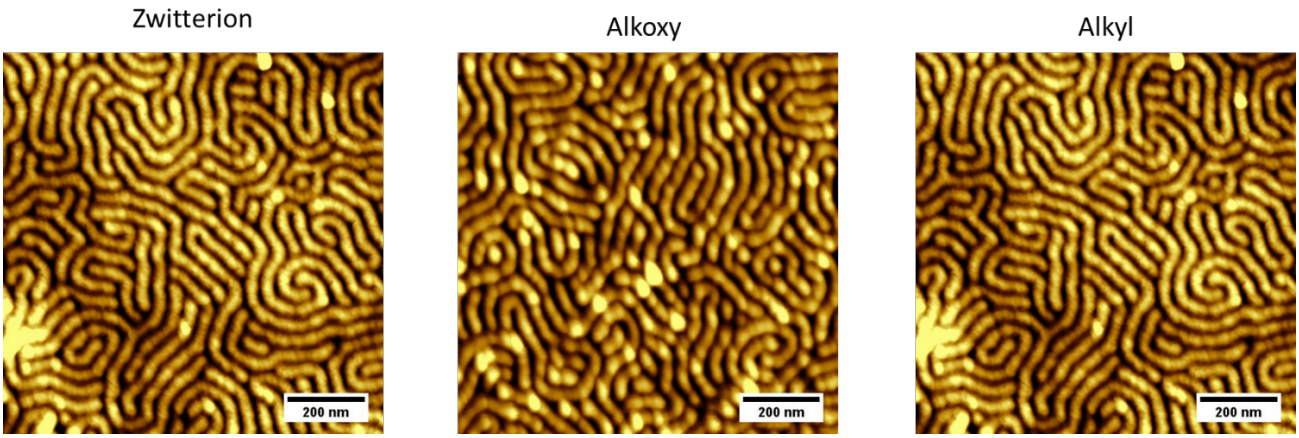

Figure 2. AFM images of the three BCEs with different side chains configurations.

Classical molecular dynamics simulations

Computational methods provide molecular level insight into the solvation structures and the ion transport mechanisms occurring within BCEs. The relationships between the microstructures of BCEs and ionic conductivity within the BCEs were investigated systematically by performing MD simulations on the three systems each consisting of 15 polymers with a specific side chain chemistry. Each BCE contains 20-mers (see Figure 3) with 10 styrene monomers followed by an equal length segment having alternating charged (pyridinium) and uncharged (pyridine) monomers. The positively charged pyridinium moieties consisted of either the alkoxy, alkyl or zwitterionic side chains. Five chloride counterions per chain and ten water molecules per pyridinium moiety were introduced in each system.

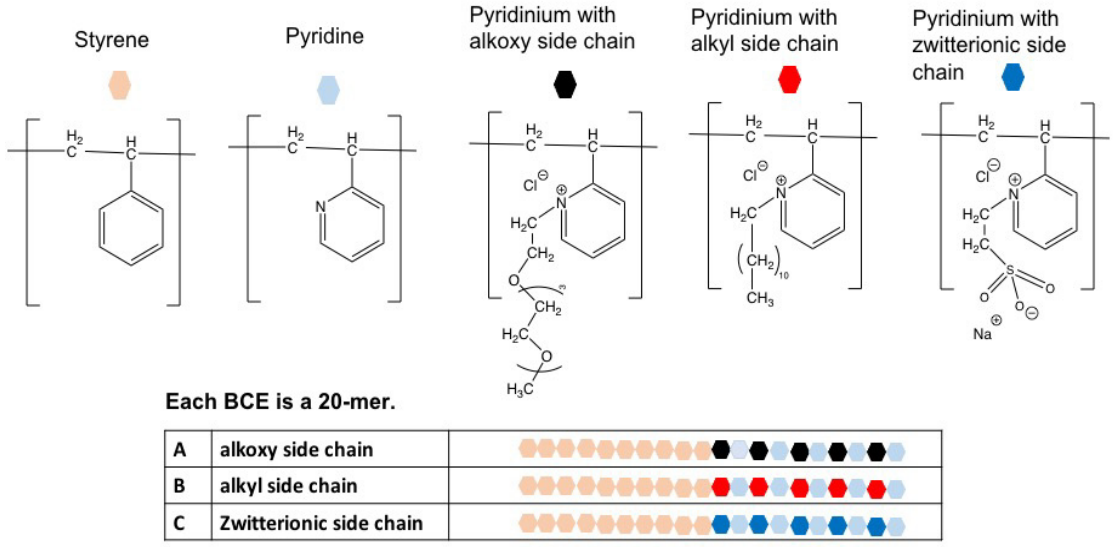

Figure 3. The model BCEs (MD simulations) consisting of different chemical groups.

The corresponding radial distribution (g(r)) functions calculated between different species in the system (chloride ions, pyridinium N, ether O, sulfate O, and water O) provides a direct measurement of the ion pairing and solvation around species. The initial results of the simulations show that ion-

charge pairs (chloride ion and positively charged pyridinium) in the BCEs are dissociated and the chloride ions are mainly solvated by water present in the system (see Figures 4a and 4b). The amount of water in the first solvation around chlorides in the zwitterionic system is less compared to the alkyl and alkoxy systems. When considering the first solvation shell around the nitrogen in pyridinium, it is evident that in the BCE system with alkoxy side chains, the positively charged nitrogen is coordinated to the ether oxygens of the side chain. Similarly, in the BCEs consisting of zwitterionic side chains, the oxygens of the sulfate group are coordinated to the nitrogen in pyridinium. Additional simulations show that the g(r) calculated between the chloride ions and sodium ions in the zwitterionic system reveal that the first solvation around chloride consists of sodium ions as well. This explains the smaller number of waters coordinated to chlorides in the zwitterionic system compared to the other two systems. Some of the waters are replaced by sodium ions present in the system.

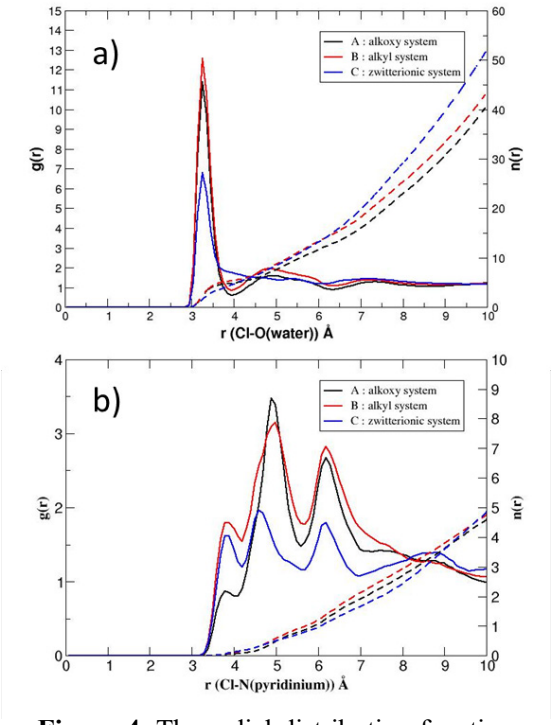

Figure 4. The radial distribution function g(r), (solid line) and coordination number, n(r), (dashed line) for (a) the Cl^- distance from the water O, b) the Cl^- distance from the pyridinium N.

Publications Acknowledging this Grant 2019-present

(I) Exclusively funded by this grant;

1. Bhattacharya, D., Kole, S., Kizilkaya, O., Strzalka, J., Angelopoulou, P. P., Sakellariou, G., Cao, D., Arges, C. G. *Small* **2021,** *17*, 2100437.
2. Ramos-Garcés, M.V.; Li, K.; Lei, Q.; Bhattacharya, D.; Kole, S.; Zhang, Q.; Strzalka, J.; Angelopoulou, P.P.; Sakellariou, G.; Kumar, R.; Arges, C.G., *RSC Adv.,* **2021,** *11*, 15078-15084.
3. Lei, Q.; Li, K.; Bhattacharya, D.; Xiao, J.; Kole, S.; Zhang, Q.; Strzalka, J.; Lawrence, J.; Kumar, R.; Arges, C. G.,*J. Mater. Chem. A*, **2020,** *8*, 15962-15975.

(II) Jointly funded by this grant and other grants with leading intellectual contribution from this grant;

N/A

(III) Jointly funded by this grant and other grants with relatively minor intellectual contribution from this grant;

4. Arges, C. G.; Li, K.; Zhang, L.; Kambe, Y.; Wu, G.-p.; Lwoya, B.; Albert, J.N.L.; Nealey, P.F.; Kumar, R. *Mol. Syst. Des. Eng.*, **2019,** *4*, 365-378.

Design and Study of High-Performance Ionene Architectures for Membrane Separations

Jason E. Bara, C. Heath Turner, Irshad Kammakakam, Kathryn E. O'Harra, Xiaoyang Liu; University of Alabama, Department of Chemical & Biological Engineering

Presentation Abstract

High-performance (HP) ionenes provide a new platform for the systematic investigation of the structural variables underlying gas transport and selectivity in polymer gas separation membranes. The rational "bottom-up" design of HP ionenes allows for the influence of key functionalities associated with state-of-the art membrane materials to be understood. HP ionenes possess synergies that can only be achieved by combining the desirable properties of polyimides, PIMs, ILs, MOFs and TR polymers, that are not necessarily available otherwise, while minimizing or eliminate the known disadvantages (e.g. aging, plasticization, difficult processing) of the individual material classes. Based on lessons already learned and the knowledge associated with each class of material, we expect to develop the core fundamental knowledge to design aromatic HP ionenes with performances that move the state of the art closer to gas phase mass transfer limited separations, with Robeson's "Upper Bounds" for the aforementioned separations being one such benchmark.

Design and Study of Hybrid Polyimide-Ionene Architectures for Membrane Separations (DE-SC0018181)

PI: Jason E. Bara (PI), C. Heath Turner (co-PI)
Postdoc(s): Irshad Kammakakam
Student(s): Kathryn E. O'Harra, Xiaoyang Liu
Affiliations(s): University of Alabama, Department of Chemical & Biological Engineering

RECENT PROGRESS

Prior to our recent efforts, the vast majority of ionenes in the literature were comprised of ammonium cations tethered by long alkyl chains and the only example of the use of ionenes in gas separation membranes was a relatively simple imidazolium ionene studied by Carlisle, Bara, and co-workers in 2010. With support from DOE BES, we have demonstrated that ionenes with far more sophisticated structures are not only feasible for gas separation membranes, but they are also highly tailorable and have synthetic methods which are highly viable for economic and efficient scale-up. The crux of our approach has been a bottom-up design where monomer selection translates to controlled structures that allow for the influence of structural components on separation performance to be understood. Our progress in membrane design has been enabled by the use of versatile "imidazole-aniline" species, which are inexpensively prepared at scales up to 200 g with excellent yield. These imidazole-aniline molecules are key to the synthesis of polyimide-ionenes and Tröger's base (TB)-containing ionenes. They impart control over the regiochemistry of the polymer backbone connectivity as well as the co-planarity of the adjacent imidazole and benzene rings, both of which influence the local conformations of the polymer chain and the nature of the free volume regions of the membrane.

Scheme 1 depicts a general approach to the synthesis of imidazole-diimide monomers from the imidazole-aniline and a dianhydride (e.g., 6FDA). This monomer can then be reacted with suitable dihalide to produce a polyimide-ionene. Commercial dihalides (e.g., *p*-dichloroxylene) (Figure 1) as well as new dihalide-diamides can provide enhanced mechanical properties through H-bonding interactions.

Scheme 1: Synthesis of imidazole-diimide monomers developed in our prior BES funding.

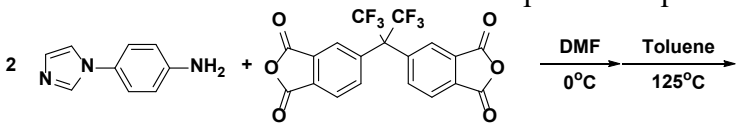

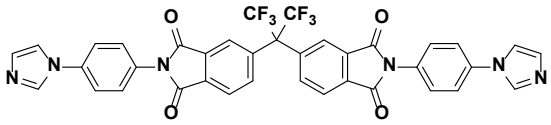

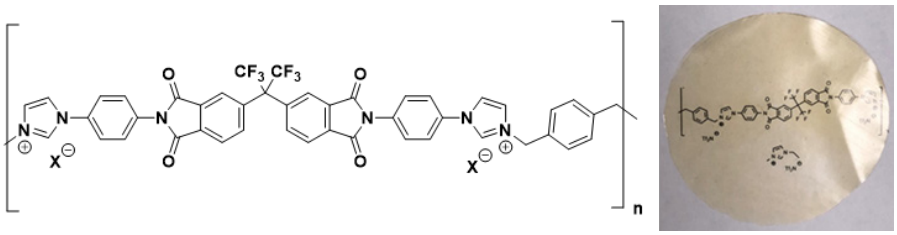

Figure 1: Example of a 6FDA based polyimide-ionene membrane developed in our prior BES funding.

Scheme 1 and Figure 1 are representative examples of many types of possible polyimide-ionenes that can be synthesized using our methods. We have achieved high MW (M_N >75 kDa) and nearly all of these materials are capable of forming thin films suitable for gas separation membranes. Polyimide-ionene materials with Tf_2N^- counter-anions generally exhibit thermal stabilities up to 400 ºC and are soluble in polar organic solvents, including CH_3CN, DMF, DMSO and DMAc, which enables them to be cast as free-standing (or supported) polymer films.

The permeabilities of these 6FDA polyimide-ionenes were modest, with only ~2 barrer for CO_2. Addition of ILs within the polyimide-ionene matrix generally increased permeability by 2-3x, with CO_2/N_2 and CO_2/CH_4 selectivity of 20-30 for both gas pairs. The amount and structure of IL added influenced the polyimide-ionene morphology, as observed by XRD.

We have shown that our imidazole-aniline species are also ideal starting materials for the formation of TB-containing ionenes. The use of TB moieties in polymer backbones is a relatively recent development in gas separation membranes and the TB group been shown to impart excellent gas permeability and separation selectivity. Scheme 2 depicts an example of a TB-containing ionene membranes which we studied in our prior funding.

Scheme 2: TB-containing ionene polymer membrane from imidazole-aniline.

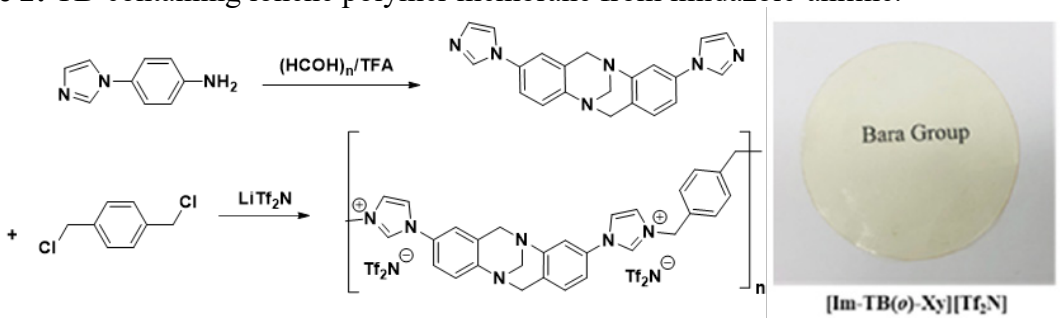

The TB-containing ionenes synthesized in our prior funding are the first examples of polymers wherein TB groups are connected to ionic species and such combinations demonstrate another tool for polymer membrane design. Our TB-containing ionenes possess thermal stability of ~400 °C and can also be formed into free-standing films through solvent casting methods. These TB-containing ionenes exhibited modest CO_2 permeabilities in the range of 2–4 barrer but with excellent CO_2/CH_4 selectivities of up to 82.5. By comparing these TB-containing ionenes to other poly(IL), ionene and TB-containing materials (*vis-à-vis* Robeson Plots), we found that TB-containing ionenes were the most selective class of TB-containing polymer materials for CO_2/CH_4 separation. Thus, there is clear synergy between the TB and ionic groups for this separation, and ionenes containing both TB groups warrant further investigation. We are currently studying TB-containing ionenes with additional functional groups appended to the imidazolium cation, as well as different linkers and the addition of "free" IL to the polymer matrix.

In our most ambitious approach to bottom-up membrane design, we have successfully realized the first combination of spirobisindane (SBI) groups commonly associated with PIMs, and ionenes using an SBI-containing dianhydride. Furthermore, the imidazole-spirobisindane is coupled with an aromatic diamide link which has been found to provide added mechanical strength and processability to our ionenes, compared to the ionenes linked by dichloroxylene. The synthesis and structure of this PIM-polyimide-ionene material is shown in Scheme 3.

Scheme 3: Synthesis of PIM-polyimide-ionene polymer membrane and photograph of membrane.

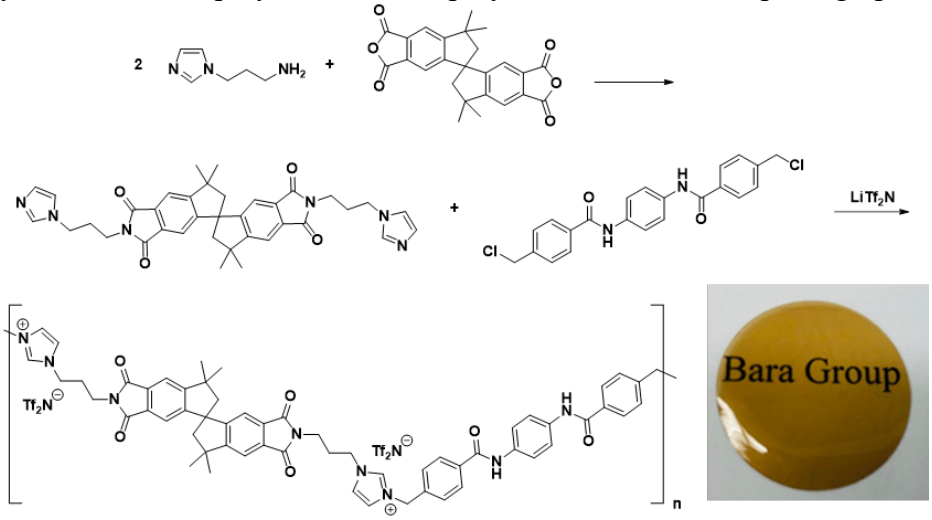

This PIM-polyimide-ionene membrane exhibits CO_2 permeability of ~300 barrer and CO_2/N_2 selectivity of 41, which is markedly higher than the other polyimide-ionenes and TB-containing ionenes, indicating that the spirobisindane group is responsible for higher FFV than other diimide (e.g. 6FDA) linkages that we have used in ionenes. The PIM-polyimide-ionene is also soluble in a range of organic solvents and thermally stable up to 400 °C. These results are encouraging as they suggest that the spirobisindane group may be a key factor to increasing permeability in ionenes, without sacrifice of selectivity. We have also recently published on benzoxazole-containing ionene membranes with improved performances and robust mechanical properties, and this approach can also be extended to "PIM-type" linkages.

The fundamental knowledge gained from this work illustrates that ionenes and ionene + IL composites are a viable and versatile class of materials for the rational design of gas separation membranes with tailored properties that can provide performances to meet the demands required to achieve cost and energy efficient chemical separations in the 21st Century. Our successes with ionenes as gas separation membranes with rationally designed structures has given us a set of guidelines as to how both the ionene structure and added IL influence gas transport and separation selectivity. These results have led us to a new set of rules and design guidelines which enable us to more clearly understand the role of charged species directed toward challenging separations involving gas pairs where the components have similar properties.

Simulations and Computational Studies

The goal of our simulations and computational studies is to develop a multi-scale simulation approach to predict experimentally-relevant membrane performance as a function of molecular-level structure/composition, the components of which are:

- Quantum mechanical (QM): calculate partial charges on polymer backbone sites;
- Molecular dynamics (MD): model the atomistic polymer structure and the short-time transport behavior of different gas molecules in the bulk polymer;
- Molecular dynamics (MD): estimate gas sorption properties at polymer interfaces;
- Kinetic Monte Carlo (KMC): simulations of a comprehensive gas/polymer/gas system to predict penetrant permeability and selectivity for the gases: CO_2/N_2, CO_2/CH_4, H_2/CO_2 and O_2/N_2.

The foundation of the modeling work is the development realistic molecular models for the molecular dynamics simulations (MD). While intramolecular parameters can be adopted from standard forcefields, the partial charge assignments need to be estimated from electronic structure methods (using Gaussian09). Different polymer fragments have been constructed, followed by energy minimization and single-point energy calculation (MP2/6-311++g(3d,3p)//B3LYP/ 6-31 g++(d,p)). Following these calculations, the partial charges are extracted using a natural bond order analysis (NBO). Currently, these calculations have been completed for the following polymer building blocks: 6-FDA, TRIPDA, and PIMDA.

We have also applied Gaussian09 to aid in the design of additional imidazole-aniline candidate compounds (cf. Scheme 1, Figure 1). The introduction of one of more methyl groups on both the imidazole and benzene rings will cause the rings to be non-coplanar, which may present further opportunities to tune void space and FFV. Computational work published to date has

focused on the influence of the counter anion on material properties and the diffusion of gases through the cavities of polyimide-ionenes.

Since these polymer materials are relatively large for atomistic-level modeling studies (severely limiting the duration and/or the sampling efficiency of the simulations), we have developed protocols for constructing coarse-grained (CG) models. These new CG models allow for time scale accelerations of 50-100x, so that much more realistic and complex environments can be simulated (e.g., entangled polymers, multi-component systems, etc.). In order to be useful, these coarse-grained models must be 'trained' using techniques such as the iterative Boltzmann inversion (IBI) approach (Figure 2), which is an incremental process for matching the polymer structures between the two different model resolutions.

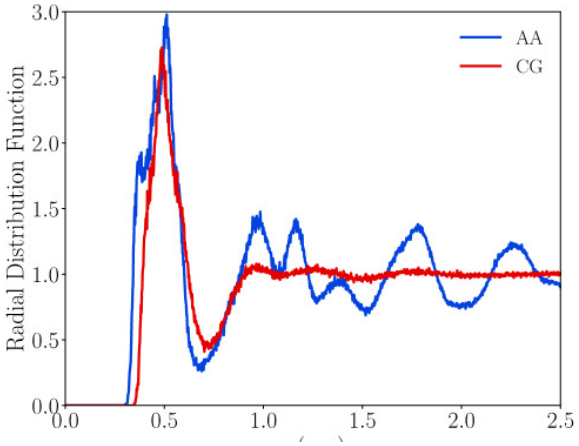

Figure 2. Iterative Boltzmann inversion approach used to extract interaction parameters for the coarse-grained (CG) model from the all-atom (AA) model.

Following convergence, the IBI approach yields a set of 'beads' which are representative of multiple atom sites (Figure 3), and the interaction parameters of these beads are able to generate structural and thermodynamic information analogous to the original all-atom polymer model. With these new models, we are now able to explore behavior of complex systems that contain these PIM-polyimide-ionene materials.

There are two main aspects of our recent modeling work that are particularly novel. First, these are the first GC representations that have ever been developed for this polymer material platform. Since these models are transferrable, others can easily adapt our approach for a variety of other applications. Second, quantifying the electrostatic interactions in CG models is extremely challenging, and as a result, these interactions are often ignored or treated in a trivial way. We are taking a very methodical approach and performing rigorous benchmarking in order to provide a framework for others in the simuation field that encounter ionenes or similarly charged polymers.

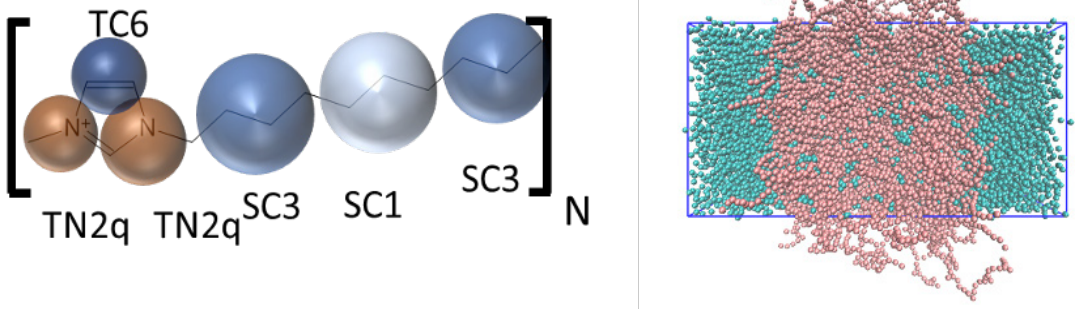

Figure 3. Representative approach for transitioning an all-atom polymer model into a coarse-grained model. *Left*: beads are parameterized to represent multiple atom sites; *Right*: system size can be significantly expanded (200 ionenes + 2000 BF_4^- in the presence of octane and benzene).

Publications Acknowledging this Grant 2018 – present

Exclusively Funded by this Grant

O'Harra, K. E.; Bara, J. E. Toward Controlled Functional Sequencing and Hierachical Structuring in Imidazolium Ionenes. *Polym. Int.* **2021**, *70*, 944-950.

O'Harra, K. E.; Devriese, E. M.; Turflinger, E. T.; Noll, D. M.; Bara, J. E. Design and Gas Separation Performance of Imidazolium Poly(ILs) Containing Multivalent, Imidazolium Fillers and Crosslinking Agents. *Polymers* **2021**, *13*, 1388. doi:10.3390/polym13091388

Kammakakam, I.; O'Harra, K. E.; Jackson, E. M.; Bara, J. E. Synthesis of Imidazolium-Mediated Poly(benzoxazole) Ionene and Composites with Ionic Liquids as Advanced Gas Separation Membranes. *Polymer* **2021**, *214*, 123239. doi:10.1016/j.polymer.2020.123239

Kammakakam, I.; Bara, J. E.; Jackson, E. M. Synthesis and Characterization of Imidazolium-Mediated Tröger's Base Containing Poly(amide)-Ionenes for CO_2 Separation Membranes. *Polym. Chem.* **2020**, *11*, 7370-7381. doi:10.1039/D0PY01038C

O'Harra, K. E.; Noll, D. M.; Kammakakam, I.; DeVriese, E. M.; Solis, G. C.; Jackson, E. M.; Bara, J. E. Designing Imidazolium Poly(amide-amide) and Poly(amide-imide) Ionenes and Their Interactions with Mono- and Tris(imidazolium) Ionic Liquids. *Polymers* **2020**, *12*, 1254. doi:10.3390/polym12061254

O'Harra, K. E.; Kammakakam, K. E.; Noll, D. M.; Turflinger, E. M.; Dennis, G. P.; Jackson, E. M.; Bara, J. E. Synthesis and Performance of Aromatic Polyamide Ionenes as Gas Separation Membranes. *Membranes* **2020**, *10,* 51. doi:10.3390/membranes10030051

Bara, J. E.; O'Harra, K. E. Recent Advances in Ionene Design – Toward Convergence with High-Performance Polymers. *Macromol. Chem. Phys.* **2019**, *220*, 1900078. doi:10.1002/macp.201900078

Bara, J. E.; O'Harra, K. E. Recent Advances in Ionene Design – Toward Convergence with High-Performance Polymers. *Macromol. Chem. Phys.* **2019**, *220*, 1900078

Kammakakam, I.; O'Harra, K. E.; Bara, J. E.; Jackson, E. M. Design and Synthesis of Imidazolium-Mediated Tröger's Base-Based Ionene Polymers for Advanced CO_2 Separation Membranes. *ACS Omega* **2019**, *4*, 3439-3448.

Bara, J. E.; Finotello, A.; Magee, J. W.; Qian, S.; O'Harra, K. E.; Dennis, G. P.; Noble, R. D. 110th Anniversary: Properties of Imidazolium-based Ionic Liquids Bearing Both Benzylic and *n*-Alkyl Substituents. *Ind. Eng. Chem. Res.* **2019,** *58,* 17956-17964. doi:10.1021/acs.iecr.9b03159

Jointly funded by this grant and other grants with leading intellectual contribution from this grant:

Liu, X.; Bara, J. E.; Turner, C. H. Understanding Gas Solubility of Pure Component and Binary Mixtures within Multivalent Ionic Liquids from Molecular Simulations. *J. Phys. Chem. B* In Press. doi: 10.1021/acs.jpcb.1c04212

Liu, X.; O'Harra, K. E.; Bara, J. E.; Turner, C. H. Solubility Behavior of CO_2 in Ionic Liquids Based on Ionic Polarity Index Analyses. *J. Phys. Chem. B* **2021**, *125*, 3665-3676. doi:10.1021/acs.jpcb.1c01508

Liu, X.; O'Harra, K. E.; Bara, J. E.; Turner, C. H. Screening Ionic Liquids Based on Ionic Volume and Electrostatic Potential Analyses. *J. Phys. Chem. B* **2021**, *125*, 3653-3664. doi:10.1021/acs.jpcb.0c10259

Liu, X.; O'Harra, K. E**.; Bara, J. E.;** Turner, C. H. Molecular Insight into the Anion Effect and Free Volume Effect of CO_2 Solubility in Multivalent Ionic Liquids. *Phys. Chem. Chem. Phys.* **2020**, *22*, 20618-20633. doi:10.1039/D0CP03424J

O'Harra, K. E.; Kammakakam, I.; DeVriese, E. M.; Noll, D. M.; Bara, J. E.; Jackson, E. M. Synthesis and Gas Separation Performances of Membranes Comprised of 6-FDA-Derived Polyimide Ionenes and Ionic Liquids. *Membranes* **2019**, *9*, 79.

O'Harra, K. E.; Kammakakam, I.; Bara, J. E.; Jackson, E. M. Understanding the Roles of Backbone and Anions in the Structure and Thermal Stability of Imidazolium Polyimide-Ionenes. *Polym. Int.* **2019**, *68*, 1547-1556. doi:10.1002/pi.5825

Szala-Bilnik, J.; Crabtree, E.; Abedini, A.; Bara, J. E.; Turner, C. H. Solubility and Diffusivity of CO_2 in Ionic Polyimides with $[C(CN)_3]_x[oAc]_{1-x}$ Anion Composition. Comp. Mater. Sci. **2020**, *174*, 109468. doi:10.1016/j.commatsci.2019.109468

Jointly funded by this grant and other grants with relatively minor intellectual contribution from this grant:

Szala-Bilnik, J.; Abedini, A.; Crabtree, E.; Bara, J. E.; Turner, C. H. Molecular Transport Behavior of CO_2 in Ionic Polyimides and Ionic Liquid Composite Membrane Materials. *J. Phys. Chem B* **2019**, *123*, 7455-7463. doi:10.1021/acs.jpcb.9b05555

Abedini, A.; Crabtree, E.; Bara, J. E.; Turner, C. H. Molecular Analysis of Selective Gas Adsorption within Composites of Ionic Polyimides and Ionic Liquids as Gas Separation Membranes. *Chem. Phys.* **2019**, *516*, 71-83. doi:10.1016/j.chemphys.2018.08.039

Transport of Complex Mixtures in Ion-containing Polymer Membranes

*Jung Min Kim[1], Yi-hung Lin[1], Pravin Aravindhan[1], Sarah Gaston[2] and **Bryan S. Beckingham**[1]; [1]Department of Chemical Engineering, Auburn University, Auburn, AL; [2]Department of Polymer and Fiber Engineering, Auburn University, Auburn, AL*

PRESENTATION ABSTRACT

Permselective ion-containing membranes are an integral component for many applications from water treatment, fuel cells, and solar fuels devices where the selective transport of molecules and ions is desired. This project aims to improve our understanding of the complex array of factors that influence transport behavior of polymer membranes when challenged by multiple solutes by investigating the interplay of membrane chemistry, membrane physiochemical properties, and complex mixture chemistry on emergent transport behavior. This project will (1) fabricate a diverse set of crosslinked ionic (and neutral control) polymer membranes with a variety of chemical compositions, water uptake, and ionic conductivity, and (2) experimentally characterize the transport behavior of these membranes to solutes and their complex mixtures. By systematically varying crosslinked polymer membrane chemistries and characterizing the resulting physiochemical and transport properties of both aqueous solute and aqueous solute mixtures, we seek to gain understanding of the relationships that drive changes in transport behavior. We challenge our membranes with aqueous mixtures of solutes in multicomponent transport experiments conducted using custom diffusion cells outfitted with in situ ATR FTIR spectroscopy to track the permeation of the multiple solutes simultaneously to extract permeability (P). Membrane solubility (S) is also characterized for single and multicomponent solutions, allowing for membrane diffusivity (D) to be calculated by the solution-diffusion equation ($P = S * D$). This presentation will focus on our recent findings for various crosslinked polyether-based cation and anion exchange membranes.

Grant Number: DE-SC0021215 Grant Title: **Transport of Complex Mixtures in Ion-containing Polymer Membranes**
PI: Bryan Beckingham (PI)
Students: Graduate Students: Jung Min Kim[1], Yi-hung Lin[1], Pravin Aravindhan[1], Sarah Gaston. Undergraduate Students: Ting Huang[1], Brock Hunter[1], Mae Baird[1]
Affiliations: [1]Department of Chemical Engineering, Auburn University, Auburn, AL, 36849
[2]Department of Polymer and Fiber Engineering, Auburn University, Auburn, AL, 36849

RECENT PROGRESS

"Transport and co-transport of carboxylate ions and ethanol in anion exchange membranes"

We have synthesized a series of anion exchange membranes (AEM) consisting of PEGDA and a quaternary ammonium-bearing comonomer (APTA) (structures shown in Scheme 1) and characterized them in comparison with crosslinked PEGDA and the commercial anion exchange membrane Selemion AMVN. Physiochemical characterization including ionic conductivity, ion exchange capacity, density, water uptake, water volume fraction and diffusion cell transport experiments challenging these membranes with ethanol, a series of salts (potassium formate, sodium formate, potassium acetate, and sodium acetate) as well as complex mixtures of ethanol with each salt has been performed.

Scheme 1: Synthesized AEM structures

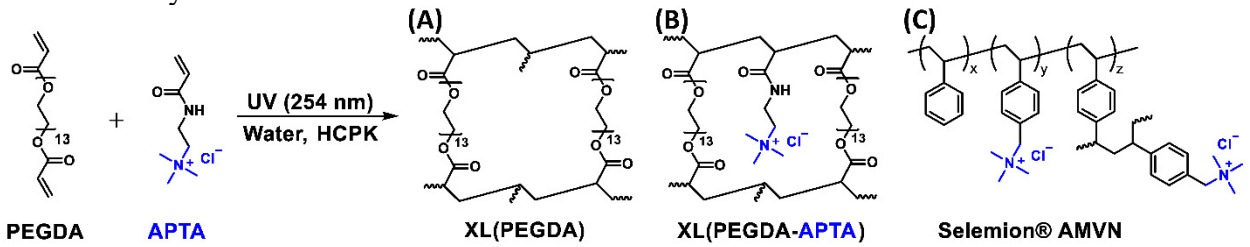

We find that permeability to ethanol is significantly higher in the PEGDA and PEGDA-APTA membranes compared to Selemion AMVN, mainly due to increased water uptake of these polyether membranes. As APTA content is increased both the water volume fraction in the hydrated membranes and, consequently, permeability to ethanol increases. Permeability to the formate and acetate salts follows similar trends with APTA content (also water uptake) with formate permeabilities greater than acetate permeabilities and potassium salt permeabilities greater than sodium salt permeabilities. The primary discrimination we ascribe to the size difference between the two carboxylate anions, formate anion (5.9 Å) < acetate anion (7.4 Å) followed by the difference between the two cations, K+ (6.6 Å) < Na+ (7.2 Å). The complex mixture transport is more complex; however, we measure permeability and solubility, and calculate diffusivity from the solution diffusion model. We find that for these mixtures of solutes the carboxylate salt diffusivities are decreased in co-diffusion with EtOH, which we currently are attributing to the screening of electrostatic attraction by the co-diffusing EtOH (charge screening). Here, the electrostatic attraction (counterion condensation) between bound cations (i.e., quaternary ammonium, QA^+) and mobile carboxylate anions (i.e., formate and acetate) can be interfered with by a co-diffusing alcohol (i.e., ethanol, EtOH) and, therefore, suppress the diffusion of carboxylate salts in co-diffusion. This result is consistent with our previous investigations on cation exchange membranes (CEM), where the electrostatic repulsion (Donnan exclusion) between bound anions (i.e., sulfonate, SO_3^-) and mobile carboxylate anions was hypothesized to be interfered with by co-diffusing alcohols and, therefore, assist the diffusion of carboxylate salts in co-diffusion. Current research is ongoing to expand the membrane chemistries and additional characterization to attain additional evidence of this behavior.

"Phenyl ether acrylates as blocking groups in co-transport of methanol-acetate in PEGDA-3-sulfopropyl methacrylate Cation Exchange Membranes"

We synthesized and investigated a series of synthesized cation exchange membranes (CEM) consisting of PEGDA and 3-sulfopropyl methacrylate (SPMAK) as a sulfonated comonomer. A series of neutral comonomers of varied side-chain length were also introduced; ethylene glycol phenyl ether methacrylate (EGPEMA), ethylene glycol phenyl ether acrylate (EGPEA), or poly(ethylene glycol) phenyl ether acrylate (PEGPEA) at a single neutral comonomer content; structures shown in Scheme 2. This work is ongoing to expand to additional comonomer contents as well as additional prepolymerization water contents (to vary fractional free volume), however we have begun our investigation of these series of membranes through 16 chemically diverse membranes.

Scheme 2: Synthesized CEM structures

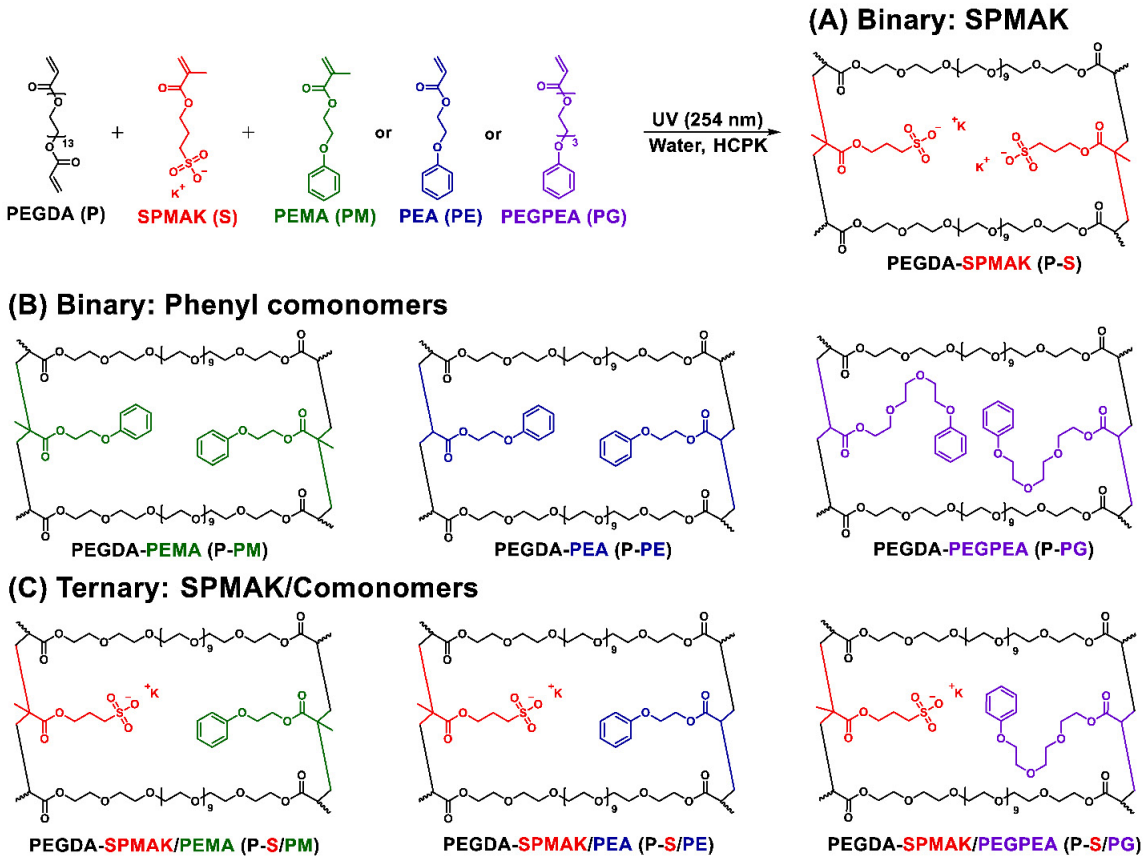

Fig. 2. Scheme of prepared (A) binary-SPMAK films, P-S, (B) binary-comonomer films, P-PM, P-PE, and P-PG, and (C) ternary films, P-S/PM, P-S/PE, and P-S/PG.

As expected, ionic conductivity increases with SPMAK content, as does water volume fraction in both PEGDA-SPMAK membranes and ternary SPMAK-containing membranes. Contrastingly, for binary PEGDA membranes with PEMA, PEA, and PEGPEA, the water volume fraction is essentially constant as the comonomer content is varied. Transport and solubility experiments of these membranes have focused on aqueous methanol and potassium acetate and their mixture. A key finding so far has been is that the diffusivities of potassium acetate in co-diffusion with methanol (MeOH) increases in both crosslinked PEGDA-based structures with a sulfonated 3-sulfopropyl methacrylate potassium (PEGDA-SPMAK) and with a hydrophobic poly(ethylene glycol) phenyl ether acrylates (PEGDA-PEGPEA), but diffusivities in co-diffusion were decreased in PEGDA-SPMAK/PEGPEA membranes. This indicates PEGPEA may be a promising candidate to act as a transport inhibiting comonomer to suppress the multi-component interactions (such as flux coupling, charge screening, etc.) and minimize the permeation CO_2 reduction products (i.e. acetate), a behavior we are investigating further.

Publications Acknowledging this Grant in 2020 – present

Nothing to report yet.

Molecular Aspects of Transport in Thin Films of Controlled Architecture

Paul W. Bohn; Department of Chemical and Biomolecular Engineering Department of Chemistry and Biochemistry,University of Notre Dame, Notre Dame, IN 46556 USA

Presentation Abstract

The scientific and technological targets of this project focus on reactions and transport in nanoscale confined volumes, because these phenomena are at the heart of a wide array of separation technologies. Studying transport on this length scale brings a core set of scientific phenomena to the fore - wetting/dewetting, hydrophobicity, stochastic fluctuations in fluid flow, electrokinetics, *etc.* - that exhibit fundamentally different behavior on the nanoscale. This occurs because scaling to nanometer dimensions changes the underlying nature of the forces that direct molecular motion, thus directly impacting molecular separations. The experiments being pursued in support of these objectives use electrokinetic, electrochemical and spectroelectrochemical probes of transport in nanoconfined flows under active control. These experiments have a collective goal to develop the design rules, structural motifs, and operating principles needed to achieve active control over molecular transport in nano-confined volumes.

DE FG02 07ER15851: Molecular Aspects of Transport in Thin Films of Controlled Architecture

Postdocs: Seung-Ryong Kwon
Students: Jin, Jia, Meredith Lee, Arielle Lopez, Christiana Oh

RECENT PROGRESS

Introduction. The scientific and technological objectives of this project are motivated by core problems in energy technologies that utilize differential transport in nanoscale confined volumes to achieve molecular separations. The core scientific phenomena that control observable behavior - wetting/dewetting, hydrophobicity, stochastic fluctuations in fluid flow, electrokinetics, *etc.* - are fundamentally different on the nanoscale, because the underlying forces that direct molecular motion are altered upon scaling to nanometer dimensions. Thus, the great potential of nanoscale fluidic architectures to effect differential control of molecular transport is apparent. In parallel, we utilize nanoelectrochemistry, drawing upon the seminal advances of Martin and coworkers who developed robust syntheses of pore-based nanomaterials[1] and strategies to combine nanopores and nanoelectrodes to yield single nanopore electrodes by Zhang and White.[2] Later, single nanopore electrodes and nanopore electrode arrays with well- defined, reproducible pore geometry and size were fabricated lithographically.[3-5] The combination of nanopores, nanofluidics, and nanoelectrochemistry has been at the heart of our efforts to develop new methods to control molecular transport.[6]

Hierarchically-Organized Nanoconfined Architectures that Support Electrowetting. Reasoning that electrowetting has almost universally been applied to macroscale planar surfaces, we are designing and testing systems that use fields to control interfacial wetting in confined nanoscale structures. In particular, we focus on nanoscale domains formed (a) stochastically in ultrathin SiN_x, and (b) by designed processing of the block copolymer poly(styrene)-*b*-(4-vinylpyridine), PS-*b*-

P4VP. In both systems, nanoscale electrowetting in nanocylindrical domains is controlled by imposing an applied potential across electrode pairs spaced ~50-100 nm apart. The PS-*b*-P4VP system exhibits the additional feature that the behavior can be controlled by pH, since the vinylpyridine domains present basic sites which can be protonated/deprotonated. This system provides a physically and chemically robust and malleable platform on which to explore electrowetting phenomena in detail. We are also exploring the fabrication of highly ordered, ultrahigh density nanochannel arrays by employing nanosphere lithography to template the graphoepitaxy of diblock copolymers. Using poly(styrene-*b*-dimethylsiloxane) as a model system and optimizing solvent vapor annealing, overcoating conditions, and subsequent reactive ion etching processes, silica nanochannel (SNC) arrays with areal densities approaching 1000 elements μm^{-2}, were obtained at wafer scale (see **Figure 1**). Furthermore, the conformal SNC array structures obtained can easily be lifted, detached, and transferred to another substrate, preserving the hierarchical organization while transferring the nanostructure-derived properties to a different substrate, thereby making it possible to template nanoscale behavior over macroscale distances

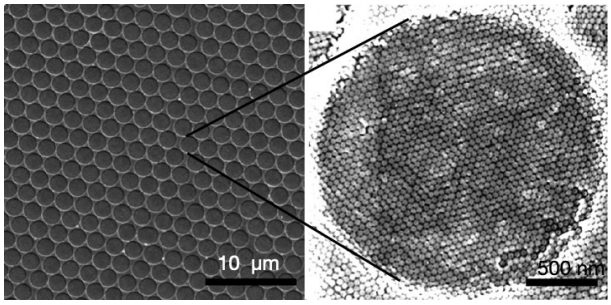

Figure 1. (Left) SEM image of highly ordered circular SiO2 corrals fabricated by nanosphere lithography. (Right) Plan- view SEM image of ultrahigh density SNC array inside a single NSL-defined trench.

Modulated Electrowetting for Transport Control. We have developed 3-electrode nanopore electrode arrays (NEAs) capable of transistor-like action and controlled electrowetting of nanoscale channels in the gate dielectric, as shown schematically in **Figure 2**. A straightforward analogy with field-effect transistors would suggest using the metal electrode as a gate, but we reason that it would be more effective to use the bottom electrode as the control element. For example, when the bottom (gate) electrode potential exceeds $|E_{BE}| > 1.7$ V, an abrupt change in amperometric behavior is observed, indicating the formation of new current pathways that we interpret in terms of voltage-induced defect channels in the SiN_X gate dielectric. These defect channels exhibit two interesting phenomena: (*a*) potential-induced wetting/dewetting, and (*b*) voltage-controlled current pathway regulation. The potential-induced wetting/dewetting phenomena represent a new route to controlling transport at these small dimensions, as evidenced by altered electrochemical reactivity in NEAs. The structures developed here hold promise for advanced ion control, which is relevant to applications in molecular separations and water purification.

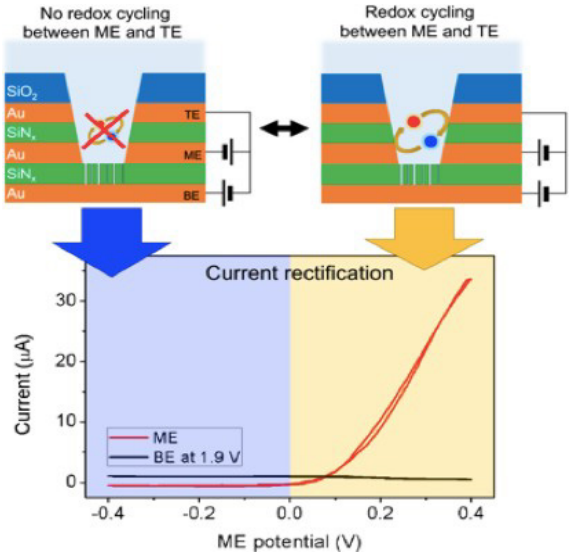

Figure 2. Schematic representation of the 3-electrode transistor-like NEA nanopores. Current rectification mediated by access to bottom electrode through SiNx nanopores.

Ion Gating. We are also studying ion gating in hierarchically-organized structures constructed from pH-responsive block copolymer PS-*b*-P4VP on NEAs, *i.e.* PS-*b*-P4VP@NEA. These membranes exhibit pH-dependent structural transitions suitable for pH- gating of the membrane nanochannels, *e.g.* on-off transport switching at pH values near the p*K*a of P4VP with excellent anion permselectivity at pH < p*K*a. As shown in **Figure 3**, operation at pH ≤ p*K*a produces a protonated state of the P4VP blocks, which is hydrophilic and swollen, while raising the pH > p*K*a collapses the P4VP blocks producing a naturally hydrophobic, *i.e.* dewetted, state. Furthermore, as suggested by the bottom right schematic in **Figure 3**, the hydrophobic state may be manipulated by potential- induced wetting and dewetting.

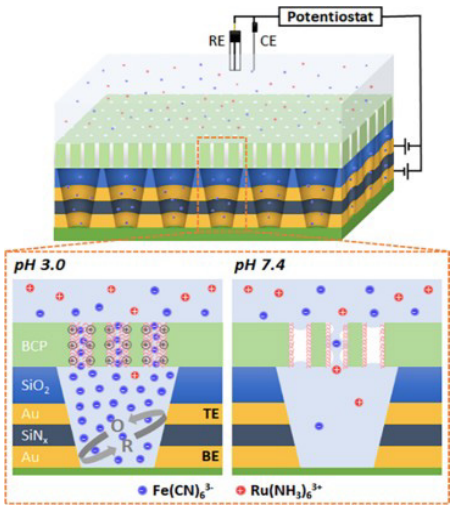

Figure 3. Schematic diagram illustrating pH-dependent structural changes to the P4VP block and its effect on transport across a PS-b-P4VP@NEA membrane. Effects of pH-dependent ion gating are read out through electrochemistry in the NEA portion of the structure.

Effects of pH-dependent ion gating are read out through electrochemistry in the NEA portion of the structure. This possibility is realized as shown in **Figure 4**, where we demonstrate the control of transport across a PS-*b*-P4VP@NEA membrane structure by effecting electrowetting/dewetting transitions of P4VP nanochannels. As shown in **Figure 4(a)**, the nanochannels at pH 7.4 are dewetted in the absence of an electric field - consistent with the lack of current at the NEA-supported electrodes. This is apparent both in the potential step experiments at |*Eappl*| < 2.5 V, **Figure 4(b)**, and in the $Fe(CN)6^{3/4-}$ cyclic voltammogram at | *Eappl* | ~ 1.0 V, **Figure 4(c)**. The current increases with increasingly negative potentials in the potential step experiments, and with increasing scan number in the cyclic voltammetry, suggesting that there is hysteresis in the wetting/dewetting phenomena and their potential dependence. These results clearly demonstrate the wetting/dewetting-induced fluctuations of transport in the nanochannels and the accompanying water evaporation/condensation dynamics, as evidenced by the noise and drift of the current signal in **Figure 4(b)** at potentials more negative than -2.5V.

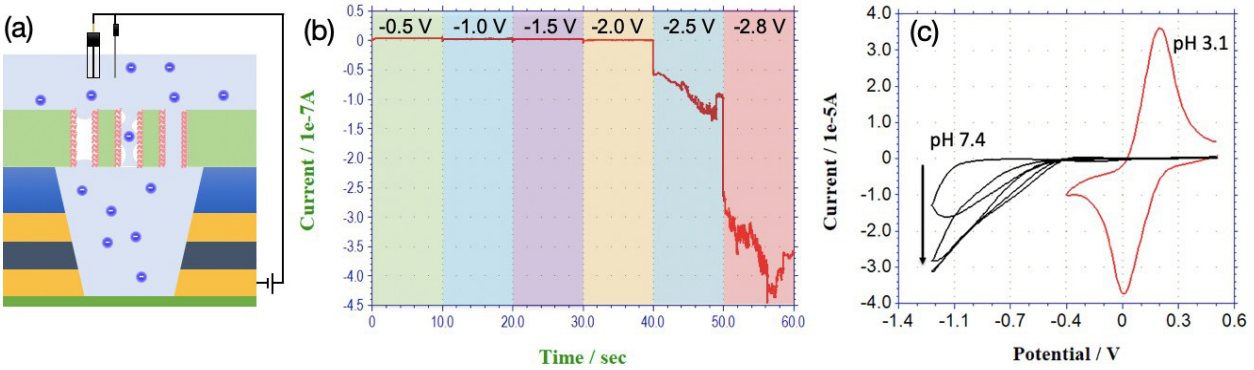

Figure 4. (a) Schematic illustration of a single nanopore in the PS-b-P4VP@NEA interrogated in the 3-electrode configuration at pH > pK_a(P4VP). (b) Potential step experiment illustrating electrowetting and evaporation/condensation dynamics at negative potentials exceeding $|E_{appl}|$ > 2.5 V. (c) Cyclic voltammetry of $Fe(CN)_6^{3/4-}$ below (3.1) and above (7.4) pK_a(P4VP).

We also investigated electrowetting transitions, such as those demonstrated in **Figure 4**, as a means to: (a) fill NEAs on-demand, and (b) retain the species after resetting the potential.

Using a new NEA, we first measured the current response before electrowetting, and as expected, almost no faradaic current response was observed owing to the inhibition of transport across the dewetted block copolymer membrane. However, once the redox probe was introduced into the nanopores and the electrowetting transition reversed, an **800x** current enhancement was observed using a 4-electrode configuration with BE and TE working electrodes, which highlights successful solution confinement with the PS-*b*-P4VP@NEA structure (**Figure 5**).

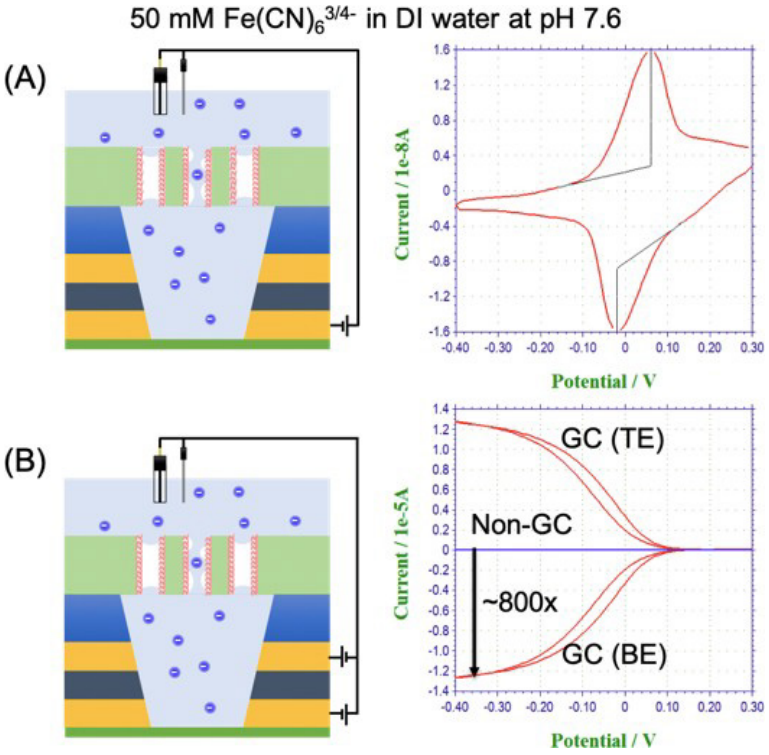

Figure 5. Cyclic-voltammograms of 50 mM $Fe(CN)_6^{3/4-}$ at pH 7.6 in (a) 3-electrode or (b) 4-electrode NEA system filled by electrowetting-mediated mass transport into the NEA with multiple potential steps.

References

1. Jirage, K.; Hulteen, J.; Martin, C.R., Nanotubule-Based Molecular-Filtration Membranes. *Science* **1997,** 278, 655.
2. Zhang, B.; Zhang, Y.; White, H.S., Steady-state voltammetric response of the nanopore electrode. *Anal. Chem.* **2006,** 78, 477-483.
3. Kuo, T.C.; Cannon, D.M.; Chen, Y.N.; Tulock, J.J.; Shannon, M.A.; Sweedler, J.V.; Bohn, P.W., Gateable nanofluidic interconnects for multilayered microfluidic separation systems. *Anal. Chem.* **2003,** 75, 1861- 1867.
4. Cannon, J., D.M.; Flachsbart, B.R.; Shannon, M.A.; Sweedler, J.V.; Bohn, P.W., Fabrication of single nanofluidic channels in poly(methylmethacrylate) films via focused-ion beam milling for use as molecular gates. *Appl. Phys. Lett.* **2004,** 85, 1241-1243.
5. Piruska, A.; Branagan, S.P.; Minnis, A.B.; Wang, Z.; Cropek, D.M.; Sweedler, J.V.; Bohn, P.W., Electrokinetic control of fluid transport in gold coated nanocapillary array membranes in hybrid nanofluidic-microfluidic devices. *Lab Chip* **2010,** 10, 1237-1244.
6. Fu, K.; Kwon, S.-R.; Han, D.; Bohn, P.W., Single entity electrochemistry in nanopore electrode arrays: ion transport meets electron transfer in confined geometries. *Acc. Chem. Res.* **2020,** 53, 719-728.

Publications Acknowledging this Grant 2015 – present

Exclusively funded by this grant;

Contento, N.M.; Bohn, P.W. "Electric Field Effects on Current-Voltage Relationships in Microfluidic Channels Presenting Multiple Working Electrodes in the Weak-Coupling Limit," *Microfl. Nanofl.* **2015**, 18, 131-140. [DOI 10.1007/s10404-014-1424-9]

Wichert, R.A.W.; Han, D.; Bohn, P.W. "Effects of Molecular Confinement and Crowding on Horseradish Peroxidase Kinetics Using a Nanofluidic Gradient Mixer," *Lab Chip* **2016**, 16, 877- 883. [DOI 10.1039/C5LC01413A; PMID: 26792298]

Xu, W.; Fu, K.; Bohn, P.W. "Electrochromic Sensor for Multiplex Detection of Metabolites Enabled by Closed Bipolar Electrode Coupling," *ACS Sens.* **2017**, 2, 1010-1026. [DOI 10.1021/acssensors7b00292]

Fu, K.; Han, D.; Crouch, G.M.; Kwon, S.-R.; Bohn, P.W. "Asymmetric Nafion-Coated Nanopore Electrode Arrays as Redox Cycling-Based Electrochemical Diodes," *ACS Nano* **2018**, 12, 9177- 9185. [DOI 10.1021/acsnano.8b03751]

Jointly funded by this grant and other grants with leading intellectual contribution from this grant;

Xu, W.; Foster, E.; Ma, C.; Bohn, P.W. "On-Demand *In Situ* Generation of Oxygen in a Nanofluidic Embedded Planar Microband Electrochemical Reactor," *Microfl. Nanofl.* **2015**, 19, 1181-1189. [DOI 10.1007/s10404-015-1636-7]

Zaino, L.P. III; Grismer, D.A.; Han, D.; Crouch, G.M.; Bohn, P.W. "Single Molecule Spectroelectrochemistry of Freely Diffusing Flavin Mononucleotide in Zero-Dimensional Nanophotonic Structures," *Faraday Disc.* **2015**, 184, 101-115. [DOI 10.1039/C5FD00072F;
PMID: 26406924]

Xu, W.; Ma, C.; Bohn, P.W. "Coupling of Independent Electrochemical Reactions and Fluorescence at Closed Bipolar Interdigitated Electrode Arrays," *ChemElectrochem* **2016**, 3, 422-428. [DOI 10.1002/celc.201500366]

Zaino, L.P. III; Ma, C.; Bohn, P.W. "Nanopore-Enabled Electrode Arrays and Ensembles,"

Microchim. Acta **2016**, 183, 1019–1032. [DOI 10.1007/s00604-015-1701-7]

Zaino, L.P. III; Wichert, R.A.W.; Crouch, G.M.; Bohn, P.W. "Microchannel Voltammetry in the Presence of Large External Voltages and Electric Fields," *Analyt. Chem.* **2016**, 88, 4200-4204. [DOI 10.1021/acs.analchem.6b00399; PMID: 27045936]

Xu, W.; Fu, K.; Ma, C.; Bohn, P.W. "Closed Bipolar Electrode-Enabled Dual-Cell Electrochromic Detectors for Chemical Sensing," *Analyst* **2016**, 141, 6018-6024. [DOI 10.1039/C6AN01415A; PMID: 27704078]

Bohn, P.W. "Science and Technology of Electrochemistry at Nano-Interfaces," *Faraday Disc.* **2018**, 210, 481-493. [DOI 10.1039/C8FD00128F]

Kim, J.-Y.; Han, D.; Crouch, G.M.; Kwon, S.-R.; Bohn, P.W. "Capture of Single Silver Nanoparticles in Nanopore Arrays Detected by Simultaneous Amperometry and Surface- Enhanced Raman Scattering," *Analyt. Chem.* **2019**, 91, 4568-4576. [DOI 10.1021/acs.analchem.8b05748]

Fu, K.; Kwon, S.-R.; Han, D.; Bohn, P.W. "Single entity electrochemistry in nanopore electrode arrays: ion transport meets electron transfer in confined geometries," *Acc. Chem. Res*. **2020**, 53, 719-728. [DOI 10.1021/acs.accounts.9b00543]

Kwon, S.-R.; Baek, S.; Fu, K.; Bohn, P.W. "Electrowetting-Mediated Transport to Produce Electrochemical Transistor Action in Nanopore Electrode Arrays," *Small* **2020**, 16, 1907249. [DOI 10.1002/smll.201907249].

Baek, S.; Kwon, S.-R.; Fu, K.; Bohn, P.W "Ion Gating in Nanopore Electrode Arrays with Hierarchically-Organized pH-Responsive Block Copolymer Membranes," *ACS Appl. Mater. Interf.* **2020**, 12, 55116-55124. [DOI 10.1021/acsami.0c12926]

Kwon, S.-R.; Baek, S.; Bohn, P.W. "Potential-Induced Wetting and Dewetting in pH-Responsive Block Copolymer Membranes for Mass Transport Control," *Faraday Disc.* **2021**, submitted.

Jointly funded by this grant and other grants with relatively minor intellectual contribution from this grant;

Ma, C.; Xu, W.; Wichert, W.R.A.; Bohn, P.W. "Ion Accumulation and Migration Effects on Redox Cycling in Nanopore Electrode Arrays at Low Ionic Strength," *ACS Nano* **2016**, 10, 3658-3664. [DOI 10.1021/acsnano.6b00049]

King, T.L.; Jin, X.; Nandigana, V.R.; Aluru, N.; Bohn, P.W. "Electrokinetic Transport and Fluidic Manipulation in Three Dimensional Integrated Nanofluidic Networks," in *Nanofluidics*, 2nd Edition, A. de Mello and J. Edel, Eds., Royal Society of Chemistry, Cambridge, UK, Ch. 2, pp. 37-75, **2017**.

Xu, W.; Zaino, L.P. III; Bohn, P.W. "Electrochemically Modulated Luminescence in Nanophotonic Structures," in Combined Luminescence and Electrochemistry: Involvements and applications in analytical chemistry, physics and biology. F. Miomandre, P. Audebert, Eds., **2017** Springer, pp. 79-104.

Fu, K.; Xu, W.; Hu, J.; Lopez, A.; Bohn, P.W. "Microscale and Nanoscale Electrophotonic Diagnostic Devices," in Bioelectronic Medicine, V.A. Pavlov and K.J. Tracey, Eds., Cold Spring Harbor Perspectives, Cold Spring Harbor Laboratory Press; **2018**. [DOI 10.1101/cshperspect.a034249]

Crouch, G.M.; Oh, C.; Fu, K.; Bohn, P.W. "Tunable Self-Organized Optical Metamaterials Enabled by Closed Bipolar Electrochemistry," *Analyst*, **2019**, 144, 6240-6246. [DOI 10.1039/C9AN01137D]

Electrically Driven Ion Separations in Permeable Membranes

Merlin L. Bruening,[a,b] *Chao Tang*[a], *Dong Ding*[a], *Andriy Yaroshchuk*,[c] *and Mykola Bondarenko*[d]; [a]*University of Notre Dame, Department of Chemical and Biomolecular Engineering*;[b]*University of Notre Dame, Department of Chemistry*;[c]*Polytechnic University of Catalonia, Department of Chemical Engineering*;[d]*National Academy of Sciences Ukraine, Institute of Colloid Chemistry*

Presentation Abstract

Highly selective ion separations are vital for recovering important salts used in a range of energy applications, and membrane-based techniques may enable environmentally friendly ion separations that operate continuously. This research demonstrates that simply opposing convective flow with electromigration in track-etched membranes leads to remarkable selectivities among monovalent ions. In the case of counter-flow cation electromigration, less mobile cations have lower electromigration velocity components and pass through porous membranes more rapidly than more mobile cations. Electromigration can occur due to either streaming or applied potentials, but applied potentials allow separations at higher ionic strength. For example, in track-etched membranes counter-flow electromigration based on an applied potential gives Li^+/K^+ selectivities >100 and Li^+/Na^+ selectivities around 30 in mixed-salt studies at 0.3 M ionic strength. However, energy costs may be prohibitive for commodity separations at high salt concentrations. Electrodialysis can occur with much lower energy costs, and the use of membranes coated with polyelectrolyte multilayers enables K^+/Mg^{2+} separations that yield 99.9% pure K^+ at 85% recovery. Li^+/Mg^{2+} selectivities are around 1000. The challenge in these separations is that limiting currents restrict fluxes. Development of membranes that show selectivities among monovalent ions would significantly enhance electrodialysis applications.

DE-SC0017618: Electrically Driven Ion Separations in Permeable Membranes

Student(s): Muhammad Ahmad, Dong Ding, and Chao Tang

RECENT PROGRESS

Counter-flow Electromigration Using Streaming Potentials

Our first studies of counter-flow electromigration demonstrated high transport selectivities among monovalent ions during flow through charged, nanoporous membranes. Charged nanopores offer unique opportunities for ion separations because at low ionic strength they exclude ions with the same charge sign as the pore surface. For a negatively charged surface, this leads to an excess of mobile cations in the pore (Figure 1A). Due to the excess mobile cations, pressure-driven flow through these pores creates streaming potentials, where the pore outlet is positive (Figure 1B). This streaming potential causes electromigration of cations toward the pore inlet and of anions toward the outlet. When a solution contains two cationic species with different electrophoretic mobilities, for example K^+ and Li^+ (see Figure 2), the streaming potential opposes the advective transport to different extents for each ion, and this leads to remarkable Li^+/K^+ separations. Li^+ has a larger hydrated radius than K^+, so the electrophoretic mobility (and hence the electrophoretic velocity) of K^+ is nearly twice that for Li^+.

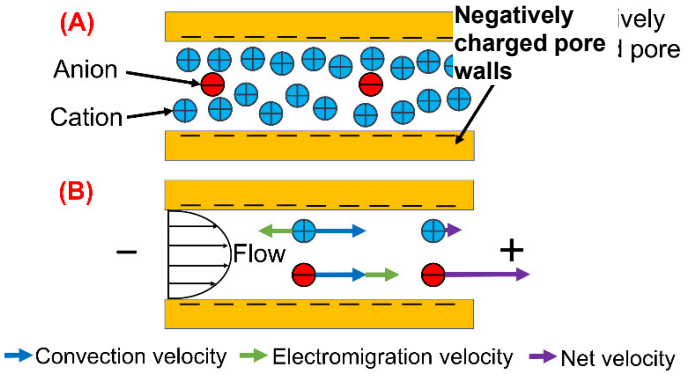

Figure 1. (A) Qualitative ion distribution in a negatively charged nanopore and (B) scheme of streaming potential and ion velocity components during flow through the pore. Due to anion exclusion, the anion velocity must be much larger than the cation velocity to maintain equal cation and anion fluxes (flux=concentration times velocity).

Figure 3 gives experimental data for such separations, and demonstrates how both passage of the less-mobile ion (Li^+) and the Li^+/K^+ selectivity increase with the transmembrane pressure, which is proportional to the flow rate. As the flow rate increases, the electromigration flux component more completely compensates the sum of advection and diffusion flux components, and the flux of the more-mobile ion (K^+) approaches zero. In contrast, the electromigration velocity of Li^+ is less than its advective velocity, so its passage can remain high. Thus, such separations can potentially overcome the permeability-selectivity tradeoff often seen in membrane processes. The maximum

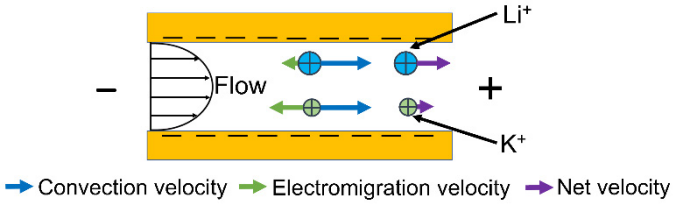

Figure 2. Scheme of Li^+/K^+ separation during flow through a negatively charged nanopore. Electromigration (green arrows) retards K^+ more than Li^+ due to the higher mobility of K^+, whereas the convective velocities of both ions (blue arrows) are the same.

selectivity of 70 in this experiment is very high for monovalent ion separations, and the Li^+ passage increases with flow rate.

Working together with Professor Andriy Yaroshchuk of Universitat Politécnica de Catalunya, we employed the extended Nernst-Planck equation to model transport in these membranes. Simulations show the possibility of much higher selectivities with control over concentration polarization (CP). In fact, the simulations in Figure 3 assume nonuniform CP (ion accumulation) above the membrane surface. (This is common in stirred cells.) Thus, future research will develop membrane cells with uniform CP. This should lead to even higher selectivities and better agreement between simulations and experiment. Nonetheless, the Li^+/K^+ selectivity of 70 is very impressive.

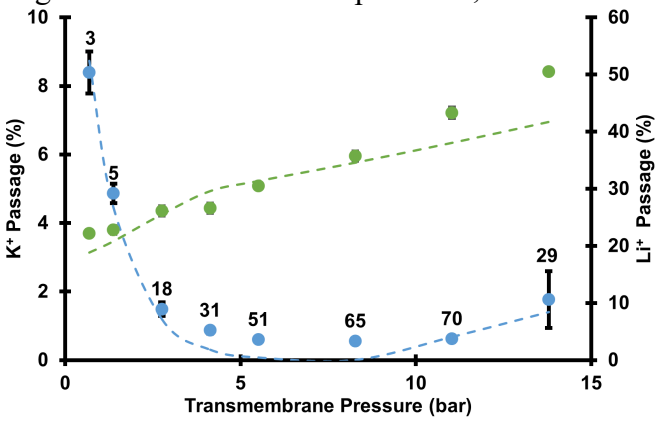

Figure 3. K^+ (blue, left y-axis) and Li^+ (green, right y-axis) passages during flow of a 0.1 mM KCl, 0.1 mM LiOH mixture through track-etched membranes (30 nm pores) using various transmembrane pressures. Dashed lines show simulation results with a linear combination of 10-µm (97%) and 75-µm (3%) unstirred layers above the membrane. The simulation assumes a surface charge density of -5 mC/m^2. The numbers above K^+ passages are Li^+/K^+ selectivities at the given pressure.

Counter-flow Electromigration Using Applied Potentials

The above separations are impressive, but at the higher ionic strengths that are common in practical separations, streaming potentials are too weak to give high Li^+/K^+ selectivities. Thus, to enable separations at higher salt concentrations, recent work on this project focused on creating a larger electric field using a DC power supply and electrodes. This allows highly selective separations at high ionic strength (0.3 M in these studies).

Figure 4 shows the K^+ and Li^+ passages during counter-flow electromigation using various applied currents. Remarkably, at high currents Li^+/K^+ selectivities are >100 for feed solutions containing a 1:1 ratio of K^+ to Li^+ at 0.3 M ionic strength. When the current (or equivalently voltage and electromigration) increases, passages of both K^+ and Li^+ decrease, but the passage of K^+ approaches zero more quickly due to its higher electrophoretic mobility. Thus, the Li^+/K^+ selectivity reaches 150 at the highest currents. The results in Figure

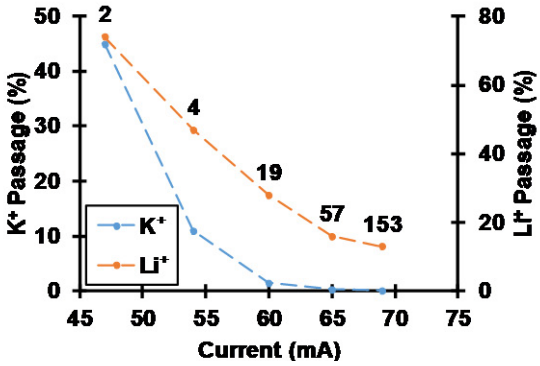

Figure 4. Ion passages as a function of applied currents at steady state during counter-flow electromigration. Note the different scales for K^+ (left axis) and Li^+ (right axis) passages. The numbers above the Li^+ passages are Li^+/K^+ selectivities. The feed contained a 50 mM K_2SO_4, 50 mM Li_2SO_4 mixture (pH adjusted to 3 with 1 M H_2SO_4). The transmembrane pressure was 0.34 bar (5 psi). Lines simply connect points.

4 demonstrate that counter-flow electromigration allows highly selective separation of Li^+ from K^+ even at 0.3 M ionic strength. Similar selectivities occur when the ratio of K^+ to Li^+ in the feed solution is 9:1. Additionally when the feed solution contains Na^+ and Li^+, the Li^+/Na^+ selectivity is 30. Expectedly the Li^+/Na^+ separations are less selective than Li^+/K^+ separations, because the electrophoretic mobilities of Li^+ and Na^+ differ less than the electrophoretic mobilities of Li^+ and K^+. Nevertheless, selectivities are high.

Experiments with replicate track-etched membranes show differences in flow rate or selectivity under similar currents due to variations in membrane porosity. To eliminate the influence of porosity, Figure 5 replots the ion passages through multiple membranes as "normalized" current, or current divided by permeate flow rate. Because the total flow rate is proportional to the number of pores (assuming constant pore diameters) and the total current is proportional to the product of the number of pores and the current density in the pores, this normalized current compares membranes under conditions where the current density in the pores should be about the same for different membranes. As Figure 5 shows, with this normalization K^+ and Li^+ passages from different membranes approximately fall on a single master curve.

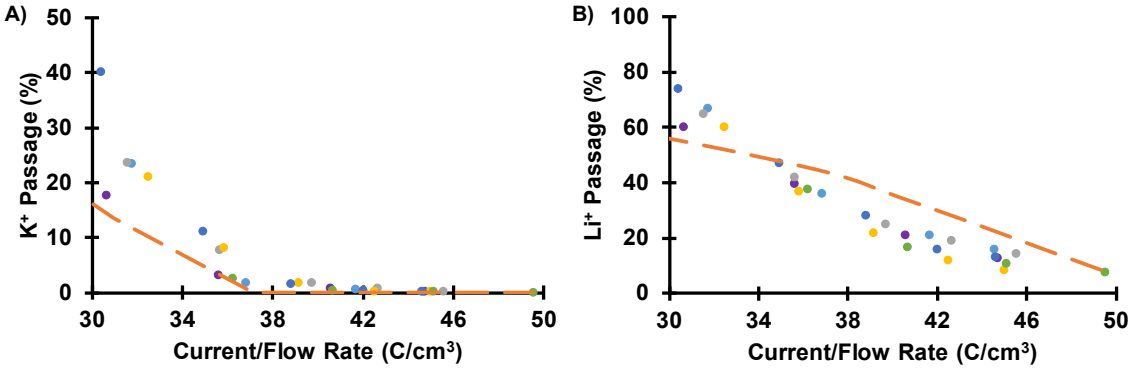

Figure 5. (A) K^+ and (B) Li^+ passages plotted as a function of "normalized" currents at steady state. The feed contained a 50 mM K_2SO_4, 50 mM Li_2SO_4 mixture (pH adjusted to 3 with 1 M H_2SO_4). Each symbol color corresponds to data from a different membrane. The dashed lines are simulation results.

Simulations of ion passages rely on the extended Nernst-Planck equation. The dashed lines in Figure 5 show that the numerical simulations follow the experimental trends. Similar agreement in trends occurs when K^+ is in excess in the feed or when separating Na^+ and Li^+. At high currents, however, simulations predict K^+ or Na^+ passages that are orders of magnitude lower than the experimental values. For example, at 40 C/cm^3 of "normalized" current, simulations predict essentially no K^+ passage (6×10^{-21} %) for Li^+/K^+ separations at a 1:1 K^+/Li^+ feed ratio, but experiments give 0.5 % K^+ passage. This likely results from a few defects in the membrane. Even if 0.001% of pores are defective, these defects will significantly increase the K^+ passage.

Electrodialysis Through Membranes Coated with Polyelectrolyte Multilayers (PEMs)

This research employs electrodialysis through cation-exchange membranes (CEMs) coated with polyelectrolyte multilayers (PEMs) to separate monovalent and divalent ions with high purities and recoveries. Electrodialysis is an energy-efficient method for ion separations, but most ion-exchange membranes show minimal selectivities among cations or among anions. Prior studies in this project showed that coating of cation-exchange membranes with PEMs can lead to monovalent/divalent cation selectivities up to 1000. Using a 4-compartment electrodialysis cell (Figure 6) and a feed solution containing equimolar KNO_3 and $Mg(NO_3)_2$, recent data show that electrodialysis with these membranes can produce *99.9% pure K^+ at >80% K^+ recovery* in a single electrodialysis stage. The current efficiency of the separations is around 75%. Separation of Li^+ and Mg^{2+} also gives high Li^+ recovery and purity.

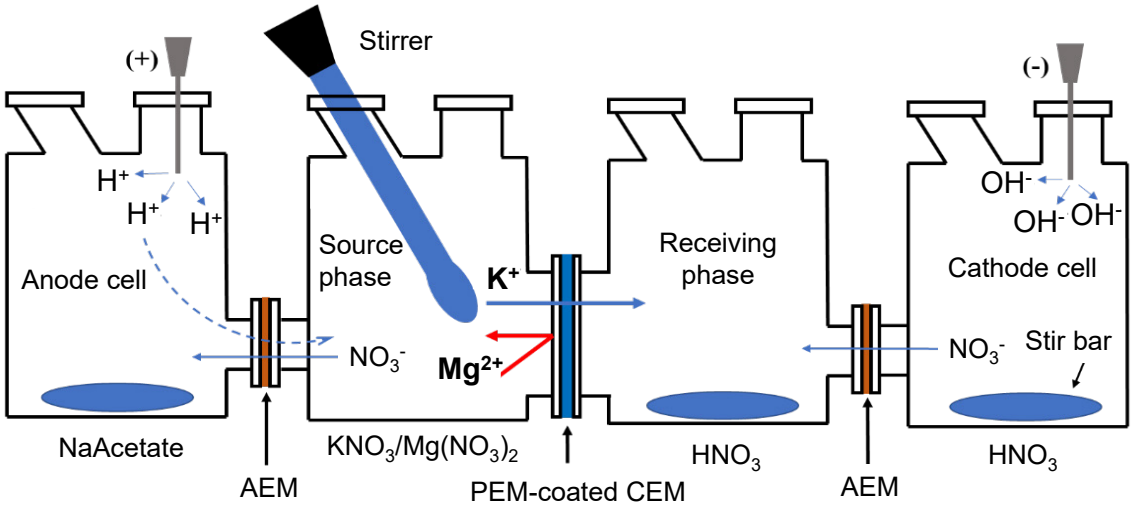

Figure 6. Diagram of the 4-compartment electrodialysis cell designed to separate K^+ and Mg^{2+} with high K^+ purity and recovery. AEM- anion-exchange membrane; PEM- polyelectrolyte multilayer; CEM- cation-exchange membrane.

The main challenge in these electrodialysis separations is a relatively small limiting current due to the low permeability of the PEM. At highly overlimiting currents, the membrane performance declines over time. Additionally, the limiting current decreases as the concentration of K^+ in the feed solution goes down. Applying a relatively low current that slowly declines as the K^+ concentration decreases in the feed achieves highly selective separations with nearly 100% current efficiency.

Publications Acknowledging this Grant in 2017 – present

(I) Exclusively funded by this grant;

1. C. Tang and M.L. Bruening, "Ion Separations with Membranes" *J. Polymer Sci.* **58**, 2831-2856 (2020).
2. Zhu, Y.; Ahmad, M.; Yang, L.; Misovich, M.; Yaroshchuk, A.; Bruening, M.L. "Adsorption of Polyelectrolyte Multilayers Imparts High Monovalent/Divalent Cation Selectivity to Aliphatic Polyamide Cation-exchange Membranes" *J. Membrane Sci.* **2017**, *537*, 177–185.

(II) Jointly funded by this grant and other grants with leading intellectual contribution from this grant;

3. M.P. Bondarenko, A. Yaroshchuk, and M.L. Bruening "Electro-osmo-dialysis Through Nanoporous Layers Physically Conjugated to Micro-perforated Ion-exchange Membranes: Highly Selective Accumulation of Trace Coions" *J. Membrane Sci.* **622**, 19022 (2021).
4. M. Ahmad, A. Yaroshchuk, and M.L. Bruening, "Moderate pH Changes Alter the Fluxes, Selectivities and Limiting Currents in Ion Transport through Polyelectrolyte Multilayers Deposited on Membranes" *J. Membrane Sci.* **616**, 118570 (2020).
5. M.P. Bondarenko, M.L. Bruening, and A. Yaroshchuk, "Current-Induced Ion Concentration Polarization at a Perfect Ion-Exchange Patch in an Infinite Insulating Wall" *ChemElectroChem* **7**, 1480-1498 (2020).
6. C. Tang, A. Yaroshcuk, and M.L. Bruening, "Flow through Negatively Charged, Nanoporous Membranes Separates Li^+ and K^+", *Chem. Comm.* **56**, 10954-10957 (2020).
7. A. Yaroshchuk, M.P. Bondarenko, C. Tang, and M.L. Bruening, "A Limiting Case of Constant Counterion Electrochemical Potentials in the Membrane for Examining Ion Transfer at Ion-Exchange Membranes and Patches" *Langmuir*, **35**, 13243-13256 (2019).
8. M. Ahmad, C. Tang, A. Yaroshchuk, and M.L. Bruening "Layer-by-layer Modification of Aliphatic Polyamide Anion-exchange Membranes to Increase Cl^-/SO_4^{2-} Selectivity" *J. Membr. Sci.* **578**, 209-219 (2019).
9. A. Yaroshchuk, M.L. Bruening, and E. Zholkovskiy "Modelling Nanofiltration of Electrolyte Solutions" *Adv. Colloid & Interface Sci.* **268**, 39-63 (2019).
10. M.P. Bondarenko, A. Yaroshchuk, and M.L. Bruening "Highly Selective Current-induced Accumulation of Trace ions at Micro-/nano-porous interfaces" *Adv. Theory & Simulations* 1900009 (2019).
11. L. Yang, C. Tang, M. Ahmad, A. Yaroshchuk, and M.L. Bruening "High Selectivities among Monovalent Cations in Dialysis through Cation-Exchange Membranes Coated with Polyelectrolyte Multilayers" *ACS Appl. Mater. Interfaces* **10**, 44134–44143 (2018).
12. Yaroshchuk, A.; Bruening, M.L. An Analytical Solution of the Solution-Diffusion-Electromigration Equations Reproduces Trends in Ion Rejections During Nanofiltration of Mixed Electrolytes *J. Membrane Sci.* **2017**, *523* 361-372.

(III) Jointly funded by this grant and other grants with relatively minor intellectual contribution from this grant;

13. S. Zhang, L. Yang, D. Ding, P. Gao, F. Xia, and M.L. Bruening "Highly Rectifying Fluidic Diodes Based on Asymmetric Layer-by-Layer Nanofilms on Nanochannel Membranes" *Anal. Chem.* **93**, 4291-4298 (2021).

Porous Organic Cage Membranes for Molecular Gas Separations

Moises A. Carreon (PI)Colorado School of Mines, Chemical and Biological Engineering Department;Praveen K. Thallapally (CoPI), Pacific Northwest National Laboratory, Physical and Computational Science Directorate, Richland, WA.

Email: mcarreon@mines.edu ;Praveen.Thallapally@pnnl.gov

Presentation Abstract

Porous organic cages (POCs) have emerged as a novel type of crystalline microporous materials which combine highly desirable properties, such as uniform micropores, high surface areas, and thermal and chemical stability, making them highly appealing candidates for industrially relevant molecular gas separations. The unique structure of POCs and their distinctive solid state molecular packing clearly differentiate them from other conventional porous materials, such as zeolites, metal organic frameworks, polymers, and carbon molecular sieves. POCs consist of covalently bonded organic cages that assemble into crystalline microporous materials displaying three-dimensional connectivity and uniform pore size. The central thrust of this collaborative proposal between CSM and PNNL is to demonstrate the development of a novel family of membranes, composed of porous organic cages which offer the possibility of displaying high separation performance for industrially relevant gas separations. POCs should display distinctive, adsorption and transport properties than those of conventional porous materials, opening the doors for a new research direction in membrane science, and molecular gas separations. The pivotal hypothesis of this collaborative proposal is that if prepared in membrane form, POCs should display the most desirable properties of polymers (facile processability and flexibility) and inorganic materials (hierarchically ordered pores with molecular sieving properties) leading to highly selective and permeable membranes for industrially relevant molecular gas separations When successful, the this research will result in the development of a novel type of microporous crystalline organic membranes capable of effectively separating industrial relevant and challenging molecular gas mixtures at high fluxes and separation selectivity. The ability to fabricate thin, chemically and mechanically stable POC membranes for societal relevant gas separations constitute a new and distinctive direction in membrane science with the goal of achieving higher combinations of permeability and selectivity overcoming the current costly conventional fractional distillation approach.

DE-SC0021357: Porous Organic Cage Membranes for Molecular Gas Separations
PI: Moises A. Carreon ; Co-PI: Praveen Thallapally
Student(s): Keerthana Krishnan

RECENT PROGRESS

Recently, we have demonstrated the successful synthesis of continuous CC3 (a prototypical type of POC) membranes grown on alumina porous tubes, a geometry that is highly amenable for potential scale-up. We evaluated the separation performance of CC3 membranes for light gases (He, CO_2, Kr, and CH_4) over Xenon. CC3 was chosen as the membrane composition based on its limiting pore aperture of ~3.6 Å which is highly suitable to molecular sieve He, CO_2, Kr, and CH_4,

having kinetic diameters of ~ 2.6 Å, 3.3 Å, 3.6 Å, and 3.8 Å, respectively from Xe having kinetic diameter of ~4.1 Å. Effectively separating Xenon from light gases can lead to a considerable reduction in its storage cost, and in potential revenue generated from its sale. For instance, once separated, Xe can be used in lighting, as high-power lamps, medical applications (e.g. imaging, anesthesia), and in the semiconductor industry.

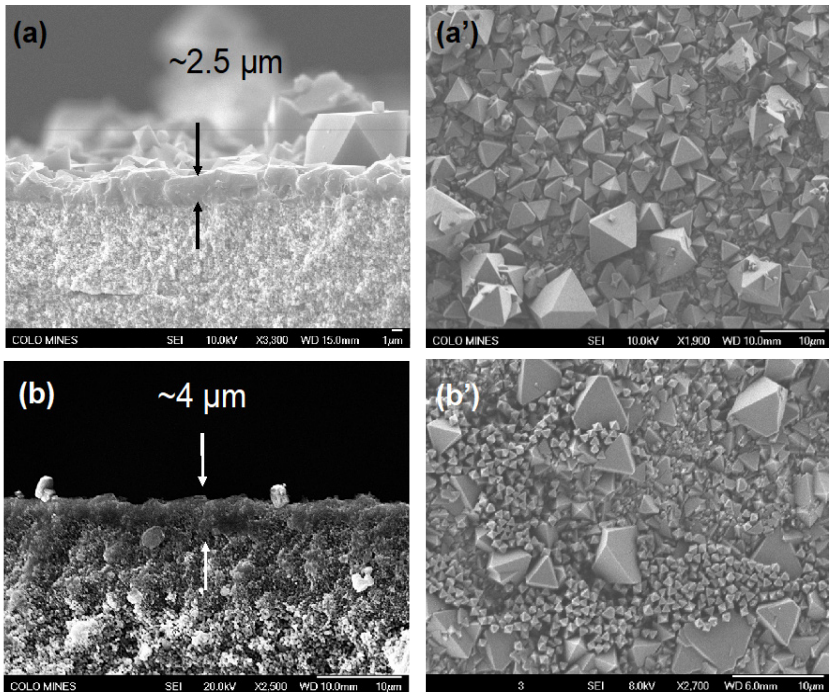

Figure 1. *Representative SEM images of synthesized CC3 membranes. Membrane M60 (a) cross-section, and (a') top-view. Membrane M120 (b) cross-section, (b') top-view.*

Figure 1 shows representative SEM images of the synthesized CC3 membranes. Figures 1a and 1a' show cross-view and top-view images respectively of a CC3 membrane synthesized solvothermally for 60 hours. This membrane is very thin, approximately 2.5 µm. From the top view, the membrane shows well intergrown and octahedral crystals, and the presence of larger crystals too. Figures 1b, and 1b' show representative SEM images for a CC3 membrane synthesized for 120 hours. This membrane is thicker (~4 µm) . The top surface is intergrown and indicates membrane continuity but shows considerable crystal overgrowth of both large and small crystals. This membrane is thicker since one additional layer was used for the synthesis of this membrane, and also due to the fact that larger seed crystals were used to synthesize this membrane. The PXRD patterns of CC3 crystals collected from solvothermal membrane synthesis, correspond to pure CC3α phase.

Table 1 summarizes the single gas permeances of the studied light gases through membranes synthesized for 60 hours (denoted as M60), and 120 hours (denoted as M120). All gas permeances were collected using a feed pressure of 223 kPa, and transmembrane pressure of 138 kPa. All gases show relatively high permeances in the ~162 - 2114 GPU range. The permeances for the studied gases through M60 were ~ 1.4-1.9 times higher than those for M120. This can be attributed to the membrane thickness increasing by about 62.5% from 2.5 µm up to 4 µm for M60 and M120

respectively. In this particular study, we focused on evaluating the separation performance of several light gases from Xenon. Ideal selectivities for the following gas pairs, CH_4/Xe, CO_2/Xe, He/Xe, Kr/Xe, are shown in Table 1.

***Table 1**. Single gas permeances and ideal selectivities for light gas i over Xe for CC3 membranes.*

Permeance *[mol/m² s Pa] (GPU)*		
Gas	**M120**	**M60**
CH_4	3.89E-07 (1162)	6.57E-07 (1962)
CO_2	2.97E-07 (887)	5.71E-07 (1705)
He	4.63E-07 (1382)	7.08E-07 (2114)
Kr	1.89E-07 (564)	2.59E-07 (773)
Xe	8.71E-07 (260)	5.44E-08 (162)
Ideal Selectivity		
Gas Pair	**M120**	**M60**
CH_4/Xe	4.5	12.1
CO_2/Xe	3.4	10.5
He/Xe	5.3	13
Kr/Xe	2.2	4.8

Ideal selectivities as high as 12 and 13 for CH_4/Xe and He/Xe gas pairs respectively were observed. Selectivities for each gas pair were about ~2.5-3 times higher for membrane M60 than M120. This can be possibly attributed to the crystal size and size distribution of the seeds employed during secondary seeded growth. The small 60 hour synthesized seeds have a narrow size distribution, and when membrane seeding takes place, these smaller crystals are able to effectively create a tightly packed seed layer on the surface of the alumina support. When solvothermal synthesis is performed, the use of smaller, more uniform seeds allows for a better crystal intergrowth leading to a more uniform membrane growth. Alternatively, when larger crystals are used for seeding, the coverage of alumina support is not uniform, and after membrane growth, there is a higher chance of the formation of higher concentration of defects. Larger seed crystals also contribute negatively to the formation of thicker membranes. The higher observed permeances for the studied light gases over Xenon may be associated to the thinner nature of the membranes. In addition, the presence of defects (non-selective pore pathways) could potentially contribute to these high permeances. While much higher ideal separation selectivities were expected due to the CC3 limiting pore size aperture of ~3.6 Å lying between the kinetic diameters of the studied gas pairs (He, 2.6 Å; CO_2, 3.3 Å; Kr, Å; 3.6; CH_4,3.8 Å; vs Xe, 4.1 Å) it is clear that the well-known flexibility of the CC3 cage, and the presence of defects may have limited this potential sharp molecular sieving effect.

Interestingly, the ideal selectivities for the separation of light gas i from Xe over CC3 membranes correlated linearly with the diffusivity of gas i, (Figure 2) suggesting that differences in diffusivities is the main separation mechanism.

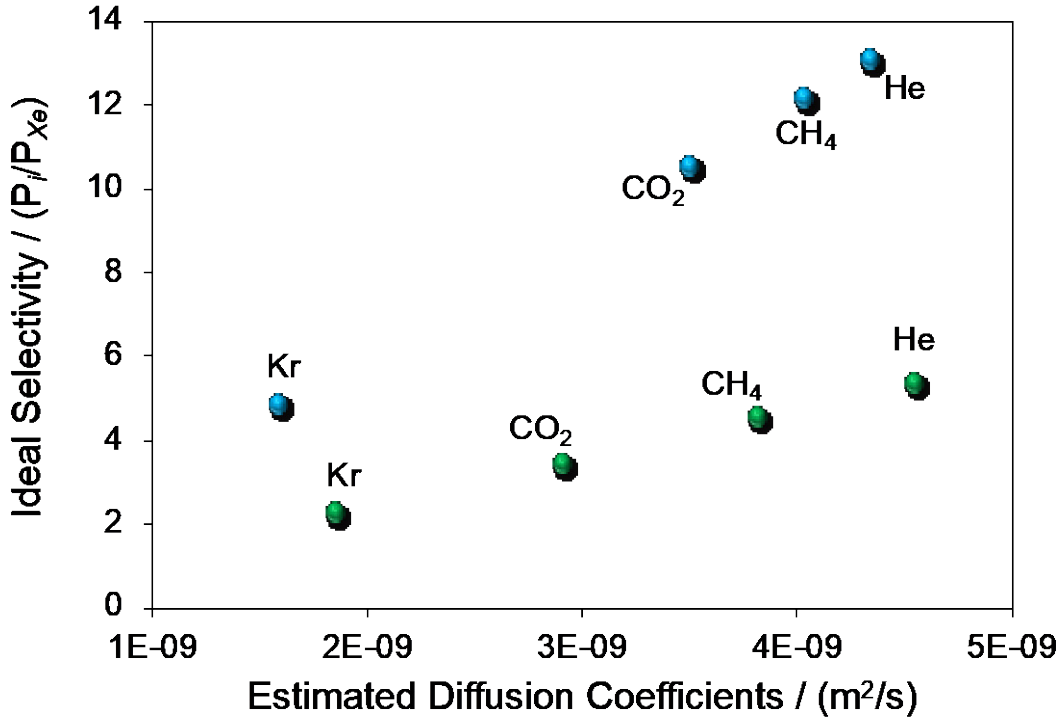

***Figure 2**. Ideal selectivity of gas i over Xe as a function of diffusivity coefficients*

Figure 3 shows the ideal selectivities of CC3 membranes as a function of molecule size. CC3 has a limiting pore aperture of 3.6 Å, and therefore molecules having smaller size than the membrane pore size such as He, and CO_2, should be able to permeate through the CC3 membrane with low resistance, leading to high permeances. Therefore, differences in molecule size for He/Xe and CO_2/Xe gas pairs led to moderate ideal selectivities of 13, and 10.5 respectively. Larger gases such as Kr displayed low ideal selectivities. Kr molecule size is slightly larger, or as large as the CC3 limiting window aperture, and therefore the permeance of this molecule through CC3 is hindered (lower) as compared to CO_2 and He. Interestingly, in the case of CH_4/Xe, the moderate ideal selectivity ~12 suggests that size of the molecule is not the key factor that leads to this observed selectivity. It is likely that the unique diamondoid pore network of CC3 can potentially impart pore shape selectivity resulting in moderate CH_4/Xe ideal selectivities. In fact, it is known that regular micropores with different geometries can potentially discriminate molecules based on their different molecular configurations. In particular, lower hydrocarbons are known to display different molecular configurations leading potentially to this entropic selectivity. In addition, as

supported by diffusivity calculations, CH_4 diffuses faster than all studied gas molecules (except He) a factor that should contribute positively to the observed moderate ideal selectivities.

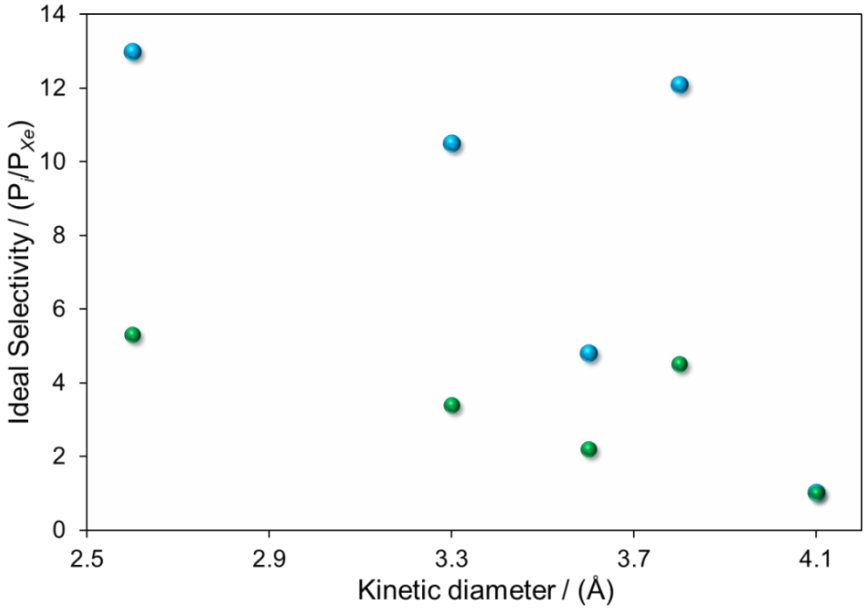

Figure 3. *Ideal separation selectivity of light gas i over Xe with respect to kinetic diameter of M60 (blue), and M120 (green) CC3 membranes.*

While in principle, molecular sieving could be possible for the studied light gases over Xenon, the CC3 framework flexibility, and potential disordered CC3 molecule packing should result in the formation of non-selective pore pathways leading to limited sieving effect. Adsorption may play an important role in the transport properties of the studied gases over CC3. Of all the studied molecules, Xe is the one having the highest isosteric heat of adsorption, and highest uptakes capacities over CC3 crystals. The reported isosteric heat of adsorption values in kJ/mol for He, CO_2, CH_4, Kr, and Xe are 4.8, 27.6, 22, 22.6, and 31 respectively. These values are calculated zero-coverage heats of adsorption taken from a multicomponent competitive adsorption simulation. Relative heats of adsorption ordered from lowest to highest are: He < CH_4 < Kr < CO_2 < Xe. These relative heats of adsorption correlate directly to the polarizability of each gas. Therefore, as compared to all studied gases, Xe will adsorb preferentially over CC3. This Xe preferential adsorption has been associated to a strong competing separation mechanism in zeolite and MOF membranes. Although our CC3 membranes display low to moderate ideal selectivities of diverse light gases over Xe, they exhibit one of highest reported Kr permeances over Xe, and unprecedented permeances for He, CO_2, and CH_4 over Xe.

In summary, we have demonstrated the *proof of concept* on the successful development of continuous CC3 membranes grown on tubular supports displaying the ability to separate light gases from Xe at high gas permeances. The quality and integrity of the membranes was highly dependent on the crystal size, and size distribution of the seeds employed for membrane synthesis. Specifically, the smaller CC3 seeds with narrow size distribution led to membranes displaying enhanced separation performance. Mechanistically, the membranes separated He, CO_2, Kr, and CH_4 from Xe mainly via differences in diffusivities. Therefore, the separation was kinetically driven. The ideal separation selectivities correlated linearly with respect to gas diffusivity

coefficients. While the synthesized CC3 membranes in this study displayed low to moderate ideal selectivities of the light gas over Xenon (2.2-13), they displayed unprecedented high gas permeances. Specifically, He, CO_2, Kr, and CH_4 permeances of 2114, 1705, 773, 1962 GPUs were observed. These membranes may be promising for extracting Xenon from different important gas sources, including air, natural gas, medical mixtures, and nuclear based gases. Future work will focus on assessing the performance of these membranes for gas mixtures at industrially relevant feed gas compositions, as well as on evaluating its long-term stability. Furthermore, we will center our future research efforts on improving membrane reproducibility, targeting different gas mixtures in which POC membranes can potentially separate gas mixtures via molecular sieving.

Publications acknowledging this grant (September 2020-present)

1) F. Gorky, J. M. Lucero, J.M. Crawford, B. Blake, M.A. Carreon, M.L. Carreon, Plasma-Induced Catalytic Conversion of Nitrogen and Hydrogen to Ammonia over Zeolitic Imidazolate Frameworks ZIF-8 and ZIF-67, *ACS Applied Materials & Interfaces* **2021**, 13, 18, 21338–21348.
2) D. Saha, M. Kim, A.J. Robinson, R. Babarao, P.K. Thallapally, Elucidating the Mechanisms of Paraffin-Olefin Separations using Nanoporous Adsorbents: An Overview, *iScience* **2021**, *in revision.*

Bespoke Liquid/Liquid Interfaces that Modulate Solute Transport Mechanisms in Solvent Extraction

Aurora E. Clark, Zhu Liu, Enrique Alvarado, Nitesh Kumar Department of Chemistry, Washington State University Pacific Northwest National Laboratory

Presentation Abstract

Hierarchical structural organization and collective motions at the interface are an essential element of mass transport within solvent extraction process chemistry. Mathematics and data science approaches, combined with atomistic simulations of complex liquid-liquid interfaces are providing new insight into the mechanisms of mass transport. Recent work has identified two major classes of transport mechanisms that are based upon characteristically different interfacial organization and energetics. Changes to diluent composition can smoothly traverse the mechanistic landscape and provide new routes to tailor interfacial reactant concentrations, transport pathways and associated kinetics, and speciation of extracted solutes in the organic phase.

Grant or FWP Number: DE-SC0001815

PI: Aurora E. Clark

Postdoc(s): Zhu Liu*

Student(s): Nitesh Kumar*, Enrique Alvarado**

Affiliations(s): *Department of Chemistry, Washington State University; **Department of Mathematics, Washington State University

RECENT PROGRESS

The goal of the current work is to develop a new chemical theory and rationale behind the two major transport mechanisms that we have identified for liquid-liquid extraction. Within our previous and ongoing studies we have been able to classify transport processes across the oil/water phase boundary depending upon: 1) if they leverage the heterogeneity at the instantaneous oil/water interface and as such result in what we have labelled “primary structure transport”, or 2) utilize hierarchical organization beyond the instantaneous surface (including bilayers and micellar phenomena) in what we have labelled “secondary structure transport”.

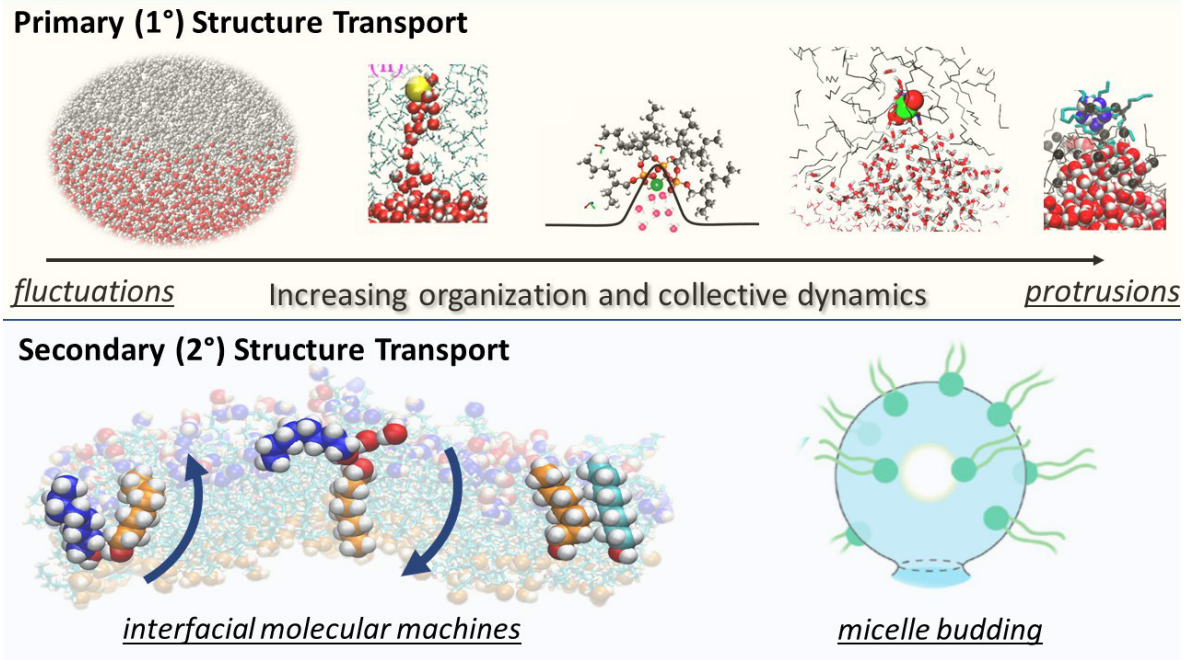

(A) Foundations of Primary Structure Mediated Solute Transport.

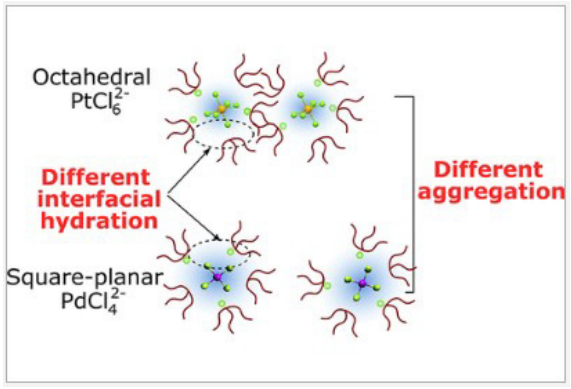

Characterizing Liquid/Liquid Interfaces. As part of our ongoing collaborations with surface spectroscopist Ahmet Uysal at ANL, we used molecular dynamics and subensemble analsysis to develop a molecular-scale interpretation of how different interfacial hydration at the water/oil phase boundary may end up influencing aggregation characteristics in the organic phase of transported metal ions (https://doi.org/10.1021/acsami.0c23158).

Complementing these characterization tools we continue to advance new data science methods to be able to quantify interfacial organization so as to develop new correlating relationships between solution composition and mass transfer properties. We now have two robust algorithms that are capable of identifying primary structures on a surface and their associated transport properties (10.1021/acs.jctc.0c00260; 10.1021/acs.jpca.0c11320). Thus far, however, we have lacked metrics to quantify changes to the spatial and chemical heterogeneity at the phase boundary that is correlated to the formation of these primary transporting structures. Toward that end we have been developing new computational topology methods that encode variations in chemical speciation, densities, and local environments into a compact form that can be used in the future for machine learning applications. In preliminary work have used image analysis methods to develop a bitmap representation that is used with sublevel set persistent homology to create barcodes that

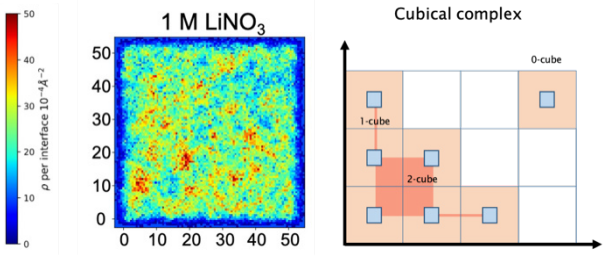

completely capture the chemical heterogeneity both along the instantaneous surface and through the instantaneous surface.

Complexation and Transport Processes. Building upon our prior work that has identified primary surface structures – so called "protrusions" – as transporting units on the instantaneous surface, we have begun to explore the generality of these structures for transport of a large variety of solutes. In submitted work we have demonstrated that ion- pairs like $LiNO_3$ and metal-ligand complexes like $UO_2(NO_3)_2TBP_2$ can also be transported by protrusion mechanisms. There are, however, several interesting features of these transport processes. First, the transport of multiple solutes is a competitive process at the interface and as such the introduction of a transporting solute can alter the transport mechanisms of other different solutes that are moving across the phase boundary. This is the case in $LiNO_3$, where Li^+ interacts with two TBP molecules to form a transporting TBP(Li^+)TBP species that subsequently associated with an interfacial NO_3^-. Yet when the Li TBP dimer is formed it decreases the ability of individual H_2O to be transported by TBP dimeric species and as such its transport mechanism is altered. Although H_2O is still transported across the oil/water phase boundary it does so by single H_2O-TBP interactions rather than TBP(H_2O)TBP species as occurs in the non-electrolyte system. A similar phenomena is observed for metal-ligand complexation and transport processes. A second major observation lies in the fact ion concentration gradients have the simultaneous ability to decrease amphiphilic extractant concentration at the interface while enhancing rates of protrusion-based transport.

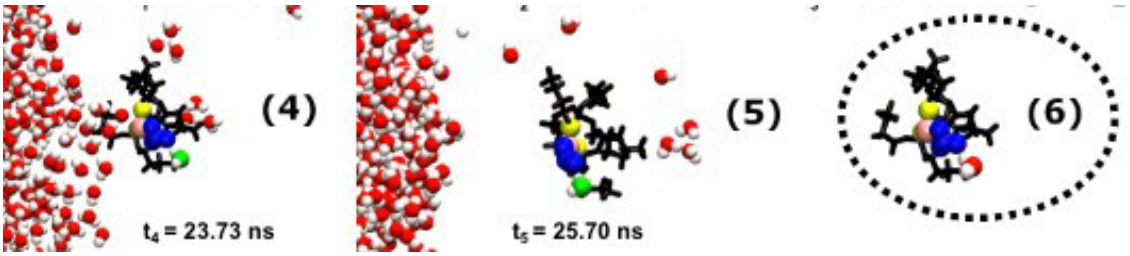

(B) Secondary Structures – Foundations of Transporting Molecular Hinges.

Transport Processes. In work performed during this last funding period we identified a new class of transport mechanisms that is based upon hierarchical organization that extends beyond the instantaneous surface (10.1039/D0SC04782A). In the original case we examined the transport of water by octanol, where octanol forms a semi-bilayer structure that consists of a highly organized instantaneous surface and a semi-organized second layer. Within the second layer islands of octanol form that are capable of flipping back and forth between the instantaneous layer and the second layer. Binding and release events with a solute (in this case water) can occur at either the instantaneous surface or the second layer. The flipping motifs are called "molecular hinges" and are well-represented by a double harmonic potential as occurs with simple molecular machines. Ongoing preliminary work is exploring the extent to which larger solutes can be transported by molecular hinge motifs.

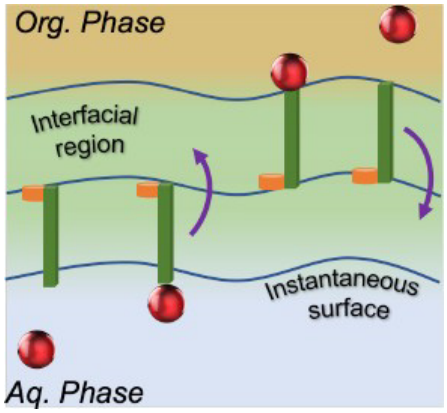

Publications Acknowledging this Grant in 2016 – present
Exclusively funded by this grant;

Kumar, N.; Servis, M.; Clark, A. E. Uranyl Speciation in the Presence of Ion Gradients at the Electrolyte/Organic Interface, *Solvent Extraction and Ion Exchange*, **2021**, *Accepted.* https://doi.org/10.26434/chemrxiv.14415818.v1

Liu, Z.; Clark, A. E. An Octanol Hinge Opens the Door to Water Transport, *Chemical Science*, **2021**, *12*, 2294 –

2303. DOI: 10.1039/D0SC04782A.

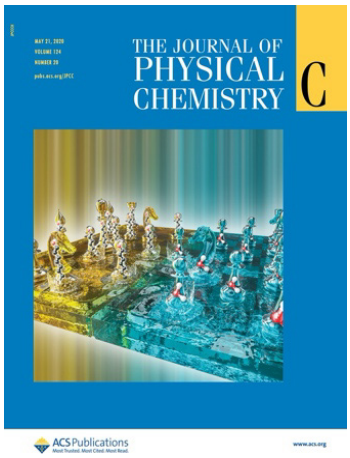

Kumar, N.; Sadhu, B.; Clark, A. E. Essential Aspects of Solvent Effects and Solution Conditions Upon the Modeling and Simulation of Lanthanide and Actinide Complexes, in *Computational Actinide and Lanthanide Chemistry*, ed. Windus, T.;

Pederson, C.; Penchoff, D. *ACS Books*, **2021** *In Press.*

Servis, M. J.; Martinez-Baez, E.; Clark, A. E. Hierarchical Phenomena in Multicomponent Liquids: Methods, Analysis, Chemistry. *Physical Chemistry Chemical Physics* **2020**, ***22***, 9850-9874. DOI: 10.1039/D0CP00164C.

Kumar, N. ; Servis, M. J.; Liu, Z.; Clark, A. E. Competitive Interactions at Electrolyte/Octanol Interfaces

– A Molecular Perspective. *Journal of Physical Chemistry C*. **2020**, *124*, 10924–10934 DOI:

10.1021/acs.jpcc.0c00302.

Servis, M.; Clark, A. E. Interfacial heterogeneity is essential to water extraction into organic solvents, *Phys. Chem. Chem. Phys.*, **2019**, *21*, 2866 – 2874. DOI: 10.1039/C8CP06450D. *2018 Hot Article.*

Jointly funded by this grant and other grants with leading intellectual contribution from this grant;

Nayak, S.; Kuma, R.; Liu, Z.; Qiao, B.; Clark, A. E.; Uysal, A. Origins of Clustering of Metalate- Extractant Complexes in Liquid-Liquid Extraction. *ACS Applied Materials and Interfaces*, **2021**, *ASAP article* https://doi.org/10.1021/acsami.0c23158

Rock, W.; Qiao, B.; Zhou, T.; Clark, A. E.; Uysal, A. Heavy Anion Complex Creates a Unique Water Structure at a Soft Charged Interface, J. Phys. Chem. C, **2018**, *122*, 29228-29236 DOI:

10.1021/acs.jpcc.8b08419, Cover article.

Alvarado, E.; Liu, Z.; Servis, M. J. ; Krishnamoorthy, B.; Clark, A. E. A Geometric Measure Theory Approach to Identify Complex Structural Features on Soft Matter Surfaces, *Journal of Chemical Theory and Computation*, **2020**, *16,* 4579-4587. DOI: 10.1021/acs.jctc.0c00260.

Servis, M.; Liu, Z.$^{+}$; Martinez-Baez, E.; Su, J.; Stetina, T.; Wildman, A.; Newcomb, K.; Autshbach, J.; Dixon, D. A.; Maginn, E. J.; Batista, E. R.; Yang, P.; Li, X.; Clark, A. E. Solvent Extraction Through the Lens of Advanced Modeling and Simulation, in Ion Exchange and Solvent Extraction, **2019**, Ed. Bruce Moyer, *CRC Press.* ISBN: 9781315114378

Servis, M.$^{+}$; Wu, D.; Shafer, J.; Clark, A. E. Square supramolecular assemblies of uranyl complexes in organic solvents, *Chemical Communications*, **2018*, 54,*** 10064 - 10067 DOI: 10.1039/C8CC05277H

Kelley, M. P.$^{\#}$; Yang, P.; Clark, S. B.; Clark, A. E. Competitive Interactions Within Cm(III) Solvation in Binary Water/Methanol Solutions, *Inorganic Chemistry,* **2018**, *57,* 10050-10058. DOI: 10.1021/acs.inorgchem.8b01214

Clark, A. E.; Braley, J.; Yang, P. Coordination of Actinides and the Chemistry Behind Solvent Extraction, *Experimental and Theoretical Approaches to Actinide Chemistry*, Wiley, **2018**, DOI*:* 10.1002/9781119115557.ch5 ISBN: 978-1-119-11552-6.

Kelley, M. P.; Davis, A.; Clowers, B.; Clark, A. E.; Clark, S. B. Acceleration of Metal- Ligand Complexation Kinetics by Electrospray Ionization. *The Analyst*, **2017**, *142*, 4468- 4475. DOI*:* 10.1039/C7AN01142C

Zhou, T.; McCue, A.; Ghadar, Y,$^{+}$; Bako, I.; Clark, A. E. Structural and Dynamic Heterogeneity of Capillary Wave Fronts at Aqueous Interfaces, *Journal of Physical Chemistry B*, **2017**, *121*, 9052-9062. DOI: 10.1021/acs.jpcb.7b07406.

Freiderich, J. W.; Burn, A. G.;$^{\#}$ Martin, L. R.; Nash, K. L.; Clark, A. E. A Combined Density Functional Theory and Spectrophotometry Study of the Bonding Interactions of $[NpO_2\square M]^{4+}$ Cation-Cation Complexes, *Inorganic Chemistry*, **2017**, *56*, 4788–4795 DOI: 10.1021/acs.inorgchem.6b02369.

Kelley, M. P., Yang, P.; Clark, S. B.; Clark, A. E. Structural and Thermodynamics Properties of the Curium(III) Ion Solvated by Water and Methanol, *Inorganic Chemistry,* **2016**, *55*, 4992-4999. DOI: 10.1021/acs.inorgchem.6b00477.

Exploiting Insertion Processes for Continuous Membrane-free Ion Separations

Richard M. Crooks, *Jonathan R. Thompson, and Collin D. Davies; Department of Chemistry, The University of Texas at Austin*

Presentation Abstract

The main goal of our DOE-sponsored research is to develop a fundamental understanding of how to use electrochemical processes to continuously redirect and separate ions. The basic research approach to this goal is to use electrochemical processes to form concentration gradients in solution. This results in a region of solution characterized by a decrease in conductivity relative to the bulk solution (i.e., an ion-depletion zone, IDZ). Upon application of a driving voltage, the IDZ forms a corresponding electric field gradient that can control the motion of ions in solution even in the absence of a membrane. In previous work, an IDZ was formed by neutralizing buffer ions via water electrolysis at a metal electrode. Here, we describe a new method for forming electric field gradients which does not rely on the formation of an IDZ and is therefore not restricted to buffer-containing solutions. Specifically, within a microchannel, we introduce a parallel pathway for current to pass (in the form of electrical current, instead of ionic current) through a fraction of the channel to yield ionic current gradients. These ionic current gradients contribute to forming electric field gradients which can be used to manipulate ion motion. In this presentation we will briefly discuss our characterization of ionic current gradients and demonstrate how the concomitant electric field gradients can be used for filtering or continuously separating charged microplastics from solution.

DE-FG02-06ER15758: Exploiting Insertion Processes for Continuous Membrane-free Ion Separations

RECENT PROGRESS

Filtering and continuously separating microplastics from water using electric field gradients formed electrochemically in the absence of buffer

The main goal of our DOE-sponsored research is to develop a fundamental understanding of how to use electrochemical processes to continuously redirect and separate ions. The basic research approach to this goal is to form ionic concentration gradients in solution by using electrochemical processes. Such concentration gradients create a region of solution with fewer ions (i.e., a local ion-depletion zone, IDZ) and a corresponding decrease in solution conductivity relative to the bulk solution. In the presence of an applied electric field, a disproportionate amount of the voltage is dropped within the IDZ, which yields an electric field gradient. We have previously shown electric field gradients can be useful for manipulating ions in interesting ways.

In the past, we formed an IDZ by converting buffer ions to neutral species via water electrolysis at an electrically floating bipolar electrode (BPE). One key limitation associated with this method, however, is that the process requires the presence of a buffer in solution to facilitate the formation of the IDZ and corresponding electric field gradient. Therefore, the goal of this project is to develop an alternative method for modulating the local electric field in microchannels without requiring a buffer in solution.

Recently, we showed that water electrolysis in the absence of buffer redistributes the electric field and can be used to manipulate the motion of charged microplastics. Figure 1a is a schematic diagram of the microfluidic configuration used for separation experiments. Here, a BPE is situated within a straight microchannel. Figure 1b shows the region of the microfluidic device that contains the BPE cathode (Figure 1a, dashed red box) after applying a driving voltage but before activating the BPE. In this frame, negatively charged microplastics are evenly distributed throughout the microchannel because the electric field is uniform. In contrast, Figure 1c shows the device after connecting the BPE poles. Here, microplastics are filtered from the microchannel because water electrolysis at the BPE redistributes the electric field. This result is important because it represents a buffer-free, electrochemical method for manipulating ion motion.

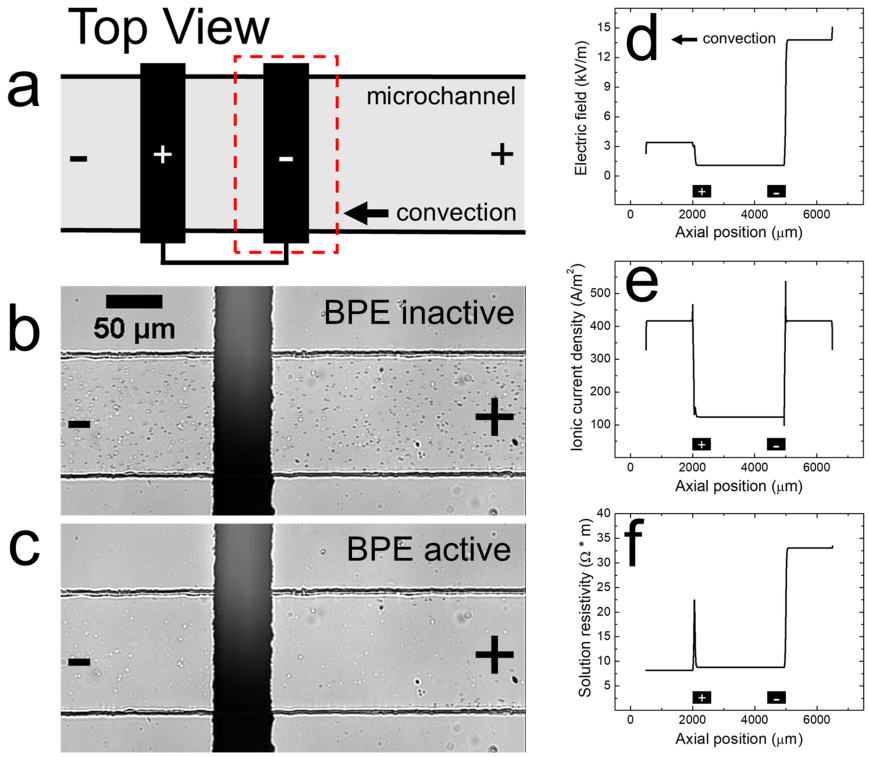

Figure 1. (a) Schematic illustration of the microfluidic device used for filtering microplastics. The dashed red box outlines the region of the microchannel containing the BPE cathode, where optical micrographs were captured (b) before and (c) after activating the BPE during a filtration experiment. 30.0 V was applied across the length of the microchannel. The BPE was 3.0 mm and the solution initially contained 1.0 mM KCl and 15 fM carboxyl-functionalized, ~1 μm, polystyrene microbeads. Simulated line plots along the center cutline of the microchannel showing the (d) electric field, (e) ionic current density, and (f) solution resistivity as a function of axial position. The black rectangles in (d-f) represent the two poles of the BPE.

Numerical simulations were then performed to understand how the electric field is redistributed to remove microplastics from the channel. Figure 1d is a line plot showing the simulated electric field as a function of axial position in a straight microchannel when the BPE is active. Most importantly, the simulated electric field reveals the presence of sharp electric field gradients in solution above the BPE poles (x = 2000 μm and 5000 μm), which are responsible for microplastic filtration. This result is interesting, because in the absence of a buffer there is no mechanism for forming an IDZ and corresponding electric field gradient. In other words, the origin of these electric field gradients was not immediately obvious. As a result, we plotted the simulated ionic current density and simulated solution resistivity separately in Figures 1e-f to more closely investigate the source of the electric field gradients in solution.

Figure 1e is a line plot of the simulated ionic current density as a function of axial position within the microchannel. The ionic current density is lower between the BPE poles (2000 μm < x < 5000 μm) relative to outside of the poles because the BPE provides an alternative pathway for current (in the form of electrical current) to pass through the system. Figure 1f is a line plot of the simulated solution resistivity as a function of axial position within the microchannel. The key result here is that solution resistivity upstream of the BPE cathode (x > 5000 μm) is much higher than the downstream resistivity (x < 5000 μm). This difference in solution resistivity along the length of the microchannel arises from the redistribution of ionic species in solution (i.e., generation of highly mobile of H^+ and OH^- at the BPE).

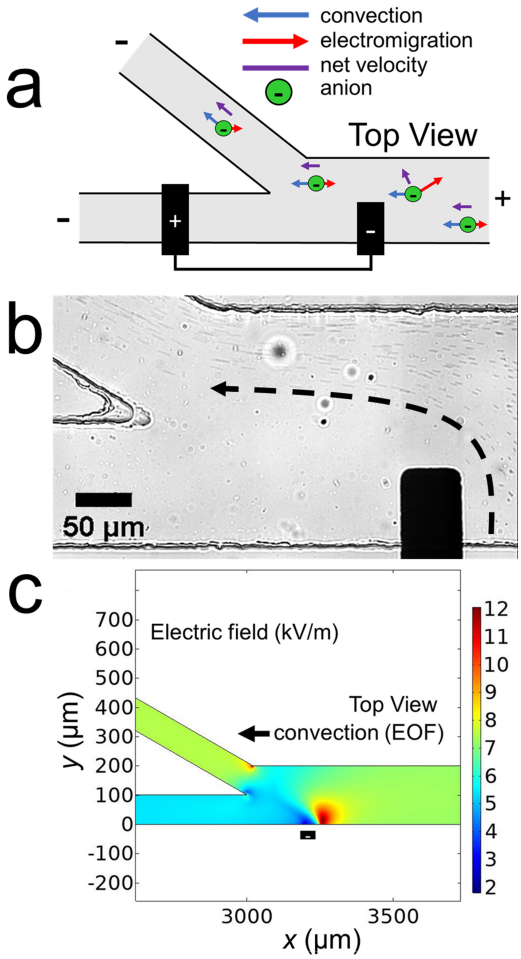

Figure 2. (a) Schematic illustration of the microfluidic device used for continuously separating microplastics. (b) Optical micrograph of the region of the microchannel containing the BPE cathode and channel bifurcation during a continuous separation experiment. 30.0 V was applied across the length of the microchannel. The BPE was 3.0 mm and the solution initially contained 5.0 mM KCl and 15 fM carboxyl-functionalized, ~1 μm, polystyrene microbeads. (c) Simulated plot of the electric field within the bifurcated microchannel when the BPE is active. The black rectangle represents the location of the BPE cathode.

When considered together, Figures 1e,f indicate that the ionic current density and solution resistivity gradients near the BPE poles (x = 2000 μm and 5000 μm) are directly responsible for the simulated electric field gradients shown in Figure 1d. This is a significant finding because, while electric field gradients have previously been formed using solution resistivity gradients (e.g., an IDZ), ionic current density gradients represent a new approach for forming electric field gradients in solution. This result improves our fundamental understanding of electrochemical separations in the absence of buffer.

Finally, we hypothesized that the electric field gradient near the BPE cathode could facilitate the continuous separation of microplastics in a bifurcated microchannel. Figure 2a is a schematic illustration of the experimental design. Here, because the BPE cathode only partially extends across the width of the main microchannel, we anticipated that the electric field gradient associated with the BPE cathode would be confined to the bottom half of the microchannel and therefore would redirect and continuously separate microplastics into the top outlet channel.

Figure 2b is an optical micrograph showing the BPE cathode and channel bifurcation within a device after applying the driving voltage and connecting the BPE poles. The trajectory of the microplastics is indicated by the dashed black arrow. The important point is that the microplastics are redirected away from the BPE cathode and into the top outlet channel. Consequently, the solution in the bottom outlet channel no longer contains a significant amount of microplastics. This continuous separation of microplastics in the absence of buffer is a key outcome of this DOE-funded research.

Lastly, in order to confirm our hypothesis that an electric field gradient is responsible for the experimentally observed microplastic redirection, another set of numerical simulations was performed. Figure 2c displays the simulated electric field near the microchannel bifurcation when the BPE is active. This plot indicates that the electric field is quite complex near the BPE cathode in the bifurcated microchannel. The main point, however, is the presence of a sharp electric field gradient (red lobe) just to the right of the BPE cathode. This perturbation to the electric field is responsible for the redirection of microplastics into the top outlet channel, which confirms our hypothesis that the electric field gradient associated with the BPE cathode can be used for microplastic redirection. Furthermore, and more importantly, the results shown in Figures 1 and 2 confirm that buffer-free, continuous separations are possible using BPEs, informing future iterations of electrochemical separations.

Publications Acknowledging this Grant in 2018 – present

Exclusively funded by this grant (there are no co-funded publications)*

(1) J. R. Thompson; L. M. Wilder; R. M. Crooks "Filtering and continuously separating microplastics from water using electric field gradients formed electrochemically in the absence of buffer" *Chem. Sci.* **2021** (submitted).

(2) J. R. Thompson; C. D. Davies; J. Clausmeyer; R. M. Crooks "Cation-specific Electrokinetic Separations using Prussian Blue Intercalation Reactions" *ChemElectroChem* **2020**, *7*, 4108-4117 (DOI: 10.1002/celc.202001095R2).

(3) C. D. Davies; R. M. Crooks "Focusing, sorting, and separating microplastics by serial faradaic ion concentration polarization" *Chem. Sci.* **2020**, *11*, 5547-5558 (DOI: 10.1039/D0SC01931c).

(4) C. D. Davies; S. E. Johnson; R. M. Crooks "Effect of Chloride Oxidation on Local Electric fields in Microelectrochemical Systems" *ChemElectroChem* **2019**, *6*, 4867-4876 (DOI: 10.1002/celc.201901402).

(5) C. D. Davies; E. Yoon; R. M. Crooks "Continuous Redirection and Separation of Microbeads via Faradaic Ion Concentration Polarization" *ChemElectroChem* **2018**, *5*, 877-884 (DOI: 10.1002/celc.201700450).

*May include attribution to a collaborator's grant, fellowships held by graduate students, and the Robert A. Welch Foundation., which provides sustaining support for our research program in the form of an endowment.

Iminoguanidines: From Anion Recognition and Separation to Carbon Capture

Radu Custelcean, Vyacheslav Bryantsev, Santa Jansone-Popova, and Bruce A. Moyer

Chemical Sciences Division, Oak Ridge National Laboratory

Presentation Abstract

This research combines organic and materials syntheses, computations, thermodynamics, and structural analysis by X-ray and neutron diffraction with the goal to understand the principles of molecular recognition in the context of anion separations via crystallization, ion exchange, and liquid-liquid extraction. The current focus is on recognition and separation of oxyanions, an important class of anions that are ubiquitous in nature and relevant to many energy and environmental problems. Our group has developed a new class of anion receptors based on iminoguanidines, synthetically accessible molecules that upon protonation are preorganized to chelate oxyanion (e.g., sulfate, chromate, selenate, carbonate) strongly and selectively by charge-assisted bidentate hydrogen bonds. The iminoguanidinium receptors are also photoswitchable, via photoisomerization of their C=N bonds, which provides an effective mechanism for turning anion binding on and off with UV light. Finally, the aqueous basicity of iminoguanidines, and their propensity to form insoluble, crystalline (bi)carbonate salts, provides the basis for a new, energy-efficient approach to carbon dioxide capture.

ERKCC08: Principles of Chemical Recognition and Transport in Extractive Separations

Postdocs: Jeffrey Einkauf, Ping Li

RECENT PROGRESS

Photoswitchable Iminoguanidinium Receptors for Oxyanion Separation

We have recently developed a new class of photoswitchable iminoguanidinium receptors that offer a potential solution to a long-standing problem in chemical separations. As receptor molecules with increasingly stronger binding are needed to separate ionic species from increasingly dilute streams, the release of the bound ions becomes more and more difficult, requiring harsh conditions and large excess of chemicals, thereby generating excessive chemical waste. A solution to this problem can be developed through stimulated release of bound ionic species using only energy input. To date, it has been difficult to achieve both strong binding and efficient release of ions due to the synthetic challenges and the magnitude of the switching efficiency needed. To address this problem, we designed a new class of photoswitchable anion receptors endowed with diiminoguanidinium functionality that displays more than four orders of magnitude change in binding strength towards sulfate, a representative oxyanion, upon photoirradiation with UV light. Specifically, UV light irradiation photoisomerizes the open *E*,*E* binding form of the bis-2-pyridyldiiminoguanidinium cation into the *Z*,*Z* non-binding form (Fig. 1), as monitored by ^{1}H NMR spectroscopy in DMSO. The unprecedented level of photoswitching observed is caused by intramolecular hydrogen bonding between the two guanidinium –NH groups and the 2-pyridyl substituents, that essentially shuts off the ability of the diiminoguanidinium group to bind anions in the closed *Z*,*Z* form. This conclusion is supported by theoretical calculations and crystal structures that show complementary binding of sulfate by the *E*,*E* photoisomer, but no binding by

the *Z*,*Z* photoisomer. The photoisomerization-relaxation process can be cycled multiple times with no apparent loss of function. In a demonstration of photoswitched separation, precipitation of the sparingly soluble 1:2 receptor:sulfate complex of the *E*,*E* isomer reverses upon UV light irradiation.

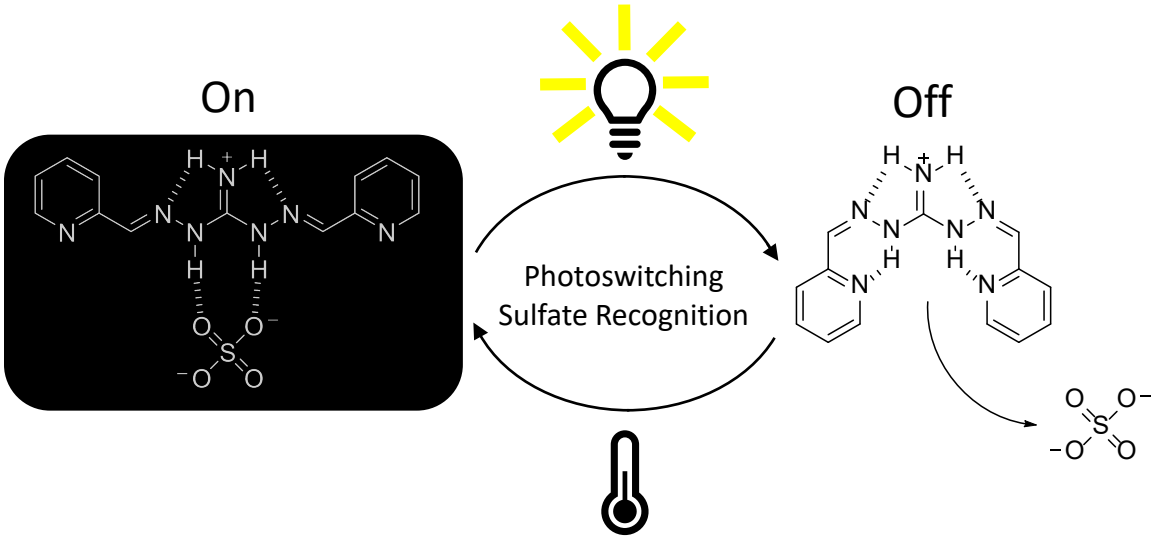

Figure 1. Photoswitchable iminoguanidinium receptor for light-induced catch-and-release separation of sulfate (Einkauf, 2021).

Anion Separation with Ionic Covalent Organic Frameworks (iCOFs)

Following up on our discovery of a novel class of iminoguanidinium-functionalized ionic covalent organic frameworks (*i*COFs) with unparalleled affinity for Cr(VI) oxyanions (Jansone-Popova, 2018), we have recently developed the second-generation *i*COFs to advance our understanding of the factors controlling selective sequestration of Cr(VI) and As(V) oxyanions in these polymeric materials (Ping, 2021). First, we studied the structure-activity relationship in the adsorption of Cr(VI) and As(V) oxyanions from water via a series of seven iCOFs with varying hydrogen bonding, steric, and electronic properties (Fig. 2A). We found that the hydrogen bonding, steric, and electrostatic interactions at/near the guanidinium-based anion binding site exert heavy influences on the uptake efficiency and selectivity of arsenate but not chromate. The study highlights the crucial role of the charge-assisted parallel bidentate hydrogen bonding interactions in the weak binding of arsenate to the guanidinium units. Second, we developed a bifunctional *i*COF with well-positioned guanidinium and phenol units for simultaneous removal of chromate and arsenate from water via a novel synergistic ion-exchange-redox approach (Fig. 2B). Specifically, the guanidinium motifs enable the ion-exchange-based adsorption of chromate in water at neutral pH with fast kinetics, high uptake capacity, and high selectivity; meanwhile, the highly hydroxylated aromatic linkers accommodate the Cr(VI)/Cr(III) redox conversion of chromate and enhance the simultaneous adsorption of arsenate through the formation of a stable 2Cr(III)-As(V) complex/cluster. As a result, the simultaneous removal of chromate and arsenate can be achieved with high adsorption efficiency and balanced Cr/As uptake ratios regardless of the change in concentration and the presence of interfering oxyanions.

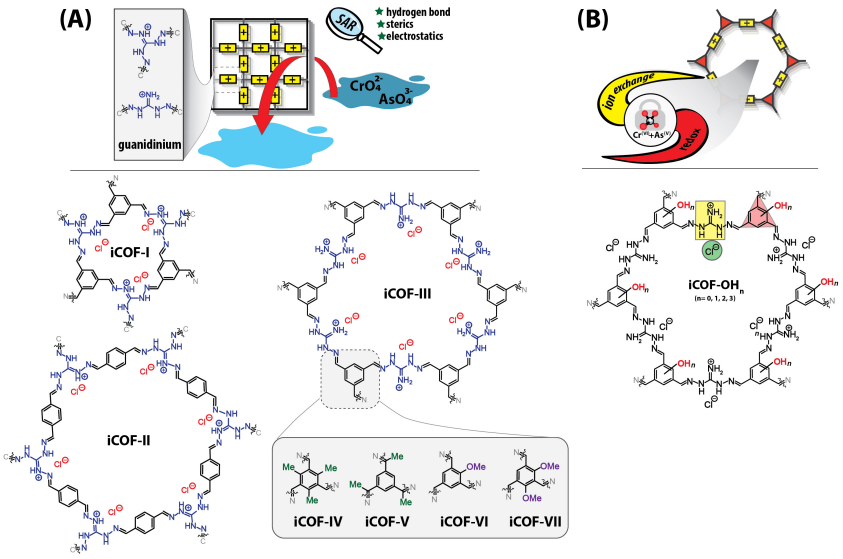

Figure 2. Iminoguanidinium-functionalized *i*COFs for selective sequestration of Cr(VI) and As(V) oxyanions.

CO_2 Separation by Bis-Iminoguanidinium (BIG) Carbonate Crystallization

We have recently discovered a novel approach to carbon capture based on CO_2 absorption by aqueous bis-iminoguanidines (BIGs) and crystallization of BIG (bi)carbonate salts (Seipp, 2017; Brethome, 2018; Williams, 2019; Custelcean, 2019). Like other oxyanions, carbonate anions tend to form BIG salts of extremely low aqueous solubility (on par with $CaCO_3$), which can drive the CO_2 absorption even from dilute sources such as air. To understand the structural factors determining the direct air capture (DAC) chemistry of BIGs, a systematic structure-properties relationship study of this class of sorbents was initiated. Along this line of inquiry, we turned our attention to the very basic series of BIG structures resulting from glyoxal (GBIG) and its simple analogs methylglyoxal (MGBIG) and diacetyl (DABIG) (Fig. 3). Their crystal structures have been analyzed by X-ray and neutron diffraction to accurately measure key structural parameters including molecular conformations, hydrogen bonding, and π-stacking. Experimental measurements of key properties, such as aqueous solubilities and regeneration energies and temperatures, were complemented by first-principles calculations of lattice and hydration free energies, as well as free energies of reactions with CO_2, and BIG regenerations. We found that minor structural modifications in the molecular structure of the BIGs result in major changes in the crystal structures and the aqueous solubilities within the series, leading to enhanced DAC. Future research will focus on mechanistic understanding of the CO_2 absorption and release by the crystalline BIGs, with the goal of maximizing the CO_2 separation efficacy and energy efficiency.

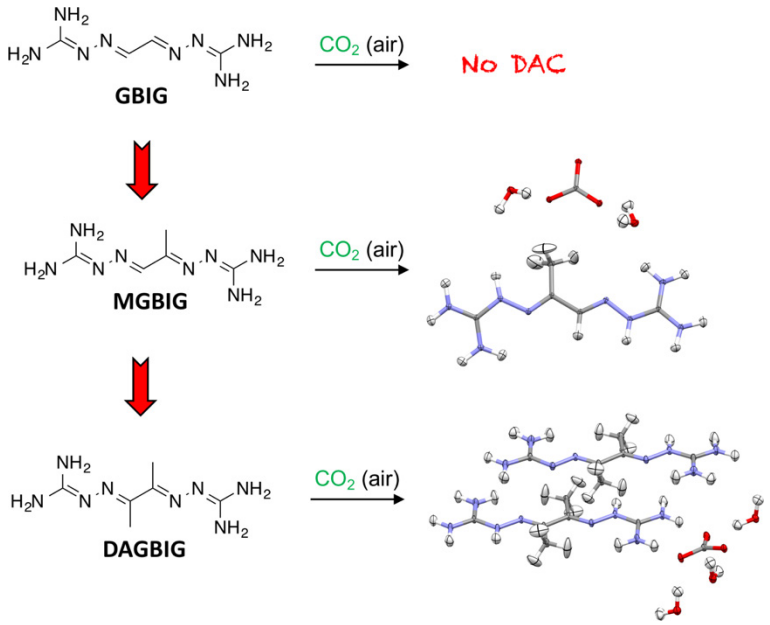

Figure 3. Direct air capture of CO_2 by carbonate crystallization with BIGs.

Publications Acknowledging this Grant in 2017 – present

(I) Exclusively funded by this grant

1. Seipp, C. A.; Williams, N. J.; Kidder, M. K.; Custelcean, R. *CO_2 Capture from Ambient Air by Crystallization with a Guanidine Sorbent. Angew. Chem. Int. Ed.* **2017**, *56*, 1042-1045.
2. Brethome, F. M.; Williams, N. J.; Seipp, C. A.; Kidder, M. K.; Custelcean, R. *Direct Air Capture of CO2 via Aqueous-Phase Absorption and Crystalline-Phase Release Using Concentrated Solar Power. Nature Energy* **2018**, *3*, 553-559.
3. Williams, N. J.; Seipp, C. A.; Garrabrant, K. A.; Custelcean, R.; Holguin, E.; Keum, J. K.; Ellis, R. J.; Moyer, B. A. *Surprisingly Selective Sulfate Extraction by a Simple Monofunctional Di(imino)guanidinium Micelle-Forming Anion Receptor. Chem. Commun.* **2018**, *54*, 10048-10051.
4. Jansone-Popova, S.; Moinel, A.; Schott, J. A.; Mahurin, S. M.; Popovs, I.; Veith G. M.; Moyer, B. A. "Guanidinium-Based Ionic Covalent Organic Framework (iCOF) for Rapid and Selective Removal of Toxic Cr(VI) Oxoanions from Water" *Environ. Sci. Technol.*, **2018**, *53 (2)*, 878-883 (featured on the cover).
5. Williams, N. J.; Seipp, C. A.; Brethome, F. M.; Ma, Y.-Z.; Ivanov, A. S.; Bryantsev, V. S.; Kidder, M. K.; Martin, H. J.; Holguin, E.; Garrabrant, K. A.; Custelcean, R. *CO_2 Capture via Crystalline Hydrogen-Bonded Bicarbonate Dimers. Chem* **2019**, *5*, 719-730 (highlighted in *Science*).
6. Williams, N. J.; Custelcean, R. *CO_2 Capture Going BIG. Carbon Capture Journal* **2019**, *68*, Mar/Apr, 4-6.
7. Williams, N. J.; Roy, S.; Reynolds, C. O.; Custelcean, R. Bryantsev, V. S.; Moyer, B. A. *Enhancing Selectivity of Cation Exchange with Anion Receptors"*, *Chem. Commun.* **2019**, *55*, 3590-3593.
8. Custelcean, R.; Williams, N. J.; Garrabrant, K.; Agullo, P.; Brethome, F. M.; Martin, H. J.; Kidder, M. K. Direct Air Capture of CO_2 with Aqueous Amino Acids and Solid Bis-Iminoguanidines (BIGs). *Ind. Eng. Chem. Res.* **2019**, *58* (51), 23338-23346.
9. Custelcean, R.; Williams, N. J.; Wang, X.; Garrabrant, K.A.; Martin, H. J.; Kidder, M. K.; Ivanov, A. S.; Bryantsev, V. S. Dialing in Direct Air Capture of CO_2 by Crystal Engineering of Bis-iminoguanidines. *ChemSusChem* **2020**, *13*, 6381-6390.
10. Custelcean, R. Iminoguanidines: From Anion Recognition and Separation to Carbon Capture. *Chem. Commun.* **2020**, *56*, 10272-10280.

11. Thievenet, A.; Custelcean, R.; Moyer, B. A.; Jansone-Popova, S. Synergistic Self-Assembly of Oxoanions and d-Block Metal Ions with Heteroditopic Receptors into Triple-Stranded Helicates, *Chem. Eur. J.* **2020**, *26*,14290 (featured on the cover).
12. Custelcean, R.; Garrabrant, K. A.; Agullo, P.; Williams, N. J. Direct Air Capture of CO_2 with Aqueous Peptides and Crystalline Guanidines. *Cell Reports Physical Science* **2021**, *2*, 100385 (featured on the cover, highlighted in C&EN News).
13. Custelcean, R. Reducing Atmospheric Carbon Dioxide Through Direct Air Capture, *Scientia* **2021**, https://www.scientia.global/dr-radu-custelcean-reducing-atmospheric-carbon-dioxide-through-direct-air-capture/.
14. Custelcean, R.; Williams, N. J.; Seipp, C.A. Guanidine Compounds for Carbon Dioxide Capture. United Stated Patent, US 10,583,387, March 10, **2020**.
15. Custelcean, R.; Williams, N. J.; Seipp, C.A. Guanidine Compounds for Removal of Oxyanions from Aqueous Solutions and for Carbon Dioxide Capture. United Stated Patent, US 10,633,332, April 28, **2020**.
16. Williams, N. J.; Custelcean, R.; Moyer, B. A.; Ellis, R. J.; Abney, C. W.; Seipp, C. A. Lipophilic Guanidinium Compounds for Removal of Oxyanions from Aqueous Solutions, United Stated Patent, US 11,001,554, May 11, **2021**.
17. Ping Li; Joshua T. Damron; Vyacheslav S. Bryantsev; Shannon M. Mahurin; Ilja Popovs; Santa Jansone-Popova. Structure-Activity Relationship Study on Sequestration of Cr(VI) and As(V) Oxoanions in Water using Guanidinium-Based Ionic Covalent-Organic Frameworks (iCOFs). **2021**, *Submitted.*
18. Ping Li, Joshua T. Damron, Gabriel M. Veith, Vyacheslav S. Bryantsev, Shannon M. Mahurin, Ilja Popovs, Santa Jansone-Popova. Bifunctional ionic covalent organic frameworks for enhanced simultaneous removal of chromium(VI) and arsenic(V) oxoanions via synergetic ion exchange and redox process. **2021**, *Submitted*.
19. Einkauf, J. D.; Bryantsev, V. S.; Moyer, B. A.; Custelcean, R. A Photoswitchable Diiminoguanidinium Receptor for Light-Induced Catch-and-Release Separation of Sulfate. **2021**, *Submitted*.
20. Custelcean, R. Direct Air Capture of CO_2 via Crystal Engineering. **2021**, *Submitted.*

(II) Jointly funded by this grant and other grants with leading intellectual contribution from this grant

1. Jia, C.; Zuo, W.; Yang, D.; Chen, Y.; Cao, L.; Custelcean, R.; Hostas, J.; Hobza, P.; Glaser, R.; Wang, Y.-Y.; Yang, X.-J.; Wu, B. *Selective Binding of Choline by a Phosphate- Coordination-Based Triple Helicate Featuring an Aromatic Box. Nature Commun.* **2017**, 938.
2. Gianopoulos, C. G.; Chua, Z.; Zhurov, V. V.; Seipp, C. A.; Wang, X.; Custelcean, R.; Pinkerton, A. A. *Direct Air Capture of CO_2 – Topological Analysis of the Experimental Electron Density (QTAIM) of the Highly Insoluble Carbonate Salt of 2,6-Pyridine- bis(iminoguanidine), $(PyBIGH_2)(CO_3)(H_2O)_4$. IUCrJ* **2019**, *6*, 56-65.
3. Huang, Z.; Jia, C.; Wu, B. Jansone-Popova, S.; Seipp, C. A.; Custelcean, R. *Selective Binding of (Thio)sulfate and Phosphate in water by Quaternary Ammonium Functionalized Oligo-Ureas. Chem. Commun.* **2019**, *55*, 1714-1717.
4. Garrabrant, K. A.; Williams, N. J.; Holguin, E.; Brethome, F. M.; Tsouris, C.; Custelcean, R. *Energy-Efficient CO_2 Capture from Flue Gas by Absorption with Amino Acids and Crystallization with a Bis-Iminoguanidine. Ind. Eng. Chem. Res.* **2019**, *58*, 10510-10515 (featured on the cover).
5. Liu, M.; Custelcean, R.; Seifert, S.; Kuzmenko, I.; Gadikota, G. Hybrid Absorption-Crystallization Strategies for the Direct Air Capture of CO_2 Using Phase-Changing Guanidinium Bases: Insight from In-operando X-Ray Scattering and Infrared Spectroscopy Measurements, *Ind. Eng. Chem. Res.* **2020**, *59*, 20953.

6. Kasturi, A.; Gabitto, J.; Tsouris, C.; Custelcean, R. Carbon Dioxide Capture with Aqueous Amino Acids: Mechanistic Study of Amino Acid Regeneration by Guanidine Crystallization and Process Intensification. *Separation and Purification Technology* **2021**, *271*, 118839.
7. Decato, D. A.; Riel, A. M. S.; May, J. H.; Bryantsev, V. S.; Berryman, O. B. Theoretical, Solid-State, and Solution Quantification of the Hydrogen Bond-Enhanced Halogen Bond. *Angew. Chem Int. Ed.* **2021**, *60*, 3685-3692.
8. Yu, X.; Einkauf, J. D.; Bryantsev, V. S.; Cheshire, M. C.; Reinhart, B. J.; Autschbach, J.; Burns, J. D. Spectroscopic Characterization of Neptunium(VI), Plutonium(VI), and Americium(VI) and Neptunium(V) Encapsulated in Uranyl Nitrate Hexahydrate. *Phys. Chem. Chem. Phys.* **2021**, *23*, 13228-13241.
9. Shih, J.-L.; Bocharova, V.; Lyu, H.; Popovs, I.; Nzuwah Nziko, V. De P.; Bryantsev, V. S.; Nawaz, K.; Custelcean, R.; Jansone-Popova, S. Design Principles Towards Exceptionally Stable Anion-Exchange Membranes. **2021**, *Submitted.*

(III) Jointly funded by this grant and other grants with relatively minor intellectual contribution from this grant

1. Stack, A. G.; Stubbs, J. E.; Srinivasan, S. G.; Roy, S.; Bryantsev, V. S.; Eng, P. J.; Custelcean, R.; Gordon, A. D.; Hexel, C. R. *Mineral-Water Interface Structure of Xenotime (YPO4) {100}. J. Phys. Chem. C* **2018**, *122*, 20232.
2. Hachtel, J. A.; Huang, J.; Popovs, I.; Jansone-Popova, S.; Keum, J.; Jakowski, J.; Lovejoy, T. C.; Dellby, N.; Krivanek, O. L.; Idrobo, J. C. "Identification of Site-Specific Isotopic Labeling in Amino Acids by Vibrational Spectroscopy in the Electron" *Science*, **2019**, *363*, 525-528.
3. Ivanov, A. S.; Parker, B. F.; Zhang, Z.; Aguila, B.; Ma, S.; Jansone-Popova, S.; Arnold, J.; Mayes, R. T.; Dai, S.; Bryantsev, V. S.; Rao, L.; Popovs, I. "Siderophore-inspired chelator hijacks uranium from aqueous medium" *Nat. Comm.*, **2019**, *10*, 819.
4. Xing, J.; Sanjeewa, L.; Meier, W.; May, A.; Zheng, Q.; Custelcean, R.; Stewart, G.; Sefat, A. Synthesis, Magnetization, and Heat Capacity of Triangular Lattice Materials NaErSe2 and KErSe2. *Phys. Rev. Mater.* **2019,** *3* (11), DOI: 10.1103/Phys. Rev. Materials. 3.114413.
5. Xing, J.; Sanjeewa, L.; Kim, J.; Stewart, G.; Du, M-H.; Reboredo, F.; Custelcean, R.; Sefat, A. Crystal Synthesis and Frustrated Magnetism in Triangular Lattice Cs RE Se 2 (RE = La–Lu): Quantum Spin Liquid Candidates CsCeSe 2 and CsYbSe 2. *ACS Mater. Lett.* **2019,** *2* (1), 71-75.
6. Sanjeewa, L.; Xing, J.; Taddei, K.; Parker, D.; Custelcean, R.; Dela Cruz, C.; Sefat, A. Evidence of Ba-substitution Induced Spin-canting in the Magnetic Weyl Semimetal $EuCd_2As_2$. *Phys. Rev. B* **2020,** *102* (10), 104404.
7. Lin, L.; Chowdhury, A. U.; Ma, Y.-Z.; Sacci, R. L.; Katsaras, J.; Hong, K.; Collier, C. P.; Carrillo, J.-M.; Doughty, B. Ion Pairing Mediates Molecular Organization Across Liquid/Liquid Interfaces. *ACS Applied Materials & Interfaces* **2021**, in press, https://doi.org/10.1021/acsami.1c09763.

Fundamental Studies of Novel Separations

Sheng Dai (PI); Shannon Mahurin, Zhenzhen Yang, De-en Jiang (UCR) (Co-PIs); Research Team: Zongyu Wang (ORNL postdoc); Xian Suo (UTK-ORNL visiting scholar); Yuqing Fu (UCR graduate student)

Overall research goals: The overarching goal of this project is to understand chemical separation phenomena enabled by novel separation media containing ionic liquids that selectively bind and/or transport target molecular species via tailored interactions at interfaces and through the control of solvation environments and the formation of structures at multiple length scales.

Significant achievements in 2019-2021:

8) Machine learning has been utilized to investigate the origin of selectivity for our porous carbon media. The major role of mesoporosity in determining selectivity was elucidated.
9) Capitalizing on our pioneering research in porous liquids, we further examined these novel nanostructured liquids with intrinsic porosity for membrane gas transport.
10) We demonstrated that highly crystalline triazine frameworks can be synthesized under super acidic conditions, highlighting highly stable covalent organic frameworks for separation.

Science objectives for 2021-2022:

The specific research topics we will investigate are:
(a) What are the design principles for Type-I porous ionic liquids to achieve tailored interactions with the separation targets?
(b) How can molecular interactions and transport be dynamically controlled via the interaction of ionic liquids with porous separation media?

Publications supported by this project (June 2019-2021):

1. Zhao, J. H.; Yang, S. Z.; Zhang, P. F.; Dai, S. Sulphur as medium: Directly converting pitch into porous carbon. *Fuel* **2021**, *286*, 119393.
2. Yang, Z. Z.; Liu, T. Y.; Wang, S.; Chen, H.; Suo, X.; Wang, T.; Thapaliya, B. P.; Jiang, D. E.; Popovs, I.; Dai, S. Fabrication of Ionic Covalent Triazine Framework-Linked Membranes via a Facile Sol-Gel Approach. *Chemistry of Materials* **2021**, *33*, 3386-3393.
3. Wang, Z. Y.; Chen, H.; Wang, Y. Y.; Chen, J. H.; Arnould, M. A.; Hu, B.; Popovs, I.; Mahurin, S. M.; Dai, S. Polymer-Grafted Porous Silica Nanoparticles with Enhanced CO2 Permeability and Mechanical Performance. *Acs Applied Materials & Interfaces* **2021**, *13*, 27411-27418.
4. Wang, S.; Mahurin, S. M.; Dai, S.; Jiang, D. E. Design of Graphene/Ionic Liquid Composites for Carbon Capture. *Acs Applied Materials & Interfaces* **2021**, *13*, 17511-17516.
5. Thapaliya, B. P.; Puskar, N. G.; Slaymaker, S.; Feider, N. O.; Do-Thanh, C. L.; Schott, J. A.; Jiang, D. E.; Teague, C. M.; Mahurin, S. M.; Dai, S. Synthesis and Characterization of Macrocyclic Ionic Liquids for CO2 Separation. *Industrial & Engineering Chemistry Research* **2021**, *60*, 8218-8226.
6. Jie, K. C.; Zhou, Y. J.; Ryan, H. P.; Dai, S.; Nitschke, J. R. Engineering Permanent Porosity into Liquids. *Advanced Materials* **2021**, *33*, 2005745.
7. Feider, N. O.; Mahurin, S. M.; Do-Thanh, C. L.; Dai, S.; Jiang, D. E. Molecular dynamics simulations of a dicationic ionic liquid for CO2 capture. *Journal of Molecular Liquids* **2021**, *335*, 116163.
8. Dai, S. Catalyst: Challenges in development of adsorbents for recovery of uranium from seawater. *Chem* **2021**, *7*, 537-539.

9. Chen, H.; Fan, J. T.; Fu, Y. Q.; Do-Thanh, C. L.; Suo, X.; Wang, T.; Popovs, I.; Jiang, D. E.; Yuan, Y. T.; Yang, Z. Z.; Dai, S. Benzene Ring Knitting Achieved by Ambient-Temperature Dehalogenation via Mechanochemical Ullmann-Type Reductive Coupling. *Advanced Materials* **2021**, *33*, 2008685.
10. Zhao, J. H.; Shan, W. D.; Zhang, P. F.; Dai, S. Solvent-free and mechanochemical synthesis of N-doped mesoporous carbon from tannin and related gas sorption property. *Chemical Engineering Journal* **2020**, *381*, 122579.
11. Zhang, Y. D.; Chen, G. J.; Wu, L.; Liu, K.; Zhong, H.; Long, Z. Y.; Tong, M. M.; Yang, Z. Z.; Dai, S. Two-in-one: construction of hydroxyl and imidazolium-bifunctionalized ionic networks in one-pot toward synergistic catalytic CO2 fixation. *Chemical Communications* **2020**, *56*, 3309-3312.
12. Zhang, J. Y.; Zhang, J. B.; Li, M. J.; Wu, Z. L.; Dai, S.; Huang, K. Solvent-free and one-pot synthesis of ultramicroporous carbons with ultrahigh nitrogen contents for sulfur dioxide capture. *Chemical Engineering Journal* **2020**, *391*, 123579.
13. Yang, Z. Z.; Guo, W.; Mahurin, S. M.; Wang, S.; Chen, H.; Cheng, L.; Jie, K. C.; Meyer, H. M.; Jiang, D. E.; Liu, G. P.; Jin, W. Q.; Popovs, I.; Dai, S. Surpassing Robeson Upper Limit for CO2/N-2 Separation with Fluorinated Carbon Molecular Sieve Membranes. *Chem* **2020**, *6*, 631-645.
14. Yang, Z. Z.; Chen, H.; Wang, S.; Guo, W.; Wang, T.; Suo, X.; Jiang, D. E.; Zhu, X.; Popovs, I.; Dai, S. Transformation Strategy for Highly Crystalline Covalent Triazine Frameworks: From Staggered AB to Eclipsed AA Stacking. *Journal of the American Chemical Society* **2020**, *142*, 6856-6860.
15. Wang, S.; Li, Y.; Dai, S.; Jiang, D. E. Prediction by Convolutional Neural Networks of CO2/N(2)Selectivity in Porous Carbons from N(2)Adsorption Isotherm at 77 K. *Angewandte Chemie-International Edition* **2020**, *59*, 19645-19648.
16. Men, S.; Licence, P.; Luo, H. M.; Dai, S. Tuning the Cation-Anion Interactions by Methylation of the Pyridinium Cation: An X-ray Photoelectron Spectroscopy Study of Picolinium Ionic Liquids. *Journal of Physical Chemistry B* **2020**, *124*, 6657-6663.
17. Men, S.; Licence, P.; Do-Thanh, C. L.; Luo, H. M.; Dai, S. X-ray photoelectron spectroscopy of piperidinium ionic liquids: a comparison to the charge delocalised pyridinium analogues. *Physical Chemistry Chemical Physics* **2020**, *22*, 11976-11983.
18. Luo, Y. L.; Yang, Z. Z.; Guo, W.; Chen, H.; Wang, T.; Liu, Y. F.; Lyu, Y. N.; Luo, H. M.; Dai, S. De novo fabrication of multi-heteroatom-doped carbonaceous materials via an in situ doping strategy. *Journal of Materials Chemistry A* **2020**, *8*, 4740-4746.
19. Jie, K. C.; Zhou, Y. J.; Sun, Q.; Li, B.; Zhao, R.; Jiang, D. E.; Guo, W.; Chen, H.; Yang, Z. Z.; Huang, F. H.; Dai, S. Mechanochemical synthesis of pillar 5 quinone derived multi-microporous organic polymers for radioactive organic iodide capture and storage. *Nature Communications* **2020**, *11*, 1086.
20. Jie, K. C.; Onishi, N.; Schott, J. A.; Popovs, I.; Jiang, D. E.; Mahurin, S.; Dai, S. Transforming Porous Organic Cages into Porous Ionic Liquids via a Supramolecular Complexation Strategy. *Angewandte Chemie-International Edition* **2020**, *59*, 2268-2272.
21. Guo, W.; Mahurin, S. M.; Wang, S.; Meyer, H. M.; Luo, H. M.; Hu, X. X.; Jiang, D. E.; Dai, S. Ion-gated carbon molecular sieve gas separation membranes. *Journal of Membrane Science* **2020**, *604*, 118013.

22. Guo, W.; Mahurin, S. M.; Unocic, R. R.; Luo, H. M.; Dai, S. Broadening the Gas Separation Utility of Monolayer Nanoporous Graphene Membranes by an Ionic Liquid Gating. *Nano Letters* **2020**, *20*, 7995-8000.
23. Fulvio, P. F.; Dai, S. Porous Liquids: The Next Frontier. *Chem* **2020**, *6*, 3263-3287.
24. Chen, H.; Yang, Z. Z.; Do-Thanh, C. L.; Dai, S. What Fluorine Can Do in CO(2)Chemistry: Applications from Homogeneous to Heterogeneous Systems. *Chemsuschem* **2020**, *13*, 6182-6200.
25. Zheng, W. T.; Huang, K.; Dai, S. Solvothermal and template-free synthesis of N-Functionalized mesoporous polymer for amine impregnation and CO2 adsorption. *Microporous and Mesoporous Materials* **2019**, *290*, 109653.
26. Zhang, Z. H.; Yang, S. Z.; Hu, X. B.; Xu, H. D.; Peng, H. G.; Liu, M. M.; Thapaliya, B. P.; Jie, K. C.; Zhao, J. H.; Liu, J. X.; Chen, H.; Leng, Y.; Lu, X. Y.; Fu, J.; Zhang, P. F.; Dai, S. Mechanochemical Nonhydrolytic Sol-Gel-Strategy for the Production of Mesoporous Multimetallic Oxides. *Chemistry of Materials* **2019**, *31*, 5529-5536.
27. Yang, Z. Z.; Wang, S.; Zhang, Z. H.; Guo, W.; Jie, K. C.; Hashim, M. I.; Miljanic, O. S.; Jiang, D. E.; Popovs, I.; Dai, S. Influence of fluorination on CO2 adsorption in materials derived from fluorinated covalent triazine framework precursors. *Journal of Materials Chemistry A* **2019**, *7*, 17277-17282.
28. Yang, Z. Z.; Chen, H.; Li, B.; Guo, W.; Jie, K. C.; Sun, Y. F.; Jiang, D. E.; Popovs, I.; Dai, S. Topotactic Synthesis of Phosphabenzene-Functionalized Porous Organic Polymers: Efficient Ligands in CO2 Conversion. *Angewandte Chemie-International Edition* **2019**, *58*, 13763-13767.
29. Wang, S.; Zhang, Z. H.; Dai, S.; Jiang, D. E. Insights into CO2/N-2 Selectivity in Porous Carbons from Deep Learning. *Acs Materials Letters* **2019**, *1*, 558-563.
30. Tian, Z. Q.; Dai, S.; Jiang, D. E. Confined Ionic Liquid in an Ionic Porous Aromatic Framework for Gas Separation. *Acs Applied Polymer Materials* **2019**, *1*, 95-102.
31. Teague, C. M.; Schott, J. A.; Stieber, C.; Mann, Z. E.; Zhang, P. F.; Williamson, B.; Dai, S.; Mahurin, S. M. Microporous and hollow carbon spheres derived from soft drinks: Promising CO2 separation materials. *Microporous and Mesoporous Materials* **2019**, *286*, 199-206.
32. Huang, K.; Li, Z. L.; Zhang, J. Y.; Tao, D. J.; Liu, F. J.; Dai, S. Simultaneous activation and N-doping of hydrothermal carbons by NaNH2: An effective approach to CO2 adsorbents. *Journal of Co2 Utilization* **2019**, *33*, 405-412.
33. Gautam, S.; Le, T. T. B.; Rother, G.; Jalarvo, N.; Liu, T. T.; Mamontov, E.; Dai, S.; Qiao, Z. A.; Striolo, A.; Cole, D. Effects of water on the stochastic motions of propane confined in MCM- 41-S pores. *Physical Chemistry Chemical Physics* **2019**, *21*, 25035-25046.
34. Che, S. Y.; Yang, Z. Z.; Popovs, I.; Luo, H. M.; Luo, Y. L.; Guo, W.; Chen, H.; Wang, T.; Jie, K. C.; Wang, C. M.; Dai, S. A succinct strategy for construction of nanoporous ionic organic networks from a pyrylium intermediate. *Chemical Communications* **2019**, *55*, 13450-13453.

Probing the Mechanisms of Liquid Extraction at Buried Liquid/Liquid Interfaces

Benjamin Doughty,Chemical Sciences Division, Oak Ridge National Laboratory, Oak Ridge, TN 37831

Poster Abstract

Understanding adsorption and self-assembly at liquid/liquid (L/L) interfaces, where key chemical transformations underlying liquid extractions take place, is central to designing chemical separations with enhanced selectivity and efficiency. However, these interfaces are notoriously hard to study due to their complexity and proximity to neighboring bulk phases that dominate traditional measurements. The overarching goal of this research is to develop a unified understanding of the molecular structure and dynamics governing the mechanisms of chemical separations at L/L interfaces. To access these complex buried interfaces, we leverage surface specific vibrational sum frequency generation (SFG) spectroscopy and surface tension methods to probe these interfaces during liquid extraction in real time. We observe marked differences in adsorption thermodynamics and assembly kinetics based on the structure and branching of the ligand tails, the nature of the non-polar phases, ion pairing interactions, and emergent H-bonding networks. We show how these chemical handles provide a means to tune interfacial structure, population, and aggregation using seemingly innocuous interactions in the opposing oil and aqueous phases. We further demonstrate, through comparisons with air/liquid interfaces, that the lack of an oil phase and associated solvation interactions results in disparate adsorption thermodynamics and structurally distinct molecular assemblies as compared to more relevant L/L interfaces. These results point to an often-overlooked interplay between oil and aqueous phase solvation that is central to connecting interfacial molecular phenomena to separations on the macroscopic scale. New directions in understanding and controlling liquid extractions and other separations are anticipated through continued work probing these fundamental interfacial interactions.

ERKCT09: Chemical Organization, Structure and Dynamics at Complex Liquid-Liquid Interfaces: Mechanistic Insight into Selective Solvent Extraction and Self-Assembly

Postdoc(s): Lu Lin, Azhad U. Chowdhury, Uvinduni I. Premadasa

RECENT PROGRESS

We have provided new insight into the mechanism of solvent extraction and assembly at L/L interfaces as determined from the first *in situ* surface specific measurements ever made *during extraction*. This comprehensive paper is published in ACS Applied Materials and Interfaces. Here we provided evidence via dynamic SFG measurements for the formation of micellar species at a L/L interface during solvent extraction. A chemical description of self-assembly driven by pH and the associated H-bonding network was developed for the L/L interface at equilibrium in the formation of water bridged aggregates in the absence of divalent ions. We showed how Co^{2+} ions substitute into this network and reverse water ordering, which is a means to create and expel micellar species from the surface during extraction. The combination of static and time-resolved measurements revealed (representative data plotted in Figure 1) the events underlying complexities of liquid extractions at high $[Co^{2+}]$:[ligand] ratios by showing an evolution of interfacially assembled centrosymmetric structures that are readily tuned on a chemical basis by altering the compositions of the aqueous phase. The results of this work point to new principles to design-applied separations through the manipulation of surface charge, electrostatic screening, and the associated H-bonding networks that arise at the interface to facilitate organization and subsequent extraction.

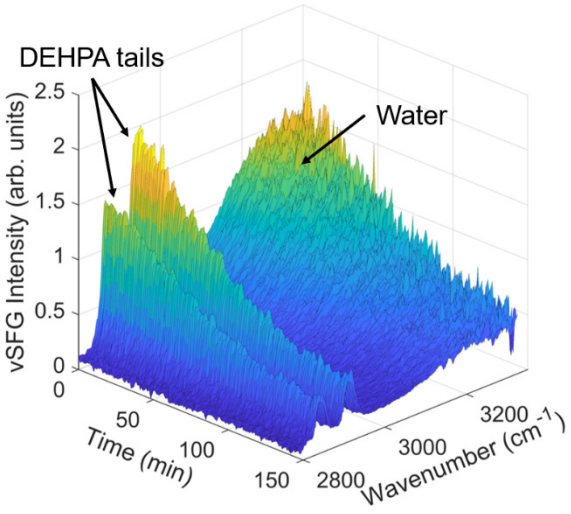

Figure 6: Time-resolved SFG spectra taking during the liquid extraction of Co^{2+} from an aqueous phase into an oil phase. The decay in the signal arises from the formation of increasingly centrosymmetric assemblies that form during the reaction.

Building off this work, we have shown how specific ion pairing, a central mechanistic process in solvent extraction and self-assembly, can be used to tune ligand tail structures and thereby imparting new function into the interface. Correlated tail packing and head-group interactions are mediated by H-bonding networks that are different from the strong/bridging interactions found the above-mentioned system, indicating that there is a means to control extraction through a direct manipulation of pairing interactions and solvation at the L/L interface (sketched in Figure 2).We show how the presence of seemingly innocuous salts can impart dramatic changes to the amphiphile tail conformations in the oil phase via specific ion effects taking place in the aqueous phase. These specific ion interactions are shown to drive enhanced amphiphile adsorption from the oil phase, induce morphological changes, and disrupt emergent H-

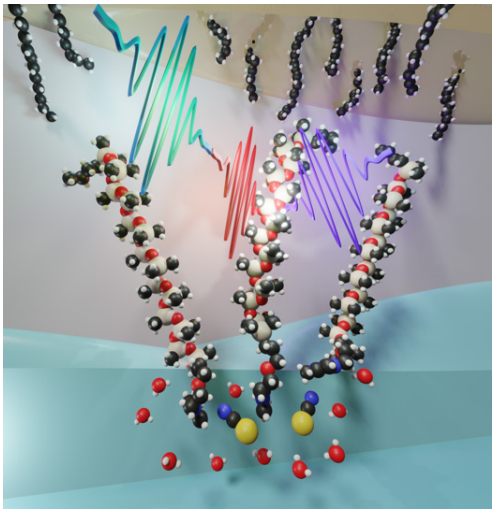

Figure 7: Sketch of amphiphile tail structures in the oil phase tuned by ion-pairing interactions in the aqueous phase, despite no direct interaction.

bonding structures at the interface. Tuning these interactions allows for independent control over the tail structure in the oil phase versus interfacial population changes and represents key mechanistic insight that is needed to control chemical reactions at L/L interfaces. This work is published in ACS Applied Materials and Interfaces.

We have since measured the equilibrium adsorption binding constants for two model ligands at the L/L and at the air/liquid (A/L) interface (air/aqueous (A/A), specifically). These results show that modest differences in binding energy appear as ligand tails are chemically changed from branched to linear species at L/L interfaces; however, the extraction rates of water and sodium counter ions are faster for linear species, indicating that, at low coverages, the curvature imparted by tail branching is not as important as mobility and an ability for ligands to approach one another. Comparisons of ligands at L/L to A/L interfaces demonstrates the importance of oil-phase solvation in the organization and chemistry of L/L interface in that both the spectral response and adsorption thermodynamic behaviors are dramatically different. Data plotted in Figure 3 shows that the SFG spectra obtained are clearly different (relative peak amplitudes and H-bonding at high frequencies) and adsorption isotherm profiles equally so – indicating that approximations in using air as the non-polar phase do not reflect real liquid extraction systems due to critical, but missing, solvation interactions on the non-polar side of the interface. This was subsequently confirmed for the model amphiphile system described above (data not shown here) in that A/A interface does not provide the needed solvation on the oil phase to drive assembly into functional moieties capable of chemical separations.

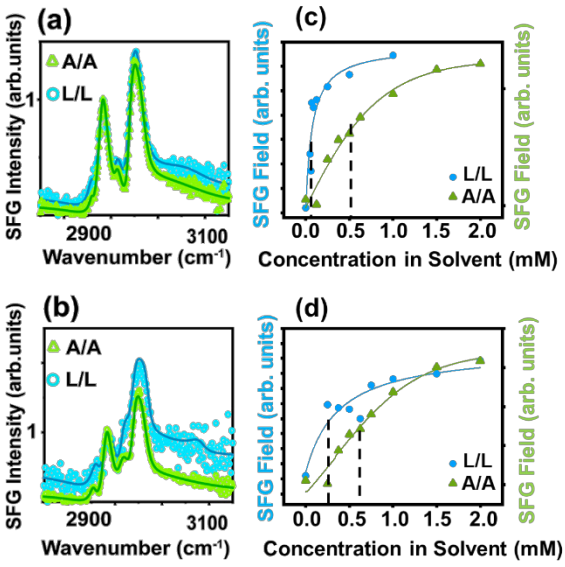

Figure 8: a) and c) show SFG spectra from the half-max of the adsorption isotherms b) and d) for two model ligands (DEHPA and DOP). Notably the spectral shapes (structure) and relative intensities (packing) are different between the interfaces, whereas the isotherms show the effect of oil-solvation in driving organization to stabilize the interface, which is not found at the air/aqueous interface.

We are also probing the effect of a model Au nanoparticle (NP) to the L/L interface to assess the role of curvature induced structural disorder at the interface and how it impacts chemical separations and overall transport. Here, we showed that Au-NPs impact substantial disorder to ligand decorated L/L interfaces through differential interactions with the coating or the hydrophilic portions of the NP to enable novel interfacial environment that facilitate transport. These interactions are central to separations science, in particular for waste remediation applications, and in the presence of non-ideal systems or those with colloidal species that can, and as we have demonstrated, create complex interfacial interactions and emergent synergies.

Finally, we have shown that the surfaces of bottlebrush and linear polymers relevant to membrane separations, are not strongly affected by molecular weight or architecture – this points to an invariance in the surface interactions that can be used in these materials to affect separations. This work is published in Langmuir and was selected as cover art (Figure 4). We show how flexibility of polymer interfaces allows for dynamics chemical and structural rearrangements in response to interfacial interactions. This study provided insights into the first steps in membrane-based separations that parallel those measurements made for liquid extractions. Along these lines, we have recently contributed spectroscopic measurements to elucidate the mechanism for enhanced binding strengths of polymers to silica materials. While not a separations science topic – the tools developed as part of this work were able to identify key interfacial interactions arising quickly and definitively from new H-bonding networks, that facilitate strong but reversible bonding. As such, this is a cross-program collaboration that leveraged tools from different communities to answer new science questions. This is an example of fundamental science enabling the understanding of real world/applied problems.

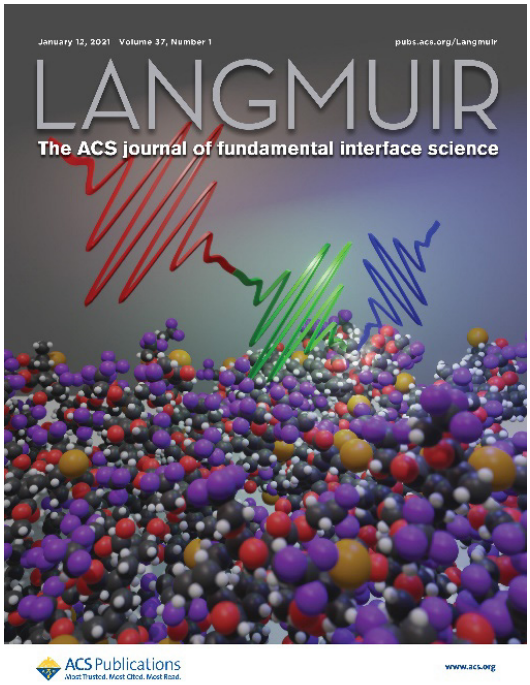

Figure 9: Cover art selected by the journal Langmuir, illustrating our work probing polymer interfaces for membrane separations.

Publications Acknowledging this FWP from 2018-present

†Advised postdoctoral researcher, *Corresponding author

(I) Exclusively funded by this grant

1. Chowdhury, A. U.†; Lin, L.†; Doughty, B.*; *Hydrogen-Bond-Driven Chemical Separations: Elucidating the Interfacial Steps of Self-Assembly in Solvent Extraction*. ACS Applied Materials & Interfaces 2020, 12, 28, 32119-32130 [DOI: 10.1021/acsami.0c06176]

(II) Jointly funded by this grant and other grants with leading intellectual contribution from this grant

1. Lin, L.,† Chowdhury, A. U.†, Ma, Y.-Z., Sacci, R. L., Katsaras, J., Hong, K., Collier, C. P., Carrillo, J.-M. Y.*, Doughty, B.*; *Ion Pairing Mediates Molecular Organization Across Liquid/Liquid Interfaces ACS Applied Materials & Interfaces*, 2021 **2021**, 13, 28, 33734–33743
2. Chowdhury, A. U.†, Chang, D., Xu, Y., Hong, K., Sumpter, B. G., Carrillo, J.-M. Y.*, Doughty, B.*; *Mapping the Interfacial Chemistry and Structure of Partially Fluorinated Bottlebrush Polymers and Their Linear Analogues*. Langmuir, **2021**, 37, 1, 211-218 Selected for Supplemental Cover Art [DOI: 10.1021/acs.langmuir.0c02786]

(III) Jointly funded by this grant and other grants with relatively minor intellectual contribution from this grant

1. Doughty, B.; Simpson M. J.; Das, S.; Xiao, K.; Ma, Y.-Z.*; *Connecting Femtosecond Transient Absorption Microscopy with Spatially Coregistered Time Averaged Optical Imaging Modalities.* Journal of Physical Chemistry A, **2020**, 124, 19, 3915-3923 [DOI: 10.1021/acs.jpca.9b11996] *Special issue in 'Time-Resolved Microscopy: A New Frontier in Physical Chemistry'*
2. Bocharova, V.; Jayakody, N.; Yang, J.; Sacci, R. L.; Yang, W.; Cheng, S.; Doughty, B.; Greenbaum, S.; Jeong, S. P.; Popov, I.; Zhao, S.; Gainaru, C.; Wojnarowska, Z.; *Modulation of Cation Diffusion by Reversible Supramolecular Assemblies in Ionic Liquid-Based Nanocomposites*. ACS Applied Materials & Interfaces **2020**, 12, 28, 31842-31851 [DOI: 10.1021/acsami.0c08323]

Binding Anions Selectively with Modular Triazolophanes and Releasing Them with Light

Amar H Flood and Krishnan Raghavachari , Department of Chemistry, Indiana University, Bloomington, IN

Presentation Abstract

Anion recognition with shape-persistent and shape-dynamic receptors offers a platform to transfer concepts from biology to synthetic systems for functional, smart, and responsive recognition. Here we seek to control and to deeply understand the binding affinity and selectivity of both rigid and flexible receptors in the form of macrocycles, cages, and foldamers. Fundamental efforts have been focused on using coupled experiment-theory approaches to test the canonical model of host-guest chemistry by measuring the energy of organization, an otherwise "dark" concept that is difficult to quantify and to learn how solvent impacts binding with size-selective binding. We have been synthetically elaborating the variety of receptors including new bis-lariat macrocycles that will enable introduction of switching modalities. Towards photoswitchable receptors, we have been tuning up the sequences of foldamers to drive double helices that offer on-off regulation of cooperativity for anion binding/releases. These topics will be covered in four posters.

Gas Transport Properties in Poly(benzimidazoles)

*Julian M. Richardson and **Benny D. Freeman**, The University of Texas at Austin, McKetta Department of Chemical Engineering*

Abstract

Several high temperature membrane-based gas separation technologies have been proposed to reduce the release of carbon dioxide into the atmosphere. For example, steam reforming of hydrocarbons produces a mixture of H_2 and CO_2 at high temperatures. If the CO_2 could be separated and sequestered, the H_2 could be used as, for example, an energy carrier. Poly(benzimidazole) (PBI) polymers exhibit high thermal and chemical stability and interesting gas transport properties at elevated temperatures. However, many fundamental polymer properties, such as rates of physical aging, are unknown at such conditions. This study focuses on understanding fundamental physical aging properties of PBIs at high temperatures and investigates the viability of a new processing technique of preparing PBI membranes produced by a polyphosphoric acid (PPA) process.

Grant Number: DE-FG02-02ER15362
Grant Title: Fundamental Structure/Property Studies of New Gas Separation Membrane Polymers

RECENT PROGRESS

Physical aging of PBI films

It is well known that thin films age differently than bulk films. This phenomenon has been investigated for many polymers at or near room temperature. However, studies which include the impact of aging temperature are very limited. Measuring aging of thin film PBI samples at multiple temperatures can shed light on how polymer relaxation times change with temperature far below T_g, which remains a subject of debate in the literature.

H_2, N_2, and CH_4 gas permeabilities of *m*-PBI thin films were measured over the course of 2000 hours at 190 °C, 175 °C, and 150 °C. All three gases exhibited qualitatively similar behavior, so only N_2 gas permeabilities (normalized relative to the bulk film permeability at each temperature) are presented in **Figure 1**.

The change in permeability with time exhibits different trends based on the measurement temperature. For example, after only 300 hours of aging, N_2 permeability of the film aged at 190°C reaches an apparent plateau 70% lower than its bulk film permeability. The permeability remained at this value for the remaining 1200 hours of aging. At 175 °C, the permeability decreased at most modestly for the first 200 hours of aging. From 200 to 1000 hours, the gas permeability decreased linearly with logarithmic time, like the reduction

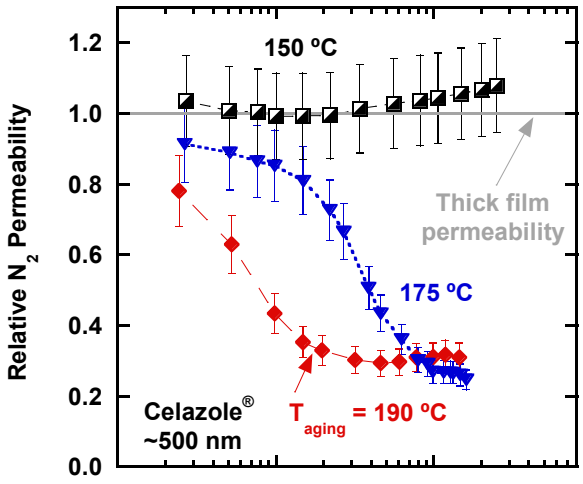

Figure 10. N_2 permeability relative to bulk film permeability vs. aging time

rate observed initially at 190 °C. After 1000 hours, the permeability decrease slowed dramatically. At 150 °C, the permeability remained practically constant for the entire 2500 hours of aging, suggesting little or no aging or that any physical aging would occur beyond the length of time probed in this experiment.

To provide a qualitative assessment of how rapid the aging process was, permeability reduction rates were calculated for portions of the experiment where reduction rates were linear with logarithmic time (cf., **Table 1**), such as between 50 and 100 hours at 190 °C and between 200 and 1000 hours at 175 °C in **Figure 1**. In most cases, the permeability reduction rates are similar for each gas at both temperatures considered, while relative permeability reduction rates are similar between N_2 and CH_4 at each temperature.

Permeability reduction rate	190 ºC	175 ºC
$-\left(\frac{d\,P_{N_2}}{d\,\log_{10} t}\right)$	0.12 ± 0.003	0.12 ± 0.003
$-\left(\frac{d\,P_{CH_4}}{d\,\log_{10} t}\right)$	0.078 ± 0.002	0.087 ± 0.002
$-\left(\frac{d\,P_{H_2}}{d\,\log_{10} t}\right)$	10.0 ± 0.5	10.8 ± 2.0
$-\left(\frac{d\,rel\,P_{N_2}}{d\,\log_{10} t}\right)$	0.72 ± 0.02	0.94 ± 0.02
$-\left(\frac{d\,rel\,P_{CH_4}}{d\,\log_{10} t}\right)$	0.74 ± 0.02	1.13 ± 0.02
$-\left(\frac{d\,rel\,P_{H_2}}{d\,\log_{10} t}\right)$	0.41 ± 0.002	0.53 ± 0.03

Note: Permeability is in Barrer, and t is in hours.
Table 2. Rate of change of permeability with the logarithm of aging time during period of rapid physical aging for ~500-nm *m*-PBI membranes.

Until now, a plateau possibly indicating the end of physical aging has not been reported for a polymer aged more than 250 °C below its T_g. Time-temperature superposition was used to calculate shift factors of the permeability reduction relative to the relaxation behavior at T_g (cf., **Figure 2**). From the shift factors, an *m*-PBI thin film membrane aged at 175 °C is predicted to reach its equilibrium permeability at ~1800 hours. Aged at 150 °C, the equilibration time is predicted to be >288,000 hours (33 years).

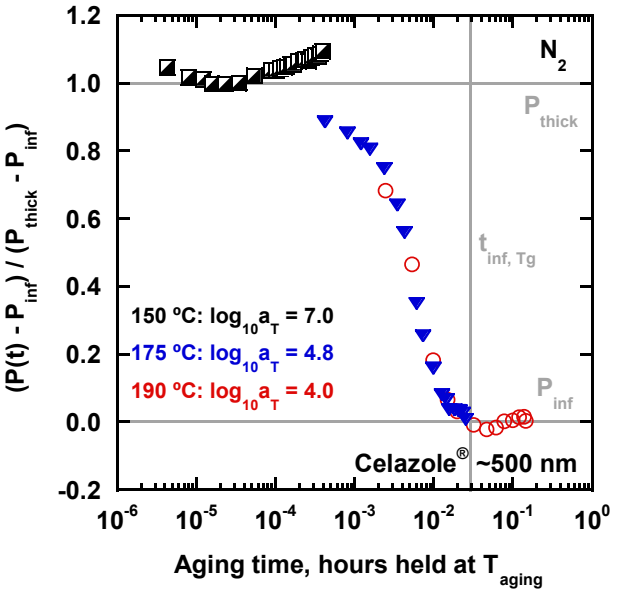

Figure 11. Time-temperature superposition of normalized permeability reductions

Novel processing of PBI films

In previous work, TADPS-based PBIs were found to have similar properties to *m*-PBI while also increasing the material's solubility in organic solvents, making PBIs easier to solution

process into membranes. Along these lines, we have also studied a new method to readily prepare bulk PBI membranes using non-organic solvents. In this method, a polyphosphoric acid (PPA) solution is directly cast into a thick film after polymerization. Humidity from the air naturally hydrolyzes the PPA to phosphoric acid, a poor solvent for PBI, solidifying the membrane. The three-step method of polymerizing, casting, and hydrolyzing the solvent is referred to as the PPA process. Recently, a densification step that can be used to remove the acid and densify the PBI structure was discovered. In this process, the acid-imbued film was clamped between two porous sheets of polyethylene and soaked in a series of water baths of varying basicity, thereby neutralizing and removing the solvent. This procedure is simple and bypasses dissolution of PBI into a volatile organic solvent, broadening the range of PBI-based materials that can be processed into membranes. One new chemistry used in this study is *p*-PBI (cf., **Figure 3**).

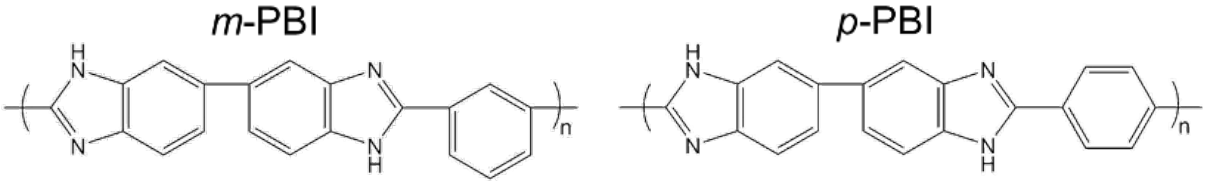

Figure 12. *m*-PBI, commercially available Celazole® and *p*-PBI, a novel PBI that can be prepared as a dense film via the PPA process

Gas separation performance and other properties of *p*-PBI were explored. The H_2/CO_2 upper bound in **Figure 4** presents *p*-PBI and *m*-PBI permeability values at high temperature for comparison.

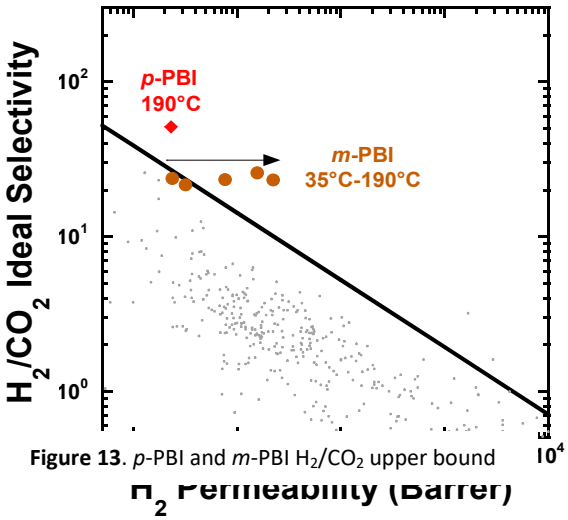

Figure 13. *p*-PBI and *m*-PBI H_2/CO_2 upper bound

Usually, aromatic polymers with para-connected rings exhibit higher glass transition temperature (T_g), higher FFV, and higher permeability than meta-connected analogs. It is believed that relatively facile flipping of the para-connected rings can increase the free volume of the system, leading to a higher permeability for para-linked isomers relative to meta-linked isomers. Similar ring-flipping motions for meta-linked isomers are more hindered than those for para-linked isomers. *p*-PBI seems to run contrary to this trend as it has lower permeability than the meta-linked isomer. X-ray diffraction, dynamic mechanical analysis, and density data in **Table 2** show *p*-PBI has a higher T_g, lower d-spacing than *m*-PBI, and higher density, consistent with the para-connected analog having more restricted local scale molecular motion than the meta-substituted analog.

	DMA	XRD	Density
	T_g (°C)	d-spacing (nm)	ρ (g/cm^3)
m-PBI	459	0.405*	1.294
p-PBI	>540	0.35	1.366

* *Literature value*

Table 3. Dynamic Mechanical Analysis, X-Ray Diffraction, and density results for *m*-PBI and *p*-PBI

Publications Acknowledging this Grant in 2015 – present

(I) Exclusively funded by this grant

1. Merrick, M. M.; Sujanani, R.; Freeman, B. D., Glassy polymers: Historical findings, membrane applications, and unresolved questions regarding physical aging. *Polymer*. **2020**, *211*, 123176.
2. Stevens, K. A.; Moon, J. D.; Borjigin, H.; Liu, R.; Joseph, R. M.; Riffle, J. S.; Freeman, B. D., Influence of temperature on gas transport properties of tetraaminodiphenylsulfone (TADPS) based polybenzimidazoles. *Journal of Membrane Science*. **2020,** *593*, 117427.
3. Dose, M. E.; Chwatko, M.; Hubacek, I.; Lynd, N. A.; Paul, D. R.; Freeman, B. D., Thermally cross-linked diaminophenylindane (DAPI) containing polyimides for membrane based gas separations. *Polymer*. **2019**, *161*, 16-26.
4. Stevens, K. A.; Smith, Z.P.; Gleason, K. L.; Galizia, M.; Paul, D. R.; Freeman, B.D. Influence of temperature on gas solubility in thermally rearranged (TR) polymers. *J. Membrane Sci.* **2017**, *533*, 75-83.
5. Galizia, M.; Stevens, K. A.; Smith, Z. P.; Paul, D. R.; Freeman, B. D. Nonequilibrium Lattice Fluid Modeling of Gas Solubility in HAB-6FDA Polyimide and Its Thermally Rearranged Analogues. *Macromolecules*. **2016**, *49, 22*, 8768-8779.

(II) Jointly funded by this grant and other grants with leading intellectual contribution from this grant

1. Moon, J. D.; Bridge, A. T.; D'Ambra, C.; Freeman, B. D.; Paul, D. R. Gas separation properties of polybenzimidazole/thermally-rearranged polymer blends. Journal of Membrane Science. *J. Membrane Sci.* **2019**, *582*, 182-193.
2. Joseph, R. M.; Merrick, M. M.; Liu, R.; Fraser, A. C.; Moon, J. D.; Choudhury, S. R.; Lesko, J.; Freeman, B. D.; Riffle, J. S., Synthesis and characterization of polybenzimidazole membranes for gas separation with improved gas permeability: A grafting and blending approach. *J. Membrane Sci.* **2018**, *564*, 587-597.
3. Moon, J. D.; Galizia, M.; Borjigin, H.; Liu, R.; Riffle, J. S.; Freeman, B. D.; Paul, D. R. Water vapor sorption, diffusion, and dilation in polybenzimidazoles. *Macromolecules*. **2018**, *51*, 7197-7208.
4. McGinnis, R. L.; Reimund, K.; Ren, J.; Xia, L.; Chowdhury, M. R.; Sun, X.; Abril, M.; Moon, J. D.; Merrick, M. M.; Park, J.; Stevens, K. A.; McCutcheon, J. R.; Freeman, B. D. Large scale polymeric carbon nanotube membranes with sub-1.27 nm pores. *Sci. Adv*. **2018**, *4*, e1700938.
5. Galizia, M.; Stevens, K. A.; Paul, D. R.; Freeman, B. D. Modeling gas permeability and diffusivity in HAB-6FDA polyimide and its thermally rearranged analogs. *J. Membrane Sci.* **2017,** *537*, 83-92.
6. Robeson, L. M.; Dose, M. E.; Freeman, B. D.; Paul, D. R. Analysis of the transport properties of thermally rearranged (TR) polymers and polymers of intrinsic microporosity (PIM) relative to upper bound performance. *J. Membrane Sci.* **2017,** *525*, 18-24.
7. Liu, Q.; Galizia, M.; Gleason, K. L.; Scholes, C. A.; Paul, D. R; Freeman, B. D. Influence of toluene on CO_2 and CH_4 gas transport properties in thermally rearranged (TR) polymers based on 3,3′-dihydroxy-4,4′-diamino-biphenyl (HAB) and 2,2′-bis-(3,4-dicarboxyphenyl) hexafluoropropane dianhydride (6FDA). *J. Membrane Sci.* **2016**, *514*, 282-293.
8. Liu, Q.; Paul, D. R.; Freeman, B. D. Gas permeation and mechanical properties of thermally rearranged (TR) copolyimides. *Polymer*. **2016**, *82*, 378-391.
9. Liu, Q.; Shaver, A. T.; Chen, Y.; Miller, G.; Paul, D. R.; Riffle, J. S.; McGrath, J. E.; Freeman, B. D. Effect of UV irradiation and physical aging on O_2 and N_2 transport properties of thin glassy poly(arylene ether ketone) copolymer films based on tetramethyl bisphenol A and 4,4′-difluorobenzophenone. *Polymer*. **2016**, *87***,** 202-214.

10. Liu, Q.; Borjigin, H.; Paul, D. R.; Riffle, J. S.; McGrath, J. E.; Freeman, B. D. Gas permeation properties of thermally rearranged (TR) isomers and their aromatic polyimide precursors. *J. Membrane Sci.* **2016**, *518*, 88-99.
11. Borjigin, H.; Stevens, K. A.; Liu, R.; Moon, J. D.; Shaver, A. T.; Swinnea, S.; Freeman, B. D.; Riffle, J. S.; McGrath, J. E., Synthesis and characterization of polybenzimidazoles derived from tetraaminodiphenylsulfone for high temperature gas separation membranes. *Polymer*. **2015**, *71*, 135-142.
12. Galizia, M.; Smith, Z. P.; Sarti, G. C.; Freeman, B. D.; Paul, D. R., Predictive calculation of hydrogen and helium solubility in glassy and rubbery polymers. *J. Membrane Sci.* **2015**, *475*, 110-121.
13. Smith, Z.P.; Hernández, G.; Gleason, K. L.; Anand, A.; Doherty, C. M.; Konstas, K.; Alvarez, C.; Hill, A. J.; Lozano, A. E.; Paul, D. R.; Freeman, B. D. Effect of polymer structure on gas transport properties of selected aromatic polyimides, polyamides and TR polymers. *J. Membrane Sci.* **2015**, *493*, 766-781.
14. Gleason, K. L.; Smith, Z. P.; Liu, Q.; Paul, D. R.; Freeman, B. D. Pure- and mixed-gas permeation of CO_2 and CH_4 in thermally rearranged polymers based on 3,3′-dihydroxy-4,4′-diamino-biphenyl (HAB) and 2,2′-bis-(3,4-dicarboxyphenyl) hexafluoropropane dianhydride (6FDA). *J. Membrane Sci.* **2015,** *475*, 204-214.

(III) Jointly funded by this grant and other grants with relatively minor intellectual contribution from this grant

1. Nebipasagil, A.; Park, J.; Lane, O. R.; Sundell, B. J.; Mecham, S. J.; Freeman, B. D.; Riffle, J. S.; McGrath, J. E. Polyurethanes containing Poly(arylene ether sulfone) and Poly(ethylene oxide) segments for gas separation membranes. *Polymer*. **2017**, *118*, 256-267.
2. Park, H. B.; Kamcev, J.; Robeson, L. M.; Elimelech, M.; Freeman, B. D. Maximizing the right stuff: The trade-off between membrane permeability and selectivity. *Science*. **2017,** *356*, 6343.

Raman Microscopy for Investigating Separation Processes within Porous Materials

Joel M. Harris, Jay P. Kitt, David A. Bryce, Maryam Zare, University of Utah – Department of Chemistry Salt Lake City, UT 84112

Presentation Abstract

In the development of new separation media, it is critical to understand how their interface composition and structure relate to their functioning for selective solute retention and separations. Confocal Raman microscopy has been adapted to examine the interior surfaces of both porous chromatographic particles and polymer films, reporting information on the structure of their interfaces and interactions with solute molecules related to their applications in chemical separations. The spatial resolution of confocal collection optics can selectively probe the *internal composition* of individual porous particles or thin films, yielding quantitative information on populations of molecules at interfaces within their pores. The technique is an *in situ* method, so that interfacial structure and composition can be monitored as conditions are varied. We apply this methodology to studies of assembly of hybrid-lipid bilayers onto n-alkyl-chain modified porous silica surfaces; these biomimetic materials can be used for separations based on the lipid-membrane affiliation of solutes with these model-membrane surfaces. Raman spectroscopy provides insight on the conformations of the acyl chains of the lipid layer, and how these conformations change with temperature and the partitioning of analytes. Assembly of supported-lipid bilayers on bare silica and lipid monolayers on nitrile-derivatized silica surfaces was also explored; the structures of these sorbent phases and their retention and selectivity for model solutes have been investigated. Mixed-charge surfactant monolayers on n-alkane-modified silica surfaces have produced similar interfacial structures as zwitterionic phospholipids. Hybrid-supported lipid bilayers produce n-alkyl chain ordering that can be systematically varied with the acyl chain length and degree of saturation of the phospholipid monolayer; this chain-ordering provides control over shape-selective separations of planar versus non-planar PAH compounds. Finally, the confocal Raman microscopy methods developed in our lab have been used in collaboration with Carol Korzeniewski at Texas Tech University to investigate the composition, structure, and ionic selectivity of porous polymer membranes that are employed as ion separators in fuel-cell applications.

DE-FG03-93ER14333: Analytical Spectroscopy Methods for Liquid/Solid Interfaces

PI: Joel M. Harris
Postdocs: Jay P. Kitt, Maryam Zare
Students: David A. Bryce, Maryam Zare, Allison Jacobsen, Aric Potter.
Faculty Collaborators: Carol Korzeniewski, Texas Tech University; Emily Heider, Utah Valley University.

RECENT PROGRESS (2019 – 2021)

Probing interior surface chemistry of porous materials: lipid-membrane-affinity based separations. Most practical applications of liquid/solid interfaces to chemical separations, including extraction, environmental remediation, chromatography, and membrane fractionation, are carried out in porous media. The high specific surface area of porous materials provides surface capacity but makes them challenging to investigate because most of the surface lies *within the interior*, making it inaccessible to traditional surface-selective spectroscopies. With DOE support, the Harris lab has pioneered the application of confocal-Raman microscopy to probe the interior composition and interface structure within porous particles [1,5] and porous polymer films [3], providing *in-situ* vibrational spectra from inside of these materials in sampling volumes of 10^{-15} L or less [8] (Figure 1). Confocal Raman microscopy has allowed investigation of a novel approach to separations based on lipid-membrane affinity, where a model lipid bilayer is supported on the interior surfaces of porous particles. These hybrid bilayers are produced through the self-assembly of a phospholipid monolayer on n-alkane-modified silica surfaces within porous particles and used for lipophilic separations of small molecules. To investigate this interfacial chemistry, we employ confocal Raman microscopy to observe the structure of hybrid-phospholipid bilayers on C_{18}-modified porous silica surfaces and their interactions with model solutes in separation applications. We applied this methodology to determine how these membrane-mimetic structures assemble onto the C_{18}–derivatized silica surfaces of reversed-phase chromatographic silica particles. Confocal Raman microscopy reports the time-dependent internal interfacial composition and structure within individual silica particles. The Raman scattering data were resolved into component Raman spectra and corresponding composition vectors that describe the time-dependent changes of the component spectra. This analysis (Figure 1) provided insight into how the structures of both the lipid and C_{18} alkyl chains of hybrid lipid bilayers evolve during deposition, formation, and organization on the internal surfaces of reversed-phase chromatographic silica particles [11].

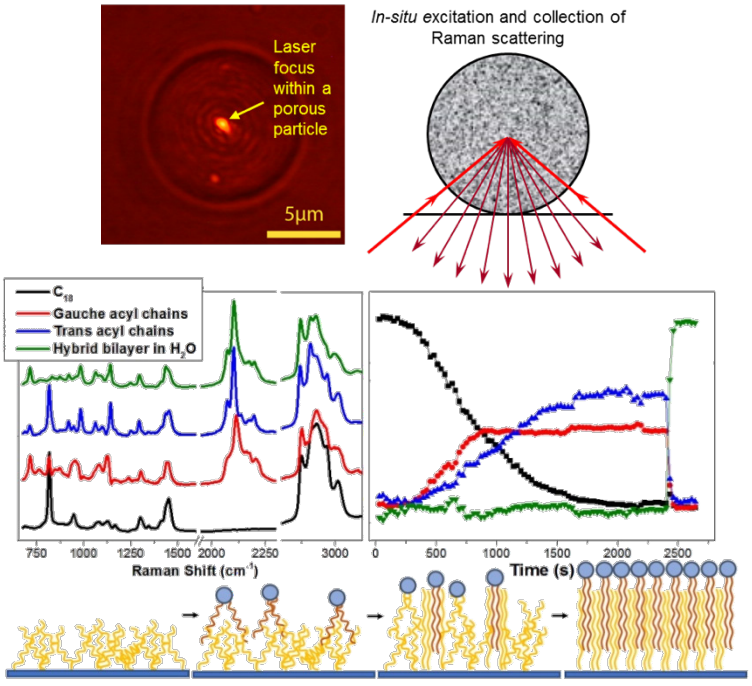

Figure 1. Raman scattering collected from within a single porous silica particle (top) during the adsorption, assembly, and ordering of a hybrid phospholipid bilayer on the C_{18}-modified surface [11].

Other hybrid models of lipid membranes for separations. Hybrid supported-phospholipid bilayers are stable membrane models for lipophilic separations prepared by self-assembly of a lipid monolayer over an n-alkane modified surface. The structure of these hybrid bilayers differs from vesicle membranes, having a greater lipid head-group spacing due to interdigitation of the lipid acyl chains with the underlying n-alkyl chains bound to the silica surface. This interdigitated structure exhibits a broader melting transition at higher temperature due to strong interactions between the lipid acyl chains and the immobile n-alkyl chains bound to silica. We recently sought to reduce the interactions between a lipid monolayer and its supporting substrate by self-assembly of 1,2-dimyristoly-sn-glycero-3-phosphocholine (DMPC) on porous silica functionalized with nitrile-terminated surface ligands. The frequency of Raman scattering of the surface -C≡N stretching mode at the lipid-nitrile interface is consistent with an n-alkane-like environment and insensitive to lipid head-group charge (Figure 2), indicating that the lipid acyl chains are in contact with the surface-nitrile groups. The head-group area of this lipid monolayer was determined from the within-particle phospholipid concentration and silica specific surface area and found to be equivalent to the head-group area of a DMPC vesicle bilayer. The structure of these nitrile-supported phospholipid monolayers was characterized below and above their melting transition by confocal-Raman microscopy and found to be nearly identical to DMPC vesicle bilayers. Their narrow gel-to-fluid-phase melting transition was equivalent to dispersed DMPC-vesicles, suggesting that the acyl-chain structure on the nitrile support mimics the outer leaflet structure of a vesicle membrane [12].

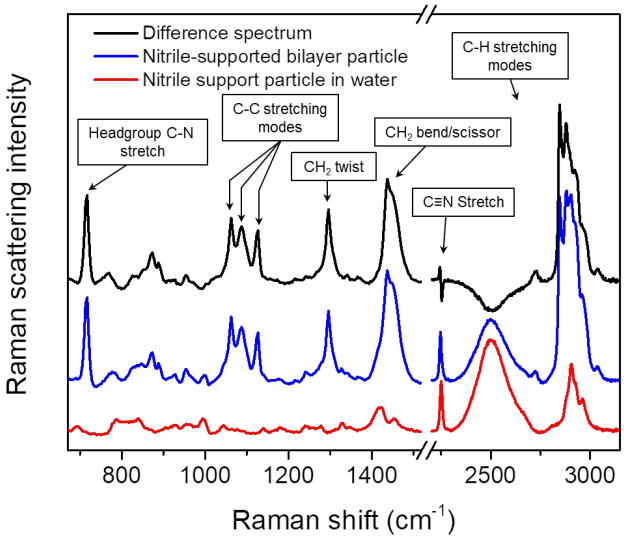

Figure 2. Raman spectra from a nitrile-support particle in water before (red) and after (blue) DMPC accumulation. Difference spectrum (black) shows phospholipid Raman bands, and a shift in the–C≡N stretching frequency (~2250 cm^{-1}) due to changes in interfacial environment.

Despite utility of membrane-mimetic hybrid-lipid bilayer interfaces for separation applications, the cost of phospholipids required to modify C_{18}- or nitrile-silica surfaces is high. We have sought less costly alternatives for membrane-like modification of C_{18}-silica surfaces by mimicking the interfacial structure of zwitterionic phosphatidylcholine lipids. To meet this goal, we have assembled stable monolayers of oppositely-charged long-chain surfactants on C_{18}-modified silica. The structure of these hybrid-supported *surfactant* bilayers on C_{18}-modified silica surfaces is similar to that of hybrid-lipid bilayers but with denser and more-ordered *n*-alkyl chains. Hybrid-supported surfactant bilayers exhibit a melting phase transition (gel to liquid-crystalline phase) with structural and energetic characteristics similar to hybrid-supported lipid bilayers prepared from a zwitterionic phospholipids of the same alkyl chain length. These mixed-charge surfactants on *n*-alkane modified silica are stable in water over time (months), results that suggest their potential use in separation applications [13].

Partitioning into small molecules into model phospholipid bilayers. The phospholipid-water partition coefficient is a commonly measured parameter that correlates with small-molecule toxicity and persistence of molecules in the environment, including compounds that derive from energy production. To address this issue, we employed *in-situ* confocal Raman microscopy to probe the partitioning of membrane-active compounds into hybrid-bilayers (lipid on C_{18}-silica) and into supported-phospholipid bilayers deposited on the pore walls of bare silica surfaces. Quantitative determination of lipid partitioning separations is achieved by using the phospholipid acyl-chains of the within-particle bilayer as an internal standard [6]. We also employed lipid-modified C_{18} stationary phases as a means of systematically varying n-alkyl chain order to control shape-selective separations. The degree of alkyl-chain order of the lipid-modified surfaces was controlled by the acyl chain length and degree of saturation of the phospholipid monolayer and quantified by the ratio of trans- versus gauche-conformers measured within individual particles by confocal Raman microscopy. This methodology was also used to assess the affinity of these surfaces for planar versus non-planar PAH molecules. The retention selectivity for planar versus non-planar compounds, thus determined, was found to vary significantly with the degree of order of the acyl/alkyl chains in hybrid-supported lipid bilayers. The results also showed the impact of solute partitioning on stationary-phase structure within porous particles [16].

Probing porous polymer separation membranes. In a very productive collaboration with Carol Korzeniewski from Texas Tech and Steve Creager from Clemson University, we have applied *in-situ* confocal-Raman microscopy in our lab to investigate the composition, structure, and ionic selectivity of porous polymer membranes that are employed as separators in fuel-cell applications. Single-layer graphene (one atomic-layer thick) was found to be an ideal thin-film material to characterize the axial spatial resolution in depth profiling by confocal Raman microscopy, useful for interpreting the depth-dependent composition of porous membranes or polymer thin films [8]. When sandwiched in porous polymer proton-exchange membranes, single-layer graphene was found to confer 100-fold faster proton transmission compared to any other cations; confocal Raman microscopy played a key role both in confirming the single-layer structure of the graphene separator and in characterizing its ability to preserve cationic separation between the two halves of the membrane sandwich [9].

Publications acknowledging this grant in 2017 – present

1. Bryce, D. A.; Kitt, J. P.; Harris, J. M. Confocal Raman Microscopy Investigation of Molecular Transport into Individual Chromatographic Silica Particles. *Anal. Chem.* **2017,** *89*, 2755-2763. *(I)*
2. Kitt, J. P.; Bryce, D. A.; Minteer, S. D.; Harris, J. M. Raman Spectroscopy Reveals Selective Interactions of Cytochrome c with Cardiolipin That Correlate with Membrane Permeability. *J. Amer. Chem. Soc.* **2017,** *139*, 3851-3860. *(I)*
3. Korzeniewski, C.; Liang, Y.; Zhang, P.; Sharif, I.; Kitt, J. P.; Harris, J. M.; Hamrock, S. J.; Creager, S. E.; DesMarteau, D. D. Vibrational Spectroscopy for the Determination of Ionizable Group Content in Ionomer Materials. *Appl. Spectrosc.* **2018,** *72*, 141-150. *(I)*
4. Bukola, S.; Liang, Y.; Korzeniewski, C.; Harris, J. M.; Creager, S. E. Selective proton/deuteron transport through Nafion | graphene | Nafion sandwich structures at very high current density. *J. Amer. Chem. Soc.* **2018,** *140*, 1743-1752. *(III)*
5. Bryce, D. A.; Kitt, J. P.; Harris, J. M. Confocal-Raman Microscopy Characterization of Supported Phospholipid Bilayers Deposited on the Interior Surfaces of Chromatographic Silica. *J. Amer. Chem. Soc.* **2018,** *140*, 4071-4078. *(I)*

6. Kitt, J. P.; Bryce, D. A.; Minteer, S. D.; Harris, J. M. Confocal Raman Microscopy for *In-Situ* Measurement of Phospholipid–Water Partitioning into Model Phospholipid Bilayers within Individual Chromatographic Particles. *Anal. Chem*. **2018,** *90*, 7048-7055. *(I)*
7. Bryce, D. A.; Kitt, J. P.; Harris, J. M. Confocal Raman Microscopy for Label-Free Detection of Protein−Ligand Binding at Nanopore-Supported Phospholipid Bilayers. *Anal. Chem*. **2018**, *90*, 11509−11516. *(II)*
8. Korzeniewski, C.; Kitt, J. P.; Bukola, S.; Creager, S.; Minteer, S. D.; Harris, J. M. Single-Layer Graphene for Estimation of Axial Spatial Resolution in Confocal Raman Microscopy Depth Profiling. *Anal. Chem.* **2019,** *91*, 1049-1055. *(II)*
9. Bukola, S.; Beard, K.; Korzeniewski, C.; Harris, J. M.; Creager, S. E. Single-Layer Graphene Sandwiched between Proton-Exchange Membranes for Selective Proton Transmission. *ACS Appl. Nano Mater.* **2019,** *2*, 964-974. *(III)*
10. Liang, Y; Cai, R.; Hickey, D. P.; Kitt, J. P.; Harris, J. M.; Minteer, S. D.; Korzeniewski, C. Infrared Microscopy as a Probe of Composition within a Model Biofuel Cell Electrode Prepared from *Trametes versicolor* Laccase. *Chem. Electro. Chem*. **2019,** *6*, 818–826. *(III)*
11. Kitt, J. P.; Bryce, D. A.; Minteer, S. D.; Harris, J. M. Confocal Raman Microscopy Investigation of Self-Assembly of Hybrid Phospholipid Bilayers within Individual Porous Silica Chromatographic Particles. *Anal. Chem.* **2019**, *91*, 7790-7797. *(I)*
12. Bryce, D. A; Kitt, J. P.; Myres, G. J. and Harris, J. M. Confocal Raman Microscopy Investigation of Phospholipid Monolayers Deposited on Nitrile-Modified Surfaces in Porous Silica Particles. *Langmuir*, **2020**, *36*, 4071-4078. *(II)*
13. Gao, R.; Edwards, M. A.; Harris, J. M.; White, H. S. Shot noise sets the limit of quantification in electrochemical measurements. *Current Opinion in Electrochemistry* **2020**, *22*, 170-177. *(III)*
14. Zare, M.; Kitt, J. P.; Harris, J. M. Hybrid-Supported Bilayers Formed with Mixed-Charge Surfactants on C_{18}-Functionalized Silica Surfaces. *Langmuir* **2020**, *36*, 7609-7618. *(I)*
15. Liang, Y.; Kitt, J.P.; Minteer, S.D.; Harris, J.M.; Korzeniewski, C. Vibrational Spectroscopic Monitoring of the Gelation Transition in Nafion Ionomer Dispersions. *Appl. Spectrosc.* **2020**, *75*, 376-384. *(III)*
16. Zare, M.; Kitt, J. P.; Wen, X.; Heider, E. C.; Harris, J. M. Hybrid-Lipid Bilayers Induce n-Alkyl-Chain Order in Reversed-Phase Chromatographic Surfaces, Impacting their Shape Selectivity for Aromatic Hydrocarbon Partitioning. *Anal. Chem.* **2021**, *93*, 4118-4125. *(I)*

(III) Exclusively funded by this grant.
(IV) Jointly funded by this grant and other grants with leading intellectual contributions from this grant.
(V) Jointly funded by this grant and other grants with relatively minor intellectual contributions from this grant.

Understanding and Control of Reactive Separations

David J. Heldebrant,[1] Vanda Glezakou,[1] Leo Bañuelos,[2] Sarah Allec,[1] Loukas Kollias,[1] Difan Zhang,[1] Jotheeswari Kothandaraman,[1] Deepika Malhotra,[1] Melissa Manetsch,[3] Omar Avina.[2]

1. Pacific Northwest National Laboratory, 2. University of Texas, El Paso, 3. University of Illinois Champaign Urbana

Presentation Abstract

Acid gases such as CO_x, NO_x, and SO_x are ubiquitous pollutants formed as byproducts of power generation, transportation, and manufacturing. Viable processes to separate acid gases from emission plumes or the atmosphere can only achieve sufficient energy efficiencies through transformative advances in our understanding of reactivity and transport in complex media. Reactive separations, by design, enable coupled separation and conversion processes in the same medium for increased energy efficiency. We present here results of a recently launched integrated experimental and theoretical research program to predict, design, and construct bespoke nanostructures within separation media and to control the interactions that govern the energy efficiency and reactivity of acid gas separations. An understanding of how gas absorption creates hierarchical ordering in solvents will help us gain control over diffusion and chemical complexation in reactive separations so that we can tune reaction free energetics, kinetics, and mass transport. We will achieve this control through our proposed work in three synergistic research objectives: (1) controlling nanoscale structuring, (2) driving far-from-equilibrium separations, and (3) creating new reactive pathways for separations of acid gases. Ultimately, these molecular-level insights will be applicable to design more efficient gas/liquid separations.

Grant or FWP Number: FWP 75428

Postdoc(s): Sarah Allec,[1] Loukas Kollias,[1] Difan Zhang.[1]
Undergraduate Students: Melissa Manetsch,[3] Omar Avina.[2]
Affiliations(s): 1. Pacific Northwest National Laboratory. 2. University of Texas, El Paso, 3. University of Illinois Champaign Urbana

RECENT PROGRESS

Our project is currently in its first year of funding, and we have spent the past half-year refining our integrated experimental and theoretical approach, more specifically the utilization of advanced spectroscopic techniques (neutron, X-ray) and theory (molecular dynamics) used to predict the feasibility of certain reaction types. Our primary aim is to utilize these techniques so we can learn how to control the hierarchical ordering to gain control over gas diffusion and design new reactivities of gases chemically fixated in water-lean solvents.

Self-assembly of hierarchical liquid structures drives transport and fixation of CO_2.

We have hypothesized that the fast CO_2 uptake and mass transfer inherent to water-lean solvents is due to the formation of channels, which were first observed through theoretical and experimental mechanistic studies.[1] In this context, we are now investigating the atomic arrangement using wide angle x-ray scattering (WAXS) and x-ray and neutron diffraction pair distribution function (PDF) analysis, in conjunction with classical molecular dynamics (MD) simulations. *Ortho*-, *meta*-, and *para*- substituent variants have been investigated as a function of CO_2 loading and temperature. While PDF analysis is being used to differentiate between the atomic structure of the nonloaded neutral liquid and the zwitterion structure resulting from CO_2 uptake, WAXS has thus far allowed detailed examination of changes in intermediate range ordering, *i.e.,*

possible channel formation, which could be responsible for the fast CO_2 uptake. Figure 9 (left) shows an intermediate range ordering (IRO) correlation of 9.0-9.5 Å for the nonloaded liquids, with the correlation becoming larger with CO_2 uptake, in the following increasing order: ortho-, meta-, para-. Additionally, the average solvent nearest neighbor distance is observed to decrease (Figure 9, middle) with CO_2 uptake. X-ray PDF experiments were carried out at BNL's NSLS-II beamline 28-ID-1, and neutron PDF using the ORNL SNS NOMAD instrument[2] (BL-1B) (Figure 9, right). Differences in neutron vs x-ray scattering sensitivity to our systems (Figure 9, bottom right) should help to obtain a refined structural model for comparison with computational efforts. MD simulations, and first-order difference analysis combined with EPSR[3-7] simulations of the experimental results, are underway to understand how the molecular-scale orientations and correlations of the CO_2-bound and neutral species of the heterogeneous composition of this liquid give rise to the observed IRO.

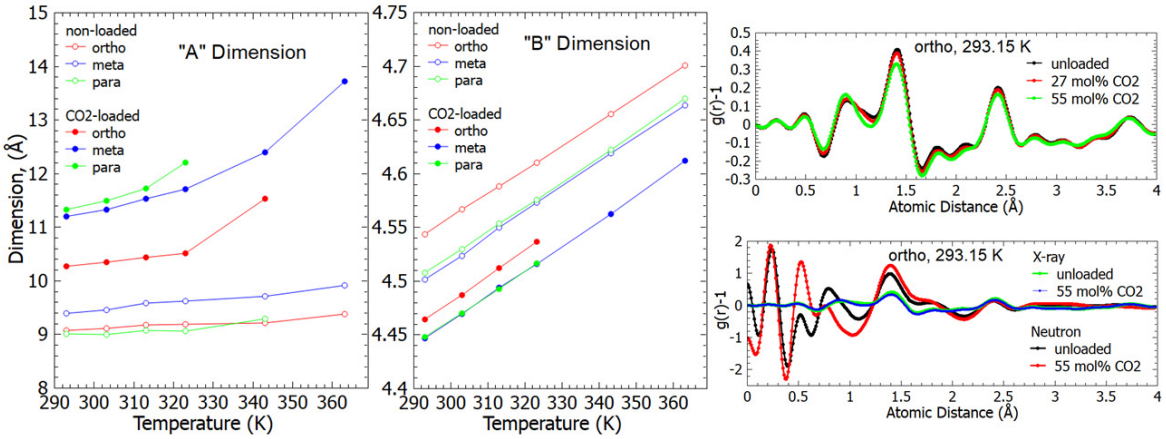

Figure 14. WAXS and x-ray and neutron PDFs of non-loaded and CO_2 bound liquids. (Left): WAXS shows IRO in non-loaded solvents compared with CO_2 loaded solvents. Increase in IRO distance due to CO_2 uptake varies as ortho- < meta- < para-. (Middle): WAXS shows that the average nearest neighbor correlation distance decreases with CO_2 uptake. (Right, top): X-ray PDF of ortho- system in 0, 27, and 55 mol% CO_2 loading conditions as well as (Right, bottom) comparison with neutron PDF. Efforts are underway to link atomic scale structural changes with IRO using molecular dynamics simulations.

We have assessed the effect of temperature and CO_2 loading on the molecular structuring of the solvent by calculating the radial distribution functions, g(r) in Figure 10, based on our experiments. Additionally, 100 ns-long simulations of systems consisting of 26,000 atoms are performed in the canonical ensemble using the OPLS-AA force field.[8-11] The latter allow us to calculate partial g(r) to assess the relative orientation of specific segments of the molecules. Ultimately, this analysis aims to provide a molecular-level understanding of solvent nanostructuring that enhances our knowledge of the origins of these molecular self-assemblies, as well as their dependence on experimental conditions, *i.e.* CO_2 loading. Our preliminary results clearly indicate distinct structures between the solvent molecules. Additional analysis codes are written to further clarify the molecular orientations, for example head-to-head or head-to-tail.

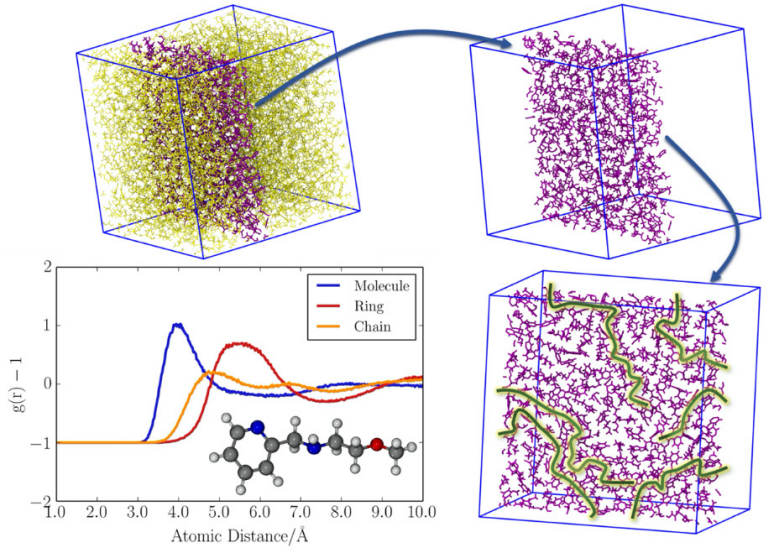

Figure 15. A representation of the simulation box (top left), and for clarity, a slice (top right) and formed channels (bottom right) are displayed. Partial pair radial distribution functions of the centers of masses (COMs) of the solvent molecules, rings, and chains that are found in the molecular structure. (Color code – C: gray, N: blue, O: red, H: white).

Tuning solvents such that more than one CO_2 could be captured per active site.

Chemically selective amines used in carbon capture materials are limited in uptake capacity as one molecule of CO_2 can be chemically fixated per amine active site. CO_2 capacity can be greatly increased if amine-containing materials could be manipulated to fixate a second equivalent of CO_2. We have hypothesized that the anionic carboxylates (e.g., carbamates or alkylcarbonates, Figure 11) in water-lean carbon capture solvents could chemically fixate a second (or more) CO_2 by tuning the nucleophilicity of anionic carboxylates to promote additional fixation (Figure 11).

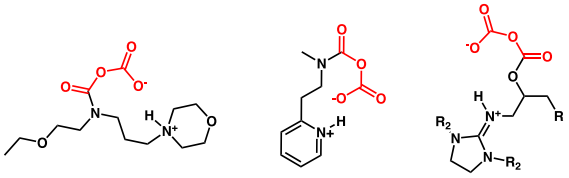

Figure 16.Proposed CO_2-anhydrides.

We have recently gathered spectroscopic evidence that carbamate anhydrides exist at elevated pressures. *In situ* high-pressure Nuclear Magnetic Resonance (NMR) studies were performed using diamines as they are the most nucleophilic class of water-lean solvents (Figure 11) and the resulting carbamate is the most likely to promote fixation of a second CO_2. Recently, 2-EEMPA[12] emerged as a promising solvent through theoretical screening and experimental testing with the lowest reported solvent regeneration energy of 2.0 GJ/tonne CO_2,[13] and the lowest total carbon capture costs reported ($47.1/tonne CO_2).[14]

2-EEMPA was pre-saturated with natural abundance CO_2, achieving the conventional 1:1 stoichiometry. The solvent was then pressurized with ^{13}C-enriched CO_2 at 500 psi, and scanned again, showing a second carbamate-like peak that was highly ^{13}C-enriched (Species B in Figure 12) that was slightly up-field of the initial carbamate (Species A in Figure 12). The area of integration of species A and dissolved natural abundance $CO_{2(d)}$ are equivalent, indicating that the expected 2-EEMPA carbamate is species **A** and the new carbamate-like peak **B** is ^{13}C-enriched, while the dissolved CO_2 has remained at natural abundance. ^{1}H-^{1}H 2D NOESY experiments ruled out the possibility that the ^{13}C-enriched CO_2 was coordinated to the molecule's morpholine nitrogen, suggesting it was closest to the carbamate. Further analysis of ^{1}H spin-lattice relaxation time constants (T_1) confirmed that this species was in a gel-like state, because the T_1 of all protons are very close or identical due to effective spin diffusion of protons through strong proton-proton

dipolar couplings. This gel-like state was also confirmed by the proton spectra having much sharper lines than conventional solid-state NMR, indicating much longer spin-spin relaxation time constants (T_2) due to less-constrained molecular motion.

After approximately ten minutes, the enriched carbamate (Species **B** in Figure 12) decreases in intensity completely, coinciding with the growth of ^{13}C-enriched dissolved $CO_{2(d)}$ at 125 ppm. The rapid decay of this second carbamate peak indicated species **B** is a transient or metastable species that ultimately transforms into a more stable resting state. It is known that carboxylic acids favor the formation of thermodynamically stable homo-associated dimers where two adjacent acids dimerize and form a 6-membered ring with strong hydrogen bonds. We posit that a similar resting state exists for 2-EEMPA under these conditions.

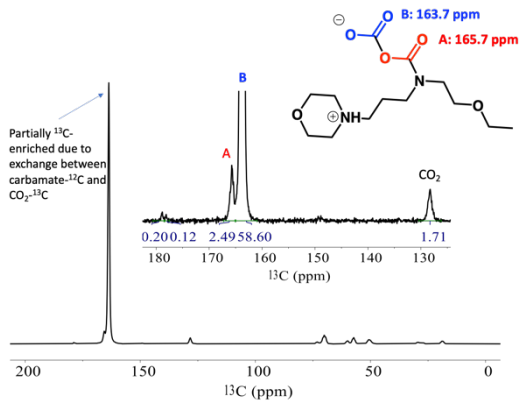

*Figure 17. ^{13}C NMR of 2-EEMPA (70 uL) saturated with natural abundance **CO_2** then pressurized with ^{13}C (99% enriched) **CO_2** (500 psi), 20 ˚C. Spectra are un-referenced.*

Theory was used to assess the relative energetics of the proposed anhydride and a plausible homo-associated carbamic acid dimer. Preliminary density functional calculations in the gas phase show that the CO_2 anhydride is approximately 185 kJ/mol uphill enthalpically as compared to the homo-associated dimer (Figure 13) suggesting the carbamate anhydride formation would not be possible unless under pressure, consistent with experimental observations.

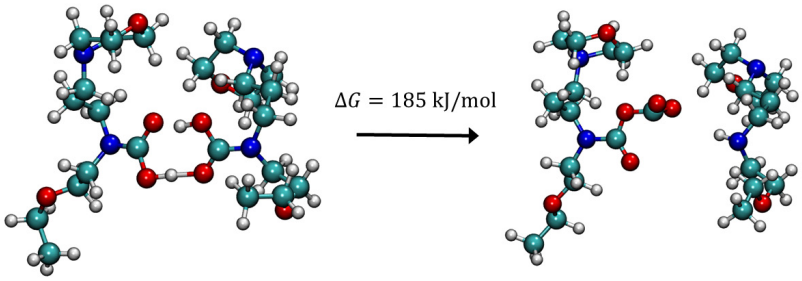

Figure 18. Calculated relative gas-phase energetics of the homo-associated carbamic acid dimer (left) and 2-EEMPA interacting with a carbamate anhydride (right).

In our quest to isolate the carbamate anhydride, we chose to block formation of the homo-associated dimer. We hypothesized that removal of the N-H proton from 2-EEMPA would prohibit formation of the homo-associated dimer due to the absence of hydrogen bonding. We have since synthesized a lithiated 2-EEMPA-amide which should still retain the ability to capture CO_2 as a lithium: carbamate salt, which could still form a lithiated carbamate anhydride, but not a homo-associated dimer. The calculated energetics of the lithiated 2-EEMPA suggests a highly exothermic sorption (-256 kJ/mol) of the first CO_2 (forming the lithium trapped carbamate) and a weakly exothermic enthalpy of binding for the second CO_2 (forming the lithium trapped anhydride). We are presently characterizing 2-EEMPA:Li and designing high-pressure NMR and IR experiments under an applied CO_2 pressure.

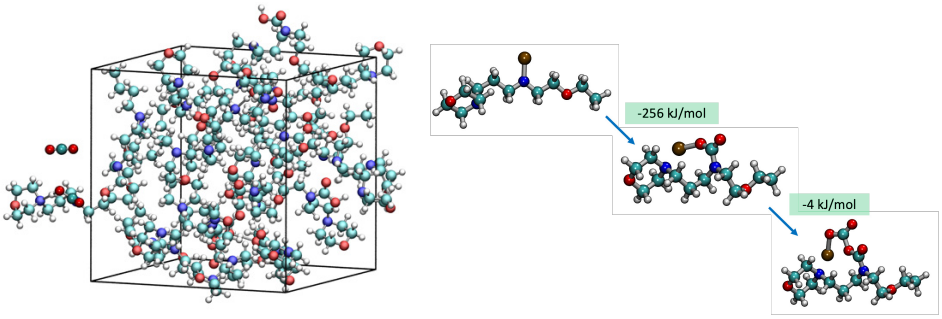

Figure 19. Left: Setup for Blue Moon calculations (2-EEMPA at 50% loading of CO_2), Right: Calculated energetics of 2-EEMPA:Li, 2-EEMPA:Li carbamate, carbamate anhydride:Li.

References

1. Yu, X.-Y.; Yao, J.; Lao, D. B.; Heldebrant, D. J.; Zhu, Z.; Malhotra, D.; Nguyen, M.-T.; Glezakou, V.-A.; Rousseau, R., Mesoscopic Structure Facilitates Rapid CO_2 Transport and Reactivity in CO_2 Capture Solvents. *The Journal of Physical Chemistry Letters*, **2018**, 9 (19), 5765-5771.
2. Neuefeind, J.; Feygenson, M.; Carruth, J.; Hoffmann, R.; Chipley, K. K. The Nanoscale Ordered MAterials Diffractometer NOMAD at the Spallation Neutron Source SNS. *Nucl. Instruments Methods Phys. Res. Sect. B Beam Interact. with Mater. Atoms.* **2012**, *287*, 68–75.
3. Soper, A. K., Empirical potential Monte Carlo simulation of fluid structure. *Chem. Phys.,* **1996**, 202, 295-306.
4. Soper, A. K., The radial distribution functions of water and ice from 220 to 673 K and at pressures up to 400 MPa. *Chem. Phys.*, **2000**, 258, 121-137.
5. Soper, A. K., Tests of the empirical potential structure refinement method and a new method of application to neutron diffraction data on water. *Mol. Phys.*, **2001**, 99, 1503-1516.
6. F Bruni, M A Ricci, and A K Soper, in Conference Proceedings Vol 76, Francesco Paolo Ricci: His Legacy and Future Perspectives of Neutron Scattering, M Nardone and M A Ricci (Eds.) (Società Italiana di Fisica, Bologna, **2001**).
7. Soper, A. K., Partial structure factors from disordered materials diffraction data: An approach using empirical potential structure refinement. *Phys. Rev. B*, **2005**, 72, 104204.
8. Dodda, L. S.; Vilseck, J. Z.; Tirado-Rives, J.; Jorgensen, W. L., 1.14*CM1A-LBCC: Localized Bond-Charge Corrected CM1A Charges for Condensed-Phase Simulations. *The Journal of Physical Chemistry B*, **2017**, 121 (15), 3864-3870.
9. Dodda, L. S.; Cabeza de Vaca, I.; Tirado-Rives, J.; Jorgensen, W. L., LigParGen web server: an automatic OPLS-AA parameter generator for organic ligands. *Nucleic Acids Research*, **2017**, 45 (W1), W331-W336.
10. Jorgensen, W. L.; Tirado-Rives, J., Potential energy functions for atomic-level simulations of water and organic and biomolecular systems. *Proceedings of the National Academy of Sciences*, **2005**, 102 (19), 6665-6670.
11. Jorgensen, W. L.; Tirado-Rives, J., The OPLS [optimized potentials for liquid simulations] potential functions for proteins, energy minimizations for crystals of cyclic peptides and crambin. *J. Am. Chem. Soc.*, **1988**, 110 (6), 1657-1666.
12. Cantu, D. C.; Malhotra, D.; Koech, P. K.; Zhang, D.; Glezakou, V.-A.; Rousseau, R.; Page, J.; Zheng, R.; Perry, R. J.; Heldebrant, D. J. *ChemSusChem*, **2020**, 13 , 3429-3438
13. Zheng, R.; Barpaga, D.; Mathias, P. M.; Malhotra, D.; Koech, P. K.; Jiang, Y.; Bhakta, M.; Lail, M.; Rabindran, A. V. R.; Whyatt, G. A.; Freeman, C. J.; Zwoster, A. J.; Weitz, K. K.; Heldebrant, D. J., A Single-Component Water-Lean Post-Combustion CO_2 Capture Solvent with Exceptionally Low Operational Heat and Total Costs of Capture – Comprehensive Experimental and Theoretical Evaluation. *Energy. Environ. Sci.* **2020** , 13, 4106-4113.

14. Jiang, Y.; Mathias, P. M.; Freeman, C. J.; Swisher, J. A.; Zheng, R.; Whyatt, G. A.; Heldebrant, D. J., Techno-economic comparison of various process configurations for post-combustion carbon capture using a single-component water-lean solvent. *International Journal of Greenhouse Gas Control*, **2021**, *106*, 103279.

Publications Acknowledging this Grant in 2021 – present

(VI) *Exclusively funded by this grant;* (*denotes corresponding author)

1. N/A

(VII) Jointly funded by this grant and other grants with leading intellectual contribution from this grant;

1. Kothandaraman, J.; Saavedra-Lopez, J.; Jiang, Y.; Walter, E.D.; Burton, S.D.; Dagle, R. A.; Heldebrant, "Integrated Capture and Conversion of CO_2 to Methane using a Water-lean Post Combustion CO_2 Capture Solvent." *ChemSusChem*, *In re-review.*

2. Jointly funded by this grant and other grants with relatively minor intellectual contribution from this grant;

1. N/A

Presentations Acknowledging this Grant in 2021 – present

1. "*Integrated capture and conversion of CO_2."* Invited, Distinguished Seminar Series, University of Toronto Department of Chemistry, March 22, 2021. Presentation by Heldebrant.
2. *"Molecular simulations in reactive separations and materials design."* Invited, University of Texas El Paso, Department of Physics, February 19, 2021. Presentation by Glezakou.
3. "*It's All About the Interface – Harnessing Molecular and Personal Interactions for a Sustainable Future."* California State University, Dominguez Hills, Physics Seminar, March 19, 2021. Presentation by Bañuelos.

Dispersible Polymeric Systems for Selective Ion Separations

Marc Hillmyer, Department of Chemistry, University of Minnesota-Twin Cities, Minneapolis, MN 55455

Presentation Abstract

Efficient and selective separations of metal cations are needed for applications such as nuclear waste remediation, metal production, and electronics recycling. Technologies using organic solvents such as solvent extraction or liquid membranes enable high selectivities based on ion/ligand complexes but suffer from instability and solvent loss to the environment. We are exploring approaches involving dispersible polymeric materials whose solid construction enables simple, physical separations and high surface areas that enable rapid kinetics. In the first approach, we synthesize hollow polymeric capsules as dispersible facilitated transport membranes, wherein ion-selective ligands solubilized in the capsule walls transport the ions into acid-filled capsule cavities, exchanging ions for protons. We demonstrate the approach with copper-selective microcapsules, with separations complete in as little as 10 minutes. To enable even more rapid kinetics, we also target nanoscale polymersomes (polymeric vesicles), with initial work on synthesizing acid-stable polymersomes. In the second approach, we develop scalable strategies to synthesize mesoporous beads with ligand-functionalized surfaces and narrow pore-size distributions. Ongoing work will demonstrate selective ion sorption in these high-surface-area materials.

DE-SC-0020210. Metal-Selective Polymersomes (MSPs) for Solvent-Free Extractive Separations of Metal Ions

PI: Marc Hillmyer **Postdoc(s):** Jay Werber **Student(s):** Colin Peterson

RECENT PROGRESS

Separation of Metal Cations with Ligand-Containing Microcapsules. Solvent extraction enables highly selective separations but has drawbacks such as solvent loss to the environment, large solvent inventories, and large mass of ligand (extractant) needed due to stoichiometric ion/ligand binding. Facilitated transport membranes, which use similar extractants as in solvent extraction, could circumvent these issues and have typically been formed in planar or hollow-fiber geometries as either "supported liquid membranes" or "polymer inclusion membranes." The former involves pores wetted with solvent, and suffers from instability, while the latter is essentially a polymer/solvent/extractant gel that is typically more stable but often has low permeability. Dispersed "emulsion liquid membranes" have also been extensively explored because of their rapid kinetics due to high surface areas but are inherently unstable. We have developed polymeric microcapsules as robust analogs of emulsion liquid membranes, retaining the rapid kinetics while increasing physical stability. As a proof of concept, we used commercially available poly(styrene)-*block*-poly(butadiene)-*block*-poly(styrene) (SBS) as the base material and the copper-selective phenolic oxime ligand Lix 84-I (BASF). SBS was chosen owing to its physical crosslinking through the hard polystyrene blocks, while the continuous polybutadiene phase allows for high diffusivities. Microcapsules were formed with 0.5 M sulfuric acid in the interior, stabilized by polyvinyl alcohol (outer interface) and a custom-synthesized poly(isoprene)-*block*-poly(4-styrene sulfonic acid) diblock copolymer (inner interface). The system breaks the extraction equilibrium between extractant and ions, instead forming a relationship between inner proton concentration and metal ion uptake. The capsules had inner cavities (Figure 1A) and diameters of 10–100 μm (Figure 1B). Batch experiments showed uptake of Cu^{2+} ions in as little as 10 min, with the uptake

rate increasing with ligand content (Figure 1C). We further showed selective uptake of copper over nickel and sodium, the ability to remove copper to below detection in packed columns with ~2 min residence time, and the ability to regenerate the columns (while recovering captured copper ions) and reuse them for at least 10 cycles. This work serves as a proof of concept for the microcapsule approach for metal ion uptake, which allows for simple processing and minimal ligand requirements. We will be submitting a manuscript based on this work shortly. The design could serve as a starting point for the selective capture of valuable metal ions using minimal quantities of complex, specialty extractants.

Synthesis of Acid-Stable Polymersomes. To further improve the kinetics of separations, the dimensions of the capsules can be further decreased, thereby decreasing the effective membrane (wall) thickness. Polymersomes self-assemble as enclosed bilayers from amphiphilic block polymers, wherein the hydrophobic block forms the ~10-nm thick, dense center of the bilayer. For the cation exchange mechanism, the polymersomes must be acid-stable, while the hydrophilic block would ideally lack interactions with the cations (i.e., neutrally charged, not polyether-based). Furthermore, crosslinking will likely be necessary to enable sufficient mechanical robustness to withstand substantial osmotic pressure differences (>20 bar). Our first goal therefore was to synthesize polymersomes from polymers matching these characteristics. Building off of chemistry developed in our laboratories, we used reversible addition-fragmentation chain-transfer (RAFT) polymerization to form polyisoprene-*block*-poly(di-boc acrylamide) diblock polymers with good control over molar mass despite some chain coupling. This polymer is soluble in some common organic solvents, enabling characterization of chemical properties (e.g., molar mass). The poly(di-boc acrylamide) (PDBAm) block could then be modified by reduction to form poly(hydroxypropylene) (PPOH) or transamidation with amines to form various poly(acrylamides), particularly polyacrylamide (PAm) using NH_3 and poly(*N*-ethyl acrylamide) using ethylamine. The resulting amphiphilic block polymers self-assembled into polymersomes in deionized water (Figure 2). However, the PPOH-based polymers precipitated in salty solutions, owing to the limited solubility of PPOH in aqueous solutions, which precludes its use in acidic solutions (≥ 0.5 M sulfuric acid). The acrylamide-based systems self-assembled in salt solutions (Figure 2C), but hydrolyze slowly in highly acidic solutions to form poly(acrylic acid). Further work is needed to develop acid-stable, crosslinkable chemistries to synthesize polymersomes for use as dispersible facilitated transport membranes.

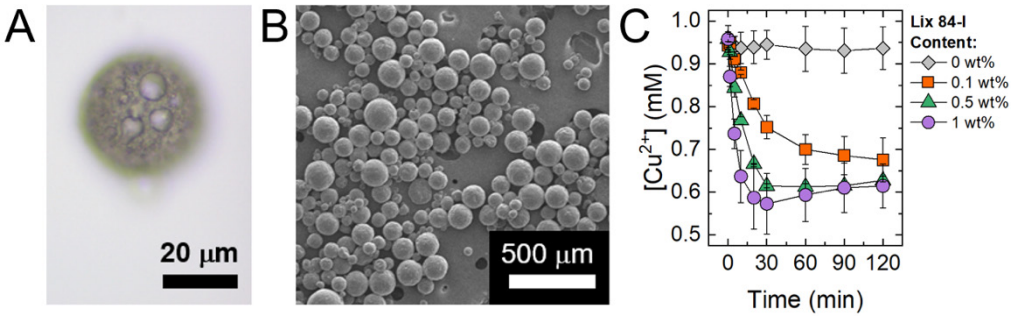

Figure 1. Polymeric microcapsules for metal ion uptake. (A) Optical and (B) scanning electron micrographs of microcapsules. (C) Batch uptake experiments for varying ligand content, in which 200 mg of beads were mixed with 15 mL of 1 mM $CuSO_4$, 20 mM NaMES, pH 5.6. The interior solution was 0.5 M H_2SO_4. Ligand wt% is relative to the capsule wall mass (i.e., ligand + SBS).

Synthesis of Mesoporous Beads with Narrow Pore-Size Distributions. Our second complementary approach is to develop selective ion-exchange materials, with porous beads functionalized with ion-selective ligands. While this approach retains the ligand/ion stoichiometry of solvent extraction, it enables physical separations and is more robust than the dispersible membrane approach due to the lack of osmotic pressure gradients. Designing advanced ion-exchange materials will require tunable control of particle size, pore diameter, and surface chemistry. We therefore explored the ability to directly form beads using polymerization-induced microphase separation (PIMS) in aqueous suspension. A polycaprolactone (PCL) macro-chain transfer agent was dissolved in a mixture of styrene, divinylbenzene, and initiator, with the mixture then dispersed in water and heated to form polymer beads by thermal RAFT polymerization. The PIMS process readily occurred in suspension at 20-g scale, resulting in beads with bicontinuous styrene/divinylbenzene and PCL domains. The PCL domains were then etched in alkaline solution, forming nearly uniform pores with diameters of ~6 nm or ~11 nm that depended on the initial PCL molar mass. Surface areas were up to ~300 m^2/g based on nitrogen sorption, and particle size could be tuned by adjusting the stir rate. Etching of PCL yielded putative hydroxyl groups, which could serve as reactive handles for surface functionalization. Work is on-going to incorporate a functional polymeric mid-block to obtain functional, ion-binding surfaces immediately upon etching. We plan to submit a manuscript detailing this work in the coming months.

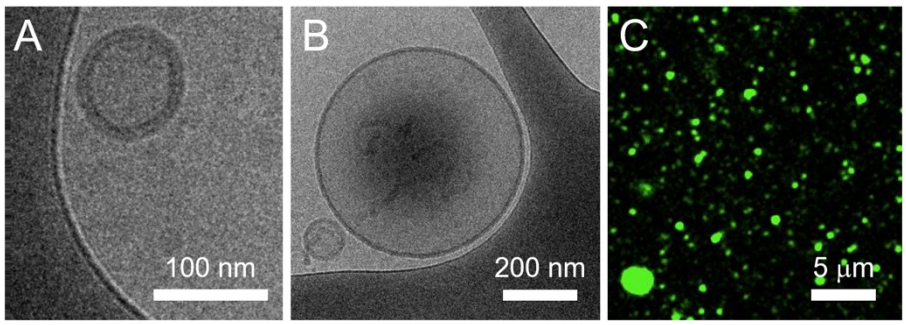

Figure 2. Vesicle formation with amphiphilic block polymers. (A-B) Cryo-electron microscopy of vesicles formed by film rehydration in deionized water using (A) polyisoprene-*block*-polyacrylamide (PI-PAm) and (B) polyisoprene-*block*-PPOH. (C) Laser scanning confocal microscopy of PI-PAm vesicles loaded with 5 mM Tris, 1 M NaCl, 15 mM carboxyfluorescein, pH 7.5, and dialyzed for 3 d to remove the residual carboxyfluorescein.

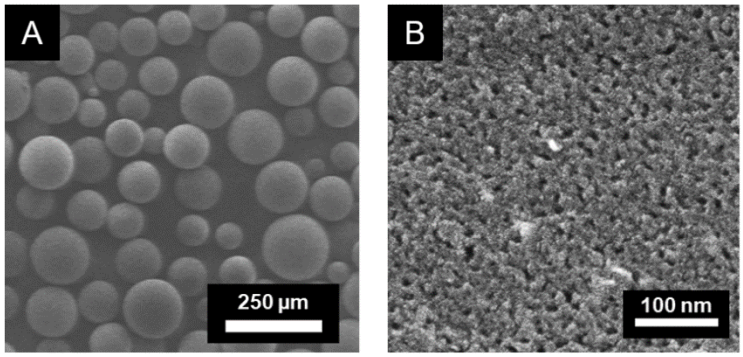

Figure 3. Scanning electron micrographs of porous beads after etching of PCL domains in base, showing (A) particle size and (B) ~6-nm diameter, nearly-uniform pores.

Publications Acknowledging this Grant in 2019–present

(I) Exclusively funded by this grant:

1. Werber, J.R.; Peterson, C.; Van Zee, N.; Hillmyer, M.A. Functionalized Polymersomes from a Polyisoprene–Activated Polyacrylamide Precursor. *Langmuir*. **2021**, 37, 490-498. DOI: 10.1021/acs.langmuir.0c03157

(II) Jointly funded by this grant and other grants with leading intellectual contribution from this grant: None

(III) Jointly funded by this grant and other grants with relatively minor intellectual contribution from this grant: None

Coordination-Chemistry-Derived Materials Featuring Nanoscale Porosity and Selective Chemical Separation Capabilities

Joseph T. Hupp, *Randall Q. Snurr, and Omar K. Farha, Northwestern University, Department of Chemistry and Department of Chemical and Biological Engineering*

Presentation Abstract

The goals of this project center on advancing and exploiting a promising predictive, iterative, and tightly interactive cycle of computational-design/experimental-synthesis/experimental-testing for discovering and understanding porous, crystalline metal-organic-framework (MOF) for energy-efficient separation of mixture of gases and vapors. The targets include several challenging, energy-relevant, small-molecule mixtures such as separations of ethylene/ethane, acetylene/ethylene, ammonia/nitrogen, carbon dioxide/nitrogen, and krypton/xenon.

This brief presentation will highlight and illustrate the idea of reversible chemical reactivity as a basis for separations. As suggested by the accompanying breakthrough curves (see figure), ammonia can be separated from other small molecules such N_2 via simple Bronsted acid/base interactions with the MOF, NU-1000-Cl.[1] Demonstrated reversible heterolytic splitting of H_2 by MOF-supported, single-metal-atom $Mo(SH)_2$ units should provide a basis for separating dihydrogen from other small molecules, as should reversible covalent bond formation between CO_2 and immobile MOF-supported macromolecules, for separation of carbon dioxide from other small molecules.

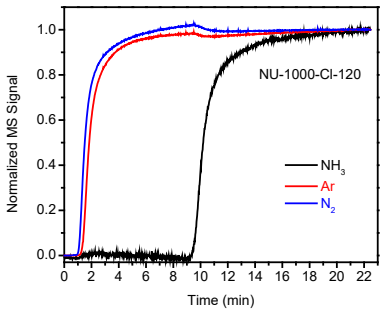

The presentation will also touch on the idea of irreversible chemical reactions (*not* irreversible binding) for accomplishing "separations." A demonstrated example[2] is "separation" of acetylene, an undesirable catalyst poison, from ethylene, a highly desirable, commodity-scale polymer building block, via Cu@MOF-catalyzed, selective partial hydrogenation of acetylene to ethylene, *i.e.* selective reaction and transformation of an impurity into the desired component of a mixture.

1. J. Liu, *et al.* "Zirconium Metal–Organic Frameworks Integrating Chloride Ions for Ammonia Capture and/or Chemical Separation," *ACS Appl. Mater. Interfaces*, **2021**, *13*, 19, 22485–22494. DOI: 10.1021/acsami.1c03717

2. M. R. Mian, *et al.* "Precise Control of Cu Nanoparticle Size and Catalytic Activity through Pore Templating in Zr Metal–Organic Frameworks," *Chem. Mater.* **2020**, *32*, 3078–3086. DOI: 10.1021/acs.chemmater.0c00059

Emerging Projects

Transforming Critical Materials Separation using Precision Control

Santa Jansone-Popova,[1] *Alex Ivanov,*[1] *Ilja Popovs,*[1] *De-en Jiang,*[2] *Juan-Carlos Idrobo,*[1] *Huimin Luo,*[1] *Sheng Dai,*[1,3] *Bruce A. Moyer*[1]; [1]*Oak Ridge National Laboratory,* [2]*University of California, Riverside,* [3]*University of Tennessee, Knoxville*

ABSTRACT

The rare earth elements (REE) Nd, Eu, Tb, Dy and Y are assessed as critical materials by the U.S. Department of Energy because of their essential roles in renewable energy, high supply risk, and difficult substitutability. The core needs in separation science are amplified by the complex and often dilute matrices in which the REEs are found as well as in the monumental challenge of separating trivalent ions whose ionic radii decrease across the lanthanide series on average by only 0.01 Angstrom per unit increase in atomic number. By applying established principles of chemical recognition, one may expect that ligands for selective REE binding must possess extraordinary preorganization to accommodate such delicate changes in guest ionic radius. Typical chelates such as the polyaminopolycarboxylic acid EDTA are flexible, exhibiting only marginal binding energy differences following linear free energy relationships and thus lack selectivity for individual REE. Extractants capable of concentrating REE ions from very dilute streams must have very high affinity, which require harsh, energy intensive conditions for release. These challenges thus bring us to the central question: *How can we design new REE host molecules for separation that incorporate both extreme recognition and a mechanism to spring the captured ions from the tight grips of the host?*

Students: Tongyu Liu (UCR), Brian Kettell (summer student, UTK)
Postdoctoral researchers: Katie Johnson (ORNL), Dhileep Reddy (UCR), Darren Driscoll (ORNL), Chi-Linh Do-Thanh (UTK)

RECENT PROGRESS

Understanding and Controlling the Interactions in the 1st Coordination Shell

We are using computational design strategy based on the variety of descriptors, such as those shown in Figure 1, to identify complexants with the optimal affinity for light versus heavy trivalent lanthanides. Specifically, density functional theory (DFT) calculations are used to compute binding free energies of a variety of organic ligands and Ln(III) ions using an implicit solvation model. Several ligands that outperform the reported preorganized systems have been selected for further investigation.

In addition to the development of new complexants, identified as most promising using

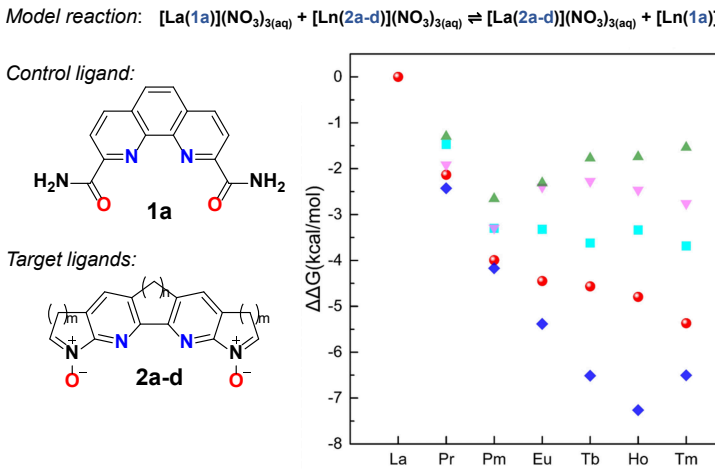

Figure 1. Calculated relative aqueous selectivity [$\Delta\Delta G_{aq(La/Ln)}$] for the preorganized ligands **2a-d** at the B3LYP/6-31+G(d) level using model reaction of ligand-exchange chemistry with the control **1a**.

computational methods, we are investigating additional stimuli responsive preorganized ligand systems. More specifically, we are working on three strategies that will allow us to gain control over selective release of Ln ions from persistent complexes: a) changes in ligand denticity, b) changes in electronic structure, and c) charge repulsion.

Additionally, we are exploring alternative options for highly efficient adjacent lanthanide separation. As depicted in Figure 2, use of dual ligand system (i.e., a hydrophobic complexant with high affinity for heavy Ln(III) in combination with hydrophilic complexant with revers selectivity) can be very effective towards enhancing the adjacent Ln(III) discrimination and therefore selectivity.

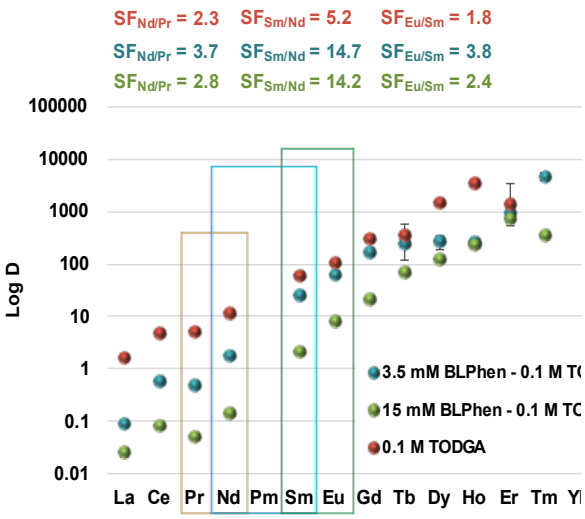

Figure 2. Combination of hydrophilic and hydrophobic complexants for targeted Ln(III) separation in 1 M HNO_3.

Understanding the Solvation Environment to Control Binding, Selectivity and Release

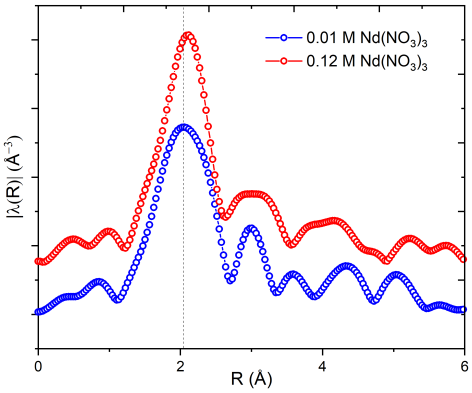

Figure 3. Comparison of Fourier transformed EXAFS data for BLPhen/Isopar contacted with 0.01 and 0.12 M $Nd(NO_3)_3$ solutions.

We are working towards acquiring fundamental knowledge of how weak interactions removed from the immediate coordination environment can be leveraged to increase selectivity through a controlled binding and release. As an initial system, we are investigating the effect of media (non-polar solvent versus ionic liquid) on the Ln(III) separation. The team was awarded the EXAFS beamtime at the Advanced Photon Source (APS) in February 2021, during which a series of samples of different composition (e.g., 2:1 and 1:1 ligand to Ln(III) complexes) were measured (Figure 3). Comparison of the two data sets corresponding to the 2:1 and 1:1 complex formation in Isopar reveals that metal concentration affects both the extent of aggregate formation and the local metal environment, indicating shorter inner sphere distances and the presence of persistent outer-sphere interactions when Ln(III) is coordinated with two rigid BLPhen ligands. The EXAFS data fitting coupled with MD simulations will provide more insights into the formation of these complexes in different media, including the role of water and ligand interactions with Ln(III) to achieve selective separations. We are currently testing force field parameters for Ln(III) ions and also evaluating methods for directly predicting distribution ratios from MD simulations. To accelerate the prediction of distribution ratios and the screening of complexants, we will also leverage machine learning and the measured distribution ratios from this project (Figure 2) and the literature to pursue a data-driven approach to guide our experimental efforts.

Publications Acknowledging this Grant (2020-present)

1. Singh, M.; Fu, Y.; Popovs, I.; Jansone-Popova, S.; Dai, S.; Jiang, D. "Molecular Dynamics Simulations of Complexation of Am(III) by a Preorganized Dicationic Ligand in an Ionic Liquid" *J. Phys. Chem. B*, **2021**, DOI: jp-2021-04410p.R1.

Design of a high-throughput platform to identify polymer scaffolds for ion separations

Abigail Knight, Department of Chemistry, University of North Carolina at Chapel Hill

Presentation Abstract

Polymer scaffolds are attractive substrates for large scale purifications such as ion separations with the necessary scalability and chemical diversity. They have yet to realize their potential in a variety of separations applications due to limitations in available design principles. We are approaching this challenge by both 1) developing new strategies for creating protein-mimetic local (secondary- like) and global (tertiary-like) structure to strategically confine ligands within a binding site and

2) developing a high-throughput platform to identify ligand distributions required to chelate desired ions. Since we began this project in September 2020, we have designed, synthesized, and characterized amphiphilic polymers with non-covalent crosslinks that create local order using a di(phenylalanine) acrylamide monomer. Concurrently, we developed an analytical assay for our "macromolecular selection" platform that will elucidate design principles for binding target ions. This platform leverages dynamic covalent chemistry with a mechanism analogous to popular dynamic combinatorial libraries composed of small molecules. The analytical assay developed will enable quantification of bound ligands. Together these results both provide novel structures and techniques for the design and characterization of polymers in aqueous solution and build the foundation of our ongoing pursuit of scaffolds for the separation of lanthanide ions.

DE-SC0021295: A Macromolecular Selection Platform for the Isolation of Lanthanide Ions
Postdoc(s): **Meredith Barbee**
Student(s): Jaqueline Warren, Peter Dykeman-Bermingham, Matthew Bogen, Jeshurun Luke

Recent Progress

Development of an analytical protocol for macromolecular selection

Inspired by the diverse binding profiles of small molecules identified with techniques implementing dynamic covalent chemistry (DCC) and previous work indicating dynamic exchange can be implemented to shift polymer properties in the presence of a template molecule,

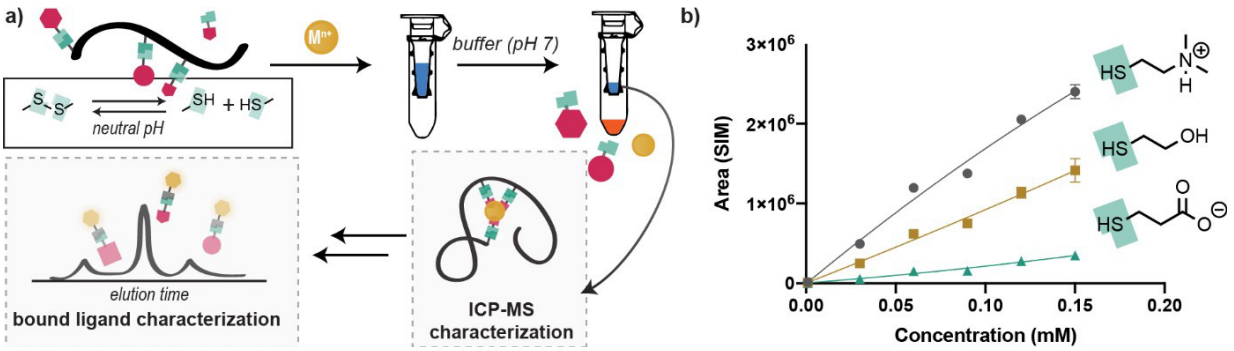

***Figure 1*. Analytical protocol for macromolecular selection**. a) Overview of the macromolecular selection strategy that will be used to identify optimal polymer composition and architecture for the isolation of lanthanide ions. b) Example LC-MS calibration curves for a series of derivatized thiols are shown (n=3, error bars = standard error).

we are developing a platform that employs dynamic covalent exchange to identify materials with the ability to capture and separate target ions. Motivated by the folding observed with single chain nanoparticles, dynamic pendent groups are embedded in a synthetic polymer scaffold consisting of a mixture of hydrophobic and hydrophilic residues to create a binding pocket. Dynamic pendent groups can exchange with complementary moieties on small molecules in solution, allowing the polymer binding site to "evolve" over time (***Figure 1a***). If a template ion (e.g., rare earth ion) is included, we hypothesize that it will shift the equilibrium such that the polymer will be preferentially bound to small molecules that interact with the templating ion.

Our results so far include the development of an analytical procedure for isolating polymers in solution away from excess small molecules and ions and characterizing both bound ions and bound small molecules. We can reproducibly quantitate the distribution of small molecules bound to a polymer scaffold using a post-modification strategy in addition to our in-house LC-MS (calibration curve shown in ***Figure 2***).

Synthesis and characterization of amphiphilic polymers with protein-mimetic structure

A significant energetic cost of the binding of macromolecules to target species is the unfavorable decrease in mobility upon binding. As non-covalent interactions (e.g., hydrophobic collapse and hydrogen bonding) play a large role in dictating protein structure, we hypothesized that these interactions would have a similar impact on the structure of synthetic polymers. Thus, we developed a monomer (FF) composed of the smallest peptide that can drive self-assembly, a phenylalanine dipeptide, identified from β- amyloid aggregation involved in Alzheimer's disease (***Figure 2a***). We compared amphiphilic copolymers with dimethylacrylamide (DMA; ***Figure 2b***) containing FF, an analogous monomer we synthesized containing a single phenylalanine (F), and benzyl acrylamide (BAA). Within this series, we identified that when normalized by weight percent, each monomer led to an equivalently compact structure (***Figure 2c***) indicating the morphology of the single chain structures were predominantly impacted by the fraction of the hydrophobic monomer. However, characterization with circular dichroism (CD; ***Figure 2d***), staining with Thioflavin T, a dye known to fluorescence in the presence of fibrils, and differential scanning calorimetry (DSC) indicated increased local structure in the polymers containing FF. These results indicate that the FF-monomer can create confinement within an amphiphilic polymer, a key part of protein structural hierarchy

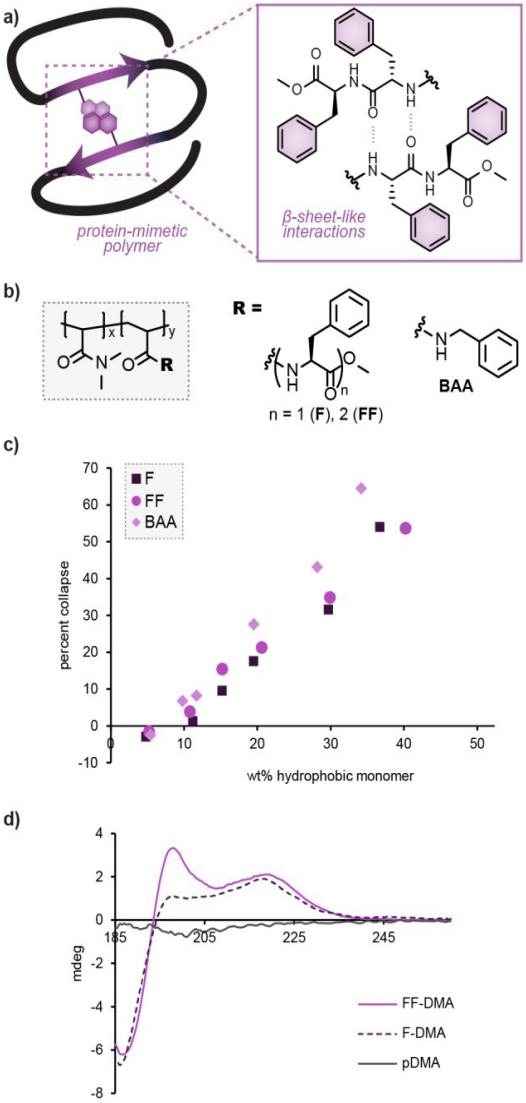

Figure 2. **Protein-mimetic structure of amphiphilic polymers.** a) Schematic of amphiphilic copolymer containing the FF monomer (structure on right) that induces local structure. b) Structures of copolymers compared using SEC (c) and CD (d). The percent collapse was calculated by comparing the apparent molecular weight using PEG standards on an aqueous and DMF SEC.

Publications Acknowledging this Grant (since Sept. 2020)

Exclusively funded by this grant

Warren, J. L.; Dykeman-Bermingham, P. A.; Knight, A. S.* Controlling amphiphilic polymer folding beyond the primary structure with protein-mimetic diphenylalanine. *Submitted*.

ChemRxiv.

Jointly funded by this grant and other grants

Barbee, M. H.[†]; Wright, Z. M[†].; Allen, B. P.; Taylor, H. T.; Patteson, E. F.; **Knight, A. S.***
Protein-mimetic self-assembly with synthetic macromolecules. *Macromolecules* **2021**. *54*. 3585– 612. DOI: 10.1021/acs.macromol.0c02826. (Highlighted with a front cover).

Plenary Talk: Jennifer Wilcox, Principal Deputy Assistant Secretary for Fossil Energy at DOE, Presidential Distinguished Professor of Chemical Engineering and Energy Policy at University of Pennsylvania

Session III: Phenomena on Surfaces and within Pores (Ruilan Guo, Chair)

Permeation Properties of Disordered Metal-Organic Framework Membranes Made by Vapor Phase Ligand Treatment

Michael Tsapatsis,[(1)] J. Anibal Boscoboinik,[(2)] J. Ilja Siepmann,[(3)] Dennis T. Lee,[(1)] Yurun Miao,[(1)] Peter Corkery,[(1)] Mueed Ahmad[(2)] and Matheus Dorneles de Mello[(2)]; [(1)] Department of Chemical and Biomolecular Engineering, & Institute for NanoBioTechnology, Johns Hopkins University, 3400 N. Charles Street, Baltimore, MD 21218 USA; [(2)] Center for Functional Nanomaterials, Brookhaven National Laboratory, Upton, NY, 11973 USA; Materials Science and Chemical Engineering Department, Stony Brook University, Stony Brook, NY 11790 USA; [(3)] Department of Chemistry and Chemical Theory Center, University of Minnesota, Minneapolis, MN 55455 USA

Presentation Abstract

The main goal of our research is to develop fundamental understanding of ZIF membranes focusing on controlled synthesis and modification of membranes to tune transport properties. We report the development of a mathematical model for the ZnO deposition in porous Al_2O_3 via atomic layer deposition, the critical first step for the fabrication of ZIF-membranes using the ligand-induced perm-selectivation process. A detailed computational fluid dynamics (CFD) model of the ALD reactor is developed using a finite-volume-based code and validated. We further probe the changes in membrane transport properties by two novel methods: first, we use vapor treatment of ZIF-8 membranes with manganese (II) acetylacetonate to tune the permselectivity of gas mixtures. We show that propylene/propane selectivity increases from 31 to 210 after the $Mn(acac)_2$ treatment at 165 °C for 30 min, while selectivities increase from 14.6 to 242 for H_2/CH_4, from 2.9 to 38 for CO_2/CH_4, from 2.4 to 29 for CO_2/N_2, and from 2.9 to 7.5 for O_2/N_2, after $Mn(acac)_2$ treatment at 175 °C for 30 min. We also explore the effect of electron beam treatment on ZIF membranes, reporting that 3.8 and 3.2-fold enhancements in selectivity for CO_2/N_2 and CO_2/CH_4 can be achieved with less than one min exposure time.

Grant Numbers: DE-SC0021212 (JHU), DE-SC0021268 (UMN), DE-SC0021304 (SBU)

Grant Title: Permeation Properties of Disordered Metal-Organic Framework Membranes Made by Vapor Phase Ligand Treatment

PI: Michael Tsapatsis (PI), J. Ilja Siepmann and J. Anibal Boscoboinik (co-PIs)

Student(s): Peter Corkery (JHU), Mueed Ahmad (SBU), Roshan Patel (UMN)

RECENT PROGRESS

ZIF-8, a zeolitic-imidazolate framework (ZIF) consisting of zinc (Zn) centers bridged by 2-methyl-imidazole (2mIm) ligands has been targeted for propane/propylene separations due to a propylene diffusivity that is over 100 times greater than that of propane. Synthesis of high-quality ZIF membranes has been achieved by the Tsapatsis group using solvent-free deposition of ZnO layers that are then converted to ZIF by exposure to 2mIm. According to this process, which we call LIPS (ligand-induced perm-selectivation), the pores of an alumina support are first blocked using atomic layer deposition (ALD) of an impermeable ZnO deposit that is then converted to a

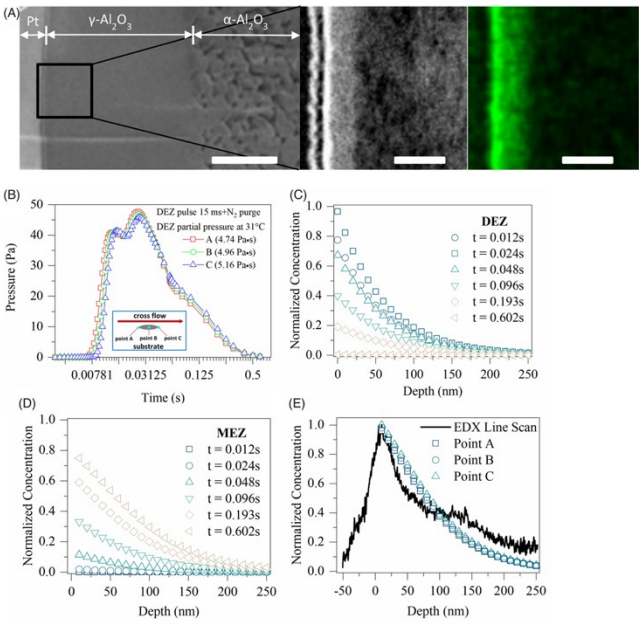

Fig. 1 (A) Cross-section of a membrane with ZnO deposit, showing the macroporous α-Al_2O_3 and mesoporous γ-Al_2O_3 support, and higher magnification cross-sectional images of the ZnO deposit (bright contrast and green color) within the γ-Al_2O_3 layer (left scale bar: 1 µm, middle and right scale bars: 250 nm). (B) Transient diethylzinc (DEZ) boundary conditions determined by the atomic layer deposition reactor model (assuming no reaction) at three positions along the membrane (A, B, and C) as indicated in the inset. (C, D) Concentration profiles of DEZ and MEZ, respectively. (E) Final concentration profile of MEZ at positions *A*, *B*, and *C* compared to profile from cross-sectional imaging.

permeable and selective ZIF layer by exposure to 2mIm vapors. In this project, our aims are to provide a detailed understanding of the LIPS process and to further improve membrane performance through post-synthetic modification, e.g., via e-beam treatment. The project is advanced through a highly collaborative approach between the Tsapatsis, Boscoboinik, and Siepmann groups.

Mathematical modeling of ZnO thin films formation by ALD. ZnO deposition in porous γ-Al_2O_3 via atomic layer deposition (ALD) is the critical first step for the fabrication of ZIF membranes using the LIPS process. This step up to now was performed empirically without quantitative understanding of the reactor design and operational parameters that can lead to a uniform and thin deposit. A detailed Computational Fluid Dynamics (CFD) model of the ALD reactor was developed using a finite-volume based code and validated. It accounts for the transport processes within the feeding system and reaction chamber and within the membrane support. The simulated precursor spatiotemporal profiles assuming no ALD reaction were used as boundary conditions in modelling diethylzinc reaction/diffusion in porous γ-Al_2O_3, the predictions of which agreed with experimental electron microscopy measurements (**Figure 1**). The modeling approach demonstrated in this work is the first comprehensive modeling of ALD for membrane formation. It allows for the design of ALD processes for the synthesis of metal–organic framework membranes as well as other thin-film membranes in porous supports.

Membrane Permselectivity Modification by Vapor Phase Treatment. We discovered a new method to modify the performance of ZIF-8 membranes based on a treatment using sublimated vapors of manganese (II) acetylacetonate. Characterization of the modified ZIF-8 films and membranes using SEM, XRD and XPS support that $Mn(acac)_2$ treatment leads to formation of a thin top layer as opposed to metal doping or metal cation exchange with framework Zn, which was our original goal. The fact that, at the surface of the modified films, we detect by XPS nitrogen but not zinc indicates the presence of a layer that is not ZIF-8 but contains 2mIm ligands from the

original ZIF-8 film. These 2mIm ligands are either bound to Mn or simply present within the $Mn(acac)_2$ layer. We found that 3 to 7 nm thick top layer drastically alters the permeation properties of the ZIF-8 membrane (**Figure 2**). Propylene/propane selectivity increases from 31 to 210 after the $Mn(acac)_2$ treatment at 165 °C for 30 min, while selectivities increase from 14.6 to 242 for H_2/CH_4, from 2.9 to 38 for CO_2/CH_4, from 2.4 to 29 for CO_2/N_2, and from 2.9 to 7.5 for O_2/N_2, after Mn(acac)2 treatment at 175 °C for 30 min. Stable equimolar propylene/propane mixture selectivity of 165 at ambient temperature and 4 bar equimolar feed with a propylene flux of 8.3×10^{-4} mol m^{-2} s^{-1} was established. Control experiments indicate that thermal treatment alone does not cause these changes.

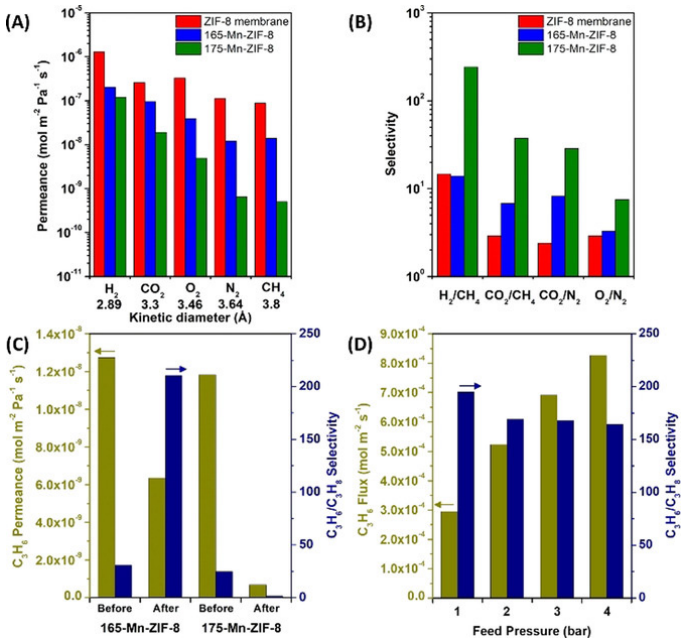

Fig. 2 A) Single gas permeances of H_2, CO_2, O_2, N_2, and CH_4, and B) ideal selectivity (ratio of permeances) for H_2/CH_4, CO_2/CH_4, CO_2/N_2, and O_2/N_2 gas pairs measured at 25 °C by the time-lag method before and after $Mn(acac)_2$ treatment at 165 °C (165-Mn-ZIF-8) and 175 °C (175-Mn-ZIF-8). C) Propylene permeance and propylene/propane equimolar feed mixture selectivity by the Wicke–Kallenbach method at 25 °C for 165- and 175-Mn-ZIF-8. D) Propylene flux and propylene/propane selectivity (equimolar propane and propylene feed) for ZIF-8 membranes before and after $Mn(acac)_2$ treatment at 165 °C (165-Mn-ZIF-8) at feed (retentate) pressure ranging from 1 bar to 4 bar, with permeate set at 1 bar with Ar sweep gas flow by

Membrane Permselectivity Modification by Electron Beam Irradiation. Electron induced modification of metal–organic frameworks (MOFs) has hardly been explored except for the well-documented beam damage problem in high-resolution microscopy and as a means for surface activation and functionalization. Our work is the first use of e-beam irradiation for the modification of MOF membranes.

E-beam modification was accomplished by exposing the as-prepared LIPS membranes to the output of an electron flood gun operating at 2 kV. We showed that electron irradiation can modify the gas permeation properties of a ZIF-8, as demonstrated by improved CO_2/N_2 and CO_2/CH_4 selectivity (**Figure 3**). Low dose exposure for less than 1 min increases CO_2 selectivity, while high dose exposure leads to reduced permeance and selectivity.

To investigate the changes caused by e-beam irradiation on the surface of ZIF-8, we collected XPS from ZIF-8 thin films irradiated by an *in situ* generated e-beam. After irradiation, while no significant changes are observed in the binding energy of Zn *2p* a small shoulder appears at 401.2 eV in the N *1s* spectrum. This change indicates the formation of N–H bonds due to the electron induced cleavage of either the Zn–N bond or the C–N/C═N bond in the imidazole ring. One

possibility is that the breakage of bonds frees the transient nitrogen species to recombine with protons in a cascade of radical reactions induced by the e-beam, and the presence of N–H bonds in open pores increases the adsorption of CO_2 in ZIF-8, leading to the improved CO_2 selectivity. At increased doses, crosslinking of imidazolate ligands could become dominant causing pore blocking and large reduction in flux.

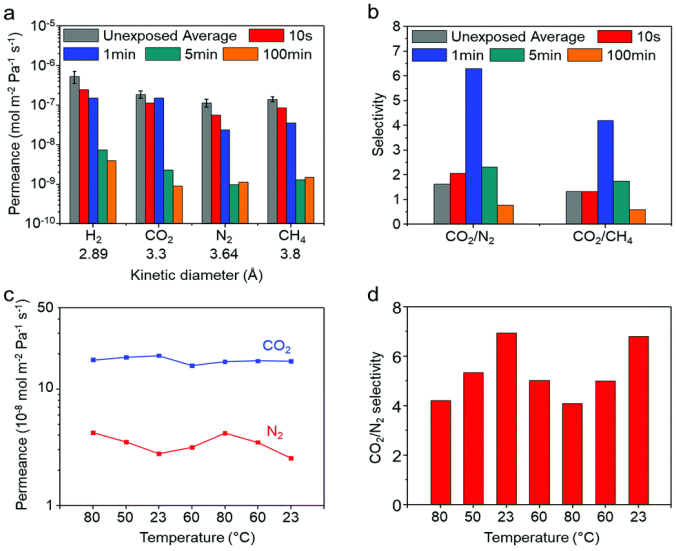

Fig. 3 (a) Single gas permeances and (b) CO_2/N_2 and CO_2/CH_4 ideal selectivities of LIPS ZIF-8 membranes before and after e-beam exposure. (c) CO_2 and N_2 permeances at various temperatures in the 23–80 °C range of a membrane exposed to e-beam for 1 min, and (d) the corresponding single-component selectivities for CO_2/N_2. Permeances for each gas are measured over a period of 24 h at each temperature, respectively. The data points in (c) are from stabilized permeances with less than 10% variation in each on-stream stability test.

Publications Acknowledging this Grant in 2020– present

(I) Exclusively funded by this grant:
None.

(II) Jointly funded by this grant and other grants with leading intellectual contribution from this grant;

1. Zhuang, L.; Corkery, P.; Lee, D.T.; Lee, S.; Kooshkbaghi, M.; Xu, Z.; Dai, G.; Kevrekidis, I.G., Tsapatsis, M. Numerical simulation of atomic layer deposition for thin deposit formation in a mesoporous substrate. *AIChE Journal.* **2021**, e17305 https://doi.org/10.1002/aic.17305

2. Hayashi, M.; Lee, D.T.; Dorneles de Mello, M.; Boscoboinik, J.A.; Tsapatsis, M. ZIF-8 Membrane Permselectivity Modification by Manganese(II) Acetylacetonate Vapor Treatment. *Angew. Chemie*., **2021**, 60, 9316-9320 https://doi.org/10.1002/anie.202100173

3. Miao, Y.; Lee, D.T.; Dorneles de Mello, M.; Abdel-Rahman, M.K.; Corkery, P.; Boscoboinik, J.A.; Fairbrother, D.H.; Tsapatsis, M. Electron beam induced modification of ZIF-8 membrane permeation properties. *Chem. Comm*., **2021**, 57, 5250-5253 https://doi.org/10.1039/d1cc00252j

Jointly funded by this grant and other grants with relatively minor intellectual contribution from this grant: None.

Fluorescence Correlation Spectroscopy with the Maximum Entropy Method for Quantitative Analysis of Molecular Diffusion in Nanostructured Media

Takashi Ito,[1] *Daniel A. Higgins,*[1] *Lainjie Xue,*[1] *Shiqiang Jin*[2]*;* [1] *Department of Chemistry, Kansas State University;* [2] *Department of Statistics, Kansas State University*

Presentation Abstract

Thorough understanding of molecular dynamic behaviors within nanostructured media will facilitate designing efficient nanoporous membranes for energy-relevant chemical separations. However, it is challenging to quantitatively evaluate key mechanisms that control the efficiency of real membrane separations because of the involvement of complex interactions of solutes and solvents with nanostructured media. We employ advanced fluorescence techniques built upon single-molecule tracking (SMT) and fluorescence correlation spectroscopy (FCS) to gain molecular-level insights into the separation-relevant dynamics of solute species within cylindrical model nanopores. This presentation will introduce our efforts toward quantitative measurements of molecular diffusion dynamics in nanostructured media using FCS with the maximum entropy method (MEM). We explore the use of the MEM for the analysis of FCS data, because the MEM can afford not only the mean diffusion times (τ_D) of solutes under different environments and their observation probability ratio, but also the probabilistic distributions of individual τ_D. Indeed, we observed differences in the τ_D distributions for uncharged, cationic, and anionic fluorescent probes diffusing in two methylimidazolium ionic liquids (ILs) with different alkyl chain lengths. These differences are attributable to solute distribution in the ILs comprising nanoscale domains. In addition, FCS measurements with the MEM analysis were applicable to measure multiple τ_D components for fluorescent molecules diffusing within/on thin films of microphase-separated block copolymers. We are currently pursuing a better understanding of factors that govern the probabilistic τ_D distribution obtained from the MEM analysis so that we can quantify the influences of material heterogeneity on molecular diffusion. We are also employing the FCS-MEM approach to measure solute diffusion in model cylindrical nanopores.

Molecular Charge and its Role in Solute Orientational Confinement, Surface Interactions, and Diffusion within One-Dimensional Surfactant- and Solvent-Filled Silica Nanopores

Daniel A. Higgins, Takashi Ito, Ruwandi Kumarasinghe; Department of Chemistry, Kansas State University

Presentation Abstract

An in-depth understanding of molecular mass transport within nanoporous media is crucial to the design of improved membranes for highly-selective chemical separations. In this study, we employed polarization-dependent single molecule tracking to assess the level of orientational confinement, the rate of diffusion, and the diffusion mechanisms for charged and uncharged fluorescent dye molecules confined within the surfactant- and solvent-filled one-dimensional (1D) pores of mesoporous silica films. Four different perylene diimide (PDI) dyes, each having different lengths and/or charges, were employed. Wide-field fluorescence videos acquired from the samples revealed that a significant fraction of the molecules followed 1D pathways and exhibited highly polarized fluorescence, consistent with their tight orientational confinement within the pores. Single-frame step size distributions prepared from the tracking data were fit to a new model that accurately describes those expected for 1D Fickian diffusion in the presence of finite localization precision. These results reveal that the molecules exhibit predominantly Fickian-like diffusion. The few molecules found to exhibit anomalous diffusion were attributed to heterogeneity in the surfactant- and solvent-filled pores. Average diffusion coefficients obtained from mean square displacement (D_{MSD}) data were 20 – 100 % larger for the uncharged PDIs than for the cationic and anionic versions, consistent with slower diffusion by the latter due to their electrostatic interactions with oppositely charged sites on the pore-filling cationic surfactant and deprotonated silanol sites on the pore walls. Polarization dependent tracking data show that the longest uncharged PDI was most strongly confined within the pores, while the three shorter dyes were less confined. The cationic PDI was least confined, suggesting it explores more of the accessible pore diameter. The results provide new knowledge on the mechanisms by which the dye molecules interact with the pore-filling medium and the pore surfaces, helping to elucidate the factors controlling the rate of mass transport.

DE-SC0002362: Molecular-Level Investigations of Diffusion Behavior within Cylindrical Nanoscale Pores

PI: Takashi Ito, **Co-PI:** Daniel A. Higgins
Postdoc: Lianjie Xue**Students:** Herman Coceancigh, Hamid Rashidi**Affiliations(s):** Department of Chemistry, Kansas State University

RECENT PROGRESS

The Role of Molecular Charge in the Nanoconfinement of Organic Molecules in Surfactant-Filled Silica Mesopores.

We investigated the translational and orientational dynamics of a series of charged and uncharged PDI dyes (**Figure 1**) within the cylindrical silica mesopores (~3.7 nm in inner pore diameter) of spin-cast films using SMT and the single-molecule emission polarization (SMEP) method. The mesopores were filled with rod-shaped micelles based on cetyltrimethylammonium bromide (CTAB) and solvents (ethanol and water) that penetrated as a vapor. SMT data showed 1D diffusing molecules in elongated cylindrical mesopores (**Figure 2**). The distributions of their frame-to-frame step sizes were consistent with a Fickian diffusion mechanism, with some evidence of anomalous diffusion (**Figure 3**). The appearance of anomalous diffusion was attributed to material heterogeneity, possibly caused by variations in the local solvent or surfactant content, or surfactant organization. The mean diffusion coefficient (D_{MSD}) was smaller for the cationic and anionic dyes (**Figure 4a**) owing to their electrostatic interactions with charged sites on the silica pore walls and with the cationic headgroups of the CTAB micelles filling the pores. SMEP studies of their confined orientational motions revealed that the longest uncharged C_{11}OPDI was most tightly confined within the pores as indicated by the smaller θ_{max}, while cationic $TAPDI^{2+}$ was apparently least confined (**Figure 4b**). Taken together with their mean D_{MSD}

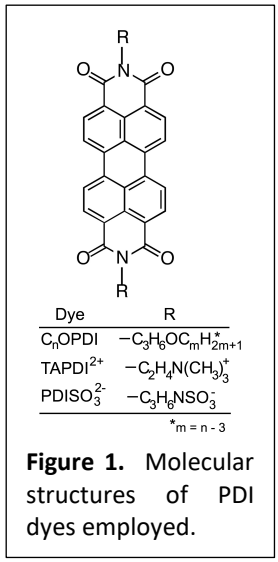

Figure 1. Molecular structures of PDI dyes employed.

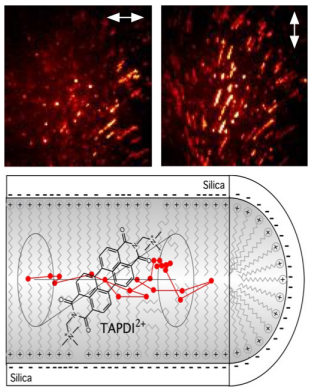

Figure 2. Z-projection images simultaneously acquired in two orthogonal polarizations for $TAPDI^{2+}$. These data show a predominance of 1D motion and strong polarization of dye emission parallel to the direction of motion, as shown in the scheme. Double-ended arrows (3 µm long) designate the detected polarizations.

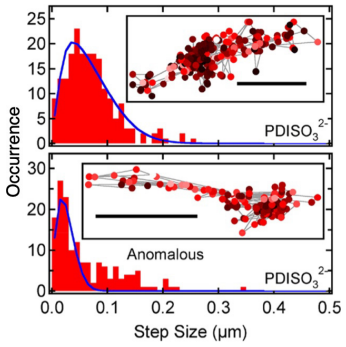

Figure 3. Representative single molecule step size distributions (red bars) and their trajectories (insets; scale bar: 250 nm) for $PDISO_3^{2-}$, depicting 1D motion. Solid blue lines represent the distribution for 1D Fickian diffusion in the presence of finite localization precision. Populations that don't fit well are labeled as "Anomalous".

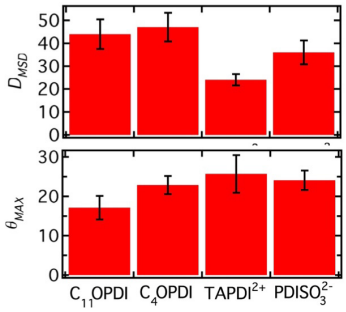

Figure 4. (a) Mean diffusion coefficients (x 10^{-3} µm^2/s) and (b) mean wobbling angles (in degree) for the four PDI dyes.

values, these results suggest the charged PDI dyes are least confined but experience the greatest electrostatic interactions with charged sites at the silica/surfactant boundaries. These results provide valuable insights into molecular transport mechanisms involving interactions with the pore surfaces and the surfactant/solvent phase(s).

Single-Molecule Fluorescence Studies on Molecular Permeability of Solvent-Swollen Block Copolymer Microdomains.

Monolithic block copolymer membranes and films have attracted considerable interest in the field of chemical separations owing to the formation of nanoscale domains with controlled structures, dimensions, and chemical/mechanical properties. For example, thin films of polystyrene-*block*-poly(ethylene oxide) (PS-*b*-PEO, **Figure 5**) have been examined as a chemical separation medium and as a polymer electrolyte, because these films comprise PEO microdomains that provide nanoscale molecular/ionic pathways. In-depth understanding of solvent-induced effects on microdomain permeability will help design better block copolymers for these energy-relevant applications. Here, we employed a series of spectroscopic methods to measure the properties of PS and PEO microdomains in thin PS-*b*-PEO films (PEO volume fraction ≈ 0.2) upon ethanol and water vapor exposure. *In situ* spectroscopic ellipsometry measurements showed a significant (6 – 10%) increase in thickness of PS-*b*-PEO films (20 – 300 nm thick) upon exposure to saturated ethanol and water vapor, indicating that these films were swollen by these vapors. Importantly, the swelling of PS-*b*-PEO films by ethanol vapor was unexpected, considering the negligible swelling of both PS and PEO homopolymer films by the vapor. The thickness of PS-*b*-PEO films gradually decreased after an initial quick increase upon ethanol vapor exposure. In contrast, no such decrease was observed for the swelling of PS-*b*-PEO films by water vapor. Subsequently, the details of the ethanol-induced swelling of PS-*b*-PEO films were investigated using FCS and SMT methods with Nile Red (NR) and sulforhodamine B (SRB) (**Figure 5**) as fluorescent probes. Solvatochromic NR molecules preferentially partitioned to the non-polar PS domains, as verified from their emission characteristics. Ethanol vapor exposure did not significantly alter the fluorescence emission properties of NR molecules and did not mobilize these molecules, implying the negligible swelling of the PS microdomains. In contrast, the diffusion of SRB molecules, which preferentially partition to the PEO microdomains, was enhanced upon exposure to saturated ethanol vapor, indicating that the swelling of PS-*b*-PEO films primarily took place at the PEO microdomains. Interestingly, the diffusion of SRB gradually slowed for longer exposure to ethanol vapor, which was consistent to the gradual deswelling of the films observed in the ellipsometry data. The unexpected ethanol-induced swelling of the PEO microdomains could reflect their amorphous nature owing to incomplete microphase separation at the PS–PEO interface.

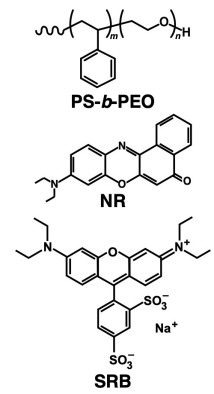

Figure 5. Molecular structures of PS-*b*-PEO, NR and SRB.

Fluorescence Correlation Spectroscopy with the Maximum Entropy Method for Quantitative Analysis of Molecular Diffusion in Nanostructured Media.

FCS has been widely used to investigate the local diffusion processes of fluorescent solutes in various media. FCS can measure faster diffusion processes than SMT. However, FCS affords only mean diffusion times (τ_D) and their observation probability ratio owing to the use of conventional fitting routines for FCS data analysis. Here, we examined the maximum entropy method (MEM) for the analysis of FCS data to quantify the probabilistic distributions of τ_D that are associated with the fluctuations of solute dynamics in nanostructured media. In FCS, the fitting is directed to minimize the sum of the squared residuals while maximizing the entropy associated with the probability distribution. We have shown different τ_D distributions for cationic, anionic, and uncharged fluorescent molecules diffusing in methylimidazolium-based ionic liquids (ILs) that could reflect the difference in distribution of the dyes in the solvents comprising nanoscale domains. In addition, FCS measurements with the MEM analysis were applicable to measure multiple τ_D components for fluorescent molecules diffusing within/on thin PS-*b*-PEO films.

Publications Acknowledging this Grant (September 2019 – present)

(I) Exclusively funded by this grant:

1. R. Kumarasinghe, T. Ito, D. A. Higgins, Nanoconfinement and Mass Transport in Silica Mesopores: the Role of Charge at the Single Molecule and Single Pore Levels, *Anal. Chem.* **2020**, *92*, 1416-1423 (DOI: 10.1021/acs.analchem.9b04589).
2. G. Ghimire, M. M. Moore, R. Leuschen, S. Nagasaka, N. Kameta, M. Masuda, D. A. Higgins, T. Ito, Influences of Hydrogen Bonding-Based Stabilization of Bolaamphiphile Layers on Molecular Diffusion within Organic Nanotubes Having Inner Carboxyl Groups, *Langmuir* **2020**, *36*, 6145-6153 (DOI: 10.1021/acs.langmuir.0c00556).
3. T. Ito, D. A. Higgins, Fluorescence Microscopic Investigations of Molecular Dynamics in Self-Assembled Nanostructures, *Chem. Rec*. **2021**, 21, 1417-1429 (DOI: 10.1002/tcr.202000173).

(II) Jointly funded by this grant and other grants with leading intellectual contribution from this grant:

NA

(III) Jointly funded by this grant and other grants with relatively minor intellectual contribution from this grant:

NA

Combinatorial Membrane Synthesis: Fundamentals of Hybrid Metal-Organic Brush (MOB) Membranes for Organic Solvent Nanofiltration (Renewal)

Pranav Ramesh, Mirco Sorci and Georges Belfort; Howard P. Isermann Department of Chemical and Biological Engineering, Rensselaer Polytechnic Institute, Troy, NY 12180;

Presentation Abstract

The goals of our current 3-year research project are (i) expansion of the novel modification technique Single Electron Transfer- Living Radical Polymerization (SET-LRP) to graft polymer brushes on a polyimide stable support followed by characterization and testing of the ensuing membrane (ii) stiffen the brush network utilizing metal organic frameworks and separately covalent bonds formed as a result of crosslinking the grafted brush network. Rose Bengal and methyl orange rejection of > 99% in ethanol was obtained with a series of hydrophilic SET-LRP-grafted polymer brushes on crosslinked polyimide membrane. Our results demonstrate that we can graft methacrylate brushes on a stable polyimide support and crosslink the brush structure to enhance stiffness of the grafted brush layer as confirmed with a quartz crystal microbalance with dissipation (QCM-D). Using a series of pure alcohols, these crosslinked brush membranes show potential for small molecule separations. The next step is to correlate the structural properties of these brush membranes with organic solvent nanofiltration (OSN) performance.

Grant Number: DE-FG02-09ER16005; Grant period: 09/01/2020–08/31/2023
Grant Title: Combinatorial Membrane Synthesis: Fundamentals of Hybrid Metal-Organic Brush (MOB) Membranes for Organic Solvent Nanofiltration (Renewal);
PI: Georges Belfort (PI) P: 518.276.6948; E: belfog@rpi.edu
Postdoc(s): Dr Mirco Sorci**; Student(s):** Graduate Students: Pranav Ramesh; **Affiliations:** Howard P. Isermann Department of Chemical and Biological Engineering, RPI, Troy, NY 12180.

RECENT PROGRESS

A. Summary:

(a) Goals: The goals of our current 3-year research project are (i) expansion of the novel modification technique SET-LRP to graft polymer brushes on a cross-linked polyimide support followed by characterization and testing of the ensuing membrane (ii) stiffen the brush network with metal organic frameworks (MOFs) and with covalent bonds formed because of crosslinking the grafted brush network.

(b) Approach: Three aspects of the research were: (i) to graft branches terminated with a carboxyl group on each bristle (or bristle branch) allowing copper-driven immobilization to form MOF-like structures between branches and separately to crosslink bristles using aliphatic or aromatic diamines; (ii) to test the performance of the membranes using organic dyes and pure solvents (alcohols); and (iii) to characterize the metal organic and crosslinked brush membranes. Since, it was assumed that crosslinking stiffens the brush membrane resulting in increased selectivity, we first confirmed increased stiffness with QCM-D. Increased selectivity resulting from increased stiffness will be tested next.

(c) Findings: The significant findings from the past one and half year are summarized below (papers resulting from this work are listed below and in **PUBLICATIONS** and **REFERENCES**).

(i) *Graft polymerization:* We extended the use of SET-LRP[1] to modify the stable crosslinked polyimide (P84) support using hydrophobic monomers (alkyl methacrylates C2, C6 and C18) with differing carbon chain length and correlated the performance of these membranes with synthesis parameters (choice of monomer and polymerization time)[2]. To understand the rate-limiting steps of SET-LRP, we simplified the number of reaction steps from 12 to 5 and then mathematically modelled the reduced reaction scheme and successfully compared the predictions of the model with previous experimental results[3]. During the current grant, we extended this knowledge with hydrophobic monomers and modified the crosslinked polyimide surface with hydrophilic monomers: Methacrylic acid (MA) and hydroxy ethyl methacrylate (HEMA). **Fig. 1A** demonstrate successful graft polymerization of the initiator-grafted crosslinked polyimide support with pMA and pHEMA in methanol using Attenuated Total Reflectance- Fourier Transform Infrared Spectroscopy (ATR-FTIR) based on the ester peak at 1726 cm^{-1} as a result of modification with the methacrylate monomers. **Fig. 1B** shows successful modification of the support in water making the process greener and cheaper. *Discovery: Surface grafting with hydrophilic monomers was successful.*

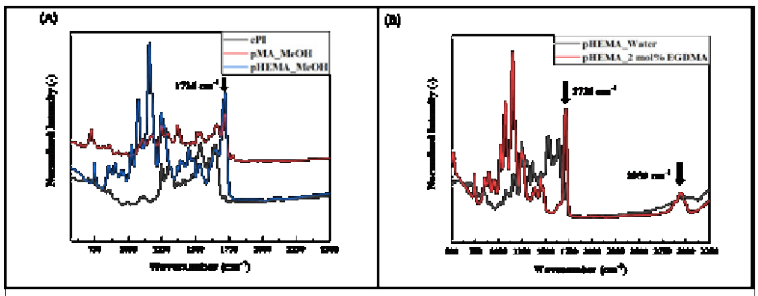

Figure 1: FTIR-FTIR spectra (A) Crosslinked polyimide (cPI), methacrylic acid (MA in MeOH) and hydroxy ethyl methacrylate (HEMA in MeOH) where polymerization is carried out in methanol (MeOH). (B) Hydroxy ethyl methacrylate modified in water with/without crosslinker diethylene glycol dimethacrylate (EGDMA). The increase in ester band at 1726 cm^{-1} (arrow) in (A) and (B) and hydrocarbon band at 2959 cm^{-1}(right arrow) in (B) indicates of a successful membrane modification.

(ii) Crosslinking pHEMA: We hypothesized in the proposal a carboxyl-amine route to crosslinking brushes. This route failed to yield stable crosslinked structures. Hence, an alternative route utilizing HEMA with n-(ethylene glycol) dimethacrylate where (n=2, 3…. poly) was investigated. n-ethylene glycol dimethacrylates comprise of a series of commercial monomers differing only in the length of the ethylene glycol chain which allows for tuning the brush network with differing lengths of crosslinkers based on the targeted separation. **Fig. 1B** demonstrates successful incorporation of ethylene glycol dimethacrylate (EGDMA, n=1) within the pHEMA framework using ATR-FTIR based on the increased intensity of the ester (1726 cm^{-1}) and hydrocarbon (2959 cm^{-1}) bands. *Discovery: Successful grafting and crosslinking of pHEMA-EGDMA demonstrated.*

***(iii) Characterization*: (a) Poly (methacrylic acid) grafting:** The surface charge of crosslinked polyimide membranes modified with methacrylic acid for 2,4,8 and12 h reaction time, t_p, and at pH 7 and solution conductivity of 150 mS/m was determined using zeta potential measurements (SurPass™ 3, Anton Paar). The polymerized brush was negative at pH 7 since the pK_a of methacrylic acid is 4.65 [4]. From **Fig. 2A**, modification of the surface leads to a change in the surface charge: from -6 mV for the initiator grafted crosslinked polyimide support to -14 mV for the methacrylic acid modified brush. The fairly constant zeta potential values between 4 and 12 h of polymerized brush is likely due to the zeta potential measurements of the charge at the

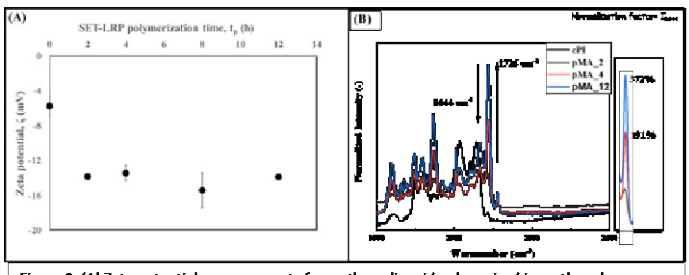

Figure 2: (A) Zeta potential measurements for methacrylic acid polymerized in methanol on a polyimide (P84) substrate for 2-12 h compared with the initiator modified crosslinked polyimide substrate (cPI). (B) Increasing ester band at 1726 cm^{-1} with increase in polymerization time of methacrylic acid (MA) polymerized for, 4h (191%) and 12 h (372%), with respect to that at 2 h.

exposed terminal of the brush and is independent of the t_p. The ATR-FTIR spectrum of methacrylic acid polymerized for 2,4,8 and 12 hours in **Fig. 2B** shows an increase in the ester peak (1726 cm^{-1}) as a function of polymerization time indicating increased grafting. *Discovery: Successful poly (methacrylic acid) grafting and increase in polymer grafting with polymerization time.* **(b) *Crosslinking pHEMA to induce stiffness:*** To measure the stiffness, two reaction cycles of HEMA grafted brushes were polymerized onto a piezoelectric quartz crystal of a QCM-D, without and with crosslinker (EGDMA). For the reactions with HEMA (**Fig. 3A**) and with HEMA and crosslinker (**Fig. 3B**), water washing after the first and second reaction cycles exhibited an increasing non-zero frequency confirming grafting. Overtone spread at the end of each cycle increased more for the non-crosslinked HEMA than for the crosslinked HEMA confirming increased stiffness for the later. The second marker of increased stiffness is obtained by comparing the dissipation change (ΔD) values of HEMA without crosslinker ($2x10^{-6}$), ($4x10^{-6}$) and with crosslinker (0), ($1X10^{-6}$) after cycles 1 and 2, respectively. *Discovery: Two independent QCM-D results provide quantitative proof of increased stiffness (rigidity) with crosslinking.*

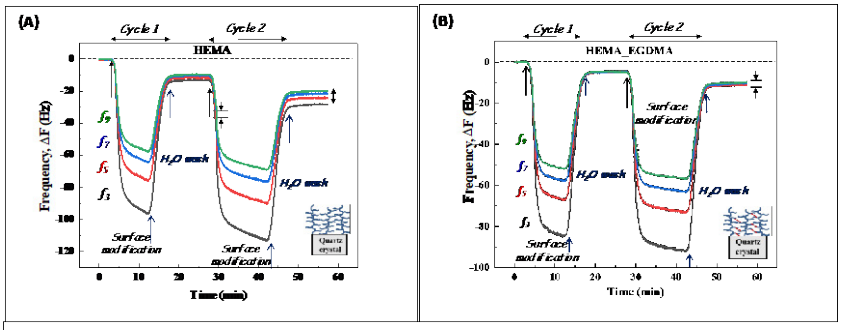

Figure 3: Variation in frequency with surface modification (A) without and (B) with crosslinker

(iv) Filtration. (a) Poly(methacrylic acid) (pMA): Crosslinked polyimide support membranes were graft-polymerized with methacrylic acid monomer for different polymerization times and the permeabilities of six alcohols (methanol, ethanol, isopropanol, butanol, isobutanol and octanol) were determined (**Fig. 4A**). Complete rejection of two negatively charged dyes: Rose Bengal (Molecular weight= 1017 g/gmol) and Methyl Orange (327 g/gmol) from ethanol were observed. Current experiments are focused on the separation of molecules much closer in size such as ethanol-isobutanol mixtures. **(b) Crosslinked HEMA:** Crosslinked polyimide membranes were modified with HEMA for 3 hours in water. The crosslinker ethylene glycol dimethacrylate (EGDMA) was added at 2, 5 and 10 mol% to the SET-LRP reaction mixture to crosslink the pHEMA brush network. The pure solvent permeabilities of the ensuing membranes were tested using six alcohols (above) (**Fig. 4B**). As in the case with methacrylic acid, complete rejection of two negatively charged dyes: Rose Bengal and Methyl Orange from ethanol were observed with HEMA modified as well as the EGDMA crosslinked variant of the membrane.

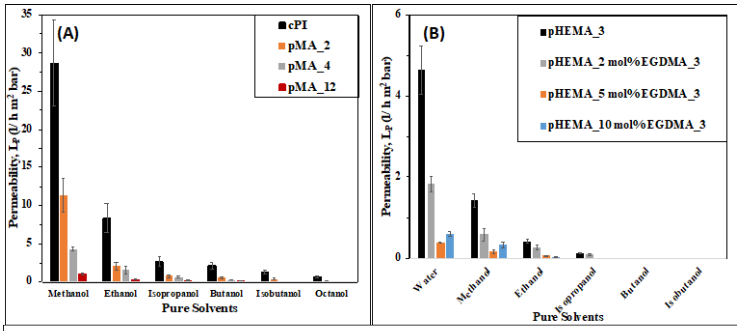

Figure 4: Permeability of six alcohols through crosslinked polyimide support (cPI) and (A) methacrylic acid modified membranes with graft polymerization for 2, 4 and 12 h on the support, and (B) HEMA modified membranes with 2, 5 and 10% crosslinker ethylene glycol dimethacrylate (EGDMA) polymerized for 3 h.

PUBLICATIONS

(a) <u>Peer-reviewed publications</u> in chronological order that specifically acknowledged DOE support from our current grant (DE-FG02-09ER16005, Period 02/01/18-to date):

S1. Belfort, G. Membrane Filtration with Liquids: A Global Approach with Prior Successes, New Developments and Unresolved Challenges. *Angew. Chem. Int. Ed.*

2019, *58* (7), 1892–1902. https://doi.org/10.1002/anie.201809548.

S2. Gunter, K.; Sorci, M.; Belfort, G. A Simplified Predictive Tool for Design and Analysis of SET-LRP Reactions with Mechanistic Insight. *ACS Appl. Polym. Mater.* **2020**, *2* (11), 4924–4935. https://doi.org/10.1021/acsapm.0c00796.

S3. Ramesh, P.; Xu, W. L.; Sorci, M.; Trant, C.; Lee, S.; Kilduff, J.; Yu, M.; Belfort, G. Organic Solvent Filtration by Brush Membranes: Permeability, Selectivity and Fouling Correlate with Degree of SET-LRP Grafting. *Journal of Membrane Science* **2021**, *618*, 118699. https://doi.org/10.1016/j.memsci.2020.118699.

(b) Manuscripts in preparation that will specifically acknowledge DOE support from our current grant (DE-FG02-09ER16005, Period 02/01/18-to date):

S4. Ramesh P, Sorci M, Behera D, Padinjarekutt S, Sengupta B, Yu M, Kilduff J, Belfort G (2021) Design and performance of hydrophilic crosslinked brush membranes for Organic Solvent Nanofiltration, *in preparation.*

S5. Ramesh P, Sorci M, Behera D, Padinjarekutt S, Sengupta B, Yu M, Feldbyum, J Kilduff J, Belfort G (2021) Synthesis and characterization of Metal Organic Brush Membranes, *in preparation.*

REFERENCES

1. Lligadas, G.; Grama, S.; Percec, V., Recent Developments in the Synthesis of Biomacromolecules and their Conjugates by Single Electron Transfer-Living Radical Polymerization. *Biomacromolecules* **2017,** *18* (4), 1039-1063.

2. Ramesh, P.; Xu, W., L.; Sorci, M.; Trant, C.; Lee, S.; Kilduff, J.; Yu, M.; Belfort, G., Organic solvent filtration by brush membranes: Permeability, selectivity and fouling correlate with degree of SET-LRP grafting. *J. Membr. Sci.* **2020,** *618*, 118699.

3. Gunter, K.; Sorci, M.; Belfort, G., Predictive Tool for Design and Analysis of SET-LRP Polymer Grafting Reactions. *ACS Applied Polymer Materials,* **2020,** *2* (11), 4924-4935.

4. Rojas-Hernandez, A.; Ibarra-Montaño, E.; Rodríguez-Laguna, N.; Sánchez-Hernández, A., Determination of pKa Values for Acrylic, Methacrylic and Itaconic Acids by 1H and 13C NMR in Deuterated Water. *Journal of Applied Solution Chemistry and Modeling* **2015,** *4*, 7-18.

5. Cho, N.-J.; Frank, C. W.; Kasemo, B.; Höök, F. Quartz Crystal Microbalance with Dissipation Monitoring of Supported Lipid Bilayers on Various Substrates. *Nat Protoc* **2010**, *5* (6), 1096–1106. https://doi.org/10.1038/nprot.2010.65.

Session IV: Trans-Interfacial Phenomena (Jovan Kamcev, Chair)

Investigations into the Nanoscale Ordering of Ionic Liquids and Deep Eutectic Solvents

Jared L. Anderson, Emily A. Smith, Jacob W. Petrich, Xueyu Song; Chemical and Biological Sciences, Ames Laboratory

Presentation Abstract

Nanoscale spatial and chemical inhomogeneity is important to many aspects of molecular transport and partitioning that affect the efficiency and scalability of separation processes. Our team is interested in understanding nanoscale ordering in ionic liquids (IL) and deep eutectic solvents (DES) as these solvents hold promise in reducing energy consumption when employed in separation systems. The existence of nanodomains, defined as nanometer-sized regions within the solvent formed by aggregation of charged ions and uncharged alkyl chains from the cation, has been predicted in many ILs. However, there has been no attempt to correlate their presence, composition, and structure to separation performance. Using various configurations of inverse gas chromatography (IGC), we will demonstrate that the solvation interactions of DESs can be measured based on the hydrogen bond donor (HBD) and acceptor (HBA) that comprise the solvents. An understanding of these solvation interactions provides fundamental insight into the unique interplay of the HBA/HBD and a clearer picture of their intricate intermolecular interactions with other molecules. We will also show that IGC can be extended to study the olefin selectivity of silver(I) ions in ILs when the silver(I) ion/IL mixture is subjected to various gases under varied temperature conditions. Machine learning studies of a model super-cooled liquid indicate the possible existence of such nano-domain and a classification scheme is developed for the molecular characterization of these domains. In combination with meso-scale FCS measurements and macroscopic chromatography, a concrete model of nano-domains is in sight.

FWP Title: Ionic liquids and deep eutectic solvents in separation science: An understanding of nanoscale ordering

PI: Jared L. Anderson
Co-PIs: Emily A. Smith, Jacob W. Petrich, Xueyu Song
Student(s): Philip Eor, Nabeel Abassi, Muhammad Qamar Farooq, Viet Nguyen, Ian Morgan, Jingzhe Li, Nicole Stephens, Kalyan Santra, Bala Gopal Maddala

RECENT PROGRESS

(I) Silver-Olefin Interactions using Silver(I) Ions in Ionic Liquids

Mixtures composed of silver salts and ILs are used as effective olefin/paraffin separation media in various techniques such as facilitated transport membranes and argentation gas chromatography. However, comprehensive information regarding the influence of different environmental conditions (e.g., carrier/exposure gas types and temperatures) and composition (i.e., silver salt types and molecular structures of ILs) on the silver(I) ion-based olefin separation system is scarce.
In our work, inverse GC was applied to systematically investigate the impacts of the aforementioned

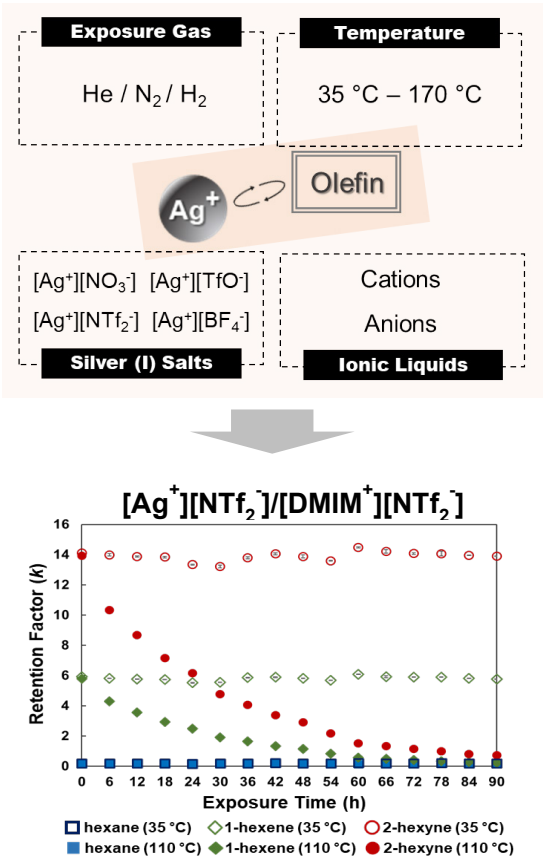

Figure 1. Experimental scheme (top) and change in retention of olefin and paraffin probes in the $[Ag^+][NTf_2^-]$ and $[DMIM^+][NTf_2^-]$ IL mixture upon exposure to hydrogen gas at different temperatures (bottom).

variables on the selectivity and stability of silver(I) ion within the olefin separation media. A series of silver salts and imidazolium-based ILs were prepared as stationary phases. The effect of different carrier gases (helium, nitrogen, and hydrogen) and increasing temperatures on the silver(I) ion-olefin complexation were studied (Fig. 1), allowing for temporal changes on silver(I) ion-olefin complexation under various environmental conditions to be evaluated. Among the silver salt/IL stationary phases examined, the silver bis[(trifluoromethyl)sulfonyl]imide ($[Ag^+][NTf_2^-]$) salt dissolved in 1-decyl-3-methylimidazolium bis[(trifluoromethyl)sulfonyl]imide ($[DMIM^+][NTf_2^-]$) IL exhibited the highest stability with moderate selectivity. The $[Ag^+][NTf_2]/[DMIM^+][NTf_2^-]$ composition was applicable in olefin separations up to 170 °C under helium conditions. Under constant hydrogen, this composition exhibited stable olefin separation capability for at least 90 hours at 35 °C. On-going work is focused at developing a molecular model that can be used to understand the role of nanoscale ordering on silver(I)-olefin separations in ILs.

(II) Elucidating the Role of Hydrogen Bond Donor and Acceptor on Solvation

Interactions in Deep Eutectic Solvents

Deep eutectic solvents (DESs) are homogenous mixtures formed through the combination of a hydrogen bond donor (HBD) and hydrogen bond acceptor (HBA). The resulting compound has a lower melting point than both individual components. An understanding of the role of the HBA and HBD on their multiple solvation interactions is important to gain insight into how these complex solvents coordinate within themselves as well as interact with solute molecules. Using inverse GC, we have measured solute-solvent interactions for two classes of DESs using a wide range of probe molecules. For DESs formed by ammonium/phosphonium salts and carboxylic acids, it was found that the hydrogen bond basicity can be modulated by (1) choosing more acidic (lower pKa) carboxylic acids as HBDs and using larger molar ratios of HBD compared to the HBA, (2) decreasing the length of alkyl chain substituents within HBA, and (3) varying the halide anion within the HBA. By using highly basic probes to examine the acidity of DESs, it was found that DESs formed with larger molar ratios of low pKa HBAs result in solvents with higher hydrogen bond acidity. Choline chloride-based ($[Ch^+][Cl^-]$) DESs comprised of HBDs with shorter alkyl chain substituents and strong organic acids possess lower hydrogen bond basicity and dispersive-type interactions as well as higher hydrogen bond acidity compared to those composed of various isomers of butane diol and hexane diol as HBDs. Choline acetate DESs possess higher hydrogen bond basicity, dispersive-type, and dipolar interactions compared to those comprised of the $[Ch^+][Cl^-]$ HBA. We are currently expanding this approach to measure additional solute-solvent interactions, such as infinite dilution activity coefficients, for other classes of DESs.

(III) Structural Characterization of Ionic Liquids by Means of Fluorescence Correlation Spectroscopy

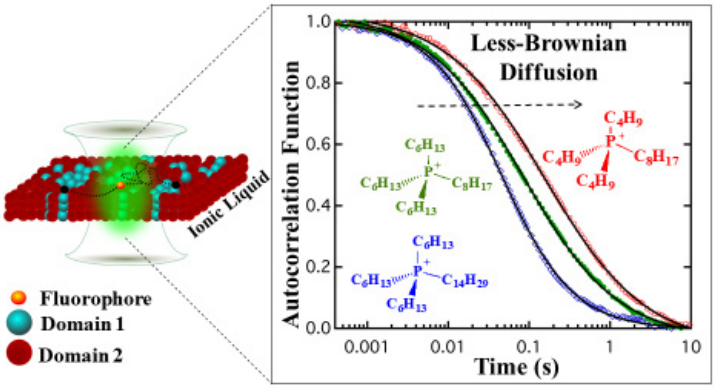

Figure 2: Autocorrelation functions of the fluorescence of Atto 590 in three ionic liquids. Deviations from Brownian motion are suggestive of the existence of nanodomains.

Fluorescence correlation spectroscopy (FCS) was applied to investigate the diffusional dynamics of hydrophilic (Atto 590) and amphiphilic (DiD) fluorophores in a series of alkylphosphonium ionic liquid (IL) films ($[P_{4448}^+][Cl^-]$, $[P_{6668}^+][Cl^-]$, $[P_{66614}^+][Cl^-]$, and $[P_{66614}^+][NTf_2^-]$) in order to determine diffusional parameters and to elucidate nanoscale structural heterogeneities within the IL. From the correlation functions, the diffusion coefficients of the fluorophores were estimated, rendering values that span from 0.39 to 1.2 and 0.146 to 5.2 $\mu m^2/s$ for Atto 590 and DiD, respectively. An increase in the diffusion coefficient values is correlated to the increase in the alkyl chain length, which in turn is correlated with a decrease in viscosity. Deviations from Brownian diffusion behavior of the fluorescent probes in the ILs are observed (Fig. 2) and are attributed to the presence of nanoscale structural heterogeneities in the tetraalkylphosphonium ILs. These results experimentally confirm the presence of nanosegregation in tetraalkylphosphonium ILs, which has been previously observed in molecular dynamics studies.

As is indicated by this abstract, these studies are currently being extended to DESs.

(IV) Theoretical Characterization of Nano-domains in Stationary Phases for Separations

Using principal component analysis and a clustering algorithm, it was found that the particles in a model of super-cooled liquids can be classified into a number of nano-domains in the configurational space. Such a classification is consistent during the 60 ns simulation run, namely, there are only few particles changing their domains in the interfacial region (Fig. 3), hence thermodynamic and kinetic quantities such as free energy and diffusion constant in the domain can be extracted from such simulations.

Armed with the above classification method, we are in the process of studying the nano-domain of 1-octyl-3-methylimidazolium chloride (C8mimCl) at various temperatures, where temperature-dependent FCS is also under way. Using the diffusion constants from various domains, we should be able to interpret the FCS measurements and thus present concrete experimental evidence of such nano-domains. Furthermore, different absorption/desorption rates of analytes in the nano-domains of chromatographic stationary phases (hence, the retention time of the analyte) can be calculated from the classification

scheme. A successful comparison with our team's chromatographic data could present strong evidence of the nano-domain picture of super-cooled liquids.

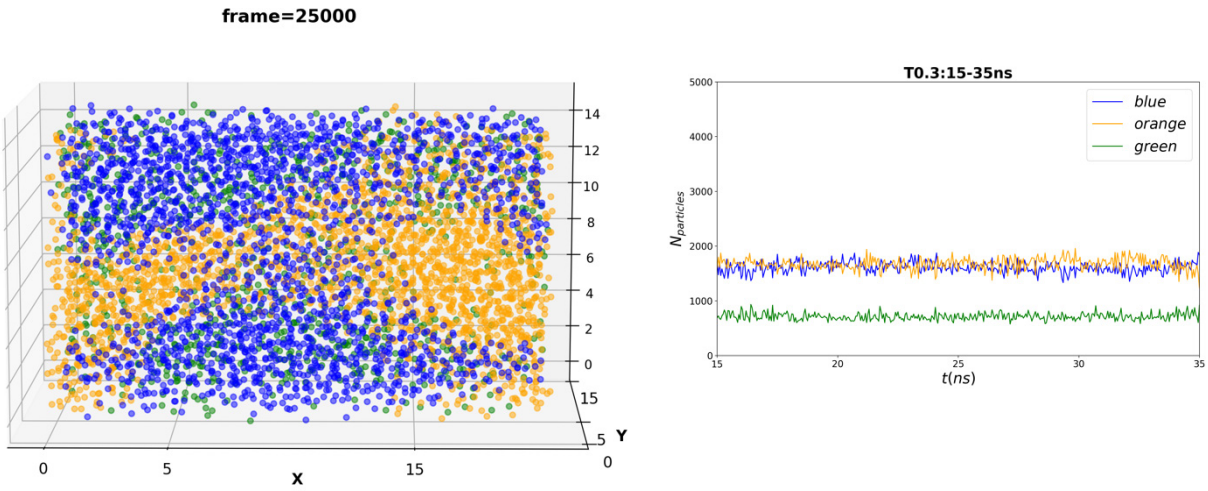

Figure 3: Panel a) is the snapshot of the simulation box at 25 ns with three domains labelled by blue, orange and green particles and the reduced temperature T=0.3. Panel b) is the number of particles fluctuations during the 15 to 35 ns simulation run. It can be shown that the domain identity changes of the particles only happens at the interface between domains.

Publications Acknowledging this Grant from 2019 – present :

1. Abbasi, N.M.; Farooq, M.Q.; Anderson, J.L. "Modulating Solvation Interactions of Deep Eutectic Solvents Formed by Ammonium Salts and Carboxylic Acids Through Varying the Molar Ratio of Hydrogen Bond Donor and Acceptor" *J. Chromatogr. A.,* 2021, 1643, 462011.

2. Eor, P.; Ryoo, D.; Nan, H.; Anderson, J.L. "Characterizing Olefin Selectivity and Stability of Silver Salts in Ionic Liquids using Inverse Gas Chromatography" *ACS Omega*, 2020, 48, 31362-31369.

3. Farooq, M.Q.; Odugbesi, G.A.; Abbasi, N.M.; Anderson, J.L. "Elucidating the Role of Hydrogen Bond Donor and Acceptor on Solvation in Deep Eutectic Solvents Formed by Ammonium/Phosphonium Salts and Carboxylic Acids" *ACS Sustainable Chem. Eng.* 2020, 49, 18286-18296.

4. Farooq, M.Q.; Abbasi, N.M.; Anderson, J.L. "Deep Eutectic Solvents in Separations: Methods of Preparation, Polarity, and Applications in Extractions and Capillary Electrochromatography" *J. Chromatogr. A* 2020, 1633, 461613.

5. Mendivelso-Pérez, D.L.; Farooq, M.Q.; Anderson, J.L.; Petrich, J.W.; Smith, E.A. Diffusional Dynamics of Tetraalkylphosphonium Ionic Liquid Films Measured by Fluorescence Correlation Spectroscopy. *J. Phys. Chem. B* 2019, *123*, 4943−4949.

Anomalous Transport in Grafted Nanoparticle Membranes

Brian Benicewicz,[1] Sanat Kumar[2]; [1]Department of Chemistry, University of South Carolina, Columbia, S.C; [2]Department of Chemical Engineering, Columbia University, New York, NY

It has now been well established that membranes comprised purely of nanoparticles grafted densely with polymer chains have anomalously enhanced gas transport properties. These unexpected results are known to be a consequence of increased free volume but the mechanical origins of this increased volume for gas transport are unknown. Here we use a suite of complementary experimental probes (neutron scattering, x-ray scattering, Brillouin light scattering, BLS) and theory to show that polymer chains grafted densely to a surface have extended conformations ("dry" brush regime). BLS shows that this dry brush regime has an unusually low modulus which thus allows for enhanced density fluctuations and hence improved gas permeabilities. While our current results shed important light on the transport behavior of these materials, the consequence of these results on designing membranes with desired (improved) gas separation performance is the ultimate goal.

Data-driven Separation Agent/Solvent Design – An Integrated Simulation Experiment Approach

Ping Yang,[1] Stosh A Kozimor,[2] Danny Perez,[1] Nicholas E Lubbers,[3] Enrique R Batista,[1] Marc J Cawkwell,[1] Benjamin Stein,[2] Sara L Adelman,[2] Daniel J. Burrill,[1] Chang Liu,[1] Rebecca Carlson,[1] Xiaobin Zhang,[1] Jan Janssen,[1] Brian T Arko,[2] Wenhao Gao,[3] Michael F Tynes[1]; [1]Theoretical Division, Los Alamos National Laboratory; [2]Chemistry Division, Los Alamos National Laboratory; [3]Computer, Computational and Statistical Sciences Division, Los Alamos National Laboratory

Presentation Abstract

Advanced separation technologies are needed to recycle the residual energy content of spent nuclear fuel, minimize nuclear waste production, optimize storage conditions, and alleviate proliferation concerns associated with reprocessing. However, rationally designing advanced separations schemes has traditionally been a time-consuming and expensive process. This project implements a multidisciplinary effort that integrates modern data-centric approaches, quantum simulations, and high-throughput experimental chemical separations screening, to develop new predictive capabilities for actinide separations. In this presentation, we share our recent progress on these integrated tasks. Separation efficiency is driven by the difference between two chemical systems. To capture the nature of this, we developed a new method, pairwise difference regression (PADRE), that is a mathematical instantiation of the intuitive concept that it is often easier to deduce relative differences between two chemical systems than it is to grasp a single system alone. This simple and generic approach is a new transformation that can be applied to machine learning models for improved performance and the generation of uncertainty quantification with improved performance compared to the state-of-the-art techniques. In parallel, we carried out fundamental separation studies and made recommendations for potential improvement for ^{241}Am processing and our results suggested that CLEAR processing of ^{241}Am would be made more robust and effective if the extraction resin used in large-scale processing was changed from *m*-CMPO to TODGA or TEHDGA.

2022LANLE3M1: Data-driven Separation Agent/Solvent Design - An Integrated Simulation Experiment Approach

Postdocs: Sara L Adelman, Daniel J. Burrill, Chang Liu, Rebecca Carlson, Jan Janssen
Students: Brian T Arko, Wenhao Gao, Xiaobin Zhang, Michael F Tynes

RECENT PROGRESS

Machine Learning for Improved Prediction in Chemical Search

Machine learning (ML) plays a growing role in the design and discovery of chemicals, aiming to reduce the need to perform expensive experiments and simulations. For such applications, ML is promising but difficult, as models must generalize to vast chemical spaces from small training sets and must have reliable uncertainty quantification metrics to identify and prioritize unexplored regions. Ab initio computational chemistry and chemical intuition alike often take advantage of the differences between chemical conditions, rather than their absolute structure or state, to generate more reliable results. We have developed an analogous comparison-based approach for ML regression, called pairwise difference regression (PADRE),

which is applicable to arbitrary underlying learning models and operates on pairs of input data points. During training, the model learns to predict differences between all possible pairs of input points. During prediction, the test points are paired with all training set points, giving rise to a set of predictions that can be treated as a distribution in which the mean is treated as a final prediction and the dispersion is treated as an uncertainty measure. Pairwise difference regression was shown to reliably improve the performance of the random forest algorithm across five chemical ML tasks. Additionally, the pair-derived dispersion is both well correlated with model error and performs well in active learning. We also show that this method is competitive with state-of-the-art neural network techniques, while being considerably simpler to deploy. Thus, pairwise difference regression is a promising tool for candidate selection algorithms used in chemical discovery.

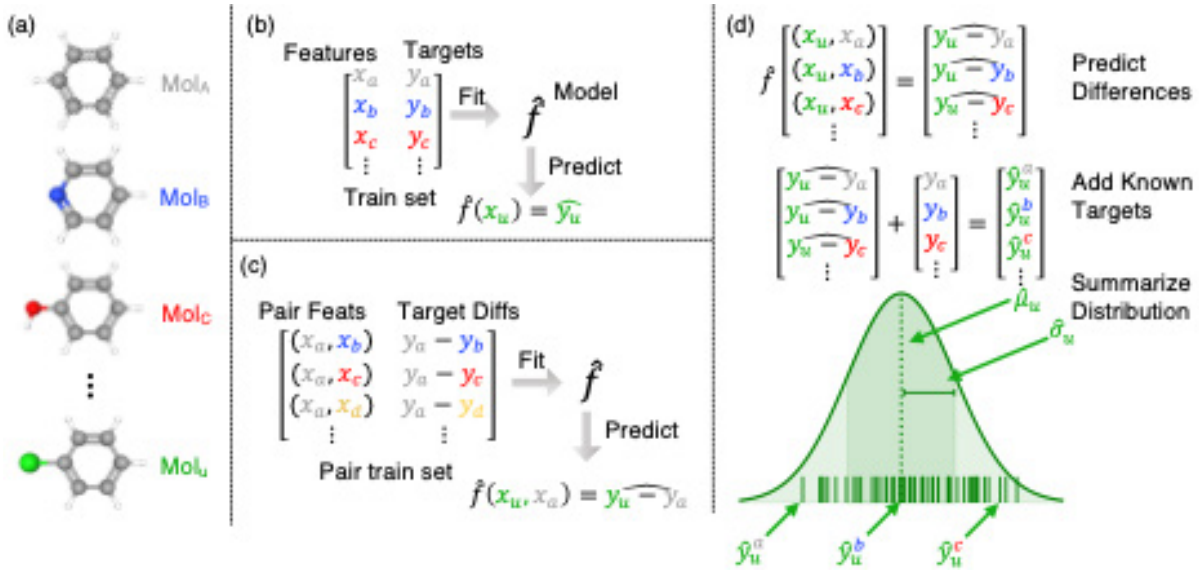

Figure 1. Illustration of PADRE. For (b–d), quantities with hats ˆ are estimates under the estimator f̂. (a) Set of seen molecules (labeled {A, B, C, ...}) used for training a regressor to predict the properties of a single unseen molecule U. (b) Classical regression approach wherein a model is fit to predict the targets y_i from the feature vectors x_i describing the molecules. (c) Construction of a pairwise training set from which a model learns to predict differences in target values from pairs of feature vectors. (d) Process of pairing an unseen feature vector with all seen feature vectors, giving a set of a set of difference predictions under the model. This set is then converted by addition of known quantities into a distribution of target predictions for the unseen feature vector.

High-throughput Advanced Simulations

Experimental exploration of the chemical space of practical ligands represents an insurmountable challenge due to the innumerable number of possible atomic configurations. Computational resources are used to reduce the complexity of the problem by identifying candidate ligands following the workflow shown in *Figure 2*. Initially, useful ligands are identified from literature and used as starting points for the generation

of new ligands. In Box 1, these ligands are used to generate metal complexes and their structures are stored in the Result Database. These initial structural guesses are then used in screening calculations conducted at a low level of theory. Density functional tight-binding theory (DFTB) was chosen as the best trade-off between computational efficiency and accuracy to estimate binding energies for the ligands in the complexes. The DFTB results are then analyzed in Box 3 where the binding energies for the most promising ligands are recalculated using Density Functional Theory. The results located in the database are then used to generate machine learning models in Box 4. The purpose of these models is to use the stored computational and experimental results to predict separation factors for the proposed ligands, identify useful features of the ligands to inform further exploration in Box 1, and finally to guide experimental efforts by selecting ligands for further evaluation. This high-throughput computational framework can effectively manage computational resources in the state-of-the-art supercomputers and automate the work flow to enable the application of modern data-science.

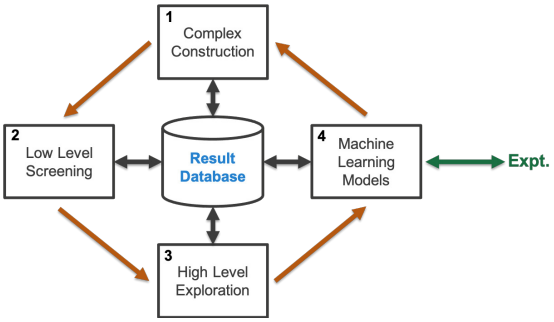

Figure 2. *Illustration of high-throughput advanced simulations*

Characterizing Extraction Chromatography for Large-scale Americium-241 Processing

- Our study focuses on improving extraction resin usage for large-scale separations and addresses a longstanding U.S. vulnerability associated with domestic supply of ^{241}Am. We cannot overstate the importance of improving recently established ^{241}Am recovery method, considering that numerous industries utilize ^{241}Am's nuclear properties. Applications range from use in smoke detectors (which have saved countless lives) to use of ^{241}Am by the petroleum industry. From 1950 to the 1990s, the U.S. maintained ^{241}Am inventories and supplied the world with this valuable radionuclide. Then, in the 1990s production ceased, the ^{241}Am inventory was depleted, and in the U.S. became reliant on foreign ^{241}Am sources. This situation recently changed (circa 2017) when the ChLoride Extraction and Actinide Recovery (CLEAR) ^{241}Am recovery line was established to provide the U.S. with a source of ^{241}Am. It is now a national priority to strengthen CLEAR processing so that the U.S. can meet existing ^{241}Am industrial needs.

- In this work, we carried out fundamental separation studies and made recommendations for potential improvement for ^{241}Am processing. For instance, our paper defines extraction chromatography characteristics that could (*1*) reduce ^{241}Am product loss, (*2*) increase ^{241}Am product recovery, and (*3*) make the ^{241}Am recovery processes accommodating to more diverse feedstocks. For instance, within the context of large-scale processing constraints, we characterized the ability of the *m*-CMPO resins – currently used industrially – to bind ^{241}Am as a function of HCl concentrations, metal contaminant concentrations, and contact time. The *m*-CMPO's performance was evaluated against the chemically similar and commercially available Rare Earth (RE) resin and against a carefully selected series of diglycolamide (DGA) resins, see *Figure 3*. Our results suggested that CLEAR processing of ^{241}Am would be made more robust and effective if the extraction resin used in large-scale processing was changed from *m*-CMPO to TODGA or TEHDGA.

- One particularly interesting observation was that binding of ^{241}Am by *m*-CMPO resin worsened drastically when the feed matrix contained relevant amounts of common metal contaminants. Surprisingly, TODGA and TEHDGA were unaffected by the metal contaminants. One would not predict this outcome if reviewing extraction chromatography data described currently in the literature. It also highlighted the importance of better

defining matrix effects on separations science, in general. Demystifying the influence of matrix effects on extractant behavior (as well other variables identified within our manuscript) would advance usage of extraction chromatography.

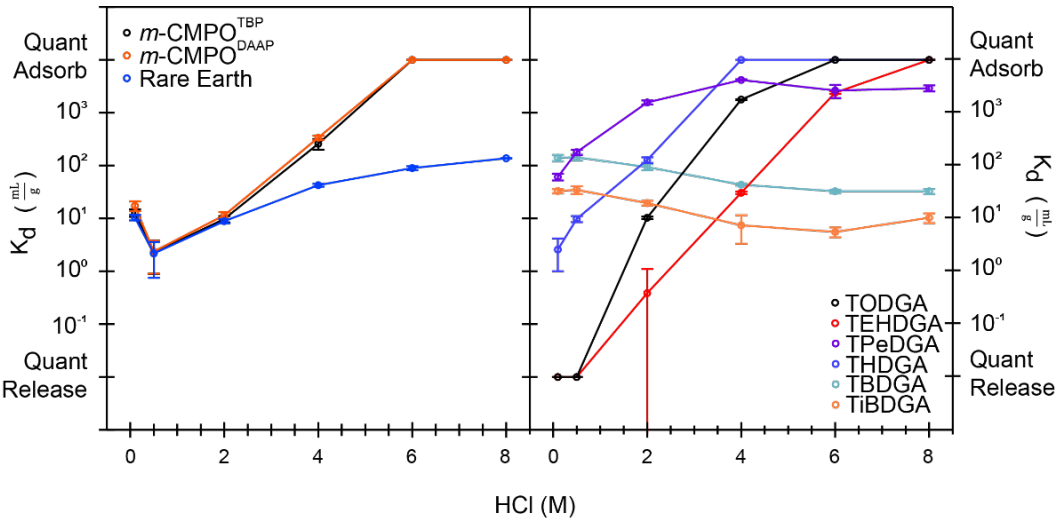

Figure 3. Temperature-controlled (25 ºC) distribution coefficients (K_d) from ^{241}Am (20 nCi) made in HCl (0.1 to 8 M) after contact times of 24 h. The CMPO resins [left; *m*-CMPO^{TBP}, *m*-CMPO^{DAAP}, and Rare Earth (RE)] are compared against DGA resins (*Right;* TODGA, TEHDGA, TPeDGA, THDGA, TBDGA, TiBDGA) with resin loading ranging from 25 ± 5 mg. Measurements were made in triplicate and uncertainty is shown as the standard deviation from the mean (at 1σ). The labels "Quant Adsorb" and "Quant Release" were defined as "quantitatively adsorbed" and "quantitatively released."

Publications Acknowledging this Grant in 2020 – present

3. Tynes, M; Gao, W; Burrill, D. J.; Batista, E. R.; Perez, D.; Yang, P.; Lubbers, N; "Pairwise Difference Regression: A Machine Learning meta-algorithm for Improved Prediction and Uncertainty Quantification in Chemical Search", *J. Chem. Inf. Model. 2021.* https://doi.org/10.1021/acs.jcim.1c00670
4. Arko, B. T.; Dan, D.; Adelman, S. L.; Huber, D.; Kimball, D. B.; Kozimor, S. A.; Lam, N. H.; Mocko, V.; Shafer, J. C.; Stein, B. W.; Thiemann, S. L.; "Characterizing Extraction Chromatography for Large-scale Americium-241 Processing", *Ind Eng Chem Res 2021, In press.*

Design and Synthesis of Molecular and Macromolecular Sequestrants for Recovery of Rare Earth Elements via Electrodialysis

Kristin M Hutchins,[1] *Michael Findlater,*[1,2] *and Weile Yan*[3]*;* [1]*Department of Chemistry and Biochemistry, Texas Tech University, Lubbock, TX;* [2]*Department of Chemistry and Chemical Biology, University of California Merced, Merced, CA;* [3]*Department of Civil and Environmental Engineering, University of Massachusetts Lowell, Lowell, MA*

Presentation Abstract

Rare-earth elements are crucial for numerous technologically-relevant industries including energy, electronics, and aerospace; however, both the supply and separation of rare earths are pressing challenges. Here, we aim to develop a class of electrodialysis membranes with novel ion-gating functionality for selective extraction of early lanthanides via molecular recognition in tandem with a conventional electrodialysis (ED) strategy. By enhancing the intrinsic ion selectivity of the ED process via incorporation of ion sequestrants at the surface of the ED membrane, we aim to maximize extraction efficiency (i.e., chemically enhanced ED, CEED). Our ongoing work has focused on the synthesis and lanthanide-binding behaviors of molecular sequestrants based on crown ether and calixarene moieties. For the crown ethers, the size of the cavity is altered to optimize binding for specific lanthanides. The sequestrants are also functionalized with a polymerizable group, which is used to incorporate them into macromolecules. Future studies will involve incorporating the molecular and macromolecular sequestrants into ED membranes and performing testing. The results will serve as feedback, and the molecular design of the sequestrants will be modified to optimize lanthanide binding.

Grant Number: DE-SC0020204 **Grant Title: Chemically Enhanced Electrodialysis (CEED) for Recovery of Rare Earth Elements**
Student(s): Deepika Bedi, Kotono Babaguchi, Jesus Daniel Loya, Mythreyi Sivaraman

RECENT PROGRESS

Synthesis of Molecular Sequestrants: Polymerizable Crown Ethers and Calixarenes

Crown ethers are macrocyclic compounds containing oxygen as donor atoms. They exhibit selective sequestering properties towards metal ions that are controlled by the size and shape of the cavity relative to the metal cations of interest. Three crown ether sequestrants functionalized with a vinyl group (for polymerization) have been synthesized in high yield and at gram scale (Figure 1). A 'boot-strapped' *p-tert*-Butylcalix[4]arene-crown-6-dicarboxylic acid has also been synthesized. Binding studies of sequestrants **1**-**3** with the lanthanides neodymium and dysprosium are in progress.

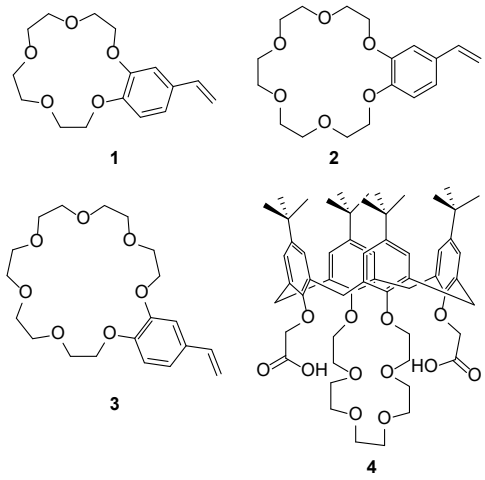

Figure 1. Molecular structures of sequestrants: **1** vinyl benzo-15-crown-5 ether, **2** vinyl benzo-18-crown-6 ether, **3** vinyl benzo-21-crown-7 ether, **4** ionizable crown-ether 'boot-strapped' *t*-butylcalix[4]arene.

Synthesis of Macromolecular Sequestrants

Ultimately, successful binding of targeted ions from solution requires a robust material that can be tailored to perform specific functions. In addition to utilizing the small-molecule-supported sequestrants **1**-**4**, macromolecular sequestrants can also be physisorbed or chemically-adhered to the ED membrane and offer numerous binding sites, as well as additional overall material robustness. The sequestrant portions of the polymer are designed to recognize and engage in dynamic noncovalent bonding; thus, binding lanthanides in a reversible fashion. Our current work is focused on synthesis of copolymers, and the ratio of the two comonomers can be tuned to optimize binding of the lanthanide. The use of a comonomer could also decreases overall cost and synthetic demand. We have synthesized a copolymer using styrene and sequestrant **2** as comonomers (Mn=3068; Đ=1.423). Synthesis of additional copolymers is underway with a focus on systematically varying the ratio of the comonomers (styrene and sequestrant monomer) and the molecular weight of the copolymers (Figure 2). Homopolymerization of the sequestrant monomers will also be investigated in the future.

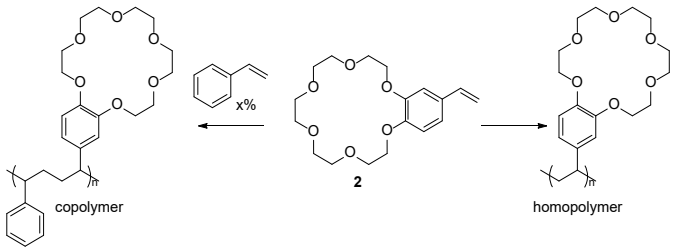

Figure 2. Synthetic strategy toward crown ether macromolecular sequestrants.

Membrane Modification and Electrodialysis

Electrodialysis (ED) is a well-established technology for desalinating brackish water with moderate to high total dissolved solids (TDS). Various forms of ED techniques are being used in the water service industry due to their modular nature, small energy footprint, and amenability to partial desalination (as opposed to general or non-selective desalination). In addition, compared to reverse osmosis (RO) and nanofiltration (NF), the ion-exchange membranes used in ED cells are more resistant to fouling, stable at elevated temperatures (thus, compatible with heated water from a deep underground environment), and are less sensitive to residue oxidizers (e.g., ClO_2) that are often used in feed water pre-treatment or membrane cleaning. Although the ED process is inherently more selective for multivalent ions than mono-valent ions due to multivalent ions possessing higher affinity to membranes and greater ion mobility, such intrinsic selectivity is inadequate for the removal of low levels of scalants or rare-earth elements from concentrated background matrix. Our team is presently augmenting ED membranes with ion-gating properties by incorporating the molecular and macromolecular sequestrants on the surface of conventional ion-exchange membranes to attain selective separation of target ions (Figure 3). Testing with neodymium and dysprosium are in progress.

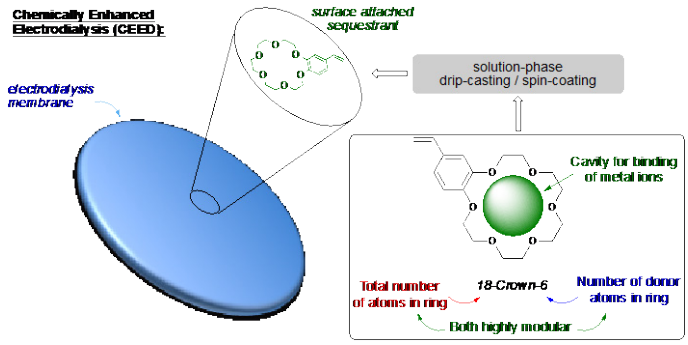

Figure 3. Depiction of CEED, physisorbed modified crown-ether shown as an example.

Publications Acknowledging this Grant in Sept 2019–present

(I) Exclusively funded by this grant:

None yet.

(II) Jointly funded by this grant and other grants with leading intellectual contribution from this grant:

Barragan, N.; Bedi, D.; Sivaraman, M.; Loya, J. D.; Findlater, M.; Hutchins, K. M.; Yan, W. "Selective Hardness and Barium Removal from Brackish Water with Chemically Enhanced Electrodialysis." *To be submitted*.

(III) Jointly funded by this grant and other grants with relatively minor intellectual contribution from this grant:

None.

Leveraging High-throughput Computation and Machine Learning to Discover and Understand Low-Temperature Fast Oxygen Conductors

Ryan Jacobs, Dane Morgan; University of Wisconsin-Madison, Madison, WI, 53706, USA.

Abstract

In this work, we seek to combine materials data mining, machine learning, high-throughput computation and experiments to (1) enable transformative basic understanding of structure-property-performance relationships governing oxygen transport in oxygen-active materials and (2) facilitate the discovery and rational design of new oxygen-active materials which transport oxygen efficiently at low temperature. We have used a hierarchy of screening criteria and computationally discovered two new oxide structural families that are predicted to rapidly conduct oxygen with an interstitial-mediated diffusion mechanism: general structure formula $A_4B_5C_4O_{22}$ and $AB_2C_4O_{12}$, with specific investigated compositions of $La_4Mn_5Si_4O_{22}$ and $ZrMn_2Ge_4O_{12}$, which have very low calculated O migration barriers of 0.44 +/- 0.02 eV and 0.34 +/- 0.03 eV, respectively. In addition, we have combined data mining and unsupervised machine learning analysis and discovered a new structural class of vacancy-mediated oxygen conductor, with the general formula Bi_2MO_4X (M= rare earth, X= halogen), which has an O migration barrier of 0.10 +/- 0.004 eV, the lowest we have found to date. Barriers were obtained from Density Function Theory (DFT) based approaches, included nudged elastic band, high-temperature ab initio molecular dynamics, and intermediate temperature machine learning potential molecular dynamics. The O diffusion mechanisms in the interstitial diffusers generally work by either an interstitial mechanism ($La_4Mn_5Si_4O_{22}$) or an interstitialcy kick-out mechanism ($ZrMn_2Ge_4O_{12}$). Bi_2LaO_4Cl has an unusual crossover in diffusion mechanism when cooling and the mechanisms active in the two domains are still under investigation. We are actively pursuing experimental investigations to synthesize, characterize, and test these newly discovered materials to confirm their exceptional predicted O diffusion properties.

DE-SC0020419: Leveraging High-throughput Computation and Machine Learning to Discover and Understand Low-Temperature Fast Oxygen Conductors

PI(s): Ryan Jacobs, Dane Morgan
Postdoc(s): Jun Meng, Sariful Sheikh, Xiangguo Li
Student(s): Lane Schultz
Affiliations: Same as above

RECENT PROGRESS

Discovery of new fast interstitial oxygen conductors. We have developed a screening approach to identify structures that are likely to enable interstitial oxygen to form and diffuse (Figure 1). Using the sequence of screening criteria as outlined in Figure 1, we mined the 33,975 oxide materials present in the Materials Project database and found that 87 of them satisfy all of our desired criteria through step 7, although screening is ongoing. For these 87 materials identified we are actively calculating their O migration energies. The final screening step 8 serves as an assessment of the ability of the material to diffuse O interstitials. Here, we use one or more of DFT-based *ab initio* molecular dynamics (AIMD) simulations[1,2], machine learning fitted Interatomic Potential (IPMD) simulations,[3,4] and Nudged Elastic Band (NEB) calculations, to study the migration pathway and barrier of the interstitial oxygen in the 87 promising oxides which were found to stably incorporate O interstitials. From the set of

presently finished calculations, we have already discovered a number of material compositions which broadly fall into two structural classes, which are calculated to have low O migration energies. These structural families have general formula $AB_2C_4O_{12}$ and $A_4B_5C_4O_{22}$, wherein A, B, and C are cations, which structures are shown in Figure 2.

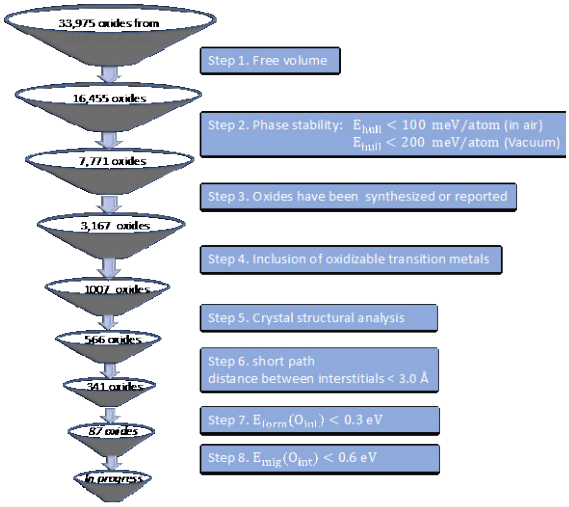

Figure 1. The flowchart of the screening procedure used for the discovery of new interstitial oxygen diffusers.

The structure of $AB_2C_4O_{12}$ (see Figure 2a) consists of (001) layers of AO_8 square antiprisms and BO_6 octahedra sharing edges, separated by layers of CO_4 tetrahedra. The CO_4 tetrahedra are linked into $[C_4O_{12}]^{8-}$ rings, which are comprised of four vertex-sharing CO_4 tetrahedra. Members of $AB_2C_4O_{12}$ which have low interstitial oxygen formation energies, include but are not limited to $ZrMn_2Ge_4O_{12}$, $ZrCo_2Ge_4O_{12}$, $ZrCo_2Ge_4O_{12}$, $Y(YMn)Ge_4O_{12}$, and $Y(YCo)Ge_4O_{12}$. Among these members, $ZrMn_2Ge_4O_{12}$ shows a very low migration barrier of ≈0.33 eV from AIMD, IPMD, and NEB calculation (see Figure 3 a-c). The $A_4B_5C_4O_{22}$ family is isostructural with the perrierite structure and crystallizes in the monoclinic space group *C2/m* (see Figure 2b). The $A_4B_5C_4O_{22}$ material displays sorosilicate C_2O_7 groups which separate rutile-like sheets of edge-shared BO_8 octahedra from single, isolated BO_8 octahedra. In general, the A-site, B-site, and C-site elements may be selected from alkali metals, alkaline earth metals, transition metals, post-transition metals, metalloids, and lanthanoids. $La_4V_5Si_4O_{22}$ and $Nd_4V_5Si_4O_{22}$ are found to have low interstitial oxygen formation energies. We have focused study on $La_4Mn_5Si_4O_{22}$, which presents low migration barriers of ≈0.4-0.5 eV for oxygen-ion diffusion in the bulk structure from AIMD, IPMD, and NEB calculation (see Figure 3 d-f). We believe all these materials are structurally distinct from the known interstitial oxygen formers, which include apatites, Ruddlesden-Popper phases (particularly A_2BO_4), hyperstoichiometric UO_{2+x}, and possibly Fe_2O_3 at low temperature.[5]

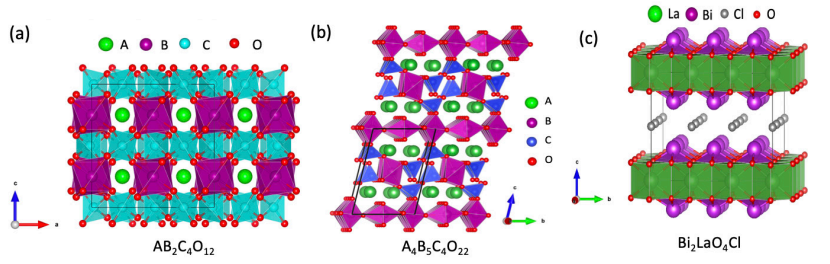

Figure 2. Structures of new fast O interstitial and vacancy diffusing materials.

Discovery of new fast vacancy-mediated oxygen conductors. Here, we seek to find new vacancy-mediated fast oxygen conductors that are structurally distinct from known good diffusers (e.g. perovskites, fluorites) in an effort to discover new oxide structural families that may be fast oxygen conductors. We combine data mining of the Materials Project, unsupervised machine learning clustering methods, and chemical intuition to suggest new oxide structural families that may be promising to explore further. To perform the unsupervised machine learning analysis, for every oxide in the Materials Project database we construct features from computationally derived X-ray diffraction (XRD) and the radial distribution function (RDF) characterizing the material structure. Next, we perform a nearest neighbors clustering analysis which provides information on structural similarity based on the calculated XRD and RDF vectors for each material. To assess structural similarity, we use three canonical material reference points which

represent compositions belonging to known good conducting materials families: $LaMnO_3$ (perovskite), BiO_2 (fluorite), and $Gd_2Zr_2O_7$ (pyrochlore), and sort all of the oxide materials based on their structural "distance" from these reference points. We examine the sorted structures for each group until a material is found that has a close neighbor distance and is structurally distinct from being a perovskite, fluorite, Bi_2O_3-type, or pyrochlore material. From this analysis, we have found a half dozen material structure types, of which representative compositions consist of Bi_2LaO_4Cl, LaZnPO, FeClO, $Ba_2Y(CuO_2)_4$, $Ba_2Mn_2Sb_2O$, and CsTlO.

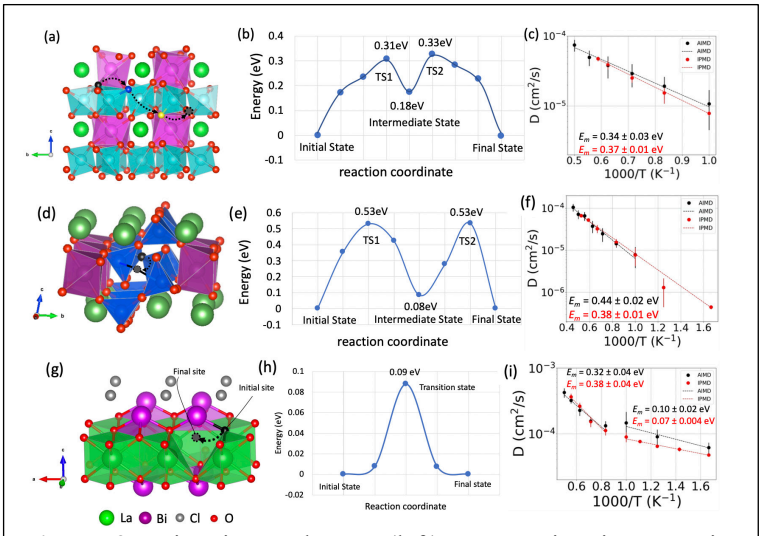

Figure 3. Migration pathways (left), NEB migration energies (middle), and AIMD (black) and machine learning potential (red) diffusivities (right) for $ZrMn_2Ge_4O_{12}$ (top), $La_4Mn_5Si_4O_{22}$ (middle), and Bi_2LaO_4Cl (bottom).

Single vacancy mediated O diffusion in Bi_2LaO_4Cl has an exceptionally small migration barrier of ≈ 0.1 eV and is currently our most promising new vacancy-mediated oxygen conductor material (see Figure 3 g-i). Bi_2LaO_4Cl belongs to the structural family with formula Bi_2MO_4X, wherein M is a rare-earth element (M= Y, La, Ce, Pr, Nd, Sm, Eu, Gd, Tb, Dy, Ho, Er, Tm, Yb, Lu) and X is a halogen element (F, Cl, Br, I). Bi_2LaO_4Cl is a tetragonal structure with space group *P4/mmm* (see Figure 2c). In the structure, $[Bi_2LaO_4]^+$ layers are interweaved with a single layer of halogen atoms, forming a layered structure. Bi is 4-fold coordinated and La is 8-fold coordinated.

Understanding oxygen conduction in novel materials families. *$AB_2C_4O_{12}$ family:* We have focused study on the promising material $ZrMn_2Ge_4O_{12}$. The AIMD simulation trajectories show that the oxygen-ion in $ZrMn_2Ge_4O_{12}$ migrates through an interstitialcy (or "kick-out") mechanism, in which the oxygen interstitial hops to an oxygen lattice site and the lattice oxygen hops to another interstitial site. *$A_4B_5C_4O_{22}$ structural family:* We have focused study on the promising material $La_4Mn_5Si_4O_{22}$. The AIMD simulation trajectories show that the oxygen-ion in $La_4Mn_5Si_4O_{22}$ migrates through an an interstitial diffusion pathway, where the oxygen interstitial directly hops in between two SiO_4 tetrahedra, without exchanging with the lattice oxygen. *Bi_2LaO_4Cl vacancy diffuser:* Bi_2LaO_4Cl shows an unexpected kink in the D vs. 1/T curve (see Figure 3i). Such kinks generally signal a change in mechanism and are frequently seen in polycrystalline materials, where they signal a crossover from bulk to grain boundary diffusion with decreasing temperature. However, here the change is occurring in a single crystal. We are presently investigating the origin of this unusual phenomenon. Another interesting aspect of O diffusion in Bi_2LaO_4Cl is that the diffusion is restricted to be effectively two dimensional, confined to the Bi_2LaO_4 layers.

Experimental evaluation of new promising materials.

We are presently focusing experimental evaluation on the $La_4Mn_5Si_4O_{22}$ and Bi_2LaO_4Cl materials.[6–8] $La_4Mn_5Si_4O_{22}$ was synthesized through the solid-state reaction method: $7MnO_2 + 4LaCl_3 + 4SiO_2 \rightarrow La_4Mn_5Si_4O_{22} + 2MnCl_2 + 4Cl_2$, where the reaction mixture of MnO_2, $LaCl_3$ and SiO_2 was ground for 20 minutes and sealed in a quartz tube. The reactant was heated at 850°C for 10 days, and the obtained sample was rinsed by alcohol to remove $MnCl_2$. The X-ray diffraction pattern of the sample was compared with the standard $La_4Mn_5Si_4O_{22}$ from literature, shown in Figure 4, and the reference peak

positions confirm that the synthesized sample is the $La_4Mn_5Si_4O_{22}$ material. Bi_2LaO_4Cl was synthesized by the flux method at 1073K in air. CsCl was mixed with Bi_2O_3, BiOCl, and La_2O_3 at the stoichiometric molar ratio of 1:2:1, with a solute concentration (Bi_2LaO_4Cl/(Bi_2LaO_4Cl + CsCl)) of 5 mol %. The mixture was ground for 20 minutes, placed in an alumina crucible with lid, and heated at 1073K for 20h. After natural cooling, the sample was washed with deionized water, collected by filtration, and dried at room temperature. XRD analysis has been performed to analysis the structure of the synthesized sample, and the comparison of the XRD pattern of the synthesized Bi_2LaO_4Cl and the Bi_2LaO_4Cl reference is shown in Figure 4 and again confirms successful synthesis of the target.

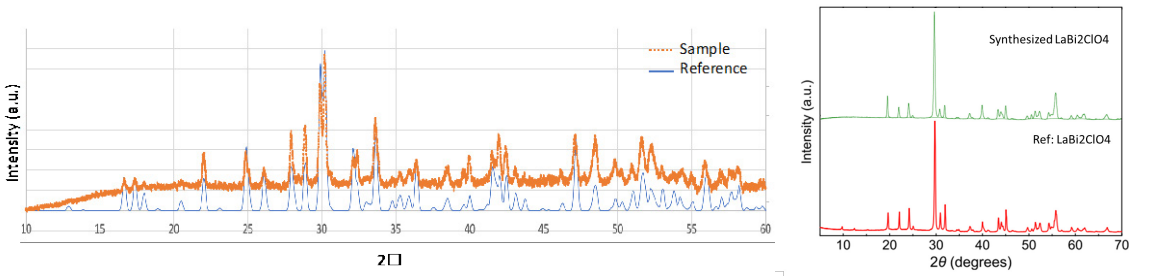

Figure 4. XRD measurements showing we have obtained correct phase $La_4Mn_5Si_4O_{22}$ (left) and Bi_2LaO_4Cl (right) materials.

With bulk structures of our promising materials confirmed, our next step is to assess the oxygen diffusion magnitude and mechanism type. We will do this by conducting electrical conductivity relaxation (ECR) measurements to measure the oxygen diffusivity and assess the defect carrier type (i.e. interstitial or vacancy) based on the diffusivity response to changes in oxygen pressure. Based on the results, we may explore sensible composition refinements to encourage the formation oxygen defects to facilitate improved diffusion.

Publications acknowledging this award (2019-present)

1.) Meng, J., Jacobs, R., Li, X., Morgan, D. "Harnessing the Materials Project and High-throughput Computation to Discover New Oxygen Interstitial Diffusers" (In preparation).
2.) Meng, J., Schultz, L., Li, X., Jacobs, R., Morgan, D. "Leveraging Data Mining, Machine Learning, and Chemical Intuition to Discover New Vacancy-Mediated Oxygen Conductors" (In preparation).
3.) Giordano, L., Jacobs, R., Akkiraju, K., Vivona, D., Morgan, D., Shao-Horn, Y. "Using Oxygen Electronic Structure to Understand and Design Catalytic Activity of Oxides" (In preparation- invited contribution for Accounts of Chemical Research).
4.) Shourov, E. H., Jacobs, R., Strohbeen, P. J., Morgan, D., Kawasaki, J. "Semi adsorption-controlled growth window for half Heusler FeVSb epitaxial films", Physical Review Materials 4 (7) (2020).
5.) Patent Application: "Oxygen Ion Transport Materials and Related Devices", by Meng, J., Jacobs, R., and Morgan, D. This patent has been accepted for support by the Wisconsin Alumni Research Foundation (WARF), which manages intellectual property for University of Wisconsin-Madison researchers. WARF is funding the legal support and a provisional patent draft has been completed and is ready for imminent submission.

References

(1) Kresse, G.; Hafner, J. Ab Initio Molecular Dynamics for Open-Shell Transition Metals. *Phys. Rev. B* **1993**, *48* (17), 13115–13118.
(2) Kresse, G.; Hafner, J. Ab Initio Molecular Dynamics for Liquid Metals. *Phys. Rev. B* **1993**, *47* (1), 558–561.

(3) Shapeev, A. V. Moment Tensor Potentials: A Class of Systematically Improvable Interatomic Potentials. *Multiscale Model. Simul.* **2016**, *14* (3), 1153–1173.
(4) Gubaev, K.; Podryabinkin, E. V.; Hart, G. L. W.; Shapeev, A. V. Accelerating High-Throughput Searches for New Alloys with Active Learning of Interatomic Potentials. *Comput. Mater. Sci.* **2019**, *156* (June 2018), 148–156.
(5) Yano, K. H.; Kohnert, A. A.; Banerjee, A.; Edwards, D. J.; Holby, E. F.; Kaspar, T. C.; Kim, H.; Lach, T. G.; Taylor, S. D.; Wang, Y.; et al. Radiation-Enhanced Anion Transport in Hematite. *Chem. Mater.* **2021**, *33* (7), 2307–2318.
(6) Gueho, C.; Giaquinta, D.; Mansot, J. L.; Ebel, T.; Palvadeau, P. Structure and Magnetism of La4Mn5Si4O22 and La4V5Si4O22: Two New Rare-Earth Transition Metal Sorosilicates. *Chem. Mater.* **1995**, *7* (3), 486–492.
(7) Nakada, A.; Kato, D.; Nelson, R.; Takahira, H.; Yabuuchi, M.; Higashi, M.; Suzuki, H.; Kirsanova, M.; Kakudou, N.; Tassel, C.; et al. Conduction Band Control of Oxyhalides with a Triple-Fluorite Layer for Visible Light Photocatalysis. *J. Am. Chem. Soc.* **2021**, *143* (6), 2491–2499.
(8) Xu, D.; Sale, M.; Avdeev, M.; Ling, C. D.; Battle, P. D. Experimental and Computational Study of the Magnetic Properties of ZrMn2-: XCoxGe4O12. *Dalt. Trans.* **2017**, *46* (21), 6921–6933.

Ion Transport in Highly Charged Polymer Membranes with Subnanometer Free Volume Elements

Jovan Kamcev, Assistant Professor; Department of Chemical Engineering, Macromolecular Science and Engineering, University of Michigan, Ann Arbor, MI 48109, USA

Charged polymer membranes are key components of several ion separation technologies (*e.g.,* electrodialysis and diffusion dialysis) and energy generation technologies (*e.g.,* reverse electrodialysis and fuel cells). Developing membranes with better selectivity and throughput will improve the efficiency of existing technologies and enable emerging environmental and energy applications such as redox flow batteries, microbial fuel cells, ion-exchange membrane bioreactors, and electrochemical CO_2 reduction. Design of new membranes with desired functionality would be accelerated by improved fundamental understanding of the connection between polymer structure and transport properties. The overarching goal of the proposed research is to establish fundamental understanding of ion transport in highly charged polymer membranes with subnanometer free volume elements (FVEs). The properties of this unique and largely unexplored class of membranes are situated in a transition region between those of gas separation membranes, in which polymer backbone dynamics influence small molecule transport, and highly swollen charged membranes, in which tortuosity and Coulombic interactions are most important. The discovery of new ion transport mechanisms in highly charged membranes with subnanometer FVEs and molecular-level understanding of such phenomena could enable the rational design of membranes with properties that are specifically tailored for a given application. To better understand the connection between polymer structure and transport properties in this class of membranes, the proposed research combines membrane synthesis, advanced morphological characterization, and characterization and modeling of membrane transport properties.

Fundamental Studies of Carbon Molecular Sieve Membranes for Energy Intensive Separations

William J. Koros, and Nicholas León; Georgia Institute of Technology, School of Chemical & Biomolecular Engineering

Presentation Abstract

Carbon molecular sieve (CMS) membranes combine high gas productivity and selectivity with economical scalability into large modules. Our BES project focuses on connecting polymer precursor type and processing to explain features of CMS responsible for its unusual abilities to separate difficult pairs such as olefins vs. paraffins. Besides traditional characterization tools, we use sorption and transport measurements and modeling to provide a self-consistent picture of the evolution from a flexible chain precursor to a rigid CMS. This approach improves the understanding of complex morphologies in CMS membrane. Recent expansion of the modeling thrust has shed light on the complex physical aging process in CMS and suggests ways to even use it to tune properties for the propylene-propane model system. Our hypothesis-driven project opens the way to a new set of CMS materials with tunable properties derived from diverse precursors to separate a broad spectrum of penetrant pairs. Temperature dependent analysis of associated diffusion coefficients is under way to assess entropic vs enthalpic factors controlling size and shape selectivity as a function of precursor and processing conditions. Our approach is significantly expanding fundamental knowledge and performance for separations relevant to the BES mission, thereby making it well-aligned with DOE's general mission and focus on fundamental science-based advances in technology.

Grant Number: No. DE-FG02-04ER15510

Students: Nicholas León (current), Sam Hays, Graham Wenz

RECENT PROGRESS

We have combined elemental analyses and WAXD, FTIR, XPS with sorption and transport measurements on diverse gas pairs having differences in effective size ranging from 0.91 Å to 0.1 Å. Especially the pairs with size difference of 0.1-0.5 Å challenge existing membranes to achieve high selectivities. We used these challenging gas pairs as probes to understand how precursor structure and pyrolysis processes change CMS structures. The result of this work was development of a self-consistent mathematical model and physical framework to understand the key attributes for such systems. The framework shares mathematical features with dual-mode transport theory for glassy polymers; however, physical connections to CMS model parameters differ greatly from glassy polymer cases. A small (typically <4 volume percent) of Langmuir sorption domains are typical in glassy polymers with a majority continuous phase. On the other hand, a very large volume fraction (> 50 volume %) of Langmuir active domains in CMS with a minority continuous phase make the two cases dramatically different. The extraordinary finding that, despite the relative percent difference in glassy polymers and CMS materials, a similar mathematical framework applies. This was both surprising and valuable, since much of the analysis for glassy polymers can simply be "imported" to the CMS case.

Fortunately, application of the dual mode framework enables evaluation of diffusion coefficients through the Langmuir and continuous (Henry's Law) domains. The ability to probe the morphology and changes in properties within the two domains provides molecular insights to phenomena like physical aging. We have found that we now have at least hypothetical connections between aging results and nanometer and sub-nanometer interpretations of the aging process. These results, while fundamentally fascinating, are also practically important, since they provide guidance on how to connect aging tendencies to molecular properties of precursors and processing conditions. Since differences in aging effects for the H_2/CH_4, CO_2/CH_4 and C_3H_6/C_3H_8 pairs that have effective size differences of 0.91 A, 0.50 A and 0.13 A, respectively can now be interpreted in terms of CMS structure and its changes with aging for a given precursor.

The dual mode framework also enables more refined understanding of the properties of CMS derived from subtly different precursors. For example, a reference standard precursor, 6FDA:BPDA-DAM has been studied for years; however, by simply changing the isomer of the BPDA to an asymmetric linkage vs. the standard symmetric linkage (e.g. sBPDA vs. aBPDA) dramatic difference are seen in the CMS created under otherwise identical conditions. Now we are studying the relative changes in the diffusion coefficients in the Langmuir and continuous Henry's Law domains of such CMS.

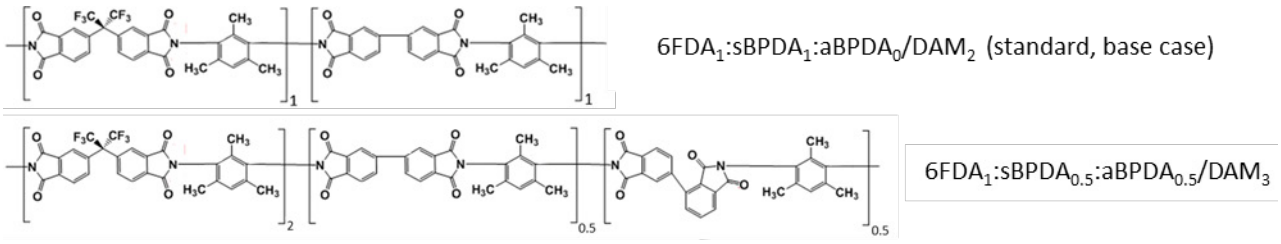

Figure 1: 6FDA:BPDA-DAM precursors without and with asymmetric BPDA isomers.

Publications—Acknowledging this Grant in 2016 → present

(I) Exclusively funded by this grant;

1. Hays, S.; Sanyal, O.; León, N.; Arab, P.; Koros, W., Envisioned role of slit bypass pores in physical aging of carbon molecular sieve membranes. *CARBON*, 157, 385-394 (**2020**).
2. Qiu, W.; Li, F.; Fu, S.; Koros, W., Isomer-Tailored Carbon Molecular Sieve Membranes with High Gas Separation Performance, *CHEMSUSCHEM*, 13(19), 5318-5328 (**2020**).
3. Kamath, M.; Itta, A.; Hays, S.; Sanyal, O.; Liu, Z.; Koros, W., Pyrolysis End-Doping to Optimize Transport Properties of Carbon Molecular Sieve Hollow Fiber Membranes, *Indus. & Engr. Chem. Res.,* 59(30), 13755-13761 (**2020**).
4. Liu, Y: Liu, Z.; Kraftschik, B; Babu,V; Bhuwania, N; Chinn, C; Koros, W; Natural gas sweetening using TEGMC polyimide hollow fiber membranes, *J. Membr. Sci*., 632, article no. 119361 (**2021**).
5. Liu, Y.; Chen, Z., Qiu, W.; Liu, G.; Eddaoudi, M.; Koros, W., Penetrant competition and plasticization in membranes: How negatives can be positives in natural gas sweetening, *J. Membr. Sci*., 627, article no. 11920 (**2021**).

6. Liu, G.; Labreche, Y.; Li, N.; Yang, L.; Zhang, C.; Miller, S.; Babu, V; Bhuwania, N.; Koros, W., Simultaneously tuning dense skin and porous substrate of asymmetric hollow fiber membranes for efficient purification of aggressive natural gas, *AICHE JOURNAL*, 65(4), 1269-1280 (**2019**).
7. Zhang, C.; Kumar, R.; Koros, W., Ultra-Thin Skin Carbon Hollow Fiber Membranes for Sustainable Molecular Separations, *AICHE J*, 65 (8), article no. UNSP e16611, DOI: 10.1002/aic.16611 (**2019**).
8. Kumar, R; Zhang, C; Itta, Arun K.; Koros, W., Highly Permeable Carbon Molecular Sieve Membranes for Efficient CO_2/N_2 Separation at Ambient and Subambient Temperatures, *J. Membr. Sci*., 583, 9-15 (**2019**).
9. Cao, Y.; Zhang, K.; Sanyal, O.; Koros, W., Carbon Molecular Sieve Membrane Preparation by Economical Coating and Pyrolysis of Porous Polymer Hollow Fibers, *Angew. Chem. Int. Ed.*,58, 11700 –11703 (**2019)**.
10. Kumar, R.; Koros, W., 110th Anniversary: High Performance Carbon Molecular Sieve Membrane Resistance to Aggressive Feed Stream Contaminants, *Indus. & Engr. Chem. Res.,* 58(16) 6740-6746 (**2019**).
11. Adams, J. ; Itta, A.; Zhang, C. ;Wenz, G. ; Sanyal, O. ; Koros, W., New Insights into Structural Evolution in Carbon Molecular Sieve Membranes During Pyrolysis, *CARBON*, 141, 238-246 (**2019).**
12. Zhang, C. Zhang, K.; Cao, Y.; Koros, W. Composite Carbon Molecular Sieve Hollow Fiber Membranes: Resisting Support Densification via Silica Particle Stabilization, *Indus. & Engr. Chem. Res*., 57 (47), 16051-16058 (**2018**).
13. Sanyal, O. ; Hicks, S.; Bhuwania, N. ; Hays, S. ; Kamath, M.; Karwa, S ;Swaidan, R.; Koros, W. Cause and Effects of Hyperskin Features on Carbon Molecular Sieve (CMS) Membranes, *J. Membr. Sci*., 551, 113-122 (**2018**).
14. Sanyal, O.; Zhang, C.; Wenz, G.; Fu, Shilu; Bhuwania, N.; Xu, Liren; Rungta, M. ; Koros, W. Next Generation Membranes-Using Tailored Carbon, *CARBON*, 127, 688-698 (**2018**).
15. Koros, W.; Zhang, C. Materials for Next-Generation Molecularly Selective Synthetic Membranes, *Nature Materials*, 16, 289-297 (**2017**).
16. Qiu, W.; Liu, L.; Koros, W. Effect of block versus random copolyimide structure on hollow fiber membrane spinnability, *J. Membr. Sci*., 529, 150-158 (2017).
17. Wenz, G.; Koros, W. Tuning Carbon Molecular Sieves for Natural Gas Separations: A Diamine Molecular Approach. *AICHE J*, **2017**, 63, 51-760.
18. Adams, J.; Bighane, N.; Koros, W. Pore Morphology and Temperature Dependence of Gas Transport Properties of Silica Membranes Derived from Oxidative Thermolysis of Polydimethylsiloxane. *J. Membr. Sci*., 524, 585-595 (**2017)**

(II) Jointly funded by this grant and other grants with leading intellectual contribution from this grant;

19. Qiu, W.; Xu, L.; Liu, Z.; Liu, Y. Arab, P.; Brayden, M.; Martinez, M.;Liu, J.;Roy, A.; Koros, W. Koros, Surprising olefin/paraffin separation performance recovery of highly aged carbon molecular sieve hollow fiber membranes by a super-hyperaging treatment, *J. Membr. Sci*., 620, article 118701 (**2021**).
20. Sanyal, O.; Hays, S.; León, N.; Guta, Y.; Itta, A.; Lively, R.; Koros, W., A Self-Consistent Model for Sorption and Transport in Polyimide-Derived Carbon Molecular Sieve Gas Separation Membranes, *Angew. Chem. Int. Ed., 59 (46), 20343-20347 (**2020**).*

21. Qiu, W.; Vaughn, J.; Liu, G.; Xu, L.; Brayden, M.; Martinez, M.; Fitzgibbons, T.; Wenz, G.; Koros, W., Hyperaging Tuning of a Carbon Molecular-Sieve Hollow Fiber Membrane with Extraordinary Gas-Separation Performance and Stability, *Angew. Chem. Int. Ed.,* 58(34),11700-11703 (**2019**).
22. Kamath, M.; Fu, S.; Itta, A.; Qiu, W.; Liu, G.; Swaidan, R.; Koros, W., 6FDA-DETDA: DABE polyimide-derived carbon molecular sieve hollow fiber membranes: Circumventing unusual aging phenomena, *J. Membr. Sci*., 546, 197-205 (**2018**).
23. Joglekar, M; Itta, A.; Kumar, R.; Wenz, G.; Mayne, J.; Williams, P. ; Koros, W. Carbon Molecular Sieve Membranes for CO_2/N_2 Separations: Evaluating Subambient Temperature Performance, *J. Membr. Sci*., 569, 1-6 (**2018).**
24. Chu, Y. H.; Yancey, D. ;Xu, L. ; Martinez, M.; Brayden, M.; Koros, W. Iron-Containing Carbon Molecular Sieve Membranes for Advanced Olefin/Paraffin Separations, *J. Membr. Sci*., 548, 609-620 (**2018).**
25. Kamath, M. G.; Fu, Shilu; Itta, Arun K.; Qiu, W. L.; Liu, G. P.; Swaidan, R.; Koros, W. J. 6FDA-DETDA: DABE Polyimide-Derived Carbon Molecular Sieve Hollow Fiber Membranes: Circumventing Unusual Aging Phenomena. *J. Membr. Sci*., 546, 197-205 (**2018**).
26. Fu, S.; Sanders, Edgar S.; Kulkarni, S.; Chu, Y. H; Wenz, GB; Koros, WJ. The Significance of Entropic Selectivity in Carbon Molecular Sieve Membranes Derived from 6FDA/DETDA:DABA(3:2) Polyimide, *J. Membr. Sci*., 329-343 (**2017**).
27. Zhang, C.; Wenz, G.B.; Williams, J.P.; Mayne, J. M.; Liu, G. P.; Koros W. J. Purification of Aggressive Supercritical Natural Gas Using Carbon Molecular Sieve Hollow Fiber Membranes. *Indus. & Engr. Chem. Res.,* 56, 10482–10490 (**2017**).
28. Zhang, C.; Koros, W. J. Ultraselective Carbon Molecular Sieve Membranes with Tailored Synergistic Sorption Selective Properties, *Adv. Mater.*, 29, 170163 (**2017**).
29. Rungta, M.; Wenz, G. B. Zhang, C.; Xu, L.; Qui, W. L.; Adams, J. S.; Koros, W. J. Carbon Molecular Sieve Structure Developments and Membrane Performance Relationships, *CARBON,* 115, 237-248 (**2017**).
30. Liu, G.P.; Li, N.; Miller S.; Kim D. ; Yi, S.; Labreche, Y.; W. Koros. Molecularly Designed Stabilized Asymmetric Hollow Fiber Membranes for Aggressive Natural Gas Separation. *Angew. Chem. Int. Ed*. 55, 13754-13758 (**2016).**
31. Fu, S.; Wenz, G.B.; Sanders, S.; Kulkarni, S.; Qiu, W.; Ma, C.H.; Koros, W. J. Effects of Pyrolysis Conditions on Gas Separation Properties of 6FDA/DETDA:DABA(3:2) Derived Carbon Molecular Sieve Membranes. *J. Membr. Sci*., 520, 699-711(**2016**).

(III) Jointly funded by this grant and other grants with relatively minor intellectual contribution from this grant

32. Liu, G., Labreche, Y.; Chernikova, V.; Shekhah, O.; Zhang, C.;Belmabkhout, Y.; Eddaoudi, M.; Koros, W.,William J.), Zeolite-like MOF nanocrystals incorporated 6FDA-polyimide mixed-matrix membranes for CO2/CH4 separation, *J. Membr. Sci*.,565, 186-193 (**2018**).
33. Chen, G., Koros, WJ, Jones, CW, Hybrid Polymer/UiO-66(Zr) and Polymer/NaY Fiber Sorbents for Mercaptan Removal from Natural Gas , ACS, Appl. Matl. & Interfaces, 8(15) 9700-9709 (**2016**).

Molecular Interactions and Layer Stacking Dictate Covalent Organic Framework Effective Pore Size

Phuoc H. H. Duong, John O. Hoberg, Bruce Parkinson, and Katie D. Li-Oakey; University of Wyoming

Abstract

Interactions among ions, molecules, and confining solid surfaces is a universally challenging and intriguing question. Lacking a molecular level understanding of such interactions in complex liquids perpetuates the intractable challenge of simultaneously achieving high membrane permeance and selectivity. Two-dimensional covalent organic frameworks (COFs) have demonstrated ultrahigh permeance, high selectivity, and stability in harsh organic solvents. Using an imine-linked carboxylated COF (C-COF) we demonstrate that unprecedented separation performance can be accomplished by well-aligned, highly crystalline pores. We applied a C-COF membrane platform to protic and aprotic solvents to probe molecular forces among solute, solvent, and COF pore walls. Our data reveal that for a given solute, changing solvents can dramatically change effective pore size and solvated solute diameter, resulting in a selectivity increase from 58% to 90%. Additionally, pH change can account for solvent permeance and solute rejection through C-COF membranes. Methanol permeance decreases with increasing NaOH and HCl concentration in filtration experiments. The membrane selectivity shifts from 23% to 98% for the same solute/solvent (Alcian Blue/methanol) pair when changing the feed pH from 2.2 to 10.1, respectively. Our study shows that dramatic changes in selectivity are not anomalous, but instead controllable via the effective pore size, solvated solute radii, and surface charges by varying pH of the feed.

DE-SC0020100: Tunable, Nanoporous, Two-dimensional Covalent Organic Frameworks for Size and Charge Separations
PI: Katie D. Li-Oakey (PI), Bruce Parkinson (co-PI), John Hoberg (co-PI)
Postdoc(s): Phuoc Duong
Student(s): Valerie Kuehl

Recent Progress

Effect of Solvent on Apparent vs. Designed COF Pore Size

A well characterized, high crystalline, imine-linked carboxylated COF (C-COF, Figure 1) platform is used with protic and aprotic solvents to probe molecular forces among solute, solvent, and COF pore walls. We also report that the C-COF membrane reached unprecedently high solvent fluxes (up to 4500 L m^{-2} h^{-1} bar^{-1}) and high selectivity (up to 95% rejection rate), as shown schematically in Figure 1. The C-COF shown in Figure 1A was synthesized by condensation polymerization using a cheap and scalable microwave method. The presence of the very stable imine-linked hydrophobic aromatic backbone and hydrophilic carboxylic functionalized pores creates ultra-fast transport channels for protic and aprotic solvents with interesting solute-solvent-C-COF interactions.

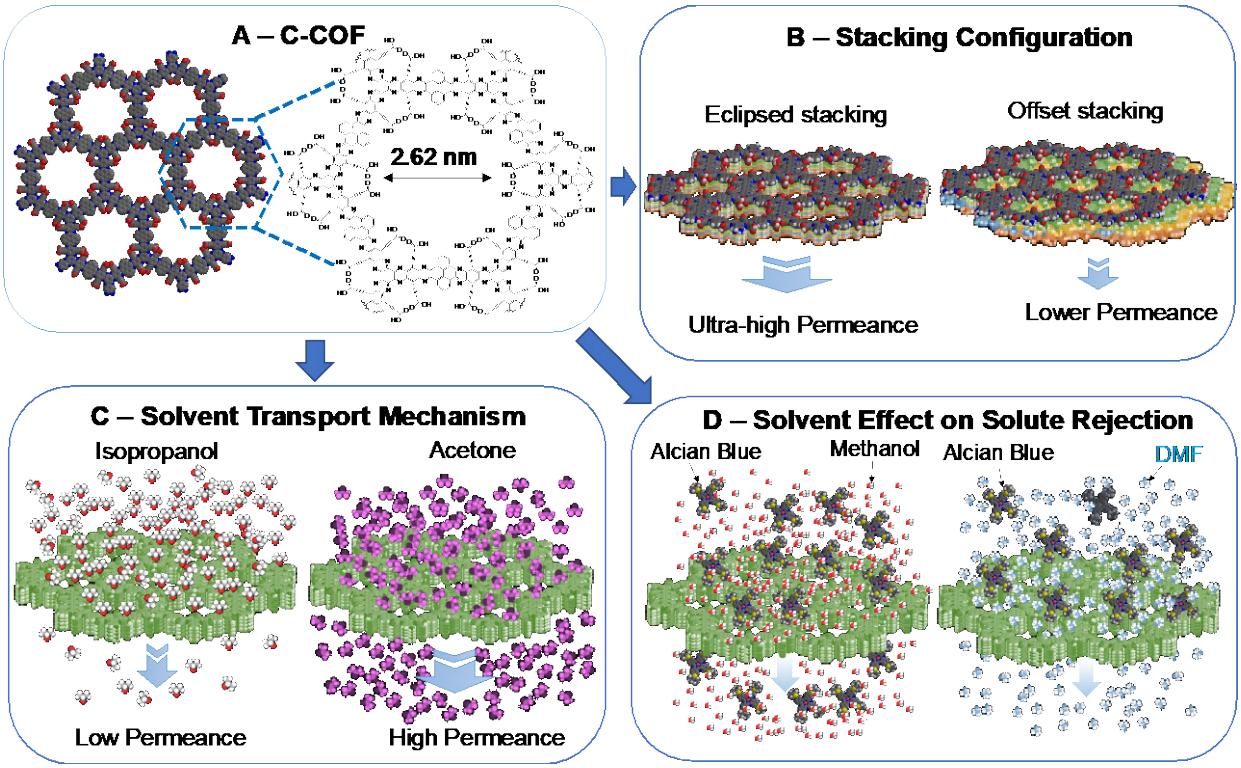

Figure 1. Schematic representations of fundamental studies at molecular level of carboxylated COF (**C-COF**). (A) Space-filling model of the 7-pore structure of C-COF, black = carbon, red = oxygen, blue = nitrogen, yellow = hydrogen, and molecular structure of C-COF in which wavy line indicates extension of the periodic structure (B) C-COF stacking configuration showing well-aligned pores (eclipsed) vs. significant slipping (offset) between layers, (C) Solvent transport mechanism through C-COF membrane showing significantly slower isopropanol permeance than acetone due to different solvent properties and solvent-COF interactions, (D) Effect of solvent on the membrane selectivity of solute revealing that simple change of solvent can dramatically increase selectivity.

Figure 2A presents the experimental permeance of various solvents through C-COF membranes, with isopropanol and acetone exhibiting the lowest (691 L m^{-2} h^{-1} bar^{-1}) and highest (4574 L m^{-2} h^{-1} bar^{-1}) permeance, respectively. Measured transport rates of protic and aprotic solvents across C-COF membranes are two orders of magnitude higher than those reported across polyamide (PA), GO, and most COF membranes (Figures 2 B – C). We hypothesize that ultrafast solvent permeance through C-COF membrane is attributed to well-aligned eclipsed stacking (Figure 1B) and favorable solvent-C- COF interactions. We show that well-aligned C-COF layers and molecular interactions involved in pore and solute solvation, discussed in the following sections, are key to achieving this unprecedentedly high permeance and selectivity.

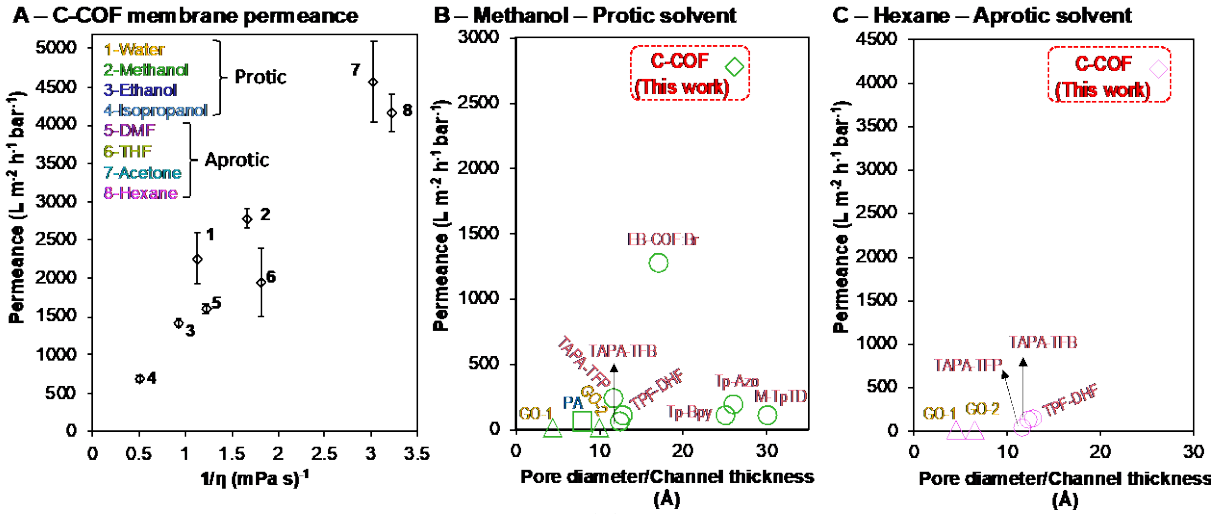

Figure 2. Ultrafast solvent permeance of C-COF membranes (A) and a comparison with a survey of COF, GO, and polyamide membranes (B & C). (A) Solvent permeance of C-COF membranes as a function of inverse viscosity (1/η). (B) Protic solvent (methanol), and (C) aprotic solvent (hexane) permeance of C-COF membrane, compared with polyamide – PA, graphene oxide [GO-1, GO-2], and COF [M-TpTD, EB-COF:Br, TPF-DHF, Tp-Bpy, Tp-Azo, TAPA-TFP, TAPA-TFB] membranes. [Detailed references of literature data for PA, GO and other COF membranes are noted in our manuscript submitted to ACS Applied Materials and Interfaces].

PublicationsAcknowledging this Grant in 2019 – present

Exclusively funded by this grant;

1. Quinoxaline Covalent Organic Frameworks: Synthesis, post-synthetic modifications and applications, Valerie A. Kuehl, Phuoc H. H. Duong, Deana Sadrieva, Samrat A. Amin, Yuqi She, Katie D. Li-Oakey, Jeffery L. Yarger, Bruce A. Parkinson and John O. Hoberg* *ACS Applied Materials & Interfaces* **2021** accepted.
2. Molecular Interactions and Layer Stacking Dictate Covalent Organic Framework Effective Pore Size, Phuoc H. H. Duong, Valerie A. Kuehl, Yun K. Shin, John O. Hoberg, Bruce Parkinson, Adrianus C. van Duin and Katie D. Li-Oakey* *ACS Applied Materials & Interfaces, under revision.*

Jointly funded by this grant and other grants with leading intellectual contribution from this grant;

1. A self-assembling, biporous, metal-binding covalent organic framework and its application for gas separation, Veronica Spaulding, Katarina Zosel, Phuoc H. H. Duong, Katie D. Li-Oakey, Bruce A. Parkinson, Diego A. Gomez-Gualdron and John O. Hoberg, *Materials Advances*, **2021**, *2*, 3362. <u>*Selected as a 2021 Popular Advance*</u>
2. The influence of disorder in the synthesis, characterization and applications of a modifiable two-dimensional covalent organic framework, Jordan Brophy, Kyle Summerfield, Jiashi Yin, Jon Kephart, Joshua T. Stecher, Jeramie Adams, Takashi Yanase, Jason Brant, Katie D. Li-Oakey, John O. Hoberg*, Bruce A. Parkinson* *Materials*, **2021**, *14*, 71.

Jointly funded by this grant and other grants with relatively minor intellectual contribution from this grant;

1. Pitfalls in the Synthesis of Polyimide-linked Two-dimensional Covalent Organic Frameworks, Valerie A. Kuehl, Michael J. Wenzel, Bruce A. Parkinson Laura de Sousa Oliveira, and John O. Hoberg[a]* *J. Mat. Chem. A*, **2021**, DOI: 10.1039/D1TA01954F.

Understanding and controlling water-organic co-transport in amorphous microporous materials

Ryan P. Lively, Young Hee Yoon; School of Chemical and Biomolecular Engineering Georgia Institute of Technology

Abstract

We are actively studying the fundamental sorption, diffusion, and permeation properties of water-organic mixtures in carbon molecular sieve (CMS) membranes to understand the conditions within the micropore that give rise to the various types of molecular motion and molecular selection processes possible in such complex systems. To develop this understanding, we have created a consistent set of samples that have well-defined pore sizes, which are determined via cryogenic sorption techniques. However, relating the void space microstructure to the structure of the carbon itself is more difficult. Neutron diffraction techniques provide this insight and an example will be given that compares the pore size from cryogenic sorption and diffraction. Finally, a relationship between void space microstructure and small molecule transport will be provided to begin creating a tentative design pathway from polymer structure to carbon-based separation device. These measurements will provide fundamental guidance in a variety of DOE-relevant challenges including wastewater remediation, transport in tight shale formations, biofuel upgrading, and other processes involving molecular transport.

Grant or FWP Number: DE-SC0019182

Student(s): Young Hee Yoon

RECENT PROGRESS

Overview—Movement of molec-ules in porous spaces is an important and active area of research with major implications in industrial separations, catalysis, and geology. In practical situations, this molecular movement occurs under highly "crowded" conditions within the pore space. This becomes even more complex in cases where the pore sizes begin to approach the size of the moving molecules. Understanding of molecular diffusion at these conditions remains a significant fundamental challenge and has largely been understood by measuring molecular movement in chemically diverse materials that exhibit different pore sizes. Beyond this, creating techniques to control the mobility of organic and water mixtures in these "crowded"

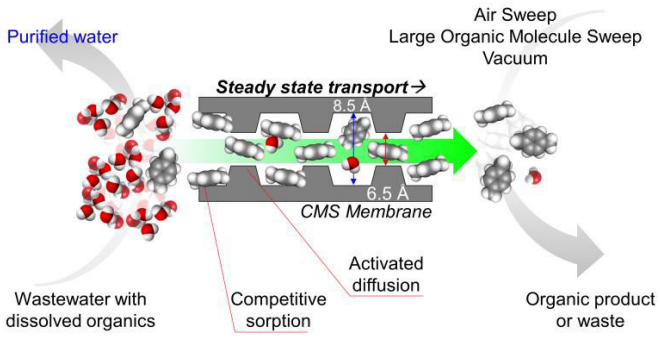

Figure 1: Illustrative example of a potential application of the proposed fundamental research. Here, a membrane continuously removes dissolved organic molecules from wastewater. Detailed co-transport insight is needed to enable concepts such as these.

porous structures will open up possibilities not accessible by current materials. For instance, the steady state removal of organic pollutants from wastewater can be envisions using a "surface selective flow" membrane with appropriate microstructure (**Figure 1**).

Creation and characterization of CMS samples—We have fabricated membranes from neat and diamine- crosslinked polyvinylidene fluoride (PVDF) and polyvinylidene chloride (PVDC), and pyrolyzed these to create carbon molecular sieve membranes with differing pore structures. We compare these to CMS samples derived from polymers of intrinsic microporosity (PIMs). We have characterized these materials using powder x-ray diffractometry, FT-IR, solid state ^{1}H- NMR, and various adsorption techniques. We primarily rely on N_2 physisorption at 77K to estimate our pore size distributions. The uncrosslinked PVDF materials exhibit a uniform pore, whereas the crosslinked materials exhibit a bimodal and narrow pore size distribution (**Figure 2, left**). However, certain CMS have sufficiently narrow pores that N_2 has difficulty accessing the entirety of the micropore structure in an experimentally reasonable amount of time. We have thus explored the use of neon vapor in the ranges of 27-40K to measure the pore size distributions of these "tighter" CMS materials. Moreover, since neon (2.75Å) is similar in size to water (~2.6-2.9Å), the use of this sorbate will allow us to fully interrogate the "water accessible" structures within the CMS. Exemplar neon-derived pore size distributions are shown in **Figure 2 (right)**, which reveal ultramicropores that were previously undetectable using N_2 as a probe.

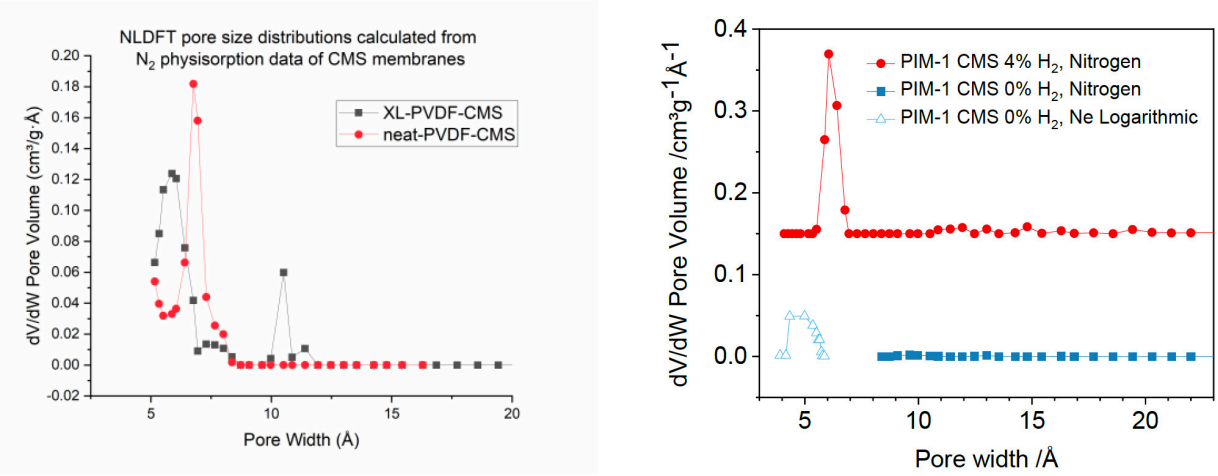

Figure 2: (left) N2-probed pore size distribution of CMS derived from neat PVDF and CMS derived from diamine crosslinked PVDF. (right) Neon-derived pore size distributions in various CMS samples at 40K.

Beyond textural approaches, an in-depth investigation of CMS structure was attempted by neutron time-of-flight total scattering data for CMS. These experiments were performed at Oak Ridge National Laboratory's NOMAD diffractometer. Our aim is to relate the physical structure of the carbon materials to the microporous (i.e., void) structure of the samples. With the sp3/sp2 carbon ratio for the CMS obtained from XPS, the structural findings of CMS from neutron scattering can be used to investigate the hypothetical CMS structure and the potential pyrolysis reaction mechanism. The updated hypothetical pyrolysis mechanism of PIM-1_CMS_4%_H2 is shown in **Figure 3**.

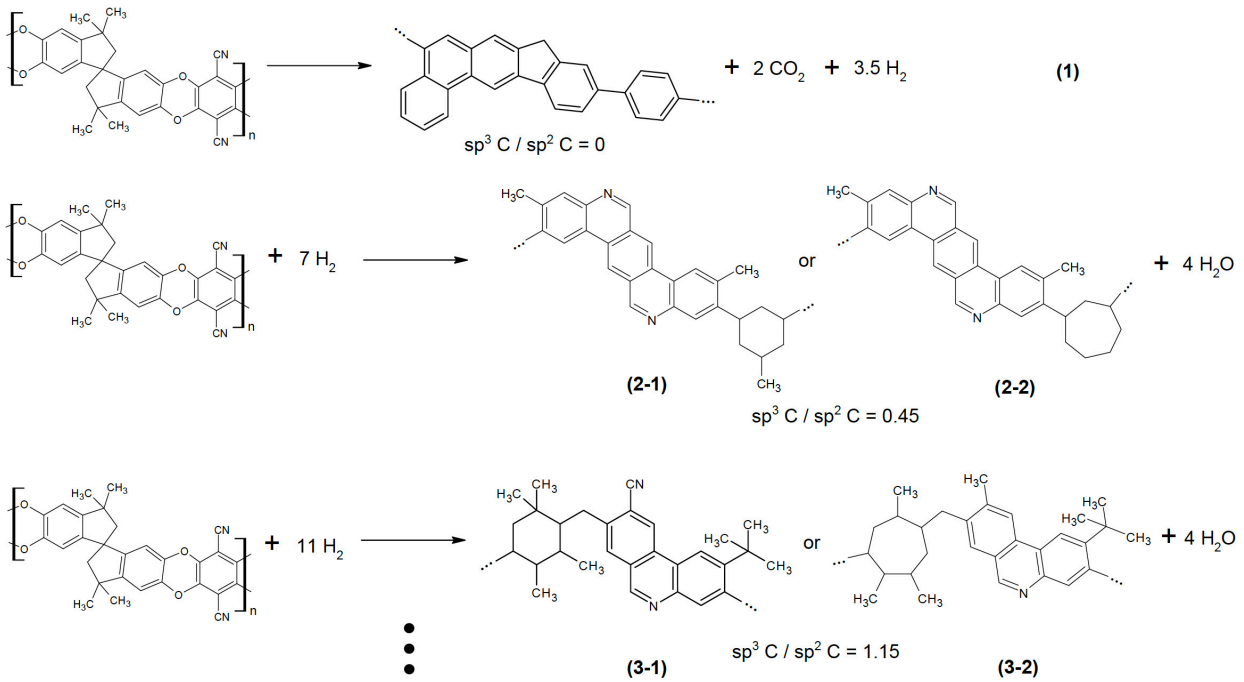

Figure 3. Hypothetical examples of pyrolysis reaction pathways of PIM-1 under the introduction of H2 in the pyrolysis atmosphere. The reaction mechanism (2-2) and (3-2) are updated based on the findings from neutron scattering data that suggests the presence of seven-membered carbon ring in 4% H2-PIM-1-CMS.

We have also collected significant amounts of single component sorption and diffusion isotherms (e.g., water sorption as shown in **Fig. 4**), which are critical starting points for our multicomponent permeation model. We will utilize these as the basis for our mixture sorption estimates, which will be experimentally probed in Year 3-4 of the project. We will discuss the foundations of our multicomponent permeation model and how these types of measurements are crucial for developing a fundamental understanding of complex mixture permeation in microporous spaces.

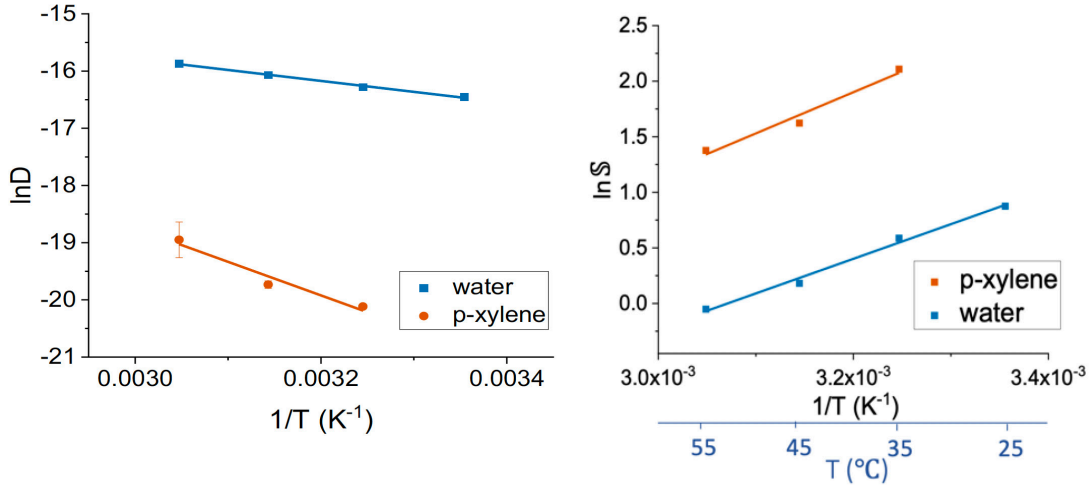

Figure 4. Temperature-dependent diffusion (left) and sorption (right) parameters for water (blue and p- xylene (orange), a representative organic contaminant.

Publications Acknowledging this Grant in 2018 – present

1. Yao Ma, Fengyi Zhang, Harry W. Deckman,‡ William J. Koros, and Ryan P. Lively*, "Flux Equations for Osmotically Moderated Sorption−Diffusion Transport in Rigid Microporous Membranes", *Industrial & Engineering Chemistry Research*, Volume 59, 5412, 2020.
2. Oishi Sanyal, Samuel S. Hays, Nicholas E. León, Yoseph A. Guta, Dr. Arun K. Itta, Ryan
3. P. Lively, William J. Koros, "A Self-Consistent Model for Sorption and Transport in Polyimide-Derived Carbon Molecular Sieve Gas Separation Membranes", *Angewandte Chemie International Edition*, Volume 59, Issue 46, 2020.
4. Haley D. White, Chunyi Li, and Ryan P. Lively, "Tailoring the Structure of Carbon Molecular Sieves derived from an Aromatic Polyamide", *Submitted.*

Precise Control Over Molecular Structure in Polynorbornene-Based Membranes

Xinyi Wang, Trevor Wilson, and Brian K. Long; Department of Chemistry, University of Tennessee, Knoxville, Tennessee, 37996*

Presentation Abstract

Our group has previously reported that alkoxysilyl substituted vinyl-addition polynorbornenes (VAPNBs) show exceptional H_2S/CH_4 separation performance, as well as good separation capabilities for CO_2/CH_4. This is intriguing as two of the most prevalent contaminants in crude natural gas are CO_2 and H_2S. Because both contaminants must be removed to meet pipeline specifications, it is desirable to develop membranes that simultaneously remove both impurities. Herein we report a next generation series of haloalkoxysilane substituted vinyl-addition polynorbornenes which are highly permeable and selective for range of gas separations that include, but are not limited to, CO_2/CH_4 and H_2S/CH_4 separations.

A second effort in our group aims to study vinyl-addition and ring-opening metathesis polymerized polynorbornene block copolymers to evaluate the impact of microphase separation on gas separation membrane performance. While block copolymers have been previously investigated for gas separating membrane materials, these segmented block copolymer systems typically lack long-range microphase separated structure that makes drawing conclusions about the influence of ordered nanodomains on gas separation performance challenging. To address this, our group has developed routes to well-defined block copolymer membranes with diverse microphase separated structures, and have begun to correlate this structure to their gas separation performance.

DE-SC0018179: Advancing Polymeric Gas Separation Membranes through Molecular Engineering

PI: Brian K. Long
Postdoc(s): none
Student(s): Trevor Wilson, Xinyi Wang, Justin Burroughs, Margret Powell, Cameron Workman
Affiliations(s): Department of Chemistry, University of Tennessee, Knoxville, Tennessee, 37996

RECENT PROGRESS

For the current reporting period, our primary efforts have focused on the synthesis and testing of halogenated polynorbornenes and the development of the underlying chemistries required to access advanced block copolymer based membranes. These two thrusts are delineated in the description below.

Project 1 – Halogenated Vinyl-addition Polynorbornenes

A series of halogenated and non-halongenated norbornene monomers were synthesized via substitution reaction followed by Diels-Alder reaction. These monomers were polymerized using a Ni-based catalyst to achieve high molecular weight homo- and co-polymers. These polymers were solution cast from THF to form robust, free-standing films for gas permeation and sorption testing.

The permeation performance of these halogenated VAPNBs and their copolymers were measured and plotted relative to the 1991 and 2008 CO_2/CH_4 Roberson upper bounds (Figure 1). We found that as halogenated content is increased, CO_2/CH_4 selectivity also increased, whereas only a minimal decrease in CO_2 permeability was observed. More specifically, **PF1** displayed a 67% increase in CO_2/CH_4 selectivity as compared to its non-halogenated VAPNB analog **P1**, whereas CO_2 permeability only decreased by 10%, thereby leading the performance closer to the theoretical upper bound for this separation. The **P2**-co-**PF2** series and **P3**-co-**PF3** series showed similar trends. Sorption studies were also performed to better understand the fundamental rationale for this improved performance.

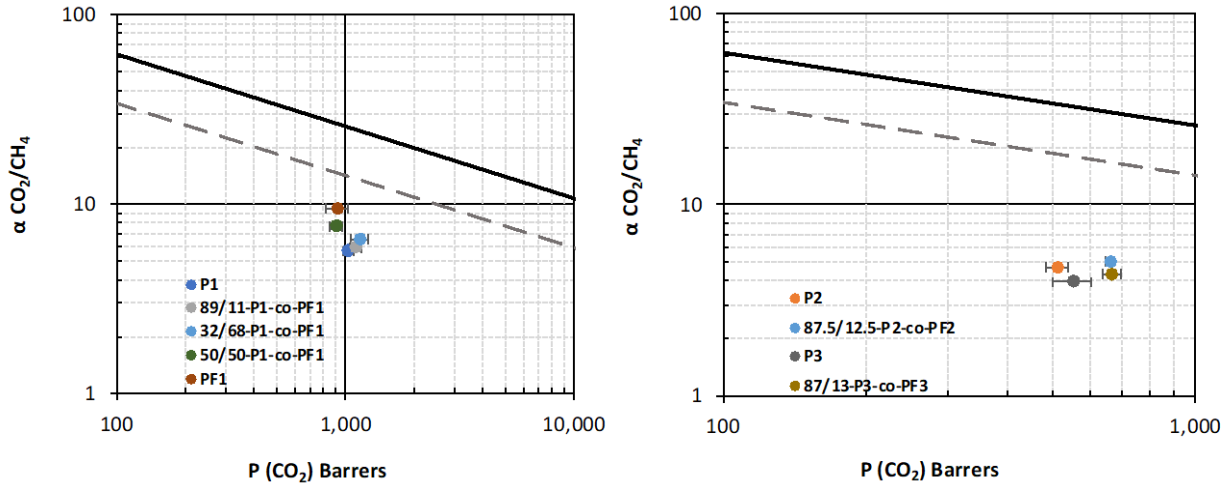

Figure 1. Gas separation performance of halogenated homo- and co-polymer series as compared to the 1991 and 2008 CO_2/CH_4 upper bounds.

Project 2 – Synthesis of Block Copolymer Membranes

Initial efforts focused primarily on the synthesis of di-block copolymers whose blocks exhibit disparate gas transport behavior such as: hexyl norbornene (PCO_2 = ~84 Barrer), and trimethylsilyl norbornene (PCO_2 = ~4400 Barrer). Not only will the differential gas transport properties between blocks allow us to elucidate the influence of microphase structural changes on overall gas transport in thin films, but the chemical incompatibilities between these repeat units should provide a thermodynamic driving force for microphase separation. We have demonstrated that alkyl substituted norbornenes prepared by this route, such as hexyl norbornene (**HexNB**), may be polymerized in a living fashion using cationic palladium catalysts wherein a linear progression of molecular weight (M_n) versus time and decreasing dispersity ($Đ$) were observed.

In contrast, monomers bearing polar and/or heteroatom functionalized substituents (such as trimethylsilyl norbornene) are more prone to differential reactivities between their *exo*- and *endo*-isomers. In certain cases, this differential reactivity may preclude complete

consumption of monomer wherein both the *endo*- and *exo*- species are initially consumed, but upon complete consumtion of the *exo*-isomer, polymerization of *endo*- monomer ceases. To obviate these differential reactivities, our group synthesized exclusively in their *exo*-isomer form. We then investigated the livingness of the polymerization of ***exo*-TMSNB** using the same cationic palladium species previously used for **HexNB**.

Despite having strong experimental evidence supporting the living polymerization behavior of both **HexNB** and ***exo*-TMSNB**, all attempts to synthesize di-block copolymers of **HexNB** and ***exo*-TMSNB** resulted in bimodal polymer samples in which only partial chain extension is observed. We have not yet fully elucidated the origins of this behavior, yet we suspect that this may be due to some trace chemical impurity that prematurely terminates the propagating chain end upon the complete consumption of ***exo*-TMSNB**.

Because partial chain-termination may be occurring upon consumption of the ***exo*-TMSNB** monomer, we hypothesized that substituting an alternative Si-containing monomer – that may not have similar impurities – and altering the monomer polymerization order may alleviate these issues. Therein, we envisioned that diblock copolymers could be accessed by first polymerizing **HexNB**, followed by the addition of a silicon containing monomer prepared through Diels-Alder, such as **Si(OMe)$_3$NB**. In this way, the lack of complete consumption of the Si containing species does not affect the growth or composition of the other block, and any unreacted silyl norbornene monomers can be removed through precipitation of the polymerization mixture. Indeed, we found that this route provides complete block extension with no observable shouldering in the GPC traces (Figure 2). We are currently pursuing this route to access a series of well-defined block copolymers, as well as establishing film annealing strategies to promote microphase separation for subsequent gas transport studies.

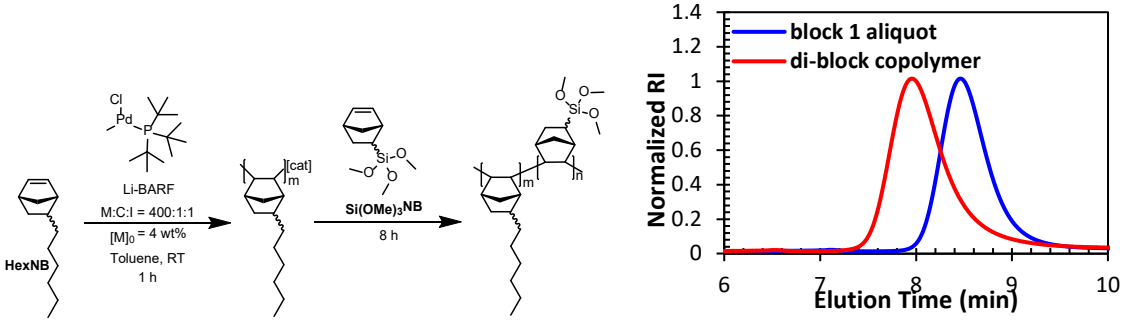

Figure 6. Synthesis of **poly(HexNB-*block*-Si(OMe)$_3$NB)**.

Publications Acknowledging this Grant in 2015 – present

(VIII) *Exclusively funded by this grant;*

a. Higgins, M. A.; Maroon, C. R.; Townsend, J.; Wang, X.; Vogiatzis, K. D.; Long, B. K. Evaluating the impact of functional groups on membrane-mediated CO2/N2 gas separations using a common polymer backbone. *J. Poly. Sci.* **2020**, *58*, 2644.

(IX) Jointly funded by this grant and other grants with leading intellectual contribution from this grant;

a. Maroon, C. R.; Townsend, J.; Gmernicki, K. R.; Harrigan, D. J.; Sundell, B. J.; Lawrence, J. A.; Mahurin, S. M.; Vogiatzis, K. D.; Long, B. K. Elimination of CO_2/N_2 Langmuir Sorption

and Promotion of "N_2-Phobicity" within High-T_g Glassy Membranes. *Macromolecules* **2019**, *52*, 1589-1600.

b. Lee, D. C.; Kensy, V. K.; Maroon, C. R.; Long, B. K.; Boydston, A.J. The intrinsic mechanochemical reactivity of vinyl-addition polynorbornene. *Angew. Chem. Int. Ed*. **2019**, *58*, 5639-5642.

c. Maroon, C. R.; Townsend, J.; Higgins, M. A.; Harrigan, D. J.; Sundell, B. J.; Lawrence, J. A.; O'Brien, J. T.; O'Neal, D.; Vogiatzis, K. D.; Long, B. K. Addition-type Alkoxysilyl-Substituted Polynorbornenes for Post-Combustion Carbon Dioxide Separations. *J. Membrane Sci.* **2020**, *595*, 117532

d. Hendren, K. D.; Higgins, M. A.; Long, B. K.; Foster, E. J. Cellulose nanocrystal-reinforced poly(5-triethoxysilyl-2-norbornene) composites. *Poly. Chem.* **2020**, *11*, 433

e. Lawrence, J. A.; Harrigan, D. J.; Maroon, C. R.; Long, B. K.; Sundell, B. J. Investigating the utility of addition-type poly(norbornene)s as membranes for sour gas separations. *J. Membrane Sci.* **2020**, *616,* 118569

f. Doerr, A. M.; Burroughs, J. M.; Gitter, S. R.; Yang, X.; Boydston, A. J.; Long, B. K. Advances in Polymerizations Modulated by External Stimuli. *ACS Catalysis* **2020**, *10*, 14457.

g. Wang, X.; Wilson, T. J.; Alentiev, D.; Gringolts, M.; Finkelshtein, E.; Bermeshev, M.; Long, B. K. Substituted polynorbornene membranes: a modular template for targeted gas separations. *Poly. Chem.* **2021**, *Just accepted* (DOI: 10.1039/D1PY00278C)

(X) Jointly funded by this grant and other grants with relatively minor intellectual contribution from this grant;

Interrogating Selective Metal-Adsorbate Interactions in Metal–Organic Frameworks

Jeffrey R. Long[1], *Jeffrey A. Reimer*[1], *Jeffrey B. Neaton*[1], *Walter S. Drisdell*[2] [1]*University of California, Berkeley, USA;* [2]*Lawrence Berkeley National Laboratory, USA*

Presentation Abstract

Separations of commodity chemicals in industry, such as O_2 from air and ethylene from light hydrocarbons, are carried out on a massive scale worldwide using energy-intensive cryogenic distillation, and account for a large proportion of global CO_2 emissions. As a part of broader efforts to reduce global energy consumption and mitigate climate change, the development of more efficient separations processes is a critical pursuit. In this context, metal–organic frameworks (MOFs) have emerged as leading candidates for energy-efficient adsorption-based separations that can be carried out under near ambient conditions. These porous materials feature well-defined, chemically tunable structures with high surface areas and are capable of selectively capturing key gases from complex mixtures based on a range of selectivity handles. In addition to their promise for use in separations that rely on cryogenic distillation, MOFs are among the most promising materials studied to date for the selective separation of CO_2 from gases such as N_2 and water vapor, as required for carbon capture processes. The further development and optimization of such next- generation adsorbents necessitates a rigorous understanding of the local physical and electronic structures that promote gas binding, and how these change upon guest uptake. Our research uses advanced *in situ* characterization methods, such as nuclear magnetic resonance, X-ray absorption spectroscopies, and X-ray diffraction, that enable direct, real-time characterization of selective metal–adsorbate binding processes at the atomic level, with relevance to a number of industrial gas separations. These methods have enabled us to identify unique adsorption mechanisms driving the selective, energy-efficient uptake of O_2, CO_2, CO, N_2, and H_2 in various MOFs. Select results will be presented along with detailed gas adsorption data and density functional theory calculations.

DE-SC0019992 (UC Berkeley) and CH19DRI01 (LBNL): Interrogating Selective Metal- Adsorbate Interactions in Metal–Organic Frameworks

PI: Jeffrey R. Long,

Co-PIs: Jeffrey A. Reimer, Jeffrey B. Neaton, Walter S. Drisdell

Postdocs: Alexander Forse, Lena Funke, Adam Jaffe, Gregory Su, Karina Riascos-Rodriguez
Students: Bhavish Dinakar, Victor Mao, Julia Okatwiec, Adam Uliana, Hao Zhuang, Alex Smith

RECENT PROGRESS

Mechanism of Selective, High-Temperature O_2 Adsorption in Chemically Reduced, Redox- Active Iron-Pyrazolate Metal–Organic Frameworks. The development of O_2-selective adsorbents capable of separating oxygen from nitrogen at ambient or elevated temperatures could dramatically enhance the efficiency of this important industrial separation. The design of O_2- selective adsorbents is particularly challenging given the similar physical properties of O_2 and N_2; however, electron affinity is one key

characteristic that distinguishes O_2 apart from the other components of air. Indeed, oxygen can readily accept up to two electrons, while N_2 and Ar are typically redox-inactive. As such, metal–organic frameworks featuring open metal sites capable of inner-sphere electron transfer to O_2 have been the focus of research in this arena. However, materials discovered to date typically bind oxygen irreversibly or very weakly at ambient temperatures. As an alternative strategy to the design of an O_2-selective adsorbent, we considered the possibility of outer-sphere electron transfer from coordinatively saturated, redox-active metal centers. In particular, we demonstrated that chemically reduced frameworks of the type $A_xFe_2(bdp)_3$ ($A = Na^+, K^+$; bdp^{2-} = 1,4-benzenedipyrazolate; $0 < x \leq 2$, Figure 1), which feature coordinatively saturated iron centers, are capable of strong and selective adsorption of O_2 over N_2 at ambient temperature (Ref. 9). A suite of characterization techniques, including gas adsorption analysis, single-crystal X-ray diffraction, as well as ^{23}Na solid-state NMR, Mössbauer, and X-ray photoelectron spectroscopies, were employed as probes of O_2 uptake. The results support a selective adsorption mechanism involving outer-sphere electron transfer to O_2 from a robust, chemically reduced framework with coordinatively saturated, redox-active metal sites. Electron transfer results in the formation of superoxide (O^{2-}) moieties, which are stabilized by intercalated alkali metal cations that reside in the one-dimensional triangular pores of the materials.

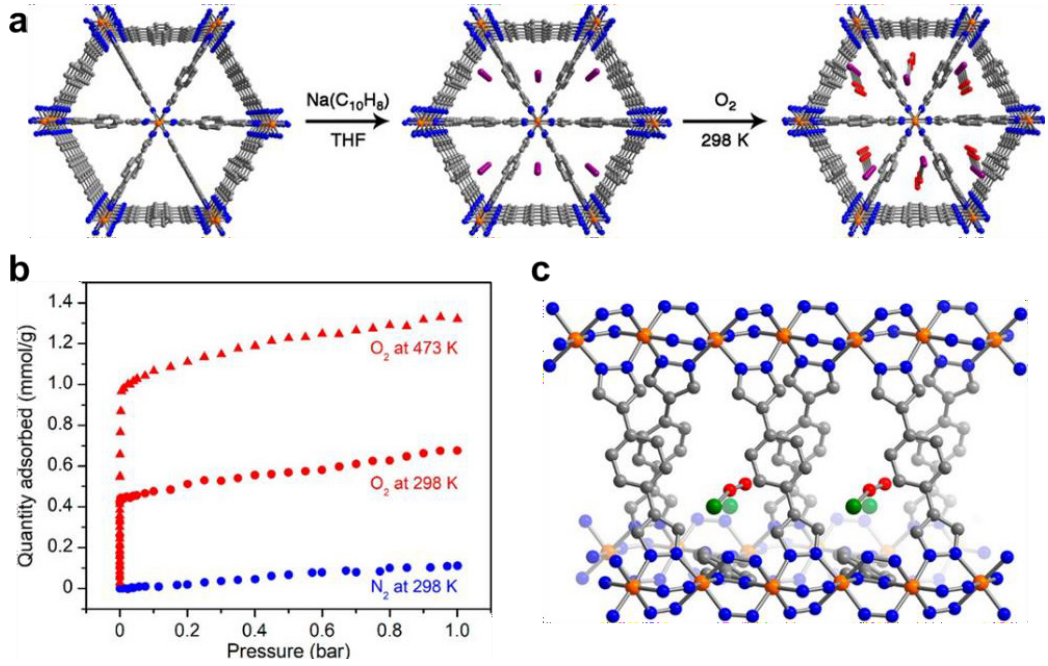

Figure 1. (a) X-ray crystal structures of $Fe_2(bdp)_3$ (left), $Na_{0.5}Fe_2(bdp)_3$ (middle), and room-temperature O_2-dosed $Na_{1.2}Fe_2(bdp)_3$ (right). (b) Adsorption isotherms of O_2 (red) and N_2 (blue) in $K_{1.09}Fe_2(bdp)_3$. (c) Expanded sideview along one pore of $K_{0.74}Fe_2(bdp)_3$ dosed with 1 bar O_2 at 298 K. Both crystallographically distinct K sites are shown. Disordered atoms created by symmetry. Orange, gray, blue, red, purple, and green spheres represent Fe, C, N, O, Na, and K atoms, respectively; hydrogen atoms are omitted for clarity.

Cooperative Carbon Dioxide Adsorption in Alcoholamine-Functionalized Metal–Organic

Frameworks. In prior efforts, we have shown that diamine-appended MOFs of the type diamine–Mg_2(dobpdc) (dobpdc^{4-} = 4,4′-dioxidobiphenyl-3,3′-dicarboxylate) adsorb large quantities of CO_2 with unprecedented selectivities and efficiencies, through a unique cooperative adsorption mechanism involving the insertion of CO_2 into the metal–amine bonds to form ammonium carbamate chains that propagate along the framework channels. This mechanism is characterized by step-shaped CO_2 adsorption profiles, and the step pressure and temperature can notably be tuned by changing the diamine. We have also recently shown that changing the structure of the appended diamine can lead to new adsorption mechanisms, including the formation of carbamic acids. Based on this finding, we envisioned that more significant structural variations in this system, such as the replacement of the appended diamines with other bifunctional molecules, could lead to new mechanisms for cooperative adsorption. Therefore, we investigated the CO_2 adsorption behavior of alcoholamine-appended variants of Mg_2(dobpdc) via gas-adsorption, spectroscopic, and computational studies (Ref. 10). Carbon dioxide adsorption isotherms for alcoholamine-appended Mg_2(dobpdc) show a sharp step, which is indicative of the cooperative CO_2 adsorption akin to that characteristic of the amine-appended variants. The post-step adsorption capacity in the new materials corresponds to one CO_2 molecule per two alcoholamines, only half that observed for diamine-appended variants. To elucidate the structure and local environment of the alcoholamine- appended MOFs, solid-state NMR spectra were collected on samples of e-2-OH–Mg_2(dobpdc) (e- 2-OH = 2-(ethylamino)ethanol) before and after dosing with $^{13}CO_2$. The data revealed the formation of hydrogen bond-stabilized carbamic acids upon CO_2 adsorption, unique from the predominant adsorption mechanism operative in diamine-appended variants. van der Waals (vdW)-corrected density functional theory (DFT) calculations support these findings and suggest that the most plausible mechanism involves the alcohol group of the original alcoholamine group serving as a hydrogen-bond acceptor (Figure 2).

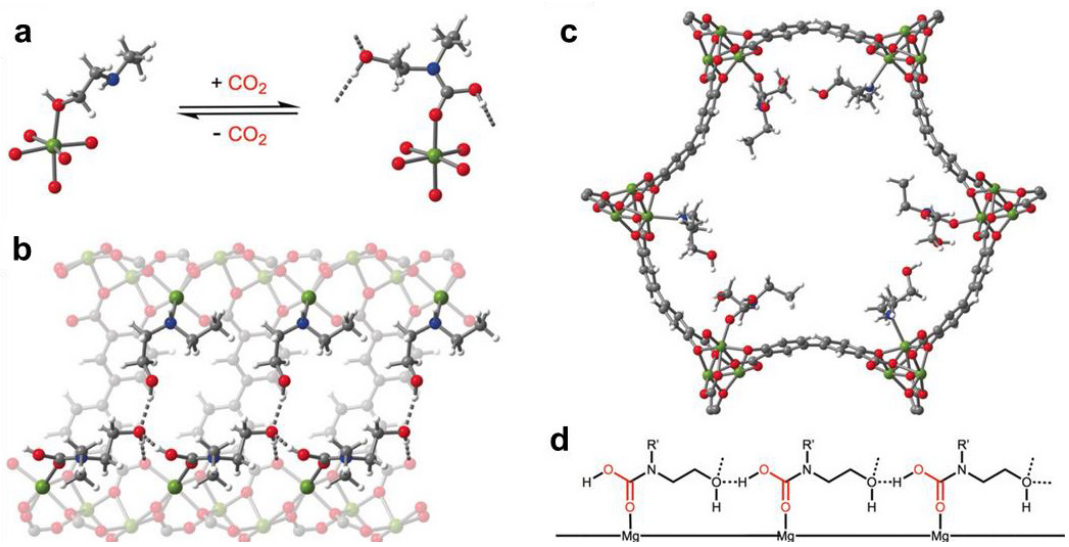

Figure 2. (a) DFT-predicted structure of e-2-OH–Mg_2(dobpdc) before and after CO_2 adsorption. Predicted structure of CO_2-inserted e-2-OH–Mg_2(dobpdc), as viewed along the pore wall (b) and down the *c* axis (c). Gray, red, blue, white, and green spheres represent C, O, N, H, and Mg atoms, respectively. (d) Proposed structure formed upon CO_2 uptake in alcoholamine-appended Mg_2(dobpdc) involving hydrogen-bond stabilized carbamic acid chains.

Backbonding Contributions to Small Molecule Chemisorption in a Metal–Organic Framework with

Open Copper(I) Centers. The framework Cu^{I}-MFU-4*l* features coordinatively unsaturated copper(I) centers that can engage in backbonding interactions with various small molecule guests, and serves as a valuable case-study toward the design of frameworks capable of engaging in backbonding and other electronic interactions for highly efficient and selective gas adsorption. We examined several gases expected to bind to the open copper(I) sites in Cu^{I}-MFU- 4*l* via different electronic interactions, including σ-donation, π-backbonding, and formal electron transfer (Ref. 4). We demonstrated that *in situ* Cu L-edge near edge X-ray absorption fine structure (NEXAFS) spectroscopy is a powerful tool for elucidating π-backbonding, as it directly probes excitations to unoccupied backbonding orbitals with Cu d-character, even for gases that participate in other dominant interactions, such as ligand-to-metal σ-donation. First-principles calculations based on DFT and time-dependent DFT additionally revealed the backbonding molecular orbitals associated with these spectroscopic transitions (Figure 3). The energies of the transitions correlate with the energy levels of the isolated small molecule adsorbates, and the transition intensities are proportional to the binding energies of the guest molecules within Cu^{I}-MFU-4*l*. By elucidating the molecular and electronic structure origins of backbonding interactions between electron rich metal centers in MOFs and small molecules, it is possible to develop guidelines for enhanced molecular- level design of solid-state adsorbents for energy-efficient separations of relevance to industry.

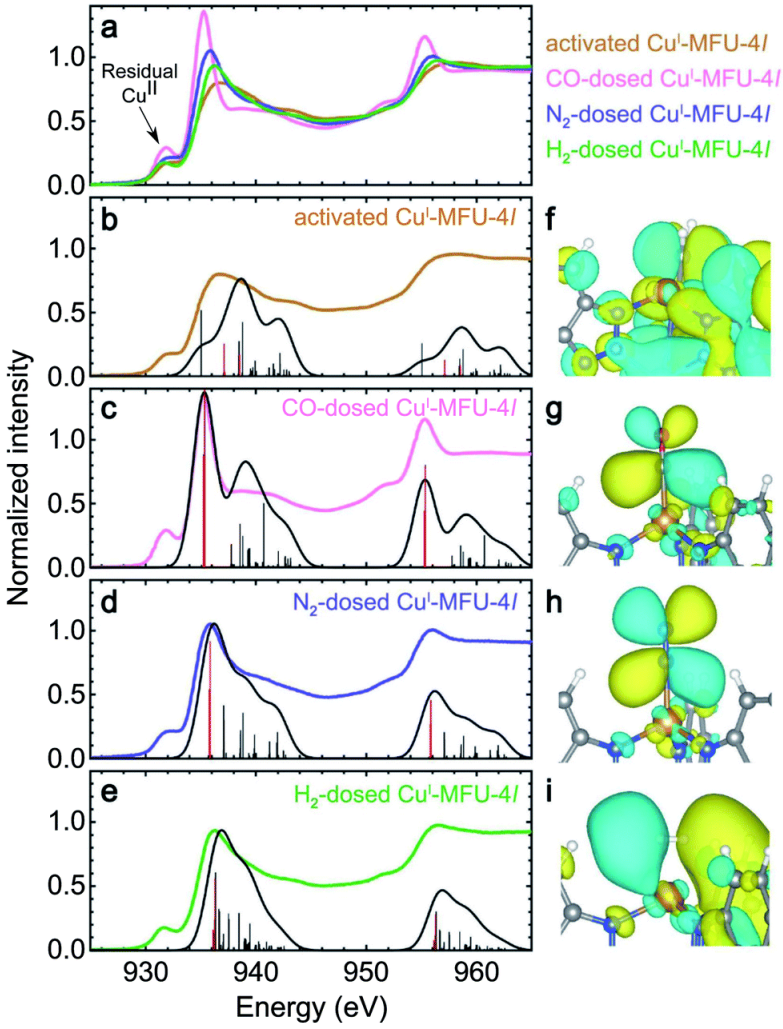

Figure 3. (a) Experimental room temperature Cu L-edge NEXAFS spectra of bare Cu^{I}-MFU-4*l* and Cu^{I}- MFU-4*l* dosed *in situ* with CO, N_2, or H_2. Individual experimental and simulated spectra are plotted together in (b) to (e) for the bare framework and Cu^{I}-MFU-4*l* dosed with CO, N_2, and H_2, respectively. Vertical lines indicate individual transitions, while the solid trace is the average Gaussian-convoluted simulated spectrum. The thick red lines correspond to major transitions from the core 2p orbitals to final states between 935 and 936 eV. The molecular orbitals of these final states are shown on the right for (f) bare Cu^{I}-MFU-4*l* and the framework dosed with (g) CO, (h) N_2, and (i) H_2. In (g)–(i), the final states correspond to unoccupied, antibonding orbitals generated upon π-backbonding between copper(I) and the given guest.

Publications Acknowledging this Grant in 2019 – present

Exclusively funded by this grant

1. "Biomimetic O2 Adsorption in an Iron Metal–Organic Framework for Air Separation" Reed, D. A.; Xiao, D. J.; Jiang, H. Z. H.; Chakarawet, K.; Oktawiec, J.; Long, J. R. *Chem. Sci.* **2020**, *11*, 1698–1702.
2. "Influence of Pore Size on Carbon Dioxide Diffusion in Two Isoreticular Metal–Organic Frameworks" Forse, A. C.; Colwell, K. A.; Gonzalez, M. I.; Benders, S.; Torres-Gavosto, R. M.; Blümich, B.; Reimer, J. A.; Long, J. R. *Chem. Mater.* **2020**, *32*, 3570–3576.
3. "Overcoming Metastable CO2 Adsorption in a Bulky Diamine-Appended Metal–Organic Framework" Dinakar, B.; Forse, A. C.; Jiang, H. Z. H.; Zhu, Z.; Lee, J.-H.; Kim, E. J.; Parker, S. T.; Pollak, C. J.; Siegelman, R. L.; Milner, P. J.; Reimer, J. A.; Long, J. R., submitted.

Jointly funded by this grant and other grants with leading intellectual contribution from this grant

1. "Backbonding Contributions to Small Molecule Chemisorption in a Metal–Organic Framework with Open Copper(I) Centers" Su, G. M.; Wang, H.; Barnett, B. R.; Long, J. R.; Prendergast, D.; Drisdell, W. S. *Chem. Sci.* **2021**, *12*, 2156–2164.
2. "Fluoroarene Separations in Metal–Organic Frameworks with Two Proximal Mg^{2+} Coordination Sites" Zick, M. E.; Lee, J.-H.; Gonzalez, M. I.; Velasquez, E. O.; Uliana, A. A.; Kim, J.; Long, J. R.; Milner, P. J. *J. Am. Chem. Soc.* **2021**, *143*, 1948–1958.
3. "Thermodynamic Separation of 1-Butene from 2-Butene in Metal–Organic Frameworks with Open Metal Sites" Barnett, B. R.; Parker, S. T.; Paley, M. V.; Gonzalez, M. I.; Biggins, N.; Oktawiec, J.; Long, J. R. *J. Am. Chem. Soc.* **2019**, *141*, 18325–18333.
4. "Ion-Capture Electrodialysis Using Multifunctional Adsorptive Membranes" Uliana, A. A.; Bui, N. T.; Kamcev, J.; Taylor, M. K.; Urban, J. J.; Long, J. R. *Science* **2021**, *372*, 296–299.
5. "Negative Cooperativity upon Hydrogen Bond-Stabilized O2 Adsorption in a Redox-Active Metal–Organic Framework" Oktawiec, J.; Jiang, H. Z. H.; Vitillo, J. G.; Reed, D. A.; Darago, L. E.; Trump, B. A.; Bernales, V.; Li, H.; Colwell, K. A.; Furukawa, H.; Brown, C. M.; Gagliardi, L.; Long, J. R. *Nat. Commun.* **2020**, *11*, 3087.
6. "Selective, High-Temperature O2 Adsorption in Chemically Reduced, Redox-Active Iron-Pyrazolate Metal–Organic Frameworks" Jaffe, A.; Ziebel, M. E.; Halat, D. M.; Biggins, N.; Murphy, R. A.; Chakarawet, K.; Reimer, J. A.; Long, J. R. *J. Am. Chem. Soc.* **2020**, *142*, 14627–14637.
7. "Cooperative Carbon Dioxide Adsorption in Alcoholamine- and Alkoxyalkylamine-Functionalized Metal-Organic Frameworks" Mao, V. Y.; Milner, P. J.; Lee, J.-H.; Forse, A. C.; Kim, E. J.; Siegelman, R. L.; McGuirk, C. M.; Porter-Zasada, L. B.; Neaton, J. B.; Reimer, J. A.; Long, J. R. *Angew. Chem. Int. Ed.* **2020**, *59*, 19468–19477.

Jointly funded by this grant and other grants with relatively minor intellectual contribution

from this grant

1. "Kinetics of Cooperative CO2 Adsorption in Diamine-Appended Variants of the Metal– Organic Framework Mg2(dobpdc)" Martell, J. D.; Milner, P. J.; Siegelman, R. L.; Long, J. R. *Chem. Sci.* **2020**, *11*, 6457–6471.
2. "Selective Nitrogen Adsorption via Backbonding in a Metal–Organic Framework with Exposed Vanadium Sites" Jaramillo, D. E.; Reed, D. A.; Jiang, H. Z. H.; Oktawiec, J.; Mara, M. W.; Forse, A. C.; Lussier, D. J.; Murphy, R. A.; Cunningham, M.; Colombo, V.; Shuh, D. K.; Reimer, J. A.; Long, J. R. *Nat. Mater.* **2020**, *19*, 517–521.
3. "Understanding 2p Core-Level Excitons of Late Transition Metals by Analysis of Mixed- Valence Copper in a Metal–Organic Framework" Wang, H.; Su, G. M.; Barnett, B. R.; Drisdell, W. S.; Long, J. R.; Prendergast, D., submitted.

Selective Electrochemical Capture and Release of Uranyl in Solution

Gabriel Ménard, *Shannon Heinrich, Maxwell Mattejat, and Zongheng Wang*

University of California – Santa Barbara, Department of Chemistry and Biochemistry

Presentation Abstract

The goal of this project is to investigate the selective, electrochemical capture and release of uranyl (UO_2^{2+}) from biphasic or heterogeneous mixtures using a class of cluster molecules, *ortho*-carboranes (Cb), containing selective binding groups (Fig. 1). Applications in PUREX, seawater UO_2^{2+} extraction, or in actinide/lanthanide (An/Ln) or Ln/Ln separations are envisioned. Harnessing the redox-switchable chelating properties (θ_1, θ_2) from the "*closo*" carborane (Cb) to the reduced "*nido*" carborane (Cb^{2-}), this presentation will describe our efforts in exploring several strategies to: 1) integrate selective coordinating groups (L) onto the carbon positions of Cb for the selective capture and release of UO_2^{2+}, and; 2) anchor these selective carboranes onto electrode and/or heterogeneous surfaces for the selective, heterogeneous capture and release of uranyl from aqueous solutions under flow conditions. Overall, this work focuses on advancing our understanding and controlling the properties of this new platform for metal capture and release chemistry which, we believe, has the potential for broader applicability in separation science.

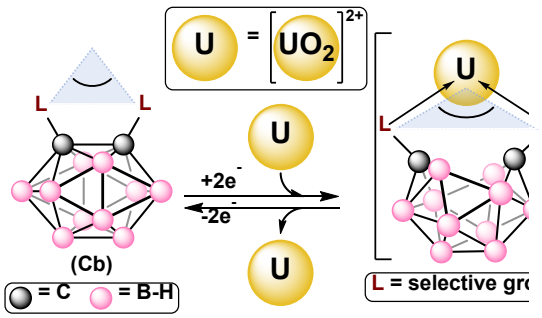

Fig. 1. Selective electrochemical UO_2^{2+} capture and release using *ortho*-carboranes (Cb).

Grant Number: DE-SC0021649

PI: Gabriel Ménard

Students: Shannon Heinrich, Maxwell Mattejat, and Zongheng Wang

RECENT PROGRESS

Size-Selective Coordination: The ability of UO_2^{2+} to adopt a high equatorial coordination number relative to competing ions (e.g. Na, V, Fe in seawater) has prompted us to investigate this possible size-selective coordination strategy using crown or poly-pyridyl binding groups (Fig. 2). Optimal, selective binding could be envisioned in the neutral *closo*-Cb with UO_2^{2+} release being facilitated in the *nido*-Cb form (or *vice versa*). We have successfully synthesized mono- and bis-Cb variants of 14-crown-4 (**1**, shown) and 18-crown-6 (not shown) and are currently investigating their coordinating abilities in the *closo* and *nido* states. We have also synthesized a bipyridyl (bipy) model compound (**2-bipy**) and are working towards the expanded terpyridyl (**2-terpy**) variant which should display an expanded equatorial coordination sphere.

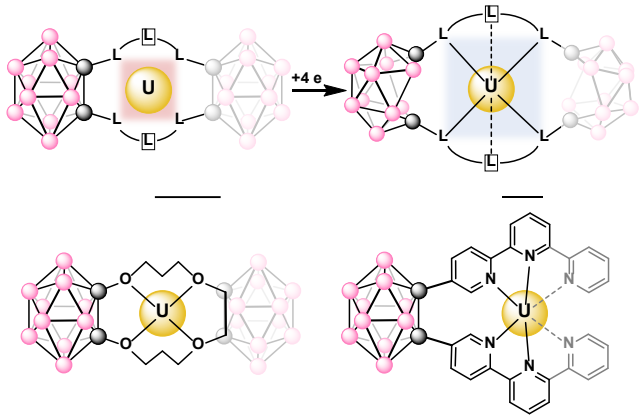

Fig. 2. Size-selective coordination strategy.

Tuning the Electrochemical and Solubility Properties of Cb: Our original report investigating UO_2^{2+} capture and release using Cb published in *Nature* (DOI: 10.1038/s41586-019-1926-4) and prior to DOE funding used L = Ph_2PO binding groups (**^{PO}Cb**, Fig. 3a). In recently submitted work (see below), we described how this system was selective for capture and release of UO_2^{2+} from mixed metal solutions containing alkali, lanthanide, and actinide metal ions under electrochemical conditions (Fig. 3a). We are currently investigating how the electronic properties of the **^{PO}Cb** cage can be tuned to favor selective metal-metal separations, in particular with respect to An/Ln or Ln/Ln separations, by modifying the Cb cage electronics (Fig. 3b). We are presently investigating how these changing redox properties affect the donicity of the PO centers and how these can be tuned for selective electrochemical separations. The effect of these groups (e.g. methyl incorporation, **^{PO}Cb-*Me*$_8$**) on the solubility of these extractants in organic phases for biphasic extractions (e.g. Fig. 3a) is also being probed.

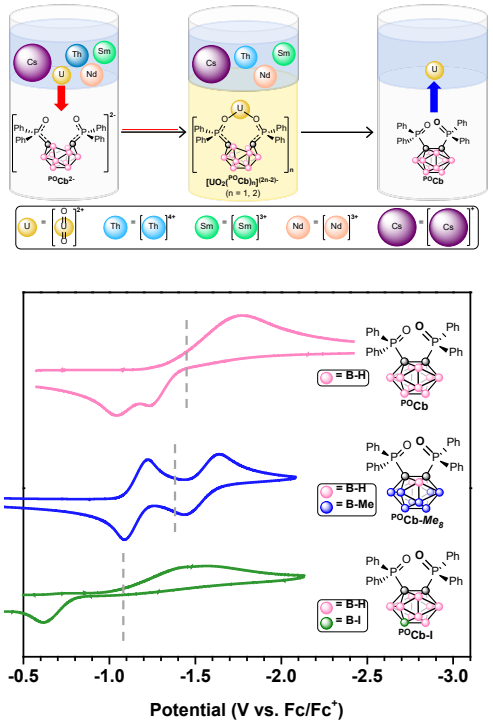

Fig. 3. a) Recently submitted work highlighting the selective biphasic capture and release of UO_2^{2+}. b) Current work investigating the electrochemical and solubility properties of modified ^{PO}Cb.

Towards Heterogenous Capture and Release: We are currently targeting Cb-functionalized flow-field electrodes for the heterogeneous capture and release of UO_2^{2+} from mixed metal solutions (e.g. seawater; Fig. 4). Anchoring groups at the 9- or 9,12- positions of the Cb framework are being synthesized with a particular focus on allyl and pyrene groups for tethering to robust carbon-based electrodes. The former are being targeted starting from known 9-I-Cb and 9,12-I_2-Cb precursors. We have successfully synthesized a bis-pyrene Cb derivative and are currently installing selective groups (L) onto the Cb prior to installing these new compounds onto carbon-based surfaces.

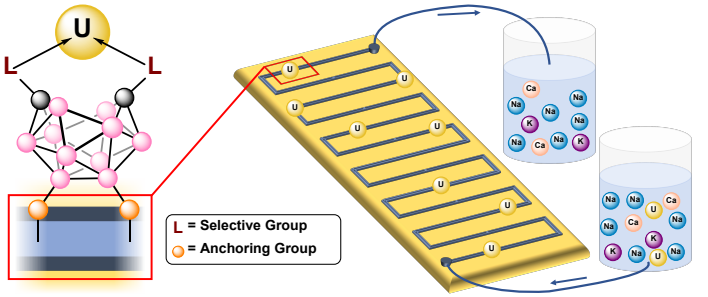

Fig. 4. Proposed electrochemical heterogeneous capture and release under flow conditions.

Publications Acknowledging this Grant in 2021 → present

(1) Exclusively funded by this grant:

None

(2) Jointly funded by this grant and other grants with leading intellectual contribution from this grant:

1. Keener, M.; Mattejat, M.; Zheng, S.-L.; Wu, G.; Hayton, T.W.; Ménard, G. Selective Electrochemical Capture and Release of Uranyl from Aqueous Alkali, Lanthanide, and Actinide Mixtures Using Redox-Switchable Carboranes. *Submitted*, **2021**.

(3) Jointly funded by this grant and other grants with relatively minor intellectual contribution from this grant:

None

New Molecular Mechanisms for Greenhouse Gas Capture in Metal–Organic Frameworks: Carbon Dioxide and Beyond

Phillip J. Milner, Department of Chemistry and Chemical Biology, Cornell University

Abstract: The goal of this project is to identify new mechanisms that enable the selective removal of greenhouse gases, including carbon dioxide, nitrous oxide, and hydrofluorocarbons, from emission streams. Different adsorption strategies will be studied within metal-organic frameworks (MOFs), with an emphasis on understanding the molecular-level interactions that lead to selectivity. Carbon dioxide adsorption will be studied in frameworks bearing oxygen-based nucleophilic sites in order to overcome the limitations of traditional amine-based materials. The initial materials to be studied are those bearing charge-balancing hydroxide sites within their pores. Nitrous oxide adsorption, which remains critically understudied in porous materials, will be studied in materials bearing redox-active metal centers in order to identify new materials capable of (reversibly) reducing this oxidizing greenhouse gas. Hydrofluorocarbon adsorption will be studied in densely iodinated Zr-based frameworks in order to determine if halogen-bonding represents a new platform for capturing these anthropogenic greenhouse gases.

DE-SC0021000: New Molecular Mechanisms for Greenhouse Gas Capture in Metal–Organic Frameworks: Carbon Dioxide and Beyond

Post-doc(s): none
Graduate Students: Mary Zick, Ronald Jerozal, Tristan Pitt, Jaehwan Kim, Tyler Azbell

Recent Progress

Carbon dioxide capture. We recently published a perspective highlighting the need for new pathways for carbon dioxide capture (Forse, Milner, *Chem. Sci.* **2021**, *12*, 508-516). To that end, we have been exploring CO_2 capture at hydroxide sites in metal-organic frameworks (MOFs), which offer a platform to carefully tune the local environment of these reactive sites and understand which structural features lead to selective CO_2 capture. As a model system, we have selected cyclodextrin-based MOFs bearing charge-balancing hydroxide sites in their pores (Figure 1). These materials, such as $Rb_2(OH)_2$(γ-CD) (γ-CD = gamma cyclodextrin), have been previously shown to chemisorb CO_2 at low pressures, but the mechanism of CO_2 capture in these materials remains unclear. We have confirmed that selective CO_2 capture in the inexpensive K-analogue, $K_2(OH)_2$(γ-CD), occurs at low pressures and with high CO_2/N_2 selectivity (Figure 2). *In situ* transmission IR and magic angle-spinning solid-state NMR spectroscopy measurements carried out in collaboration with Prof. Alex Forse at the University of Cambridge confirm that the mechanism of CO_2 capture is chemisorptive in nature, as a new carbonyl peak is observed using both methods.

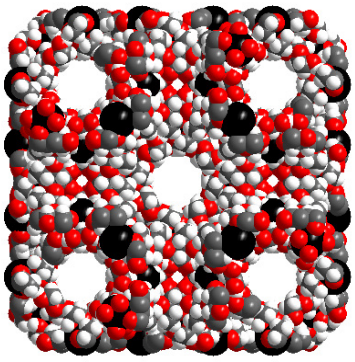

Figure 1. *Structure of CD-MOF-1.*

We hypothesized that CO_2 capture occurs via bicarbonate formation at the charge-balancing hydroxide sites in the framework pores. To test this hypothesis, we synthesized a range of new CD-MOFs bearing a range of charge-balancing anions. Consistent with our hypothesis, only MOFs prepared with hydroxide, carbonate, or bicarbonate anions displayed chemisorptive CO_2 capture (Figure 3, left). In contrast, MOFs prepared with non-nucleophilic counteranions, including acetate, chloride, and benzoate, showed little CO_2 uptake. This discrepancy can be best observed by comparing the free energy of adsorption for MOFs prepared with nucleophilic and non-nucleophilic counteranions. Density functional theory calculations carried out by Dr. Jung-Hoon Lee at the Korea Institute of Science and Technology further support that the mechanism of CO_2 capture in these materials is likely via reaction at charge-balancing hydroxide sites, likely via assistance from strongly bound water molecules in the pores.

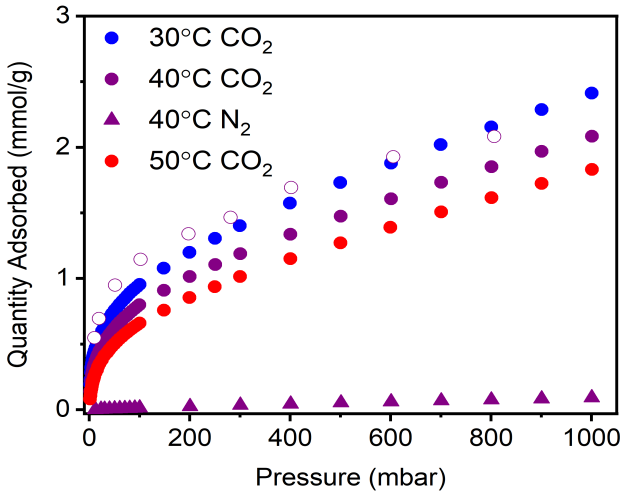

Figure 2. *Selective and reversible CO_2 capture in $K_2(OH)_2$(γ-CD).*

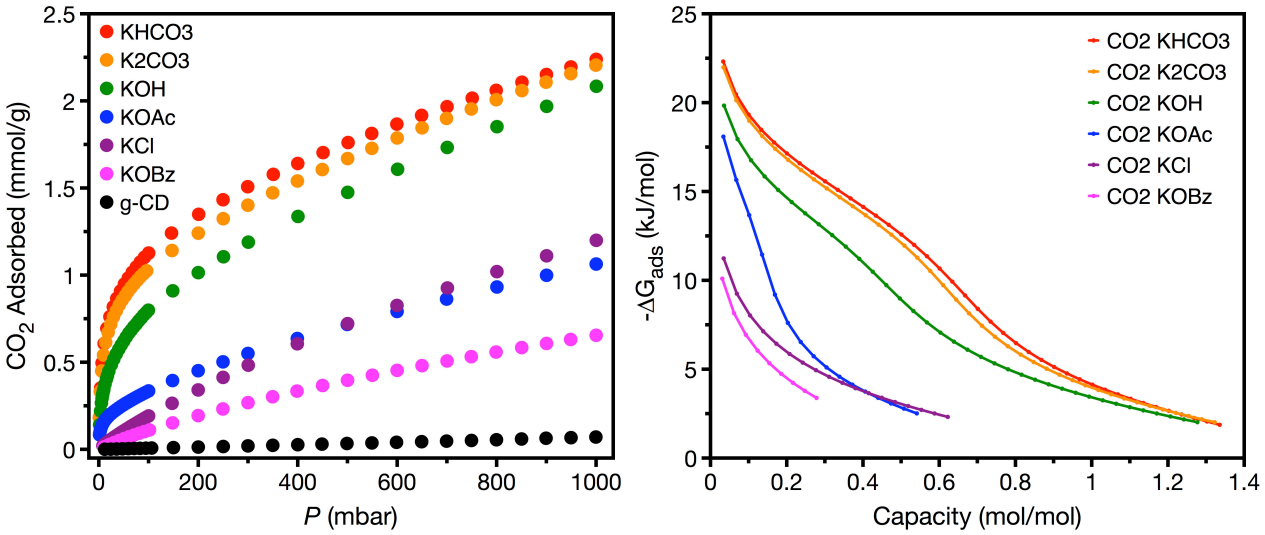

Figure 3. *CO_2 capture in $K_2(X)_2$(γ-CD) MOFs.*

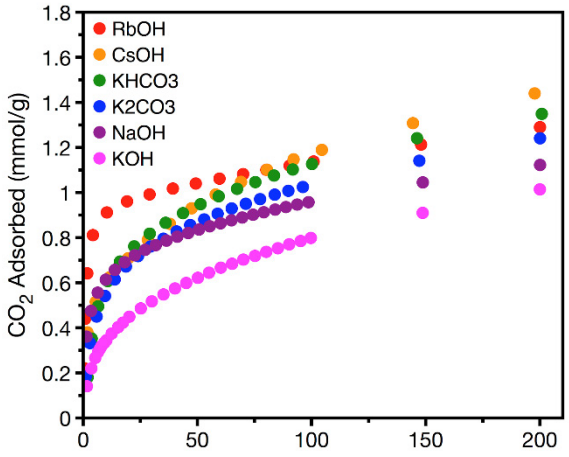

Figure 4. *Cation effect on CO_2 capture in CD-MOFs.*

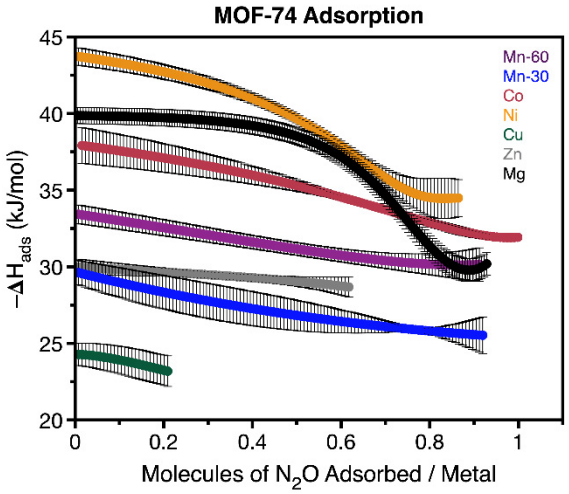

Figure 5. *N_2O capture in MOF-74.*

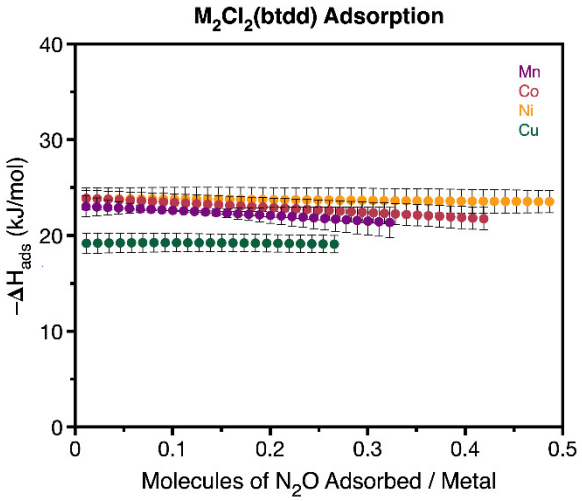

Figure 6. *N_2O capture in M_2Cl_2(btdd).*

Our studies also demonstrate that there is a pronounced effect of the cation on CO_2 capture in CD-MOFs as well (Figure 4). Of the tested materials, the unexplored CsOH-based MOF displays the highest CO_2 capacities at conditions relevant to flue gas capture as well as the highest CO_2/N_2 selectivities of all tested MOFs. Current efforts are focused on testing the cycling stability and breakthrough performance of the Cs framework.

In addition to the work outlined above, we have found that chemisorptive CO_2 capture occurs in other α- and β-CD analogues, indicating that cyclodextrin structure may offer an additional tuning handle for the strength of CO_2 binding. We have begun to expand the scope of our studies to other hydroxide-based MOFs.

Nitrous oxide capture. We have carried out an extensive evaluation of N_2O adsorption in over a dozen open metal site MOFs to identify frameworks capable of strong binding of this understudied greenhouse gas. We studied N_2O adsorption in a range of MOF-74 analogues (Figure 5). The expected trend of binding enthalpies as a function of Lewis acidity of the metal centers was observed. Near room temperature, N_2O activation was only observed in the Fe framework, leading to partially irreversible adsorption. However, calculations carried out by Heather Kulik at MIT suggest that the Mn framework may be capable of NO activation as well. Our initial results suggest that this reactivity mode may be feasible at high temperatures, as suggested by pronounced hysteresis in the adsorption/desorption isotherms even at high temperatures (>250 °C). We have also explored N2O capture in a related family of open metal site azolate MOFs, M_2Cl_2(btdd) (Figure 6). Very pronounced hysteresis in the adsorption/desorption isotherms is observed, even with very long equilibration times, indicating that there may be a kinetic barrier to N_2O desorption in these materials. We are investigating the chemical

origins of this phenomenon in order to understand how it relates to N_2O activation in MOFs.

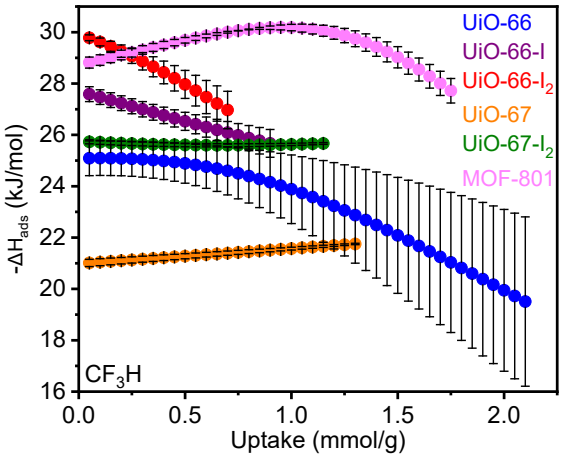

Figure 7. *Fluoroform binding in iodinated MOFs.*

Hydrofluorocarbon capture. We have prepared a range of iodinated Zr-MOFs and explored their ability to strongly bind the halogenated greenhouse gases fluoroform (CF_3H) and sulfur hexafluoride (SF_6). For fluoroform, stronger binding was observed as a function of framework iodination (Figure 7). For SF_6, the trend was less clear, with stronger binding observed in smaller-pore MOFs. Future work will focus on studying if halogen bonding is occurring in these materials and how the strength of halogen bonding interactions can be maximized to improve the selectivity for fluorinated gas capture.

Publications acknowledging this grant since 2020:

1) Forse, A. C.; Milner, P. J. "New Chemistry for Enhanced Carbon Capture: Beyond Ammonium Carbamates." *Chem. Sci.* **2021**, *12*, 508-516. DOI: 10.1039/D0SC06059C.

Defect Repair of Polyelectrolyte Bilayers Using SDS: The Action of Micelles Versus Monomers

Steven L. Regen, Nabendu B. Pramanik and Sayali Shaligram; Department of Chemistry, Lehigh University, Bethlehem, PA 18015, United States

Presentation Abstract

Defects within single, double and triple polyelectrolyte bilayers derived from poly(sodium 4-styrene sulfonate) (PSS) and poly(diallyldimethyammonium chloride) (PDDA) have been repaired using aqueous solutions of sodium dodecyl sulfate (SDS), as evidenced by a reduction in their permeability and an increase in their permeation selectivity. In contrast to the use of monomer solutions of SDS, which were moderately effective in repairing only double and triple bilayers, micellar solutions proved highly effective in repairing all three assemblies. Evidence for intact micelles or micellar fragments being deposited on the surface of single bilayers of PSS/PDDA has been obtained from a combination of atomic force microscopy, X-ray photoelectron spectroscopy, ellipsometry, and contact angle measurements. Observed CO_2 permeances of ca. 200 GPU and CO_2/N_2 selectivities of ca. 30 for SDS-repaired, single bilayers of PSS/PDDA suggests that further development of such assemblies may have practical potential for the separation of CO_2 from N_2 in flue gas.

DE-FG02-05ER15720: Hyperthin Membranes For Gas Separations

PI: Steven L. Regen
Postdocs: Nabendu B. Pramanik and Sayali Shaligram

RECENT PROGRESS

The Layer-by-Layer (LbL) deposition method is now widely used to synthesize polyelectrolyte multilayers (PEMs) that are of theoretical as well as practical interest. Our own interest in PEMs stems from their possible use as membranes for the separation of gases, especially CO_2 from N_2, which are the major components of flue gas. Because the flux of a gas across a membrane is inversely proportional to the membrane's thickness, we have been keenly interested in creating the thinnest PEMs possible, having CO_2/N_2 selectivities that are potentially exploitable; i.e., *single* polyelectrolyte bilayers having selectivities ≥ 20 and the highest permeability possible with respect to CO_2.

A requirement for the successful growth of PEMs is that an overcompensation of polyions exists during the deposition process. As a result of this overcompensation, defects (i.e., gaps between the complementary polyions that remain unfilled) are introduced into these assemblies. Because defects tend to reduce the permeation selectivity of membranes, we have been keenly interested in finding ways of repairing them. We have recently devised an experimental approach for defect repair of PEMs that is based on the use of aqueous solutions of sodium dodecyl sulfate (SDS). Our working hypothesis was that micellar solutions of SDS would repair these defects by using monomers or monomers plus intact micelles (or micellar fragments) to fill in gaps *via* ion exchange and attractive van der Waals forces (Figure 1). For proof of concept, single, double and triple bilayers were fabricated from two commonly used polyelectrolytes; i.e., poly(sodium 4-styrene sulfonate) (PSS) and poly(diallyldimethyammonium chloride) (PDDA) (Figure 2).

Experimentally, bilayers of PSS/PDDA were deposited onto highly permeable supports derived from poly[1-(trimethylsilyl)-1-propyne] (PTMSP, ca. 30 μm) that were surface modified with branched polyethyleneimine (*b*-PEI). Cast films of PTMSP are known to have exceptional permeability due to their glassy state and the presence of large permeant pores. For this reason, they have proven attractive as support material for creating composite membranes. To judge the effectiveness of such defect repair, we measured the permeability of these bilayers, before and after exposure to monomer as well as micellar solutions of SDS, with respect to H_2, CO_2 and N_2. These molecules have kinetic diameters of 0.289, 0.330 and 0.364 nm, respectively.

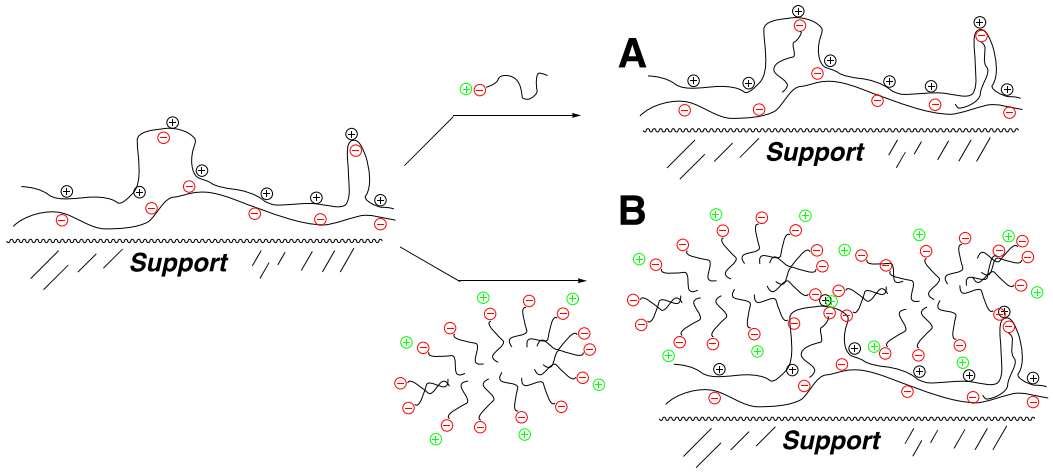

Figure 1. Stylized illustration showing SDS-based (A) monomers and (B) monomers plus micelles filling in gaps in a single polyelectrolyte bilayer.

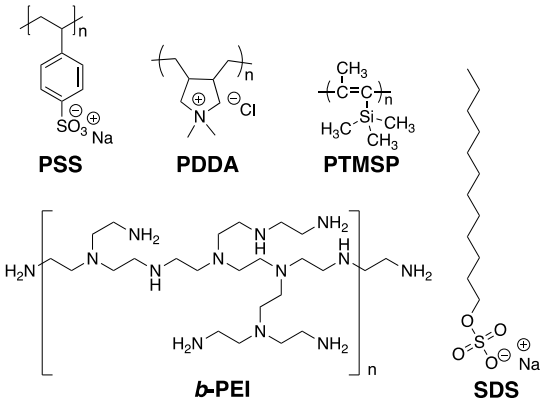

Figure 2. Structures of the polymers and sodium dodecyl sulfate (SDS) used to test defect repair.

In this work, membrane permeabilities were assessed using the solution-diffusion model for gas transport, where permeances (P/l) are defined by equation 1, P is an intrinsic permeability coefficient, l is the thickness of the membrane, Δp is the pressure gradient that is applied across the membrane and J is the observed flux. The membrane's selectivity, α, for two different permeants is then given by the ratio of their permeances.

$$\frac{P}{l}\ (\mathrm{cm^3/cm^2 \cdot s \cdot cm\ Hg}) = \frac{J}{\Delta p} \qquad (1)$$

Using experimental procedures similar to those that we have described previously, single bilayers of PSS/PDDA were deposited onto *b*-PEI-surface modified PTMSP. Subsequent immersion of these bilayers in aqueous solutions of SDS that were below and above its critical micelle concentration (i.e., 8 mM), followed by immersion in deionized water and drying in a desiccator

afforded membranes that were characterized with respect to their permeability properties. Analogous bilayers that were deposited onto silicon wafers that were silylated with *n*-octadecyltrichlorosilane (OTS), and similarly treated with *b*-PEI were characterized by a combination of atomic force microscopy, X-ray photoelectron spectroscopy, ellipsometry, and contact angle measurements.

Table 1 summarizes the permeances that were observed for (i) the PTMSP/*b*-PEI support itself, (ii) PTMSP/*b*-PEI supports that were surface-modified with single bilayers of PSS/PDDA, and (iii) PTMSP/*b*-PEI supports that were surface-modified with single bilayers of PSS/PDDA and subsequently treated with monomers or micellar solutions of SDS. As is readily apparent, the deposition of single bilayers of PSS/PDDA on PTMSP resulted in a slight decrease in permeances and a negligible change in permeation selectivity. Exposure of single bilayers of PSS/PDDA on PTMSP to monomer solutions of SDS (1 mM) resulted only in a slight reduction in permeances and a slight increase in permeation selectivities. In sharp contrast, exposure of single bilayers of PSS/PDDA on PTMSP to micellar solutions of SDS (25 mM) resulted in a dramatic decrease in permeability and a significant increase in permeation selectivities. The fact that the permeance of the larger CO_2 molecule is greater than that of H_2 for these membranes implies that solubility contributions for CO_2 are more important than for H_2 in each case.

Table 1. Permeances and Permeation Selectivities[a]

Membrane	H_2	CO_2	N_2	H_2/N_2	CO_2/N_2
PTMSP/*b*-PEI	940	1900	420	2.2	4.5
PSS/PDDA	850	1300	300	2.8	4.3
	840	1300	280	3.0	4.6
PSS/PDDA/SDS[b]	750	1100	180	4.2	6.1
	740	1200	190	3.9	6.3
PSS/PDDA/SDS[c]	125	190	6.0	21	32
	120	185	6.0	20	31

[a]Permeance values are given in GPU, where 1 GPU = 1 x 10^{-6} (cm^3/cm^2-s cm Hg). Each entry corresponds to a separate membrane that was prepared, independently. In all cases, the reproducibility of these membrane fabrications and permeation values were confirmed by two investigators (NBP and SS). All permeances are ideal values and are based on single gas measurements with a pressure gradient of 2069 Torr. [b]A monomer solution of SDS (1 mM) was used. [c]A micellar solution of SDS (25 mM) was used.

In contrast to the use of monomer solutions of SDS, which were moderately effective in repairing only double and triple bilayers, micellar solutions proved very effective for all three assemblies (not shown). Although permeance and selectivity values under mixed gas conditions tend be somewhat lower than the ideal (single gas) values that we have measured, the CO_2/N_2 selectivities of ca. 30 and CO_2 permeances of ca. 200 GPU that we have observed suggests that further development of these membranes could have practical potential for the separation of CO_2 from N_2 in flue gas. To put these numbers into perspective, some of the polymer membranes that have shown the best combination of CO_2/N_2 selectivity and CO_2 permeance values to date have been characterized by CO_2/N_2 selectivities of ca. 30-40 with CO_2 permeances of ca. 1000 GPU. Finally, it should be noted that hollow fiber analogs of our flat membranes would be of special interest because they can have surface areas that are 5 to 10 times higher. In a broader context, this simple method that we have described for repairing defects in polyelectrolyte bilayers could lead to significant improvements in the quality of other PEMs that are being considered as permeation-selective membranes, protective coatings, sensors, etc.

Publications Acknowledging this Grant in 2015 – present

Exclusively funded by this grant:

1. Yi, S.; Lin, C.; Regen, S. L. Splaying Hyperthin Polyelectrolyte Multilayers To Increase Their Gas Permeability. *Chem. Commun.*, **2015**, *51*, 1439-1441.

2. Lin, C.; Yi, S.; Regen, S. L. Consequences of Tacticity on the Growth and Permeability of Hyperthin Polyelectrolyte Multilayers. *Langmuir*, **2016**, *32*, 375-379.
3. Yi, S.; Lin, C.; Leon, W.; Vezenov, D.; Regen, S. L., Gas Permeability of Hyperthin Polyelectrolyte Multilayers Having Matched and Mismatched Repeat Units. *Langmuir*, **2016**, *32*, 12332-12337.
4. Yi, S.; Leon, W.; Vezenov, D.; Regen, S. L. Tightening Polyelectrolyte Multilayers With Oligo Pendant Ions. *ACS Macro Lett*., **2016**, *5*, 915-918.
5. Lin, C.; Stedronsky, E.; Regen, S. L. pKa-Dependent Facilitated Transport of CO_2 Across Hyperthin Polyelectrolyte Multilayers. *ACS Appl. Mater. Interfaces*, **2017**, *9*, 19525-19528.
6. Lin, C.; Jordan, L R..; Stedronsky, E. R.; Wittenberg, N. J.; Regen, S. L. A Plug and Socket Approach For Tightening Polyelectrolyte Multilayers. *ChemComm*, **2018**, *54*, 9769-9772.
7. Pramanik, N. B.; Tian, C.; Stedronsky, E. R.; Regen, S. L. Layer-By-Layer Assembly Modulated By Host-Guest Binding. *ACS Appl. Polym. Mater*., **2019**, *1*, 141-144.
8. Pramanik, N. B.; Regen, S. L. Layer-By-Layer Assembly of a Polymer of Intrinsic Microporosity: Targeting the CO_2/N_2 Separation Problem. *Chem. Commun*., **2019**, *55*, 4347-4350.
9. Pramanik, N. B.; Regen, S. L. Hyperthin Membranes for Gas Separations via Layer-by-Layer Assembly. *Chem. Rec.*, **2019**, *19*, 1-12.
10. Pramanik, N. B.; Regen, S. L. Clicking the surface of poly[1-(trimethylsilyl)propyne] (PTMSP) via a thiol-ene reaction: unexpected CO_2/N_2 permeability. *Langmuir*, **2020**, *36*, 1768-1772.
11. Pramanik, N. B.; Shaligram, S.; Regen, S. L. Defect Repair of Polyelectrolyte Bilayers Using SDS: The Action of Micelles Versus Monomers. *Langmuir*, **2021**, *37*, 5306–5310.

Accessing Kinetically Controlled Reactions for Efficient Rare Earth Separations

Eric J. Schelter, Robert F. Higgins, Alison L. Knasin, Christian Uruburo, Amit Kumar, and Patrick J. Carroll ; Chemistry Department, University of Pennsylvania

Poster Presentation Abstract

Recycling spent rare earth application materials as well as developing greener methods for the isolation and purification of rare earth containing ores represent some of the most challenging chemical separations. These separations are dictated by thermodynamic parameters, typically distribution coefficients, in solvent extraction processes. In the current work, we have developed a new separations system that operates by a hydrogen atom transfer concomitant with a rearrangement reaction that is controlled by the size of the rare earth ion. The varied solubilities of the starting materials and products of this reaction allowed for a solvent extraction enrichment process in acetonitrile-hexanes, which gave a competitive separation factor of $SF_{Nd:Dy} = 201 \pm 51$ in a single step. Importantly, trends across the rare-earth series are distinct for separations controlled by thermodynamic compared to kinetic processes, with kinetically-controlled processes showing promise for efficient separations across the entire series.

DE-SC0017259: Advancing Selective, Reactive- and Non-Reactive Separations of Rare Earth Elements through Tailored Coordination Chemistry

PI: Eric J. Schelter
Postdoc(s): (Since 2018–2021) Robert Higgins, Amit Kumar, Thibault Cheisson
Student(s): (Since 2018) Joshua Nelson, Bren Cole, Yusen Qiao, Alison Knasin, Christian Uruburo

RECENT PROGRESS

As demonstrated in our previous work, rare earth metal complexes of the proligand: H_3TriNOx ([(2-^{t}BuNOH)$C_6H_3CH_2$]$_3$N), have been shown to afford separations of simple mixtures of rare earth metal salts. In particular, separations systems were developed for applications to technologically relevant mixtures, *e.g.* Nd/Dy, and Eu/Y, for targeted, rare earths recycling chemistry. Subsequently, it was demonstrated that an electron-donating derivative of the proligand H_3TriNOx^R (([(2-^{t}BuNOH)$C_6H_3RCH_2$]$_3$N; R = 5-OMe) influenced the electronic and physical properties to effect improved separations. To further probe substituent effects, in the current work, derivatives with electron-donating and -withdrawing groups along the aryl-backbone were synthesized (R = 4-^{t}Bu, 5-Ph, 4-CF_3).[1] The new proligands were coordinated to rare earths (RE) through protonolysis reactions and the resulting complexes (RE = Nd, Dy) were characterized. Dimerization equilibrium constants and molar solubility were determined where applicable. Overall, the studies indicated that increased electron-donation of the aryl-substituents resulted in an increased driving force for the dimerization of the Nd complexes. This dimerization equilibrium and resultant solubility differences were used to separate mixtures of neodymium/dysprosium (Table 1), as well as mixtures of europium/yttrium. These findings demonstrate the tunability of TriNOx^{3-} to achieve tailored RE separations.

Table 1. Enrichment (*EF*) and Separation Factors (*SF*) for Nd/Dy(TriNOx^{tBu}), Nd/Dy(TriNOx^{Ph}), Nd/Dy(TriNOx^{CF3}), Nd/Dy(TriNOx), and Nd/Dy(TriNOx^{OMe}) mixtures in various solvents by ICP-OES. All experiments were performed in triplicate and values reported with the standard error of the mean.

Ligand	Solvent	ICP-OES Results			Avg. % Distribution/Purity		% Recovery	
		$EF_{Filtrate}$	EF_{Solid}	$SF_{Nd/Dy}$	Filtrate (% Nd)	Solid (% Dy)	% Nd Rec.	% Dy Rec.
TriNOx^{OMe}	Benzene	9.8 ± 0.4	29 ± 3	299 ± 35	90.9 ± 0.3	96.7 ± 0.3	84 ± 7	66 ± 4
TriNOx^{OMe}	Toluene	12 ± 2	22 ± 4	254 ± 10	93.3 ± 0.1	94.8 ± 0.3	79 ± 3	63 ± 5
TriNOx^{OMe}	THF	-	-	-	-	-	-	-
TriNOx^{OMe}	DME	3.5 ± 0.2	11.6 ± 0.5	41 ± 4	77.9 ± 0.9	92.0 ± 0.3	71 ± 2	54 ± 2
TriNOx^{OMe}	Et_2O	7.2 ± 0.3	1.2 ± 0.1	8.4 ± 0.6	87.8 ± 0.5	54 ± 2	17 ± 1	72 ± 2
TriNOx^{OMe}	Hexanes	-	-	-	-	-	-	-
TriNOx^{tBu}	Benzene	12 ± 3	2.5 ± 0.8	31 ± 11	91.5 ± 0.2	69 ± 6	41 ± 9	64 ± 5
TriNOx^{tBu}	Toluene	10 ± 2	2.0 ± 0.4	22 ± 7	90.1 ± 0.3	66 ± 4	25 ± 1	70 ± 3
TriNOx^{tBu}	THF	1.9 ± 0.3	7.8 ± 0.4	15 ± 2	65 ± 4	88.6 ± 0.6	46 ± 7	34 ± 2
TriNOx^{tBu}	DME	19 ± 3	3.9 ± 0.2	73 ± 5	94.8 ± 0.5	79.7 ± 0.7	56 ± 1	61 ± 7
TriNOx^{tBu}	Et_2O	18 ± 4	2.6 ± 0.2	44 ± 7	94 ± 1	72 ± 1	32 ± 2	66 ± 3
TriNOx^{tBu}	Hexanes	12 ± 5	1.6 ± 0.2	19 ± 6	91 ± 3	61 ± 2	18 ± 1	75 ± 2
TriNOx^{Ph}	Benzene	2.1 ± 0.1	5.3 ± 0.2	10.9 ± 0.7	67.4 ± 0.4	84.0 ± 0.6	46 ± 2	39 ± 3
TriNOx^{Ph}	Toluene	2.2 ± 0.1	5.3 ± 0.1	11.8 ± 0.3	68.9 ± 0.7	84.2 ± 0.2	48 ± 2	57 ± 4
TriNOx^{Ph}	THF	1.0 ± 0.1	1.5 ± 0.1	1.5 ± 0.1	49.0 ± 0.2	60 ± 1	74 ± 9	3 ± 1
TriNOx^{Ph}	DME	2.0 ± 0.1	5.2 ± 0.6	11 ± 1	66.8 ± 0.3	84 ± 1	47 ± 1	52 ± 1
TriNOx^{Ph}	Et_2O	2.1 ± 0.2	2.9 ± 0.1	6.0 ± 0.3	67 ± 2	74.5 ± 0.5	36 ± 5	60 ± 1
TriNOx^{Ph}	Hexanes	3.9 ± 0.4	1.4 ± 0.1	4.4 ± 0.3	80 ± 2	59 ± 1	10 ± 2	56 ± 1
TriNOx	Benzene	17 ± 2	18 ± 2	303 ± 19	94.3 ± 0.5	94.7 ± 0.5	77 ± 2	48 ± 2
TriNOx	Toluene	15.4 ± 0.7	1.9 ± 0.1	30 ± 2	93.9 ± 0.3	66.0 ± 0.8	50 ± 2	51 ± 1
TriNOx	THF	-	-	-	-	-	-	-
TriNOx	DME	-	-	-	-	-	-	-
TriNOx	Et_2O	-	-	-	-	-	-	-
TriNOx	Hexanes	-	-	-	-	-	-	-
TriNOx^{CF_3}	Benzene	1.2 ± 0.2	1.6 ± 0.5	1.9 ± 0.9	53 ± 5	59 ± 9	70 ± 7	7 ± 2
TriNOx^{CF_3}	Toluene	1.7 ± 0.1	6.4 ± 0.2	11.0 ± 0.3	63.0 ± 0.2	86.5 ± 0.4	67± 7	30 ± 4
TriNOx^{CF_3}	THF	-	-	-	-	-	-	-
TriNOx^{CF_3}	DME	0.9 ± 0.1	0.8 ± 0.1	0.8 ± 0.1	49 ± 1	45 ± 2	83 ± 3	1 ± 0.5
TriNOx^{CF_3}	Et_2O	2.4 ± 0.2	6.5 ± 0.4	16 ± 3	71 ± 2	86.6 ± 0.7	66 ± 8	35 ± 1
TriNOx^{CF_3}	Hexanes	0.4 ± 0.1	0.7 ± 0.1	0.3 ± 0.1	29.0 ± 0.8	40± 1	16 ± 1	29 ± 5

Figure 1. Thermal ellipsoid plot of $[Ce(H_2A)_3]Cl$ at 50% probability (Cl–, aliphatic hydrogen

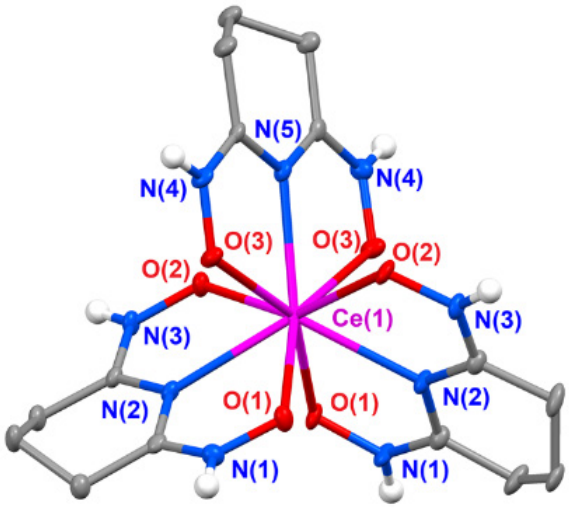

atoms, and H_2O molecules are omitted for clarity).

A Ce(IV) complex of glutarimide-dioxime

The coordination chemistry of glutarimide-dioxime (**H_3A**) has been studied previously related to applications in uranyl sequestration from seawater and for the stabilization of early d-block transition metals in high oxidation states. We report here that the **H_2A**- anion is also suitable for stabilizing Ce(IV) and acts as a tridentate ligand to form the $[Ce(\mathbf{H_2A})_3]$+ cation (Figure 1).[2] The metal complexes $[Ce(\mathbf{H_2A})_3]Cl$ and $[Ce(\mathbf{H_2A})_3][BPh_4]$ have been obtained by auto-oxidation of Ce^{III} in the presence of H_3A under aerobic conditions. UV-Vis spectroscopy and DFT calculations were performed to characterize the electronic structure and ligand-to-metal charge transfer (LMCT) bands of $[Ce^{IV}(\mathbf{H_2A})_3]$+. X-ray absorption spectroscopy (XAS) was also performed to verify the Ce(IV) oxidation state. Absent a clear electrochemical signal for cerium reduction in $[Ce(H_2A)_3]Cl$ or $[Ce(H_2A)_3][BPh_4]$ under a range of conditions, DFT calculations predicted a Ce(III/IV) redox couple of -1.22 V vs Fc/Fc^+. These results further expand the coordination chemistry of glutarimide-dioxime to tetravalent cerium.

Publications Acknowledging this Grant in 2020 – present

1. (I) "Understanding Molecular Factors That Determine Performance in the Rare Earth (TriNOx) Separations System" Cole, B.E, Cheisson, T.; Nelson, J. J. M.; Higgins, R. F.; Gau, M. R.; Carroll, P.J.; Schelter, E. J. *ACS Sustainable Chem. Eng.* **2020**, *8*, 14786.
2. (II) Yang, Q.; Qiao, Y.; McSkimming, A.; Moreau, L. M.; Cheisson, T.; Booth, C. H.; Lapsheva, E.; Carroll, P.J.; Schelter, E. J. *Inorg. Chem. Front.* **2020**, *8,* 934.
3. (III) Knope, K. E.; Vanagas, N. A.; Higgins, R. F.; Wacker, J. N.; Asuigui, D. R. C.; Warzecha, E.; Kozimor, S. A.; Stoll, S. L.; Schelter, E. J.; Bertke, J. A. *Chem. Eur. J.* **2020**, *26*, 5872-5886.
4. (I) Nelson, J. J. M.; Cheisson, T.; Rugh, H. J.; Gau, M. R.; Carroll, P. J.; Schelter, E. J. *Commun. Chem.* **2020**, *3*, 7.
5. (I) Higgins, R. F.; Cheisson, T.; Cole, B. E.; Manor, B. C.; Carroll, P. J.; Schelter, E. J. *Angew. Chem. Int. Ed.* **2020**, *59*, 1851-1856.

X-ray studies of molecular ordering at the liquid/liquid interface in solvent extraction

Mark L. Schlossman[1] and Ilan Benjamin[2]; [1]Department of Physics, University of Illinois at Chicago, Chicago, IL 60607, USA; [2]Department of Chemistry and Biochemistry, University of California at Santa Cruz, Santa Cruz 95064, USA

Presentation Abstract

During solvent extraction of rare earth ions, an aqueous electrolyte solution is placed in contact with an immiscible organic solution of extractants to enable extractant-facilitated transport of ions into the organic solvent. Although experimental methodologies such as x-ray and neutron scattering have been applied to characterize ion-extractant complexes, identifying the site of initial ion-extractant complexation has proven challenging. Here, we use tensiometry and surface-sensitive x-ray scattering to study the surface of aqueous solutions of lanthanide chlorides and the partially water-soluble extractant HDEHP, in the absence of a coexisting organic solvent. These studies restrict interactions of HDEHP with lanthanide ions to either the aqueous phase or the liquid-vapor interface. This allows us to explore the consequences of one mechanism proposed for liquid-liquid solvent extraction, that is, partially water-soluble extractants diffusing from the organic into the aqueous phase, forming a complex with metal ions in the aqueous phase, then diffusing back to the aqueous-organic interface and into the organic solvent. Unexpectedly, we find that light lanthanides preferentially occupy the liquid-vapor interface. This contradicts our expectation that heavy lanthanides should preferentially occupy the interface since they are preferentially extracted by HDEHP in the presence of an organic phase. These results reveal the antagonistic role played by initial ion-extractant complexation within the aqueous phase and clarify the potential advantages of water-insoluble extractants that interact with ions primarily at the interface during the process of solvent extraction.

DE-SC0018200: The Role of Molecular Ordering at the Liquid/Liquid Interface in Solvent Extraction

PI: Mark Schlossman (PI), Ilan Benjamin (co-PI)
Postdoc: Zhu Liang
Student(s): Trung Vo, Frederick Richard

RECENT PROGRESS

Antagonistic role of aqueous complexation in the solvent extraction and separation of trivalent lanthanides

We study the liquid-vapor interface of aqueous solutions of water-soluble bis(2-ethylhexyl) phosphate (HDEHP) and lanthanide chlorides with tensiometry, x-ray reflectivity and x-ray fluorescence. Figure 1 presents surface tension measurements from this system for different values of pH (2.0, 3.0, and 4.5). These curves illustrate the variation of surface tension with time as well as the equilibrium value attained after measuring for a sufficiently long time.

In the absence of lanthanide ions, aqueous solutions of HDEHP have an equilibrium value of surface tension that decreases as the pH is lowered. Aqueous solutions containing HDEHP and lanthanide chlorides at pH 2.0, 3.0, or 4.5 produce an equilibrium surface tension that is largest for solutions containing the heaviest lanthanide ions (Lu) and sequentially smaller for solutions containing lighter lanthanide ions (from Lu to Er, Dy, Gd, Nd, to La). X-ray measurements confirm the interpretation that surface adsorption is greater when lighter lanthanides are present, consistent with the lower surface tension.

Figure 1. Surface Tension Measurements.[1] Relaxation and equilibrium values of the liquid-vapor surface tension of (H)DEHP-aqueous solutions in the absence ("no Ln ions") or presence of lanthanide chlorides. (A) pH 2.0, (B) pH 3.0, (C) pH 4.5, (D) equilibrium values of the surface

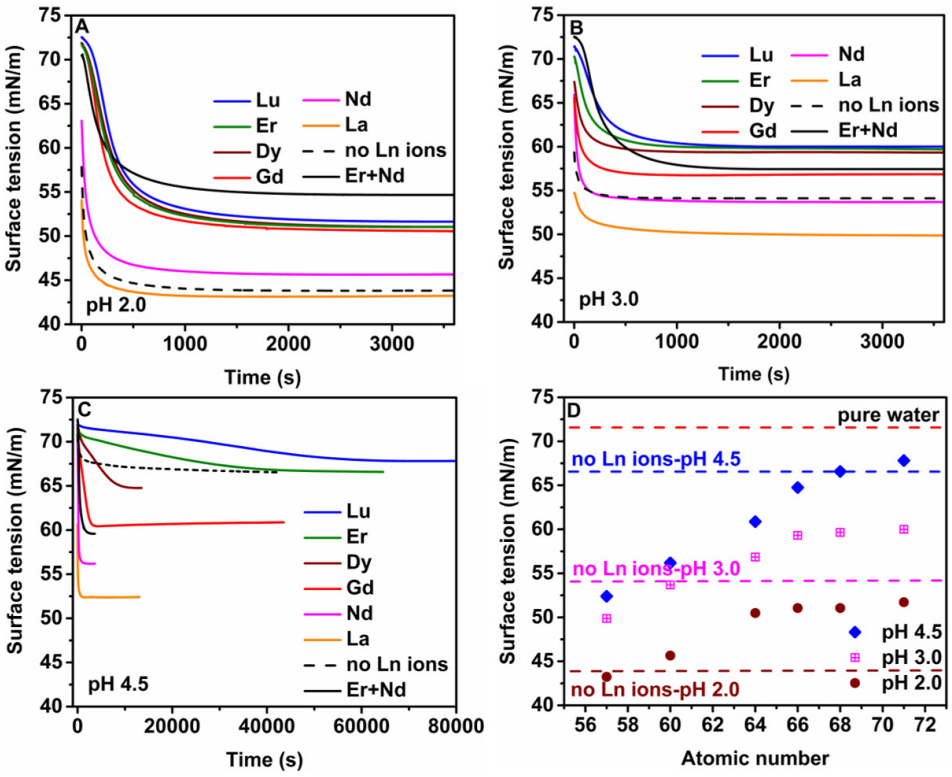

tension vs. atomic number [La(57), Nd(60), Gd(64), Dy(66), Er(68), Lu(71)] for different values of pH, where dashed lines indicate the values in the absence of lanthanide ions. Note that the total ionic strength of the mixtures (Er+Nd) in panels A-C is twice that of the single ionic component solutions.

Figure 1 also illustrates the kinetics of attaining equilibrium. It is generally observed that solutions with lighter lanthanides equilibrate quickly, more or less at the rate with which (H)DEHP equilibrates in the absence of ions, but the kinetics is slower for solutions with heavier lanthanides. This is particularly apparent at pH 4.5 where it can be observed that the surface tensions for the single-Ln-ion component samples containing Er and Lu ions persist at values near that of pure water for many thousands of seconds, suggesting that these ions stabilize an interface that has little extractant even on time scales much longer than required for the equilibration of (H)DEHP in the absence of Ln ions. Eventually, the surface tension relaxes to

values lower than that of pure water, indicating a slow adsorption to the liquid-vapor interface, an adsorption that is confirmed by x-ray measurements. On the other hand, the surface tension of solutions with lighter lanthanides, for example Nd ions, relaxes on the same time scale as in the absence of ions, suggesting that the relaxation is dominated by the adsorption kinetics of HDEHP to the interface. Similar effects are observed to a lesser extent at pH 2.0 and 3.0.

Figure 2 illustrates XFNTR measurements which probe the interfacial density of ions at the liquid-vapor interface of samples with the same composition as for the surface tension measurements, though limited to lanthanides Nd(III) and Er(III). Panel A in Figure 4 illustrates the increase in XFNTR signal with pH for equilibrated samples containing either Nd or Er ions. Analysis of these data is summarized in Fig. 4C, which demonstrates the increase in the interfacial density of ions as the pH increases from 2.0 to 4.5. More Nd ions are adsorbed to the interface than Er ions at each value of pH.

Aqueous samples of (H)DEHP that contain a 1:1 mixture of $NdCl_3$ and $ErCl_3$, both in a ratio of 6:1 (H)DEHP:ion, demonstrate the result of competitive adsorption between these Ln ions. Under these conditions, Fig. 4B/D demonstrates that Er at the interface drops to very low levels as Nd dominates the surface adsorption at all values of pH. The surface adsorption of Nd ions in mixtures with Er ions is similar to that in the absence of Er ions.

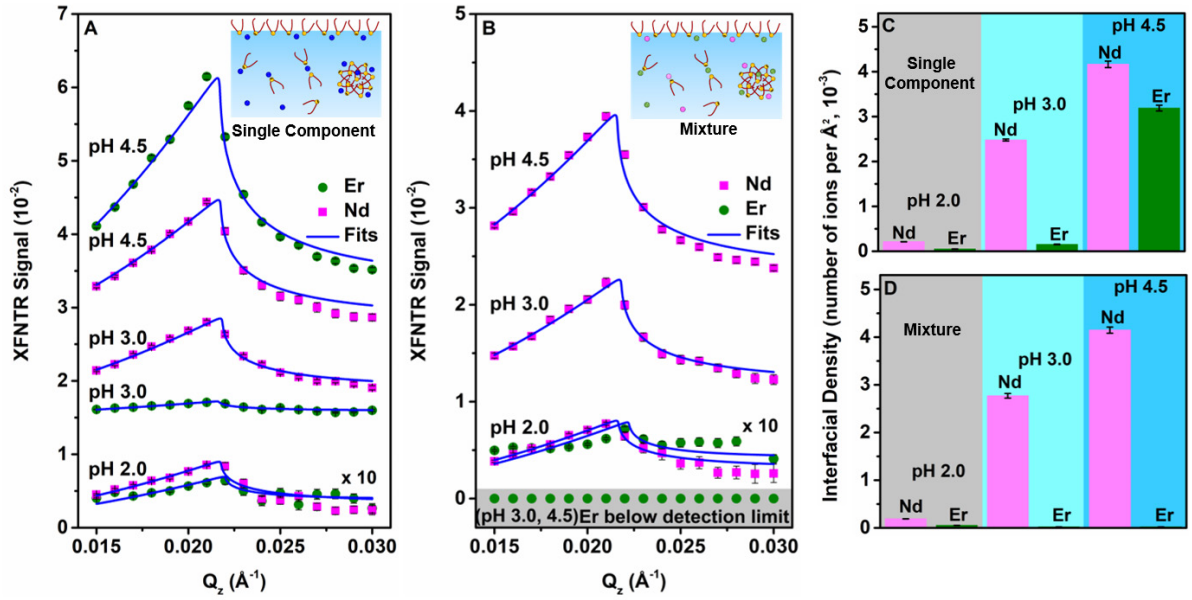

Figure 2. XFNTR measurements of the interfacial density of Nd and Er ions at the liquid-vapor interface of equilibrated aqueous solutions of water-soluble HDEHP.[1]

The extractant HDEHP is commonly used in rare earth processes and preferentially extracts heavy over light lanthanides. In this process, a solution of HDEHP in an organic solvent such as dodecane or kerosene is placed in contact with a multi-component acidic aqueous solution of lanthanides. It is believed that ions complex with HDEHP near the interface as the result of one or both of the following processes: (1) weakly amphiphilic HDEHP (H)DEHP adsorbs to the liquid-liquid interface, where it then interacts with ions approaching from the water-side of the interface, or (2) the partially soluble HDEHP dissolves in the aqueous phase boundary layer

where it complexes with ions, then the ion-extractant complex diffuses back into the organic solvent. Here, we have shown that HDEHP solvation in the aqueous phase, which might occur in the boundary layer or in the bulk, will be antagonistic to the intended preferential extraction of heavy over light lanthanides. First, the aqueous solubility of HDEHP and HDEHP -ion complexes will hold back heavier lanthanides in the aqueous phase that might have otherwise been extracted into the organic solvent. The preferential attraction of a heavy lanthanide, Er(III), over a lighter lanthanide, Nd(III), for $DEHP^-$, is supported by MD simulations shown in Figure 3. Second, by preferentially solvating heavier lanthanides in the aqueous solution, this process opposes the preferential extraction of heavier lanthanides by HDEHP into the organic solvent. Complementary to this is the overwhelming preference of the light lanthanide Nd over the heavy lanthanide Er for the liquid-vapor interface of HDEHP solutions under conditions of competitive adsorption. Third, once complexed with HDEHP in bulk aqueous solution, the kinetics of heavier lanthanide adsorption to the interface is longer by hundreds to tens of thousands of seconds than for lighter lanthanides. These results raise several issues for the mechanism of liquid-liquid extraction of lanthanides with HDEHP that require further study.

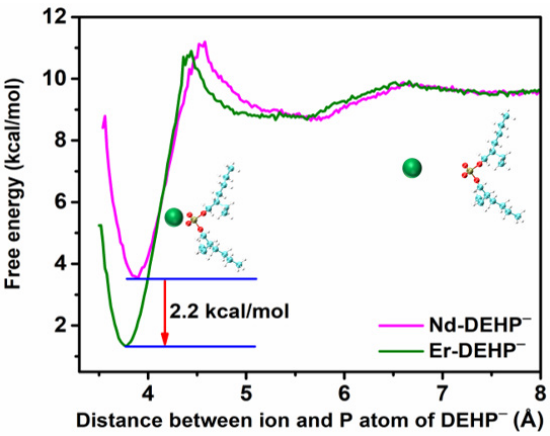

Figure 3. MD simulations of the potential of mean force (PMF or free energy) between Er(III) and $DEHP^-$, and Nd(III) and $DEHP^-$.[1]

(1) Sun, P.; Binter, E; Liang, Z.; Brown, M. A.; Gelis, A. V.; Benjamin, I.; Bera, M.; Lin, B.; Bu, W.; Schlossman, M. L. Antagonistic Role of Aqueous Complexation in the Solvent Extraction and Separation of Rare Earth Ions, ChemRxiv 2021.

Publications Acknowledging this Grant in 2018 – present

(II) Liang, Z.; Bu, W.; Schweighofer, K. J.; Jr., D. J. W.; Harvey, J. S.; Hanlon, G. R.; Amoanu, D.; Erol, C.; Benjamin, I.; Schlossman, M. L. A Nanoscale View of Assisted Ion Transport across the Liquid-Liquid Interface. *Proceedings of the National Academy of Sciences (USA)* **2019**, 116, 18227-18232.

(II) Bu, W.; Schlossman, M. L. X-ray Studies of Liquid Interfaces in Model Solvent Extraction Systems. In *Ion Exchange and Solvent Extraction*; Moyer, B. A., Ed.; CRC Press: New York, **2019**; Vol. 23; pp 115-146.

Single-molecule Dynamics in Interface-rich Separations Environments

Daniel K. Schwartz, University of Colorado Boulder

Presentation Abstract

The dynamic behavior of molecules and nanoparticles in confined environments, such as at interfaces and within porous materials, lead to complex and highly-varied phenomena, where heterogeneity may arise from spatial variation of the material/interface itself, from structural configurations (i.e. conformation, orientation, aggregation state, etc.), or temporally, through inhomogeneous dynamic behavior. In order to capture relevant information about these complex dynamics, we have developed highly multiplexed single- molecule/single-nanoparticle tracking methods that are capable of acquiring $>10^5$ trajectories in a given experiment; automated unbiased data analysis methods are used to interpret these large data sets. Recent work in our lab has extended the tracking methods to acquire fully 3D trajectories, enabling tracking of individual molecules and nanoparticles in complex environments, including porous media, thin polymer films, interfacial nanofilms, and dynamically fluctuating porous environ,ents. Results will be shown that provide new insights into the transport of nanoparticles within porous 3D environments, of polymers in confined gaps, and of small molecules within polymeric films and aqueous nanofilms.

Single-molecule Dynamics in Interface-rich Separations Environments DE-SC0001854

PI: Daniel K. Schwartz

Postdoc(s): Raphael Sarfati (2018), Daniel Kienle (2019-2021)
Student(s): Gregory Morrin (2018-2020), Haichao Wu (2019-2021)

RECENT PROGRESS

3D Tracking of Transport in Confined Environments

We have developed methods to study the 3D motion of nanoparticles and molecules near surfaces, within the void space of porous materials using double-helix point-spread- function (DH-PSF) imaging and also using a new method that combines super-resolution imaging with FRET. Temporal sequences of images are acquired, and trajectories linked, providing long-duration 3D trajectories for tens of thousands of particles or molecules simultaneously. Trajectories are subjected to statistical analyses, including multivariate machine-learning analytic approaches, e.g. to identify time intervals where particles arein confined/retained vs. freely diffusing “states”

DH-PSF with Variable-Angle Illumination Epifluorescence Microscopy
We demonstrated that the signal-to-noise ratio (SNR) and three-dimensional localization precision of a double helix point spread function (DH-PSF) were greatly improved by applying variable-angle illumination epifluorescence microscopy.

Nanoparticle diffusion within ordered porous void spaces
3D diffusion of nanoparticle probes was observed within a model porous material, an inverse opal,

comprising an interconnected network of hexagonally close packed spherical cavities. Each nanoparticle trajectory was analyzed to determine its dwell time within each cavity to determine comprehensive escape-time distributions as a function of size of the channels connecting the cavities. We found that nanoparticle motion was inhibited near cavity walls and cavity escape was slower than predicted by existing theories and random- walk simulations. A combined computational-experimental analysis indicated that translocation through a nano-channel is barrier-controlled rather than diffusion-controlled. In subsequent work, interactions were mediated via ionic strength. The effects of electrostatic interactions on nanoparticle transport were surprisingly large. For example, an increase in the Debye length of only a few nm (in a material with a hole diameter of ~100 nm) increased the mean cavity escape time three-fold. A combination of computational and experimental analyses indicated that this hindered cavity escape was due to an electrostatic energy barrier in the region of the hole, which was quantitatively explained using DLVO theory. These findings explicitly demonstrate that the cavity escape process was and dominated by electrostatic effects.

Connecting transport in porous media across length scales: single-pore to macroscopic While hindered transport is widely observed in various porous media, like filtration membranes and porous rocks, there is no universal model able to predict this transport due to the heterogeneity of porous structures and complex underlying microscopic mechanisms, like electrostatic and hydrodynamic effects. Here we used a highly-ordered porous media (a silica inverse opal film) to explicitly explore the effects of geometric parameters (i.e., pore size, pore throat and tracer particle size) and microscopic interaction parameters (i.e. ionic strength) on nanoparticle transport in porous media using DH-PSF three-dimensional single-particle tracking methods. Interestingly, we found a linear scaling relation between the macroscopic diffusion coefficient and a particular combination of parameters associated with microscopic features and behaviors, which include both geometric effects and microscopic interactions. The proportionality coefficient relating micro and macro behaviors was complex, and related to the connectivity of the matrix in the context of percolation theory. Moreover, we found pore size variation could lead to tortuous diffusion pathways, leading to macroscopic hindered transport. These findings provide important insights into nanoparticles and macromolecules transport in various porous media.

Motion of ions in a polyelectrolyte multilayer

The diffusion of small, charged molecules incorporated in polyelectrolyte multilayers (PEMs) was tracked in three dimensions by combining single-molecule fluorescence localization (to characterize lateral diffusion) with Förster resonance energy transfer (FRET) between diffusing molecules and the supporting surface (to measure diffusion in the surface-normal direction). Analysis of the surface-normal diffusion required model- based statistical analysis to account for the inherently noisy FRET signal. These distinct imaging methods, which are inherently sensitive to different length scales permitted simultaneous characterization of severely anisotropic diffusion, which was more than three orders of magnitude slower in the surface-normal direction. We hypothesize that the anomalously slow surface-normal diffusion was related to the, periodic distribution of charge in the PEM, which created electrostatic barriers. The motion was strongly subdiffusive, with anomalous temporal scaling exponents in lateral and normal directions, suggesting a connection to the fractal conformation of polymer chains in the film's matrix.

Transport Enhancement of Self-Propelled Nanoswimmers in a Porous Matrix Micro/nanoswimmers convert diverse energy sources into directional movement, demonstrating tremendous promise for biomedical and environmental applications, many of which involve complex tortuous or crowded environments. Here, we investigated the transport behavior of self-propelled catalytic Janus particles in a complex interconnected porous void-space, where the rate-determining step involves the escape

from a cavity and translocation through holes to adjacent cavities. Surprisingly, self-propelled nanoswimmers escaped from cavities more than 20x faster than passive (Brownian) particles, despite the fact that the mobility of nanoswimmers was less than 2x greater than that of passive particles in unconfined bulk liquid. Combining experimental measurements, Monte Carlo simulations and theoretical calculations, we found that the escape of nanoswimmers was enhanced by nuanced secondary effects of self-propulsion which were amplified in confined environments. In particular, active escape was facilitated by anomalously rapid confined short-time mobility, highly efficient surface-mediated searching for holes, and the effective abolition of entropic and/or electrostatic barriers at the exit hole regions by propulsion forces. The latter mechanism converted the escape process from barrier-limited to search-limited. These findings provide general and important insights into micro/nanoswimmer mobility in complex environments.

Mass Transport in Complex Interface-rich Environments

Our studies of molecular motion at solid/liquid interfaces have described the transport in the context of a continuous time random walk (CTRW) process, in which diffusion switched between desorption-mediated "flights" (i.e. hopping) and surface-adsorbed waiting-time intervals during which the molecules were either immobilized or engaged in slow 2D diffusive motion. We recently extended this work to include interfacial transport under more complex conditions, where the surface itself exhibited some degree of fluidity and/or where molecules were increasingly crowded at the interface.

Surface Diffusion in Confined Slit-Pore Geometries

Strongly confined environments (confined dimensions between 1-100 nm) represent unique challenges and opportunities for understanding and manipulating molecular behavior due to the significant effects of electric double layers, high surface-area to volume ratios, and other phenomena at the nanoscale. Convex Lens-induced Confinement (CLiC) can be used to analyze the dynamics of individual molecules or particles confined in a planar slit geometry with continuously varying gap thickness. We developed an interferometry-based method for precise measurement of the slit pore geometry that approach permitted accurate characterization of separation distances as small as 5 nm, with 1 nm precision, without a priori knowledge or assumptions about the contact geometry. This method was used to study the diffusion of a polyelectrolyte (PLL) in a planar slit geometry slit heights below 100 nm. Independent of surface chemistry, the effective surface diffusion coefficient increased with height until saturating for slit heights <30nm. The evolution of the diffusion coefficient with slit height was faster for surfaces with which PLL exhibited stronger short-range interactions, which influenced the intermittent random walk behavior by increasing the waiting times between flights and the re-adsorption probability (a.k.a sticking coefficient) during flights.

Diffusion of Short Semi-Flexible Polymer Chains in Strong and Moderate Confinement

In many separations (and other) applications, semi-flexible polymer chains are confined within nano-environments that are smaller than the size of the unconfined polymer in solution. However, the dependence of the diffusion coefficient on molecular weight and characteristic confinement dimension remains poorly understood in this regime. Here, Convex Lens-induced Confinement (CLiC) was leveraged to examine how the diffusion of short DNA fragments varied as a function of slit height using single-molecule fluorescence tracking microscopy. The diffusion coefficient followed approximate power law behavior versus confinement height, with exponents of 0.27 ± 0.01, 0.32 ± 0.02, 0.42

± 0.06 for 692, 1,343, and 2,686 base pair chains, respectively. The weak dependence on slit height suggests that shorter semi-flexible chains may adopt increasingly rod-like conformations, and therefore experience weaker excluded volume interactions as the confinement dimension is reduced. The diffusion coefficient versus molecular weight also exhibited apparent power law behavior, with exponents that varied slightly (from –0.89 to
–0.85) with slit height, consistent with hydrodynamic interactions intermediate between Rouse and Zimm model predictions.

Temporally anticorrelated subdiffusion in water nanofilms

Single-molecule tracking was used to probe the local rheology of interfacial water. Fluorescent rhodamine molecules were tracked on silica surfaces as a function of ambient relative humidity, which controlled the thickness of condensed water nanofilms. At low humidity, the molecules exhibited confined diffusion in the vicinity of isolated adsorption sites characterized by a broad distribution of binding stiffness constants; subsequent chemical or physical surface passivation selectively eliminated stiffer binding sites. At increased humidity, molecularly thin water films condensed, permitting near-surface transport of rhodamine molecules. Motion was subdiffusive, with an anomalous exponent increasing with the nanofilm thickness. Molecular trajectories were temporally anticorrelated, ergodic, but also featured transient binding and intermittent diffusion. Statistical modeling demonstrated that this complex motion in water nanofilms had the characteristics of fractional Brownian motion combined with a continuous-time random walk. This was consistent with diffusion within viscoelastic nanofilms, suggesting persistent molecular structuring in the vicinity of the silica surface.

Enhanced diffusive transport in fluctuating porous media

Mass transport within porous structures is a ubiquitous process in biological, geological, and technological systems. Despite the importance of these phenomena, there is no comprehensive theory that describes the complex and diverse transport behavior within porous environments. While the porous matrix itself is generally considered a static and passive participant, many porous environments are in fact dynamic, with fluctuating walls, pores that open and close, and dynamically changing crosslinks. Here we present a direct comparison of the diffusion of nanoparticles of various sizes within a fluctuating porous matrix and a geometrically equivalent static matrix, in conditions spanning a range of regimes from obstructed to highly confined. The experimental system comprised a close- packed layer of colloidal spheres that were either immobilized to a planar surface or allowed to fluctuate locally, within the space defined by their nearest neighbors. Interestingly, the effective long-time diffusion coefficient was approximately 35-65% greater in the fluctuating porous matrix than in the static one (depending on the size of the nanoparticle probes), regardless of the geometric regime. This was explained by considering the enhancing effects of matrix fluctuations on the short-time diffusion coefficient and cooperative “gate-opening" motions of matrix particles and nanoparticle probes.

Publications Acknowledging this Grant in 2019 – present

Exclusively funded by this grant;

1. Dapeng Wang, Lijun Liu, Haichao Wu, Jizhong Chen, and Daniel K. Schwartz, "Diffusive Escape of a Nanoparticle from a Porous Cavity", *Phys Rev Lett,* **123**, 118002 (2019)
2. Raphael Sarfati and Daniel K. Schwartz, "Temporally anticorrelated subdiffusion in water nanofilms on silica suggests near surface viscoelasticity", *ACS Nano*, **14**, 3041- 3047 (2020);
3. Raphael Sarfati, Christopher P. Calderon, and Daniel K. Schwartz, "Enhanced Diffusive Transport in Fluctuating Porous Media", *ACS Nano*, **15**, 7392-7398 (2021); doi:10.1021/acsnano.1c00744
4. Daniel F. Kienle and Daniel K. Schwartz, "Anisotropic and Anticorrelated Motion of Ions in a Polyelectrolyte Multilayer", *Analytica Chimica Acta*, **1154**, 338331 (2021); doi:10.1016/j.aca.2021.338331
5. Gregory T. Morrin, Daniel F. Kienle and Daniel K. Schwartz, "Diffusion of Short Semi- Flexible DNA Polymer Chains in Strong and Moderate Confinement" (under review)

Jointly funded by this grant and other grants with leading intellectual contribution from this grant

6. Gregory T. Morrin, Daniel F. Kienle and Daniel K. Schwartz, "Standalone Interferometry-Based Calibration of Convex Lens-Induced Confinement Microscopy with Nanoscale Accuracy", *Analyst*, **144**, 2628-2634 (2019).
7. Gregory T. Morrin, Daniel F. Kienle, James S. Weltz, Jeremiah C. Traeger, and Daniel
8. K. Schwartz, "Polyelectrolyte diffusion in a nanoslit geometry: Effects of height and surface chemistry", *Macromolecules,***53**, 22640-22649 (2020)
9. Haichao Wu, Raphaël Sarfati, Dapeng Wang, Daniel K. Schwartz, "Electrostatic Barriers to Nanoparticle Accessibility of a Porous Matrix", *J. Am. Chem. Soc.* **142**, 4696-4704 (2020)
10. Dapeng Wang and Daniel K. Schwartz, "Non-Brownian Interfacial Diffusion: Flying, Hopping, and Crawling" (Invited Perspective), *J. Phys Chem C* (2020); doi:10.1021/acs.jpcc.0c05834
11. Haichao Wu and Daniel K. Schwartz, "Nanoparticle Tracking to Probe Transport in Porous Media" (Invited review), *Accounts of Chemical Research,* **53**, 2130-2139 (2020); doi:10.1021/acs.accounts.0c00408
12. Haichao Wu, Dapeng Wang, and Daniel K. Schwartz, "Connecting Hindered Transport in Porous Media Across Length Scales: From Single-Pore to Macroscopic", *J Phys Chem Lett*, **11**, 8825-8831 (2020); doi:10.1021/acs.jpclett.0c02738
13. Haichao Wu, Benjamin Greydanus, and Daniel K. Schwartz, "Mechanisms of Transport Enhancement for Self-Propelled Nanoswimmers in a Porous Matrix", *Proc. Natl. Acad. Sci. U.S.A.* **118**, e2101801118 (2021); doi:10.1073/pnas.2101807118

Using Machine Learning to Search Adsorption Space: Many Molecules in Many MOFs

David Sholl, AJ Medford, Sihoon Choi and Xiaohan Yu; School of Chemical & Biomolecular Engineering, Georgia Institute of Technology

Because of the vast number of distinct molecular species that exist there are many near-azeotropic pairs of molecules whose bulk boiling points are very similar. These pairs are interesting and challenging candidates for adsorption-based separations. We have developed machine learning (ML) methods to model adsorption of diverse collections of molecules in MOFs in the dilute limit. This limit is important both because it drives selectivity in mixture adsorption and because it is dominated by molecule-adsorbent interactions, which have not been captured accurately in previous ML models. By developing models for the molecular Henry's constants and heat of adsorption we are able to predict adsorption selectivity as a function of temperature. Testing these models with a diverse array of near-azeotropic mixtures highlights the key physical features necessary for accurately modeling adsorption and reveals the limitations of our current model.

A top-down and bottom-up strategy to generate free volume for membrane-based gas separations

Katherine Mizrahi Rodriguez,[1] Sharon Lin,[2] Francesco M. Benedetti,[2] and Zachary P. Smith[2]; [1]Materials Science and Engineering, MIT, Cambridge, MA 02139; [2]Chemical Engineering, MIT, Cambridge, MA 02139

Polymers of intrinsic microporosity (PIMs) have outstanding gas permeabilities and adequate selectivities. These properties result from the rigid and contorted backbone structure of PIMs, which produce significant non-equilibrium free volume as these polymers vitrify during solvent casting. Unfortunately, it is difficult to manipulate and predict the nascent free volume architecture of these polymers. This presentation will describe two alternative strategies to generate high free volume polymers. The first strategy is to construct bottlebrush polymers with pre-designed side chains that can generate free volume. In this bottom-up approach, rigid side chains are tethered to flexible backbones to generate a new class of PIM materials. The second strategy is a top-down approach, where a polymer is pre-functionalized with a labile protecting group. After casting, *in situ* solid-state deprotection and crosslinking significantly increases free volume and tightens free volume distribution, resulting in enhanced permeability and selectivity for various gas pairs.

Trivalent and Tetravalent Ion Adsorption at Graphene and Graphene Oxide Surfaces

Ahmet Uysal, Chemical Sciences and Engineering Division, Argonne National Laboratory, Lemont, IL 60439

Graphene based membrane and sorbent materials have been extensively studied in recent years. They are especially attractive due to their mechanical stability, unique structural and functional properties, tunability, and high surface area. Graphene based materials, alone or as additives, can be very useful under harsh conditions of heavy element separations, where the stability of polymer based materials fail.

In spite of their popularity, molecular scale details of ion adsorption at graphene and graphene oxide interfaces are poorly understood. Especially, understanding the interplay between the ion hydration and adsorption is very challenging at these interfaces. Graphene is hydrophobic and conductive and graphene oxide is amphiphilic and nonconductive. A typical graphene-based material has hydrophobic and hydrophilic patches that can lead to complex adsorption trends that is hard to resolve with a single experimental probe.

We utilize *in situ* synchrotron X-ray scattering and vibrational sum frequency generation (VSFG) spectroscopy techniques to study multivalent ion adsorption at graphene and graphene oxide surfaces. Our studies initial studies focus on the two end points of the broad graphene based materials spectrum. High quality pristine graphene (epitaxial graphene on silicon carbide) and graphene oxide (thin films at air/water interface).

Atomically flat epitaxial graphene allows high resolution crystal truncation rod (CTR) studies of aqueous/graphene interface. We determine the layered structure of interfacial water and how it changes with the adsorbed ions. A combination of X-ray scattering and spectroscopy, where the X-ray energy is tuned around the X-ray absorption edge of adsorbed ions provides direct information about the coverage and distance of the adsorbed ions at the interface. The ion adsorption was controlled by the applied potential to the graphene surface.

Ion adsorption at graphene oxide thin films at the air/aqueous interface are studied by surface sensitive X-ray fluorescence and VSFG spectroscopy. X-ray fluorescence provides a direct quantitative measure of the adsorbed ions on the graphene oxide film. VSFG spectroscopy elucidates the response of the interfacial water to the adsorbed ions. We identify how the bulk solution conditions affect the adsorption and investigate possible differences between the bulk and interfacial speciation of tetravalent ions.

Computer Simulation of Complex Systems at the Extremes of pH

Gregory A. Voth, The University of Chicago, Department of Chemistry

Presentation Abstract

This project involves the development and application of an accurate and efficient multiscale reactive molecular dynamics approach to simulate a variety of complex heterogeneous systems at the extremes of pH (< 0 or > 14). Such systems are fundamentally important in separations science, but currently little is known about their physical properties and very limited simulation tools are available to study them. The research addresses this challenge by further developing this multiscale computational framework to accurately bridge electronic structure data with an efficient MD methodology, which is in turn is able to access the relevant large time and length scales. A fundamental understanding is being obtained for highly acidic and basic systems, including those for water-organic liquid interfaces, water-amphiphile mixtures, systems in nanoscale confinement, micelles and polymers, systems under applied voltage, and proton exchange membrane-catalyst layers. The project is also carried out in close contact with experimental characterization for certain of the key systems. In addition to providing fundamental basic knowledge, the proposed research helps to open the door to new breakthroughs in the design and control principles for novel separations processes and materials.

DE-SC0018648: Computer Simulation of Complex Systems at the Extremes of pH

Student(s): Paul Calio, Zhefu Li, Chenghan Li

RECENT PROGRESS

Our research focuses on the outstanding and important challenge of simulating highly acidic and basic systems in both homogeneous and heterogeneous environments. We are addressing this challenge by further developing our multiscale computational framework based on a multiscale reactive molecular dynamics (MS-RMD) method that recapitulates state of the art electronic structure data but with an efficiency capable of accessing the relevant time and length scales. Specific accomplishments in the past year include:

Hydrated excess protons in heterogeneous environments

We investigated the behavior of an excess proton in non-ionic reverse micelles of various sizes. We observed the hydrated excess proton has a strong affinity to the water-micelle interface, and such affinity diminishes as the micelles increase in diameter. Strong affinity to the interface results in reduced proton transport due to (1) slow micellar water diffusion that leads to slow vehicular transport of proton and (2) the distorted structure of interfacial hydrated proton complex that leads to hindered proton hopping. We additionally see strong correlations between the proton dynamical properties as the micelle increases in size due to the reduced affinity to the surface. Furthermore, we observe a bi-exponential relaxation of the overall hydrogen bonds in

reversed micelles, with the larger relaxation timescale comparable to that in a bulk water. A slow-relaxing component of the hydrogen bond network also contributes to the slow proton transport.

We also studied the behavior of a hydrated excess proton at the water-vapor interface. We used enhanced free energy sampling techniques to calculate the potential of mean force (PMF) for two interface definitions: (1) the Gibbs Dividing interface (GDI), which is an average interface over the entire time series, and (2) the Willard-Chandler Interface (WCI), which is an instantaneous interface calculated for each timestep. In both cases, the excess proton shows similar trends that weakly attract the hydrated proton to the interface. When the excess proton moves to the interface, the reduced water density in the interfacial region causes the coordination number of the hydrated proton (hydronium-like) structure to decrease, thus causing the dipole moment of the hydronium cation to align perpendicular to the interface. This leads to the solvation structure of the hydronium to form in a relatively higher density water region. We also discovered that the curvature of the WCI is very dependent on the location of hydrated excess proton, which we propose is a result of the alteration of water density by the solvation shells of the hydronium-like cation.

We employed molecular dynamics simulations, quantum theory of atoms in molecules (QTAIM) analysis, and free energy sampling to investigate the thermodynamic, structural, and dynamical properties of protonated water clusters found in a heterogenous water-acetonitrile mixture. Recent 2D-IR spectroscopy experiments have proposed that protonated water clusters in acetonitrile reveal the solvation structure of the hydrated excess proton as a Zundel cation. From our simulations, however, we discovered that the Zundel cation $H_5O_2^+$ is not the predominant species in these water clusters as had been proposed. Multiple species of protonated water clusters were identified in the system, with the primary cluster species being an Eigen cation $H_9O_4^+$, followed by a three-water $H_7O_3^+$ cation. Further analysis of the structural properties and anisotropy decay trends identified the $H_7O_3^+$ cluster as an Eigen-like cation with an acetonitrile replacing one of the solvating water molecules, not a Zundel cation with an additional water molecule as has been previously suggested. The overall Eigen-like nature of the protonated water clusters was found to be the result of the localization of the excess proton charge defect. We concluded that an acetonitrile-acid-based water system contains multiple species of protonated water clusters.

Of special pertinence to separations science, we also studied the impact of acidification on the solubility of hydrophobic species in the aqueous phase with our MS-RMD simulations. The radial distribution functions (RDF) of neopentane in water, acid, and salt solutions of different concentrations were calculated and compared. The RDFs reveal that the solvation of neopentane in salt solution is more structured (the salting-out effect). In acid solution, on the other hand, the solvation becomes less structured and is aided by the hydrated excess protons, arising from an “amphiphilic” character of hydrated excess protons predicted in the Voth group more than 15 years ago. Additionally, to obtaint a quantitative picture of hydrophobic solubility in water/acid/salt solutions, we further investigated the transfer process of neopentane from aqueous phase to oil phase by utilizing free energy sampling. The profile of transfer free energy was calculated, and reveals consistent conclusions arising from the amphiphilic character of

hydrated excess protons, which significantly affects the transfer free energetics of hydrophobic species from aqueous to oil phase. Acid solutions (low pH) are different from equivalent concentration salt solutions and both are different from neutral pH solutions.

Publications To Date Acknowledging this Grant

1. Calio, P. B.; Li, C.; Voth, G. A. Molecular Origins of the Barriers to Proton Transport in Acidic Aqueous Solutions. *J. Phys. Chem*. *B*. **2020**, *124*, 8868–8876. *Exclusively funded by this grant*
2. Arntsen, C.;* Chen, C.;* Calio, P. B.; Li, C.; Voth, G. A. The Hopping Mechanism of the Hydrated Excess Proton and Its Contribution to Proton Diffusion in Water. *J*. *Chem*. *Phys*. **2021**, *154*, 194506. (*Authors contributed equally). *Exclusively funded by this grant*
3. Li, Z.; Li, C.; Wang, Z.; Voth, G. A. What Coordinate Best Describes the Affinity of the Hydrated Excess Proton for the Air-Water Interface? *J. Phys. Chem. B*, **2020**, *124,* 5039–5046. *Exclusively funded by this grant*
4. Li, Z.; Voth, G. A. Interfacial Solvation and Slow Transport of Hydrated Excess Protons in Non-ionic Reverse Micelles, *Phys. Chem. Chem. Phys*. **2020**, *22*, 10753-10763. *Exclusively funded by this grant*
5. Calio, P. B.; Hocky, G. M.; Voth, G. A. Minimal Experimental Bias on the Hydrogen Bond Greatly Improves *Ab Initio* Molecular Dynamics Simulations of Water. *J. Chem. Theory Comp*. **2020**, *16*, 5675–5684. *Jointly funded by this grant and other grants with leading intellectual contribution from this grant*
6. Calio, P. B; Li, C.; Voth, G. A. Understanding the Essential Nature of the Hydrated Excess Proton Through Simulation and Interpretation of Recent Spectroscopic Experiments. *J. Am. Chem. Soc*. (under review). *Exclusively funded by this grant*
7. Li, C.; Voth, G. A. Using Constrained Density Functional Theory to Formulate Accurate and Transferable Reactive Molecular Dynamics Models. *J. Phys*. *Chem*. *B*. (under review). *Jointly funded by this grant and other grants with leading intellectual contribution from this grant*
8. Li, C.; Voth, G. A.; Using Constrained Density Functional Theory to Track Proton Transfers and to Sample Their Associated Free Energy Surface. *J*. *Chem*. *Theory Comp*. (in press). *Jointly funded by this grant and other grants with leading intellectual contribution from this grant*
9. Calio, P. B.; Voth, G. A. Proton Transport in Perfluorosulfonic Acid Membranes Under External Electric Fields. *J*. *Phys*. *Chem*. *C* (to be submitted). *Exclusively funded by this grant*
10. Li, Z.; Li, C.; Beckett, D.; Voth, G. A. Unusual Behavior of Protonated Water Clusters in Heterogeneous Solutions. *J. Am. Chem. Soc.* (to be submitted). *Jointly funded by this grant and other grants with leading intellectual contribution from this grant*

Field-enhanced Ion Selectivity and Transport Throughput: From Single Nanopores to Anodized Aluminum Oxide Membranes

Gangli Wang, Warren Brown, Ruoyu Yang, Maksim Kvetny, Dipak Baram, Georgia State University, Department of Chemistry*

Abstract

Symmetry-breaking and time-/history- dependent electrokinetic transport properties discovered from single asymmetric nanopores provide fundamental insights on ion selectivity and transport throughput at nano-structured interfaces, and suggest new avenues to mitigate the tradeoff between selectivity and throughput/efficiency in separation and energy processes. Transport hysteresis in the rectified electrokinetic transport is successfully resolved in anodized aluminum oxide (AAO) membranes for the first time. Discovery of these time-/history-dependent transport features from macroscopic ensemble membranes constitutes significant advances of the fundamental insights on the transport selectivity and dynamics learnt from single nanopores toward separation and desalination, energy storage, harvesting and conversion, sensing, and other applications.

DE-SC0019043: Ion Transport Dynamics at Nanoscale Interfaces in Single Asymmetric Nanopores and Nanopore Arrays
PI: Dr. Gangli Wang
Affiliations: Department of Chemistry, Georgia State University

RECENT PROGRESS

I: Discovery of Rectified and Hysteresis Ion Transport through AAO membranes

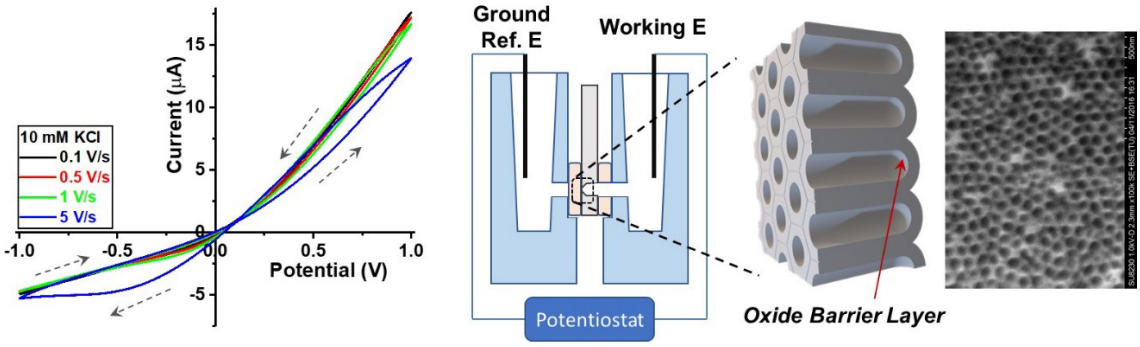

Figure 1. **Left:** Representative current-potential (*i-V*) curves demonstrating the rectified ion transport and time-dependent hysteresis in AAO membranes. Data recorded in 10 mM KCl aqueous solution at noted potential scan rates. Arrows indicate the potential scan directions. **Right:** Experimental setup and scanning electron microscopy imaging of in-house fabricated AAO membranes with the oxide barrier layer remaining.

Predicted by our earlier experimental and simulation work on single nanopores, multiple pinched current-potential hysteresis loops are successfully resolved in the voltammetric measurements with AAO membranes. Literature fabrication conditions are modified after the

confirmation that commercial AAO membranes do not display these transport properties. The time- or history-dependent electrokinetic ion transport behaviors of 1. the deviation of the ionic current from linear ohmic behavior, i.e. ion current rectification (ICR), and 2. the history-dependent transport hysteresis evident by the two i-V loops separated by a non-zero point that does not shift with scan rate (**Figure 1A**), are characterized by varying measurement parameters such as potential scan rate, ionic strength and membrane characteristics through fabrication. Combined with finite element simulation by solving Poisson, Nernst- Planck (PNP) and Navier-Stokes (NS) equations, ion selectivity and concentration polarization are quantitated and interpreted by the compositions of the available mobile charge carriers and electrostatic effects at the transport-limiting region. Those quantitative insights lay the foundation for future ion separation and energy harvesting/conversion applications.

II: Quantitation of the Hysteresis Charges and Ion Selectivity in Single Nanopores

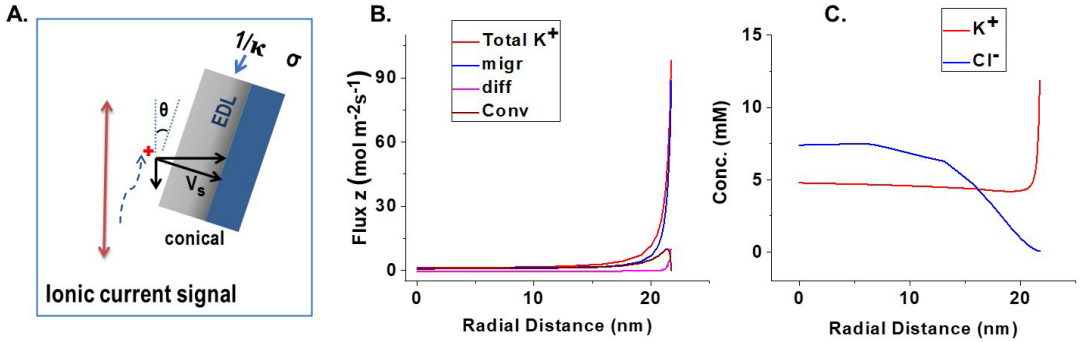

Figure 2.

A: Sketch of localized electrical field and ion flux inside a conical nanopore (side view of one substrate-electrolyte interface). **B:** flux and **C:** concentration profiles in radial direction from the simulation of rectified and hysteresis ion transport current-potential (*i-V*) features (parameters validated by fitting of experimental results). Finite element simulation using Comsol by solving PNP-NS equations: radius 20 nm, 1 mM KCl, V = + 0.7 V at cutline z= 10 nm shown.

A very counterintuitive concept has been established where ion flux and transport selectivity can be enhanced simultaneously by the localized electrical field effects in asymmetric nanopores. A dimensionless parameter of nanopore radius over Debye length is established to show that the enhancement is sustained up to tens of nanometers and hundreds of millimolar, characterized by the cation transfer number approaching unity for selectivity and high flux for throughput. This is achieved through electroosmotic flow (EOF) effects in rectified nanoscale electrokinetic transport (panel A illustrates the directions of flux, applied and surface electrical fields). Panels B & C emphasize the inhomogeneous distribution of concentration and flux resulting from the force vectors in A. The high flux and concentration near the interface present unique opportunities to improve transport throughput and ion selectivity by employing the emerging i-V transport phenomena emerge at nanometer scale interfaces shown in Fig. 1A.

Publications Acknowledging this Grant

(XI) Exclusively funded by this grant:

1. Brown, W.; Kvetny, M.; Yang, R.; Wang, G., Higher Ion Selectivity with Lower Energy Usage Promoted by Electro-osmotic Flow in the Transport through Conical Nanopores. *J. Phys. Chem. C* **2021,** *125* (6), 3269-3276.
2. Brown, W.; Li, Y.; Yang, R.; Wang, D.; Kvetny, M.; Zheng, H.; Wang, G.*, *Deconvolution of electroosmotic flow in hysteresis ion transport through single asymmetric nanopipettes. Chem. Sci.* **2020,** *11* (23), 5950-5958.
3. Kvetny, M.; Baram, D.; Brown, W.; Wang, G., Rectified Ion Transport and Hysteresis in Al2O3 Membranes with Broken Symmetry. **submitted**.
4. Brown, W.; Kvetny, M.; Yang, R.; Wang, G., Transport Hysteresis for Enhanced Selectivity of Ion Enrichment and Storage in Conical Nanopipettes **submitted**.
5. Kvetny, M.; Yang, R.; Brown, W.; Wang, G., Negative Differential Conductivity Induced by Pressure in the Rectified and Hysteresis Ion Transport in Single Nanopipettes with Broken Symmetry. **Manu. in Prep**.

Prior publications closely relevant to this grant within the past three years:

1. Wang, G.; Brown, W.; Kvetny, M., Structure and dynamics of nanoscale electrical double layer. *Current Opinion in Electrochemistry* **2019,** *13*, 112-118.
2. Wang, D.; Brown, W.; Li, Y.; Kvetny, M.; Liu, J.; Wang, G.* *Hysteresis Charges in the Dynamic Enrichment and Depletion of Ions in Single Conical Nanopores. ChemElectroChem (invited, special issue)* **2018,** *5* (20), 3089-3095.

Data Science enabled investrigation of the mechanisms for multiscale ion transport in functional electrolytes and for the radical generation in crystalline assemblies.

Sophya Garashchuk[1], Jianjun Hu[3], Linda Shimizu[1], Chuanbing Tang[1], Qi Wang[2]

University of South Carolina, [1] Dept of Chemistry & Biochemistry, [2] Dept of Mathematics, [3] Dept of Computer Science & Engineering

The objective of this study is to investigate ion transport mechanisms and morphology-property relationships in copolymer-based functional electrolyte membranes by integrating machine learning (ML) and multiscale modeling with innovative experiments. The experimental system investigated consists of cobaltocenium ($CoCp_2^+$) polymers composed of hydrophobic polyethylene backbone for mechanical stability and hydrophilic side chains for rapid hydroxide transport. The scientific questions here are (1) how to stabilize cobaltocenium ions? (2) what is the mechanism of OH^- transport within anionic exchange membrane (AEM)? We evaluate the chemical stability of the cations by dissolving them in deuterated methanol and potassium hydroxide solution at elevated temperatures to accelerate the degradation. We found that multiple substitution and steric effects play important roles in determining the stability, and tetra-tert-butyl cobaltocenium was proven to be highly stable against a strong base. Since the Bond dissociation energy (BDE) in water is a proxy for cobaltocenium stability, we conduct electronic structure analysis on a series of cobaltocenium ($CoCp_2^+$) polymers with various substitutes using DFT calculations. Based on the computed BDE data together with a set of identified molecular descriptors, we devise a neural network-based approximant to the BDE with relative errors ~ 0 2 kcal/mol or 10% accuracy of the BDE prediction. Significant non-linear dependence on the electron-donating/withdrawing descriptor (H) is also identified/confirmed.

Tuning the Thermophysical Properties of Thermally Robust Ionic Liquids Through the Subtle Modification of Ion Structure

*Brooks D. Rabideau[†], **Kevin N. West**[†], Mohammad Soltani[‡], Rome Parker[†], James H. Davis, Jr.[‡], E. Alan Salter[‡], Andrzej Wierzbicki[‡]; University of South Alabama Departments of [†]Chemical & Biomolecular Engineering and [‡]Chemistry*

Presentation Abstract

Ionic liquids have shown promise a separations agent for a variety of industrially relevant chemical processes including those involving vapor/liquid, solid/liquid and liquid/liquid equilibria. Although ionic liquids are often described as having high thermal stability, in fact, many common ionic liquids begin to break down in minutes to hours at temperatures a low as 150-200 °C, making their use at these temperatures for long periods of time impractical. Recently, our groups have developed a class of perarylphosphonium- and perarylsulfonium-based ionic liquids which are stable in the presence of air at 300-350 °C for weeks to months with little evidence of decomposition. These salts and similar species were the inspiration for the 2019 DOE EPSCoR Implementation Grant which created the Alabama Advanced Solvents Cluster (AASC) a collaborative effort between the University of South Alabama, the University of Alabama, Tuskegee University and the University of North Alabama. The cluster's work is focused developing an understanding of the molecular-level interactions between theses salts and molecular species which govern processes related to three industrially relevant areas: 1) separation of aliphatic/aromatic mixtures, 2) high temperature chemical reactions and 3) the synthesis and processing of ultrahigh performance polymers.

In this presentation, the focus will be on one aspect of the separations topic related to the molecular-level interaction between cations in the perarylphosphonium ionic liquids. Specifically, we have shown that subtle modification of the cation structure which induce an increase in the cation's dipole moment can have a significant effect on the enthalpy and entropy of fusion, and thus on the melting point of the salt. These effects are understood through molecular dynamics simulation of the liquid and solids states, showing strong agreement with the experimental measurements, and demonstrated that the decrease in enthalpy with increasing dipole moment is due to an increase in enthalpy of the crystalline state resulting from the formation of cationic domains in the solid which prevented favorable cation-anion interaction which were recovered upon melting. This understanding will inform future ionic liquid design choice and enable the creation of new thermally robust ionic liquids with lower melting points and thus larger thermal operating windows.

DE-SC0020282: Understanding the Molecular-Level Interactions Between Ionic Liquids and Molecular Species to Design and Develop Novel Solvent Systems for Energy Efficient Processes

PI: Kevin N. West – University of South Alabama

PM: W. Matthew Reichert – University of South Alabama

Co-PIs:

James H. Davis, Brooks D. Rabideau, Christy Wheeler West – University of South Alabama

Jason E. Bara, C. Heath Turner, Paul A. Rupar – University of Alabama

Michael L. Curry – Tuskegee University

Amanda H. Coffman – University of North Alabama

Post-Docs: Azin Eftekhari, Santosh Rathan Paul Bandlamudi, Mohammed Soltani, Chandan Giri, Gabriel Barbosa, Praveenkumar Sappidi, Irshad Kammakakam, Sourav Chatterjee, Sudhir Ravula, Manish Maurya

Graduate Students: Edward Anderson, Johnathan Anderson, Jimmie McGehee, Rome Parker, Bryan Christa, Amber Kinnebrew, Johnathan Mitchell, Morgan Fair, Katheryn O'Harra, Keith Watson, Corey L. Patton, Sarah E. Sisk, Xiaoyang Liu, Henry Atkinson

Undergraduate Students: Ryan Gray, Garrett Hawkins, Brittney Mack, Adrian Carter, Imani Mason

Recent Progress

Lowering the Melting Point of Perarylphosphonium Bistriflimides Through Modification of Cation Dipoles

Unlike many classes of ionic liquids whose thermophysical and chemical properties can be modified by using a broad palette of organic chemistry, the family of perarylphosphonium and perarylsulfonium salts which we are studying are limited in structural diversity due to the desire for high thermal stability (e.g. no alkyl groups, limited organic functional groups.) Thus, developing structure property relationships for the viable structural variations is often complex and not as intuitive as for simpler structures. One technique that we employ to understand how structural modifications effect melting point is to break down the thermodynamics of melting into the enthalpy and entropy of fusion (at equilibrium $\Delta G^{fus} = 0 = \Delta H^{fus} - T_m \Delta S^{fus} \rightarrow T_m = \Delta H^{fus}/\Delta S^{fus}$). Thus, from simply DSC measurements, we are able to understand how structural variations change the enthalpy and entropy of fusion. However, such studies do not explain the molecular-level origins of the changes, nor are they able to explain whether the changes in the properties of fusion were primarily from changes in the liquid or the solid phases. However, coupling these experiments with molecular dynamics simulation of the liquid and solid phases can provide a complete picture of the structure property relationships. Recently, we studied the influence of increasing the polarity of the cation (through substitution of a fluorine for a hydrogen) on various positions on the cation. In general, we found that increasing the polarity of the cation decreases the melting point, a phenomenon that was controlled by a corresponding decrease in the enthalpy of fusion.

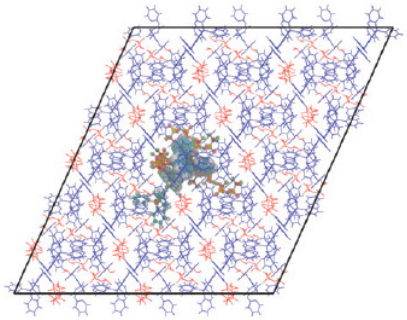

Experimental crystal structure of fluorinated perarylphosphonium salt, showing domains of cations (blue).

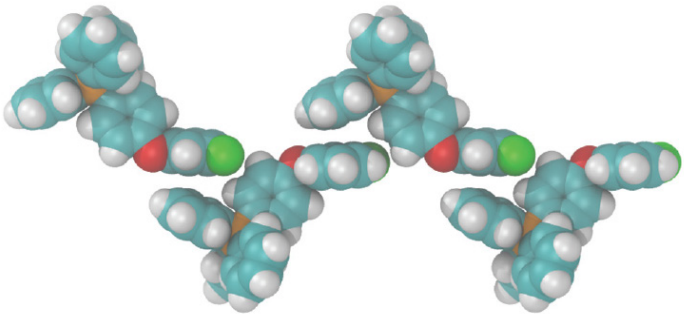

Alignment of fluorinated perarylphosphonium cations in the solid phase.

Molecular simulation provided a surprising explanation for this observation that was tied to changes in the solid phase. By increasing the polarity of the cation, the cations better align, or formed domains, in the solid phase, decreasing the potential for cation-anion interactions, and increasing the enthalpy of the solid phase. The cation-anion interactions were recovered upon melting, and the liquid phase structures/enthalpies of fluorinated vs non-fluorinated species were similar. These results were featured as a DOE Highlight earlier this year.

Molecular Simulation of Toluene/p-Xylene separation using Perarylsulfonium Salts

Separations of simple aromatics (benzene, toluene, ethylbenzene, xylenes or BTEX separations) are a challenging but important part of petroleum refining as these compounds represent key building blocks for many commercial chemical products. Many source streams containing these aromatics form azeotropes, driving extraction as the dominant process rather then distillation, particularly at low BTEX concentration. Ionic liquids have proven effective for a number of liquid-liquid extraction processes including aliphatic/aromatic and BTEX separations, however, improvements in selectivity and mass transfer (ionic liquids often have higher viscosities than many molecular liquids) must be achieved for ionic liquids processes to be commercially viable. Perarylonium salts are particularly promising as BTEX and aliphatic aromatic separation media for two reasons: their aromatic nature and their high thermal stability. The former provides the needed specific solvation for the aromatic species and the latter allows for higher operating temperatures where mass transfer limitations are decreased. Recently, the cluster has used molecular dynamics simulations to examine the solvation of toluene and *p*-xylene in one perarylphosphonium salt, triphenyl-*p*-phenyl sulfonyl phenyl. The free energy of transfer of the aromatics from *n*-hexane/*n*-heptane into the perarylonium salt was calculated (by calculating the difference in free energy of solvation of the aromatic in each solvent). The free energy of transfer of *p*-xylene being more favorable than that of toluene at all temperatures (300-420K), with transfer of each aromatic less favorable at high temperature.

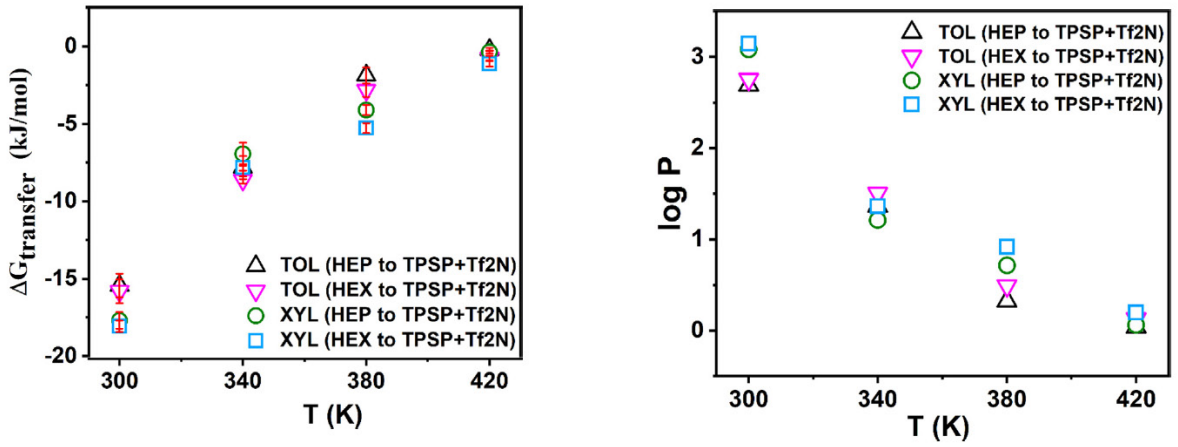

(Left) Free energy of transfer of aromatics (toluene and *p*-xylene) from aliphatic (*n*-hexane/*n*-heptane) to the perarylphosphonium salt as a function of temperature. (Right) Partition coefficient for the aromatic between the aliphatic phase and the salt phase as a function of temperature.

Furthermore, although, as expected, computed diffusivities of the aromatic solutes were about a factor of twenty lower in the ionic liquids than in the aliphatic solvent, the diffusivities increase significantly with temperature. Thus, the higher thermal limit of the perarylonium salts provides the opportunity to optimize solvation and mass transfer effects. These results will aid in the future development of this class of materials for aromatic separations.

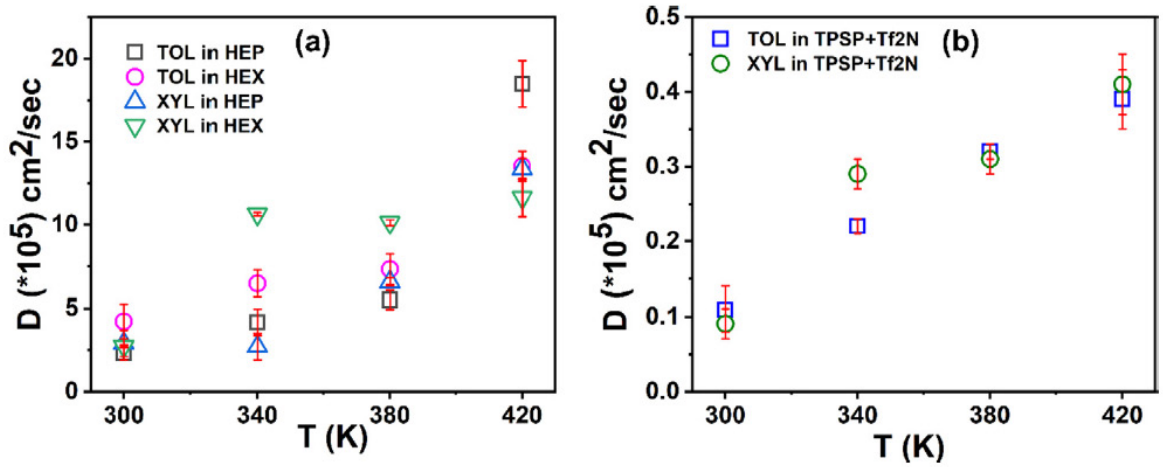

Computed diffusivities of toluene and *p*-xylene in *n*-hexane/*n*-heptane and in the perarylphosphonium salt.

Publications Acknowledging this Grant

1. Rabideau, B. D.; Soltani, M.; Parker, R. A.; Siu, B.; Salter, E. A.; Wierzbicki, A.; West, K. N.; Davis, J. H., Tuning the melting point of selected ionic liquids through adjustment of the cation's dipole moment. *Physical Chemistry Chemical Physics* **2020,** *22* (21), 12301-12311.

2. Kammakakam, I.; Bara, J. E.; Jackson, E. M., Dual Anion-Cation Crosslinked Poly(ionic liquid) Composite Membranes for Enhanced CO_2 Separation. *ACS Appl. Polym. Mater.* **2020,** *2* (11), 5067-5076.

3. Kammakakam, I.; Bara, J. E.; Jackson, E. M.; Lertxundi, J.; Mecerreyes, D.; Tome, L. C., Tailored CO_2-Philic Anionic Poly(ionic liquid) Composite Membranes: Synthesis, Characterization, and Gas Transport Properties. *ACS Sustainable Chem. Eng.* **2020,** *8* (15), 5954-5965.

4. Sappidi, P.; Rabideau, B. D.; Turner, C. H., Molecular simulation of the separation of toluene and p-xylene with the thermally-robust ionic liquid triphenyl-p-phenyl sulfonyl phenyl phosphonium. *Chem. Eng. Sci.* **2020,** *224*, 115790.

5. Alshaikh, A.; O'Harra, K. E.; Liu, X.; Whitley, J. W.; Mittenthal, M. S.; Taylor, W. F.; Turner, C. H.; Bara, J. E., Scalable, safer and greener syntheses of vinylimidazoles via reactive distillation of hydroxyethylimidazole intermediates. *Polym. Int.* **2020**, 70(5), 582-593.

6. Sappidi, P.; Bara, J. E.; Turner, C. H., Molecular-level behavior of imidazolium-based ionic liquid mixtures. *Chem. Eng. Sci.* **2021,** *229*, 116073.

7. Sappidi, P.; Liu, X.; O'Harra, K. E.; Bara, J. E.; Turner, C. H., How Do Ionic Liquids "Fold" Ionenes? Computational and Experimental Analysis of Imidazolium Polymers Based on Ether and Alkyl Chain Variations Dissolved in an Ionic Liquid. *Macromolecules* **2021,** *54* (4), 1611-1622.

8. Sappidi, P; Barbosa, G. D.; Rabideau, B. D., Weinman, S. T., Turner, C. H. Molecular Simulation of High-Salinity Brines in Contact with Diisopropylamine and Tripropylamine Solvents. *Ind. Eng. Chem. Res.* **2021**, 60 (21), 7917-7925.

9. Barbosa, G. D.; Bara, J. E., Weinman, S. T., Turner, C. H. Molecular aspects of temperature swing solvent extraction for brine desalination using imidazole-based solvents. *Chemical Engineering Science*, **2022**, 247, 116866

Emerging Projects

Systematic study on the phase transition of confined fluid mixture up to the critical region

Hertanto Adidharma,[1,2] *Morteza Dejam,*[1] *Sugata P. Tan*[3], *Xingdong Qiu,*[1] *Huan Yang,*[1] *Kevin Jayaatmaja,*[2] *Anitha Kommu*[1] ;[1]*Department of Petroleum Engineering, University of Wyoming* [2]*Department of Chemical Engineering, University of Wyoming* [3]*Planetary Science Institute*

Presentation Abstract

The phase transition of fluid mixtures confined in nanoporous media is a vital topic at the frontier that has a broad range of scientific and engineering applications, especially in separation science. Despite its importance, there have been insufficient studies to date that dealt with the *measurement of phase transition for fluid mixtures* in nanopores. In this presentation, the results of the ongoing calorimetric measurements of capillary phase transition of pure fluids in well-defined nanopores, i.e., methane, ethane, and propane in MCM-41 and SBA-15, are discussed, along with the development of procedure for measuring capillary evaporation of binary mixtures in nanopores. The latter coupled with the previously developed capillary-condensation measurement enables us to rigorously study the capillary phase-transition hysteresis and con- vincingly demonstrate that binary fluid mixtures confined in nanopores, at a specified bulk composition, behave similarly to confined pure fluids, and therefore do not exhibit phase-coexistence region in a *P-T* diagram, which is different from the views most conventional works have suggested so far. This study is also demonstrated to produce datasets useful for developing a self-consistent equation of state that can correctly describe the phase behavior of nanoconfined fluids.

Grant Number: DE-SC0021318
Grant Title: Systematic study on the phase transition of confined fluid mixture up to the critical region

PIs: Hertanto Adidharma (PI), Morteza Dejam (co-PI), Sugata P. Tan (co-PI)

Postdoc: Anitha Kommu

Students: Xingdong Qiu, Huan Yang, Kevin Jayaatmaja

Recent Progress

Experiments with pure fluids

The measurements of capillary condensa- tion condition and pore critical points of pure me- thane, ethane, and propane are still underway, the re- sults of which will be used to evaluate simulation re- sults in a later stage of the study. Figure 1 shows the measured capillary condensation of methane in MCM-41 in a *P-T* diagram obtained using our new high-pressure low-temperature differential scanning calorimeter, implementing our novel isochoric Differential Scanning Calorimetry (DSC) cooling pro- cedure.[1]

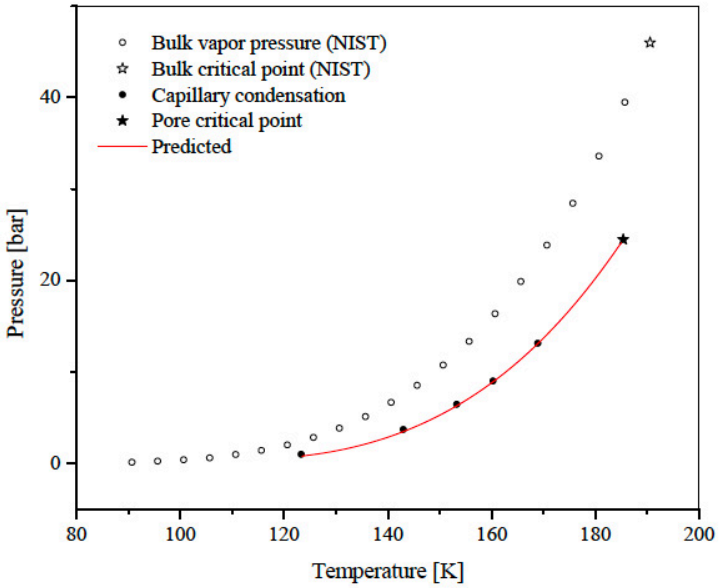

Figure 1. Bulk vapor pressure and capillary condensation of methane in MCM-41 (3.18 nm). Solid line is the pre- dicted capillary condensation using our new EOS.

As expected, the capillary condensation of methane in MCM-41 occurs, isothermally, at a lower pressure than that in bulk. The pore critical point (PCP) is also shown in Figure 1, which has been determined using the three-line approach from our preliminary work.[2] The shifts of the critical tem- perature and pressure of methane confined in MCM- 41 from that of bulk are proven to have different or- der of magnitude, the behavior of which is the same as that of CO_2 and ethane in SBA-15.[2]

Development of procedure for measureing capillary evaporation of mixtures in nanopores.

We successfully extended the DSC measure- ment procedure to measure the capillary evaporation of mixtures in confined space. Figure 2 shows the capil- lary evaporation of a methane/ethane mixture ($15 \pm 0.3\%$ $CH_4/85 \mp 0.3\%$ C_2H_6) in SBA-15 (8.1 nm), along with the capillary condensation, in a *P-T* dia- gram.[3] Both capillary condensation and capillary evap- oration unambiguously coincide with each other except at low-temperature range where hysteresis occurs, which is also well known in the case of confined pure fluids. Therefore, the phase transition can only occur when the bulk mixture outside the nanopores is in the vapor phase, and the phase transition is complete upon crossing the capillary-condensation or evaporation curve. Evidently, this work demonstrates for the first time that confined mixtures at a

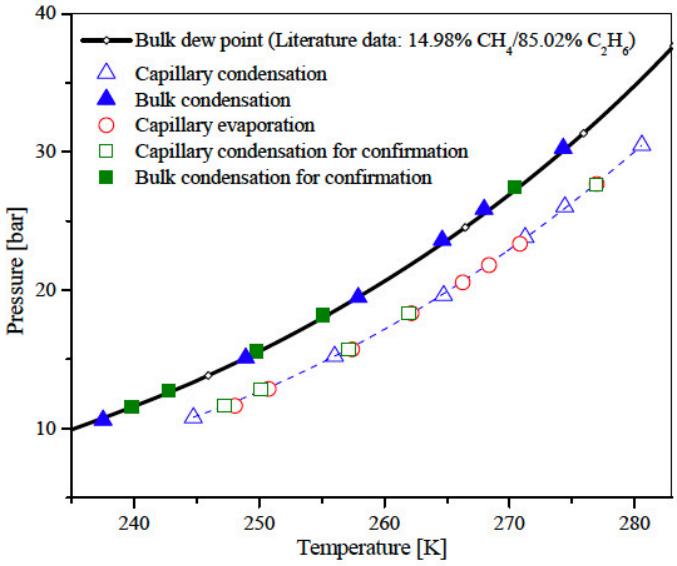

Figure 2. Comparison of capillary condensation and capillary evaporation of a CH_4/C_2H_6 mixture in SBA- 15 (8.1 nm).3 Literature data of bulk dew point of the mixture are taken from Bloomer et al.[4]

specified bulk composition do not exhibit phase-coexistence region as the bulk mixtures do. In other words, they behave similarly to confined pure fluids in their phase transition.

Experiments on the capillary phase transition hysteresis of confine pure fluids and binary mixtures

Since our isochoric procedure can be used to measure both capillary condensation and evaporation points for confined pure fluids and mixtures even up to high pressures, hysteresis phenomenon can be experimentally studied using our instrument in the whole range of its existence until the hysteresis end point T_{he}, beyond which capillary condensation and capillary evaporation occur reversibly, as demonstrated in our recent publication.[5] It should be noted that T_{he} is different from T_{Cp}. The hysteresis end point is a point at which the nucleation barrier is so low that the experimental condition allows the capillary condensation (adsorption) and capillary evaporation (desorption) branches to appear reversible.[6]

The capillary condensation/evaporation hysteresis end point T_{he} for a specific system is determined by performing a series of measurements with different densities by increasing the initial temperature and pressure.[5] By plotting the hysteresis width, *i.e.*, T_{ce} - T_{cc}, as a function of bulk vapor density ρ at phase transition, which is proportional to P/T (= $ZR\rho$), T_{he} can be determined, as shown in Figure 3; Z is the compressibility factor, R is the universal gas constant, P and T are pressure and temperature at phase transition, and subscripts ce and cc denote capillary evaporation and capillary condensation, respectively.

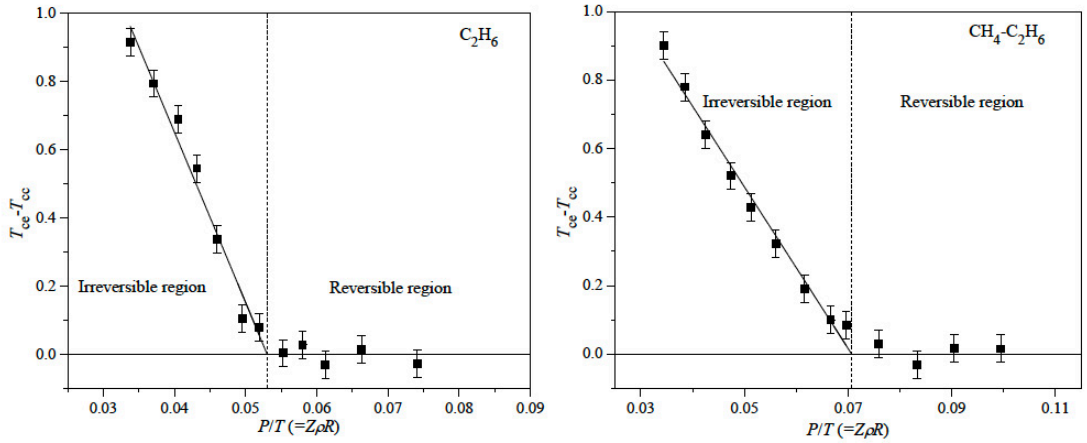

Figure 3. Hysteresis width (T_{ce}-T_{cc}) as a function of P/T (=ZρR) for ethane and a mixture of methane/ethane (15±0.3% CH_4/85 ± 0.3% C_2H_6) in SBA-15 (8.1 nm).[5]

We confirm that for a pure component, T_{he} is lower when confined in smaller nanopores, whereas T_{he} for CH_4/C_2H_6 mixtures at the specific composition investigated (15±0.3% CH_4/85 ± 0.3% C_2H_6) is higher than that of pure C_2H_6, when confined in the same nanopores. To the best of our knowledge, this is the first time that T_{he} of fluid mixture is experimentally studied, which further demonstrates that binary mixtures behave similarly to pure fluids when confined in nanoporous media.

Prototype equation of state for phase transition of confined fluids

We have also developed a new EOS for the phase transition of pure spherical fluids confined in MCM-41 based on the Generalized van der Waals partition function. Experimentally derived critical temperature and pressure of confined fluid are the only information needed to find the model parameters of the EOS, which subsequently can be used to predict the whole capillary-condensation curve. This resembles the simple but effective cubic-type EOS that is widely used for bulk fluids. The new EOS has been demon- strated to accurately predict the capillary condensation of argon, nitrogen, and oxygen in MCM-

41.[7] There- fore, this EOS can also be used to cross-check the accuracy of PCP obtained in our lab. If the model can accurately predict the experimental capillary condensation while using the model parameters derived from experimental PCP without any adjustment, the experimental PCP can be deemed accurate and consistent with the experimental capillary condensation. Figure 1 presents the EOS prediction of the capillary con- densation of methane, which matches the measured data very well.[1] This encouraging result opens the way to proceed to a more advanced model valid for larger molecules with longer chains, and even for mixtures.

Development of program codes for Monte Carlo simulations of capillary phase transition

In another front of the project, we have developed the program codes for Grand Canonical Monte Carlo (GCMC) and gauge-cell Monte Carlo (MC) for confined spherical molecules. GCMC simulation will be needed to crosscheck the results of the gauge-cell MC. For the verification of our GCMC codes, we reproduce the adsorption isotherm of methane in 3.143 nm MCM-41 at 237 K reported by Cao et al.[8] The LJ parameters of methane and MCM-41 are taken directly from their paper. As in the paper, MCM-41 is modeled as a cylindrical pore and the interaction between a methane molecule and MCM-41 solid wall is represented by the Tjatjopoulos–Feke–Mann (TFM) potential,[9] which was obtained by integrating the in- teraction between a fluid molecule and all atoms of single cylindrical pore wall. Figure 4 shows the good agreement of the calculated adsorption isotherm with the literature data.

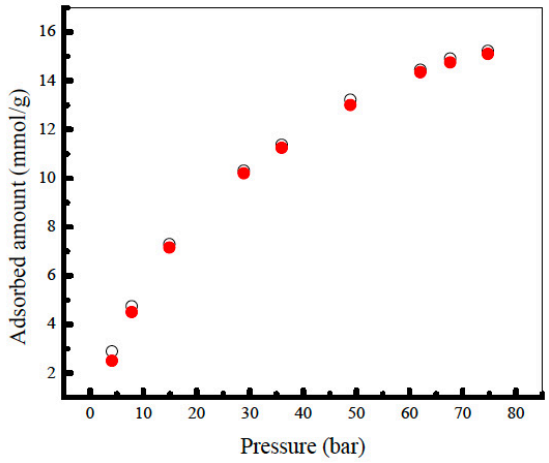

Figure 4. Adsorption isotherm of methane in MCM-41 at 237 K; open circles (literature data8), solid circles (this work).

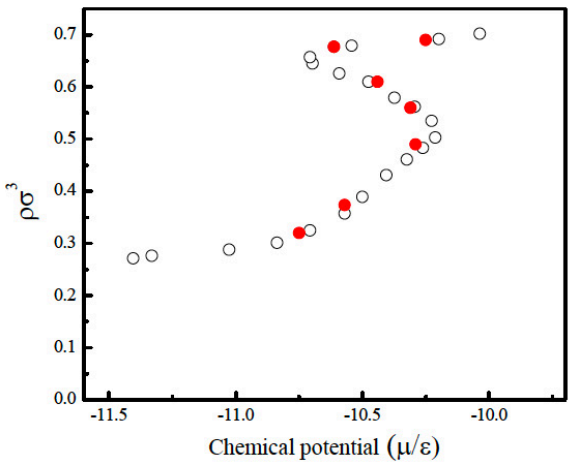

Figure 5. Adsorption isotherm of N_2 in MCM-41 (pore size of 10σ) at 77.4 K obtained using gauge-cell MC; open circles (literature data[10]), solid circles (this work)

To verify the gauge-cell MC codes, we reproduce the adsorption isotherm of N2 in MCM-41 with a pore size of 10 at 77.4 K reported by Neimark abd Vishnyakov,[10] which has a phase transition in the pores. Solid-fluid interactions are modeled as the LJ interaction of a fluid molecule with a single structure- less cylindrical layer of atoms composing the pore wall, as described in their paper. The fluid-fluid and solid-fluid parameters to represent nitrogen in silica pores of MCM-41 are therefore directly taken from the paper. Figure 5 shows the good agreement of the calculated isotherm, including points in the metastable and unstable regions, with the literature data. Therefore, we are

now preparing to proceed with simulations in accordance with the purpose of this project, i.e., to evaluate the interaction potential model employed in the simulation, as it is now possible to compare the results with experimental data.

Publications acknowledging this grant (September 2020-present)

E*xclusively funded by this grant*:

1. Qiu, X.; Yang, H.; Dejam, M.; Tan, S.P.; Adidharma, H., Experiments on the Capillary Condensation/Evaporation Hysteresis of Pure Fluids and Binary Mixtures in Cylindrical Nanopores, *Journal of Physical Chemistry C*, 125, 5802, 2021.
2. Adidharma, H.; Tan, S.P., Prototype equation of state for phase transition of confined fluids based on the Generalized van der Waals partition function, *Journal of Chemical Physics*, 154, 111104, 2021.
3. Qiu, X., Tan, S.P., Dejam, M., Adidharma, H., Binary fluid mixtures confined in nanoporous media: Experimental evidence of no phase coexistence, *Chemical Engineering Journal*, 405, 127021, 2021.
4. Yang, H.; Jayaatmaja, K.; Dejam, M.; Tan, S.P.; Adidharma, H. Phase Transition and Criticality of Me- thane Confined in Nanopores, 2021, *in preparation*.

Jointly funded by this grant and other grants with leading intellectual contribution from this grant:

None

Jointly funded by this grant and other grants with relatively minor intellectual contribution from this grant:

None

References

1. Yang, H.; Jayaatmaja, K.; Dejam, M.; Tan, S.P.; Adidharma, H. Phase Transition and Criticality of Methane Confined in Nanopores, 2021, in preparation.
2. Tan, S.P., Qiu, X., Dejam, M., Adidharma, H. Critical point of fluid confined in nanopores: Experimental detection and measurement. J. Phys. Chem. C, 2019, 123, 9824−9830.
3. Qiu, X., Tan, S.P.; Dejam, M.; Adidharma, H. Binary fluid mixtures confined in nanoporous media: Experimental evidence of no phase coexistence. Chem. Eng. J., 2021, 405, 127021.
4. Bloomer, O.T., Gami, D.C., Parent, J.D. Physical Chemical Properties of Methane Ethane Mixtures. Institute of Gas Technology Bulletin, 1953, 22, 1-39.
5. Qiu, X.; Yang, H.; Dejam, M.; Tan, S.P.; Adidharma, H. Experiments on the Capillary Condensation/ Evaporation Hysteresis of Pure Fluids and Binary Mixtures in Cylindrical Nanopores. J. Phys. Chem. C, 2021, 125, 5802−5815.
6. Neimark, A. V.; Vishnyakov, A. Phase Transitions and Criticality in Small Systems: Vapor-Liquid Transition in Nanoscale Spherical Cavities. J. Phys. Chem. B, 2006, 110, 9403-9412.
7. Adidharma, H.; Tan, S.P. Prototype equation of state for phase transition of confined fluids based on the Generalized van der Waals partition function. J. Chem. Phys., 2021, 154, 111104.
8. Cao, A.; Shen, Z.; Chen, J.; Zhang, X. Experiment, molecular simulation and density functional theory for investigation of fluid confined in MCM-41. Micropor. Mesopor. Mat., 2004, 67, 159-166.
9. G.J. Tjatjopoulos, D.L.; Feke, J.A.; Mann, J. Molecule-Micropore Interaction Potentials. J. Phys. Chem., 1988, 92, 4006-4007.
10. Neimark, A. V.; Vishnyakov, A. Gauge cell method for simulation studies of phase transitions in con- fined systems. Phys. Rev. E, 2000, 62, 4611.

Exploiting the Emergent Behavior in Ionic Liquids for Advanced Rare Earth Separations

George S. Goff,[1] Enrique R. Batista,[2] Joan F. Brennecke,[3] Yamil J. Colón,[4] Mark D. Dadmun,[5] Andrew J. Gaunt,[6] Jason C. Lashley,[1] Edward J. Maginn,[4] Wolfgang Runde,[1] and Ping Yang[1]; [1]Materials Physics and Applications Division, Los Alamos National Laboratory; [2] Theoretical Division, Los Alamos National Laboratory; [3] Department of Chemical Engineering, The University of Texas at Austin; [4] Department of Chemical and Biomolecular Engineering, University of Notre Dame; [5] Department of Chemistry, The University of Tennessee Knoxville and Oak Ridge National Laboratory; [6] Chemistry Division, Los Alamos National Laboratory

Abstract

The mining, processing, and separation of Rare Earth Elements (REEs) is performed using conventional hydrometallurgical processes. Separation processes often rely on the dissolution of natural feedstocks using concentrated mineral acids or caustic solutions, followed by various solvent extraction steps. New processes are needed to increase process efficiency, lower costs, and minimize waste streams. Ideally these solvent systems would be nonvolatile, highly stable, cost-effective, and require minimal acid/base consumption. Ionic liquids (ILs) have shown great promise and recent advances in IL chemistry have opened the door for designing novel separations processes that exploit the unique properties of this class of material. *The overarching goal of this project is to utilize recent advances in molecular-level design to develop ILs with improved physical and thermodynamic properties that incorporate tunable functional groups in order to control metal complexation and enable novel selective separations strategies.* This project takes a multi-faceted, multi-scale approach that will significantly advance our understanding of emergent phenomena and molecular-level f-element chemistry in ILs. Our project integrates experiment and theory to understand and control Ln-IL interactions and emergent phenomena in ILs to develop new separations schemes. These concepts define the three research themes and represent a bottoms-up approach towards developing novel separations, starting with the building blocks of fundamental science. Due to the importance of water in industrial REE processing, we will focus on developing robust IL chemistries that are water stable, targeting lanthanide (Ln) separations from U and Th and Ln-Ln separations. We will achieve this by taking advantage of recent discoveries in the emergent phenomena of ILs combined with the extensive experience of this team in the areas of *f*-element chemistry, IL synthesis, condensed matter physics, separations, and advanced simulation techniques. In this talk, we will provide an overview to the project and present some initial results related to REE separations.

Postdocs: Melissa Fairley Rier,[1] Lauren Stevens[6]
Students: Dinis Abranches,[4] Fernando Carmona,[4] Jacob Fischer,[5] RayVen Gonzales,[1] JaeSong Lee,[3] Shelby Sanders[5]

Recent Progress

Newly initiated award

Plenary talk: Molecular Dynamics Studies of Activated Events

Michele Parrinello, Istituto di Technologia, Genoa, IT.

Session V: Phenomena on Surfaces and within Pores (Kristin Hutchins, Chair)

Functionalized Interfaces for Efficient Ion Separations

Grant E. Johnson, Vassiliki-Alexandra Glezakou, Manh-Thuong Nguyen and Venkateshkumar Prabhakaran; Physical Sciences Division, Pacific Northwest National Laboratory, Richland, WA 99352

Presentation Abstract

Our research aims to obtain a predictive molecular-level understanding of intermolecular interactions at solid/liquid interfaces that will enable efficient and selective separation of ions with functionalized membranes, sorbents, and electrodes. Graphene oxides (GOs) are potentially transformative materials for ion separation. However, it is not sufficiently understood how different functional groups on GO influence the competitive adsorption of solvated ions and water. Using state-of-the-art computations accompanied by experiments on well-defined model systems, we demonstrate that hydroxyl (-OH) and carboxyl (-COOH) groups on GO exert a stronger influence on water adsorption than other functional groups. Proton dissociation is observed in the COOH groups, and the resulting carboxylate anions ($-COO^-$) are shown to stabilize Pb(II) through strong electrostatic interactions. An increase in Pb(II) adsorption with increasing pH is also observed due to deprotonation of the carboxyl groups, while lower pH releases the adsorbed Pb(II) so the GO may be reused. These findings address the challenge of understanding and controlling selective water and ion transport through laminate membranes widely used in ion separations.

Selective adsorption of ions at electrochemical interfaces used in electrodialysis-based critical mineral extraction may be modulated by capacitive and Faradaic (redox) approaches. However, a knowledge gap exists in our understanding of the effect of hydrophobic domains and redox-active species on interfacial solvation, ion and molecule transport, and selective adsorption at electrified interfaces. It is also not sufficiently understood how the functionality of ionic liquids (ILs) may be tailored to influence the controlled formation of hydrophobic domains to achieve efficient and targeted ion extraction under local electric fields. We are employing ion soft landing, a versatile mass spectrometry-based deposition method, combined with *in situ* vibrational spectroscopy and machine learning (ML)-based simulations to prepare, characterize, and model well-defined electrochemical interfaces functionalized with IL clusters (*e.g.,* 1-n-alkyl-3-methylimidazolium cations $[C_nmim]^+$, n = 1, 3, 5, 7, and 9) and multi-electron redox-active polyoxometalates (POMs). These species impart controlled hydrophobicity and Faradaic adsorption/reduction capacity at electrified interfaces, respectively. We demonstrate that electrodes functionalized with specific ILs

provide stable and reversible adsorption sites for model anions. We also show that the potential applied to POMs at interfaces may be used to modulate the selective strong binding of Na^+ compared to the weaker reversible binding of Pb^{2+} and La^{3+}.

Grant or FWP Number: 72353

PI: Grant E. Johnson

Postdoc(s): Eric Baxter, Shuai Tan, Jun Zhang, and Difan Zhang

Other staff: Manh-Thuong Nguyen

Affiliations(s): Pacific Northwest National Laboratory

RECENT PROGRESS

1. Structure and Stability of Ionic Liquid Clusters for Electrochemical Separations

Controlled functionalization of electrodes with ionic liquid (IL) clusters has the potential to improve the efficiency and selectivity of electrochemical separations. However, critical knowledge gaps exist in our understanding of the effect of hydrophobic domains on interfacial solvation, ion and molecule transport, and selective ion adsorption at electrified interfaces. It is also not sufficiently understood how the functionality of ionic liquids may be tailored to enable the formation of hydrophobic domains that promote efficient targeted ion extraction.

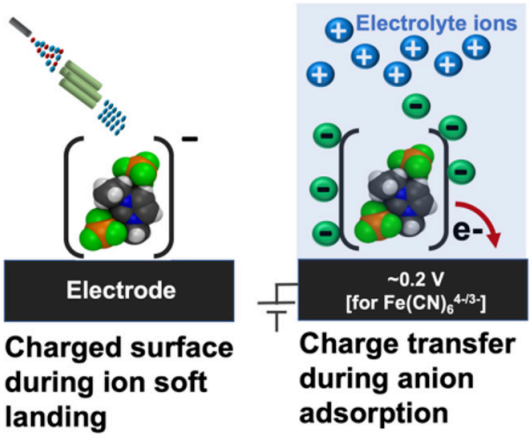

Fig 1. Pictorial representation of the applicability of ionic liquid functionalized electrodes for efficient ion separation.

In the last funding period, we addressed this challenge through a combined experimental and theoretical investigation of the IL clusters 1-ethyl-3-methylimidazolium tetrafluoroborate $[EMIM]_n[BF_4]_{n+1}^-$ (n = 1 − 9) and demonstrated their efficiency toward adsorption of targeted ions from aqueous solution. The structures and energies of the IL clusters, predicted with global optimization theory, allowed us to interpret the ion abundances and stabilities measured by high-mass-resolution electrospray ionization mass spectrometry and collision-induced dissociation (CID) experiments. The $[EMIM][BF_4]_2^-$ cluster,

which was identified as the most stable IL cluster by CID, was selectively deposited onto a working electrode using our distinguishing capability for soft landing of mass-selected ions. Electrochemical impedance spectroscopy measurements revealed a lower charge transfer resistance on the electrode functionalized with soft landed $[EMIM][BF_4]_2^-$ compared to a similar electrode prepared by drop-casting of an IL solution containing a distribution of IL clusters, counterions, and solvent. Our findings indicate that specific IL clusters may be used to increase the efficiency of electrochemical separations by lowering the overpotentials involved. These results were published in the *Journal of Physical Chemistry Letters*.

2. Rational Design of Graphene Oxide Membranes for Efficient Lead Separation from Water

A critical challenge associated with the design of graphene oxide (GO) materials for ion separations is how specific functional groups influence the competitive adsorption of different solvated ions and water at liquid/graphene interfaces. Theoretical calculations, accompanied by detailed experiments on well-defined model systems, show that hydroxide (-OH) and carboxyl (-COOH) groups on GO exert a stronger influence on water adsorption than -O and -H functional groups. The $-COO^-$ anions on GO, which are formed following deprotonation of -COOH, stabilize Pb(II) cations through strong electrostatic interactions. This observation indicates that, among the different functional groups studied, -COOH offers the best Pb(II) adsorption capacity. Remarkably, the -COOH functionalized GO sorbent may be regenerated through a simple pH swing mechanism. In agreement with the computational predictions, following experiments revealed that a substantial increase in Pb(II) adsorption capacity occurs with increasing solution pH. Our findings provide a systematic framework for the controlled design and implementation of regenerable carbon-based sorbents used in ion separations. These results were published in the *Journal of the American Chemical Society Gold* (*JACS Au*) and highlighted on the journal cover.

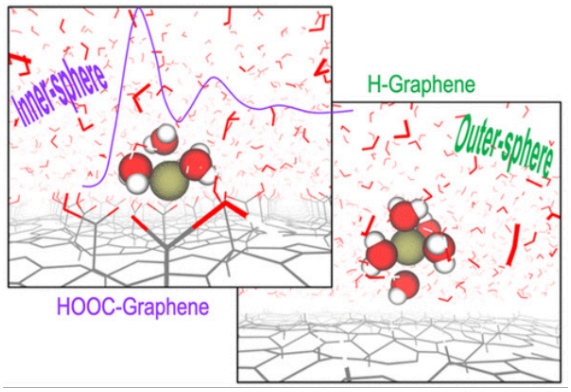

Fig 2. Schematic representation of the stronger inner-sphere interactions that bind Pb^{2+} to COO^- on GO enabling separation from water.

Publications Acknowledging this Grant in 2018 – present

(I) Exclusively funded by this grant;

1. S. Tan, J. Zhang, D. Zhang, M.-T. Nguyen, V. Prabhakaran, E.T. Baxter, V. Shutthanandan, R. Rousseau, G.E. Johnson, V.-A. Glezakou, Tuning the Charge and Hydrophobicity of GO Membranes for Efficient Separations using Ionic Liquids, **2021**, *to be submitted*.
2. E.T. Baxter, J. Zhang, S. Tan, M.-T. Nguyen, X.-B. Wang, V. Prabhakaran, V.-A. Glezakou, G.E. Johnson, Size and Composition Tunable $[EMIM]_x[Cl]_{x+1}^-$ Ionic Liquid Clusters for Electrochemical Separations, **2021**, *to be submitted*.
3. M.-T. Nguyen, J. Zhang, V. Prabhakaran, S. Tan, E.T. Baxter, V. Shutthanandan, G.E. Johnson, R. Rousseau, V.-A. Glezakou, Graphene Oxide as a Pb(II) Separation Medium: Has Part of the Story Been Overlooked? *Journal of the American Chemical Society Au* **2021**, 1, 766-776. http://dx.doi.org/10.1021/jacsau.0c00075
4. J. Zhang, E.T. Baxter, M.-T. Nguyen, V. Prabhakaran, R. Rousseau, G.E. Johnson, V.-A. Glezakou, Structure and Stability of the Ionic Liquid Clusters $[EMIM]_N[BF_4]_{N+1}^-$ (N = 1 – 9): Implications for Electrochemical Separations. *Journal of Physical Chemistry Letters* **2020**, *11*, 6844-6851. http://dx.doi.org/10.1021/acs.jpclett.0c01671
5. J. Zhang, V.-A. Glezakou, R. Rousseau, M.T. Nguyen, NWPEsSe: an adaptive-learning global optimization algorithm for nanosized cluster systems. *Journal of Chemical Theory and Computation*, **2020**, *16*, 3947-3958. https://doi.org/10.1021/acs.jctc.9b01107
6. J. Zhang, V.-A, Glezakou, Global optimization of chemical cluster structures: Methods, applications, and challenges. *International Journal of Quantum Chemistry*, **2021**, 121, e26553. https://doi.org/10.1002/qua.26553

(II) Jointly funded by this grant and other grants with leading intellectual contribution from this grant;

1. M.A. Hewitt, H. Hernández, G.E. Johnson, ESI-MS Identification of the Cationic Phosphine-Ligated Gold Clusters $Au_{1–22}$: Insight into the Gold–Ligand Ratio and Abundance of Larger Clusters. *Journal of the American Society for Mass Spectrometry* **2021**, *32*, 237-246. http://dx.doi.org/10.1021/jasms.0c00293
2. M.R. Ligare, K.A. Morrison, M.A. Hewitt, J.U. Reveles, N. Govind, H. Hernandez, E.S. Baker, B.H. Clowers, J. Laskin, G.E. Johnson, Ion Mobility Spectrometry Characterization of the Intermediate Hydrogen-Containing Gold Cluster $Au_7(PPh_3)_7H_5^{2+}$. *Journal of Physical Chemistry Letters* **2021**, *12*, 2502-2508. http://dx.doi.org/10.1021/acs.jpclett.0c03664

3. M.A. Hewitt, H. Hernández, G.E. Johnson, Light Exposure Promotes Degradation of Intermediates and Growth of Phosphine-Ligated Gold Clusters. *Journal of Physical Chemistry C* **2020**, *124*, 3396-3402. http://dx.doi.org/10.1021/acs.jpcc.9b10920
4. J. Edgecomb, X. Xie, Y. Shao, P.Z. El-Khoury, G.E. Johnson, V. Prabhakaran, Mapping Localized Peroxyl Radical Generation on a PEM Fuel Cell Catalyst Using Integrated Scanning Electrochemical Cell Microspectroscopy. *Frontiers in Chemistry* **2020**, *8*, 572563. http://dx.doi.org/10.3389/fchem.2020.572563
5. R.C. Shiery, J.L. Fulton, M. Balasubramanian, M.-T. Nguyen, J.B. Lu, J. Li, R. Rousseau, V.-A. Glezakou, D.C. Cantu, Coordination sphere of lanthanide aqua ions resolved with *ab initio* molecular dynamics and X-ray absorption spectroscopy. *Inorganic Chemistry*, **2021**, *60*, 3117-3130. https://doi.org/10.1021/acs.inorgchem.0c03438
6. A.J. Campanella, M.-T. Nguyen, J. Zhang, T. Ngendahimana, W.E. Antholine, G.R. Eaton, V.-A. Glezakou, J.M. Zadrozny, Ligand control of low-frequency electron paramagnetic resonance linewidth in Cr(iii) complexes. *Dalton Transactions*, **2021**, *50*, 5342-5350. https://doi.org/10.1039/D1DT00066G
7. J.-B. Lu, D. Cantu, C.-Q. Xu, M.-T. Nguyen, H.S. Hu, V.-A Glezakou, Rousseau, R., Li J., 2021, Norm-Conserving Pseudopotentials and Basis Sets to Explore Actinide Chemistry in Complex Environments, *Journal of Chemical Theory and Computation*, **2021**,17, 3360-3371. https://doi.org/10.1021/acs.jctc.1c00026

(III) Jointly funded by this grant and other grants with relatively minor intellectual contribution from this grant;

1. E. Aprà, A. Bhattarai, E.T. Baxter, S. Wang, G.E. Johnson, N. Govind, P.Z. El Khoury, Simplified *Ab Initio* Molecular Dynamics-Based Raman Spectral Simulations. *Applied Spectroscopy* **2020**, *74*, 1350-1357. http://dx.doi.org/10.1177/0003702820923392
2. P. Gao, J. Zhang, Q. Peng, J. Zhan, V.-A. Glezakou, General protocol for the accurate prediction of molecular $^{13}C/^{1}H$ NMR chemical shifts *via* machine learning augmented DFT. *Journal of Chemical Information and Modeling*, **2020**, *60*, 3746-3754. https://doi.org/10.1021/acs.jcim.0c0038

Structure and potential-dependence in redox-active metallopolymers for ion-selective electrochemical separations

Xiao Su, Raylin Chen, Riccardo Candeago, Kwiyong Kim, University of Illinois Urbana-Champaign

Abstract

Redox polymer electrodes offer a modular platform for electrochemical separations, by ease of synthetic control and tunability of electrochemical properties. Establishing structure-function relationships between redox-interfaces and target ions is key for tailoring molecular selectivity. Electrochemical modulation of the separation process can lead to reduced chemical input, lower generation of waste, and energetic advantages. The main focus of our research program is the investigation of supramolecular interactions on molecularly-designed polymeric electrodes, and the elucidation of the underlying mechanisms for reversible binding of critical elements. Here, we pursue three integrated objectives: (i) investigation of charge-transfer interactions at redox-metallopolymers, (ii) investigation of potential-dependent multicomponent separations, and (iii) nanoscale ion transport and spatial distribution within redox-films under operando conditions. We investigate synthetic control for achieving specific separations of transition metal oxyanions, and the possibility of orthogonal modulation by potential, through both electrosorption measurements and quantum-chemical calculations. Next, we describe ongoing work on operando spectroscopy/gravimetric investigations, including electrochemical quartz crystal microbalance (EQCM) and *in situ* neutron reflectometry. These non-destructive *in situ* characterization techniques can correlate oxidation states of the redox-active centers with migration of ions and solvent within the polymer film, under electrochemical conditions. Through these combined studies, we seek to tease out and quantify the individual energetics associated with charge transfer, solvation, and electrostatics. Our long-term goal is to achieve predictive control of selectivity by enhancing specific charge-transfer interactions, and to provide a fundamental understanding of both thermodynamic and kinetic mechanisms at play during electrochemical separations.

Grant DE-SC0021409: Supramolecular control of redox-mediated interactions for ion-selective electroseparations

PI: Prof. Xiao Su

Postdoc: Dr. Kwiyong Kim

Students: Raylin Chen, Riccardo Candeago

Recent Progress

Anion selectivity through polymer structure. First, we showed how metal ion selectivity can be controlled through polymer structure, with differential ion selectivity shown between polyvinylferrocene (PVF), with pendant ferrocenes, and polyferrocenylsilane (PFS), with main-chain ferrocenes, and through applied electrochemical potential. Metallopolymers with distinct chemical structure (pendant group PVF and main-chain PFS) were synthesized, and conjugated into heterogeneous composites (PVF-CNT and PFS-CNT). Systematic electrochemical separation

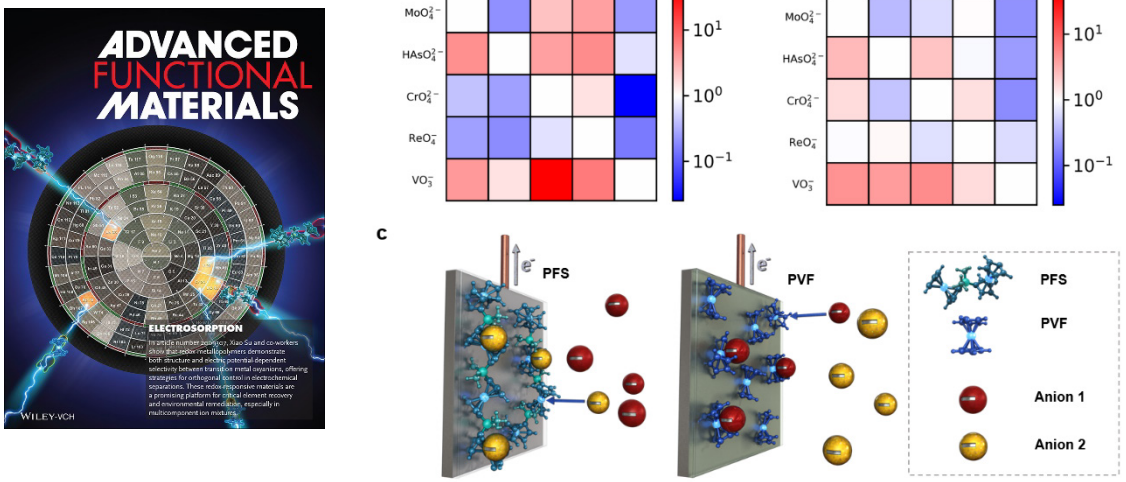

Figure 20. (Left) Cover image (Frontispiece) depicting how polymer structure is used to target critical elements of interest. Image taken from Adv. Funct. Mater., 31: 2170103. **a)** Heat map of separation factors obtained using PFS-CNT for pairs of oxyanions (1 mM each) at 0.8 V Ag/AgCl. **b)** Heat map of separation factors obtained using PVF-CNT for pairs of oxyanions (1 mM each) at 0.8 V Ag/AgCl. **c)** Due to differences in selectivity, PFS and PVF can be used to target different ions.

measurements were carried out with a series of transition metal oxyanions across a range of applied electrochemical potentials. **Figure 1a,b** show binary ion-selectivity heat maps for the separation factors obtained using PVF-CNT and PFS-CNT at 0.8 V vs Ag/AgCl. In 8 of the 10 binary adsorption tests at 0.8 V vs Ag/AgCl, PVF and PFS favored the same anion. As a highlighted example, $\alpha_{VO3-,CrO42-}$ was 5.2 for PVF-CNT and 39 for PFS-CNT, indicating VO_3^- had a greater affinity toward PVF-CNT and PFS-CNT than CrO_4^{2-}, but PFS was almost an order of magnitude more selective. In the remaining two binary adsorption tests ($MoO_4^{2-} + CrO_4^{2-}$, $HAsO_4^{2-} + ReO_4^-$), PVF-CNT and PFS-CNT favored different ions ($\alpha_{MoO42-,CrO42-} = 0.60$ and $\alpha_{HAsO42-,ReO4-} = 0.91$ for PVF-CNT, $\alpha_{MoO42-,CrO42-} = 2.4$ and $\alpha_{HAsO42-,ReO4-} = 5.2$ for PFS-CNT), demonstrating that a change in structure from a pendant ferrocene polymer to a main-chain ferrocene polymer can alter the ion-selectivity trend and furthermore, demonstrating that redox-active polymers can be structurally tuned for targeted ion selectivity (**Figure 1c**).

Electronic structure calculations. In collaboration with Prof. Diwakar Shukla (ChBE UIUC), electronic structure calculations were performed with our redox-centers and anions. Results indicate an inverse correlation between the ionization energy of the anion and the difference in binding energy between that anion and ferrocenium (Fc^+) and a trimethyl silane substituted ferrocenium ($FcSi(CH_3)_3^+$) (**Figure 2**). We hypothesize that a charge-transfer binding mechanism may be dictating this correlation. Anions with a low ionization energy may be more willing to give up electron density to the cationic binding site, and as such, the electronegativity of the binding site strongly affects the binding energy and subsequent selectivity. In contrast, anions with a high ionization energy bind primarily through electrostatics. This charge-transfer

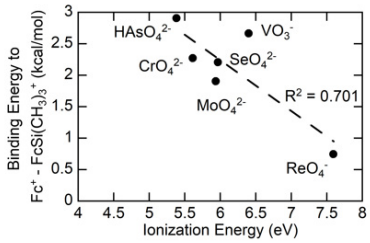

Figure 2 Ionization energy versus the difference in binding energy to Fc^+ and $FcSi(CH_3)_3^+$ for the six anions tested. Linear least-squares regression shown by dotted line.

modulation demonstrates the opportunity for tunable ferrocene polymers with specific substituents for highly targeted ion capture.

Anion selectivity through electrochemical potential. The selectivity of PFS-CNT and PVF-CNT changes depending on the applied potential. **Figure 3a,b** highlights two special cases where ion preference switched for the ferrocene polymers at different potentials. $\alpha_{MoO42-,CrO42-}$ at an applied potential of 0.5 V vsv Ag/AgCl was 0.28 and 0.43 for PVF-CNT and PFS-CNT, respectively. At 1.0 V vs Ag/AgCl $\alpha_{MoO42-,CrO42-}$ was 1.5 and 4.6 for PVF-CNT and PFS-CNT, respectively. A similar swap occurred with $\alpha_{MoO42-,ReO4-}$ changing from 0.17 for PVF-CNT and 0.48 for PFS-CNT at 0.5 V Ag/AgCl to 1.8 for PVF and 35 for PFS at 1.0 V vs Ag/AgCl. Tracking the anion speciation through Pourbaix diagrams and XPS show no evidence of changing anion speciation that would result in changing selectivities. Between 0.6 and 1.0 V vs Ag/AgCl, the separation factor shifts in favor of the anion that transfers more charge, an effect seen in 16 out of the 20 anion pair tests at 1.0 V vs Ag/AgCl. We hypothesize that this may be the result of a driving force toward satisfying charge neutrality at a microscopic level. These studies set the stage for potential-dependent control, which may eventually lead to orthogonal or synergistic to structure-control of molecular selectivity.

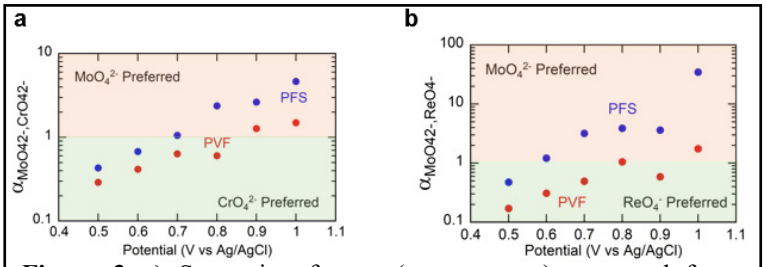

Figure 3 a) Separation factors ($\alpha_{MoO42-,CrO42-}$) measured from electrosorption in 1 mM MoO_4^{2-} and 1 mM CrO_4^{2-} at various potentials. b) Separation factors ($\alpha_{MoO42-,ReO4-}$) measured from electrosorption in 1 mM MoO_4^{2-} and 1 mM ReO_4^- at various potentials.

In situ studies: electrochemical quartz crystal microbalance, neutron reflectometry, and in situ ellipsometry. Competitive adsorption studies of perchlorate anions against perrhenate anions were carried out using EQCM. Solutions of 100% ClO_4^- (20 mM), 100% ReO_4^- (20 mM), and 50% ClO_4^- (10 mM) + 50% ReO_4^- (10 mM) were considered. ~100 nm thin poly(ferrocenylpropyl methacrylamide) (PFPMAm) films were spin coated on 14 mm Au/Ti EQCM sensors. By comparing the coulometric data with the gravimetric information, it was possible to

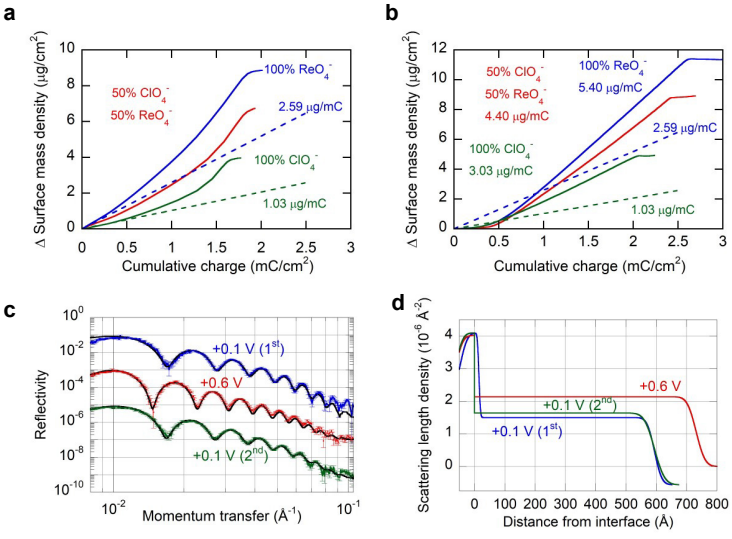

Figure 4. EQCM data, change in surface mass density over cumulative charge. Solutions are 20 mM of indicated ion for 100%, and 10 mM + 10 mM for 50% 50% solution. Data acquired during **a)** a cyclic voltammetry, 10 mV/s scan rate **b)** a potential step of 600 mV vs Ag/AgCl. **c)** Fitted neutron reflectivity profiles for 20 mM ClO_4^- in H_2O and PVF film, showing a reduction, oxidation, reduction cycle (0.1 and 0.6 V vs Ag/AgCl.) **d)** Corresponding scattering length density depth profiles for PVF films. The film displays a reversible swelling of ~26%.

distinguish the contributions of solvent ingression and counterion ingression, and dynamic information. As depicted in **Figure 4a,b,** solvent ingression accelerates as charge is passed, with an estimated 11 H_2O molecules inserted per each ClO_4^- anion, and 15 H_2O molecules inserted per each ReO_4^- anion. Notably, a linear potential sweep at 10 mV/s (**Figure 4a**) and a potential step at 600 mV vs Ag/AgCl (**Figure 4b)** resulted in significant selectivity of ReO_4^- over ClO_4^-. However, EQCM studies alone cannot provide a full picture of the distribution of solvent in the film. *In situ* neutron reflectometry studies provide accurate depth profile of solvent ingression, and spatiotemporal information. A preliminary analysis on PVF films (~55 nm thick) coated on Pd-sputtered silicon wafers at Oak Ridge National Lab (IPTS-26749) allowed us to investigate selectivity in redox-active polymer interfaces. The results showed that PVFc swelling was ~26% upon oxidation (with ClO_4^-), in good agreement with previous studies (**Figure 4c,d**). The reflectivity over momentum transfer and scattering length density (SLD) depth profiles are displayed in **Figure 4c,d** for 20 mM ClO_4^- in H_2O ($\chi^2 < 4$). These equilibrium selectivity studies will be our starting point for the next stage, in-depth dynamic studies of competitive adsorption kinetics. By coupling this dynamic information with the EQCM and coulometric data, it will be possible to deconvolute the contributions to polymer swelling (solvent ingression, target ion and counterion contributions) and gain a multiscale understanding of molecular selectivity.

Publications Acknowledging this Funding (2020-Present):

Exclusively Funded by this grant:

R. Chen, J. Y. Feng, J. Jeon, T. Sheehan, C. Ruttiger, M. Gallei, D. Shukla, **X. Su**, "Structure and Potential-Dependent Selectivity in Redox-Metallopolymers: Electrochemically Mediated Multicomponent Metal Separations." *Advanced Functional Materials*, **2021**, 31(15), *2009307.*

Jointly funded by this grant and other grants with leading intellectual contribution from this grant:

N. Kim, **X. Su**§, C. Kim§, "Electrochemical Lithium Recovery System through the Simultaneous Lithium Enrichment via Sustainable Redox Reaction", *Chemical Engineering Journal*, **2020**. 127715.

Y. Kim, K. Kim, H. Eom, **X. Su**§, J. Lee§. Electrochemically-assisted removal of cadmium ions by redox active Cu-based metal-organic framework. *Chemical Engineering Journal,* **2021**, 421, 129765.

Jointly funded by this grant and other grants with relatively minor intellectual contribution from this grant:

K. Kim, R. Candeago, D. Raymond, G. Kim, A. H. Park, **X. Su**., "Electrochemical Approaches for Selective Recovery of Critical Elements in Hydrometallurgical Processes of Complex Feedstocks." *iScience*, invited issue on *Material Criticality*. **2021**, 24(5), 102374.

From Captured CO_2 to Value-added Chemicals: A Photochemical Approach

Ksenija D. Glusac,[†] Lin Chen,[†] Amy Cordones-Hahn,[‡] David Kaphan,[†] Alex Martinson,[†] Karen Mulfort,[†] David Tiede,[†] Peter Zapol[†]; [†]Chemical Sciences and Engineering Division, Argonne National Laboratory, Lemont, Illinois 60439; [‡]Stanford PULSE Institute, SLAC National Accelerator Laboratory, Menlo Park, California 94025

Presentation Abstract

Carbon dioxide is an abundant and inexpensive reagent that, if captured from the air, can serve as a source of value-added chemicals. However, efficient approaches toward direct-air capture (DAC) of CO_2 rely on the formation of strong chemical bonds with the capturing reagent, which require prohibitively large energy inputs when CO_2 release is needed, rendering the overall capture process impractical. To circumvent this challenge, we investigate a photoreactive capture approach that combines the DAC of CO_2 with its direct conversion into value-added chemicals, such as methanol, acrylic acid derivatives and oxalic acid, using visible light as an energy input. This molecular reactor is composed of a porous, three-dimensional architecture, where light-harvesting, CO_2-capturing and catalytic moieties are assembled into a metal-organic framework (MOF), which provides high surface area for efficient DAC, precise orientation of chromophores for successful light harvesting and catalyst deposition needed for selective and fast synthesis of relevant products (Figure 1).

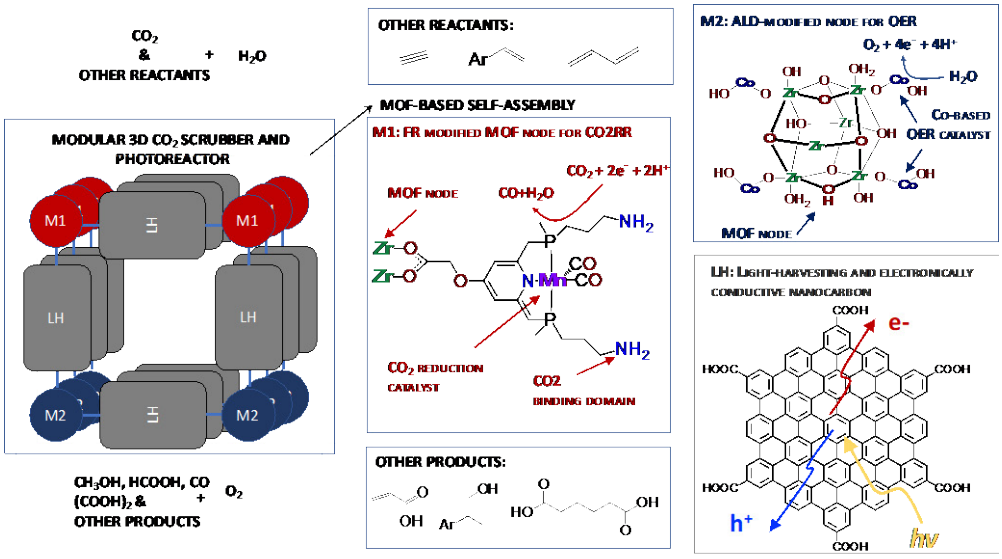

Figure 1. Proposed photoreactive CO_2 capture project. Three-dimensional MOF-based architectures composed of light-harvesting nanographene-based chromophores, amine-based groups for DAC of CO_2, and transition metal-based catalysts for carbamate reduction and oxygen evolution reactions.

The chemical processes are driven using light as an energy source and water as an electron and proton source (through the oxygen evolution reaction). Chemically tunable catalytic sites are deposited at the MOF nodes using atomic layer deposition or functionalization reactions to contain CO_2 binding motifs as well as the catalytic metal site in the proximity and optimal geometry for desired CO_2 reduction reaction to useful chemicals. The light harvesting is accomplished using MOF ligands composed of nanocarbon-

based chromophores with tunable absorption frequencies (due to quantum confinement effects) and high electrical conductivity (due to high degree of π- conjugation).

FWP #34698: From Captured CO_2 to Value-added Chemicals: A Photochemical Approach

PI: Ksenija Glusac, **Co-PIs**: Lin Chen, Amy Cordones-Hahn, David Kaphan, Alex Martinson, Karen Mulfort, David Tiede, Peter Zapol

Postdocs: Thabiso Kunene, Sayontani Sinha Roy, Tabitha Miller

Students: Alice Zheng, Matthew Drummer, Boris Kramar, Nick Weinegartz.

RECENT PROGRESS

We recently synthesized and characterized MOFs with nanographene-containing chromophore ligands (Figure 2A). The synthesis starts with polyphenylene precursor with carboxylate groups and $ZrCl_4$ precursors to form pre-MOF. The benzene rings in pre-MOF are not planarized, resulting in poor absorption in the visible range (Figure 2B). The post-synthetic oxidation of pre-MOF generates nanographene flake ligands and the formation of MOF-flakes. The conversion leads to significant darkening of the MOF crystals, from transparent crystals observed in microscope image in Figure 2C to darker and darker crystals shown in Figure 2D. We scaled-up the MOF-flake synthesis and are now anchoring metal-based catalytic units and DAC groups to its nodes. Future experiments will involve the study of DAC of CO_2 and its photochemical conversion to value-added chemicals using node-modified MOF-flakes.

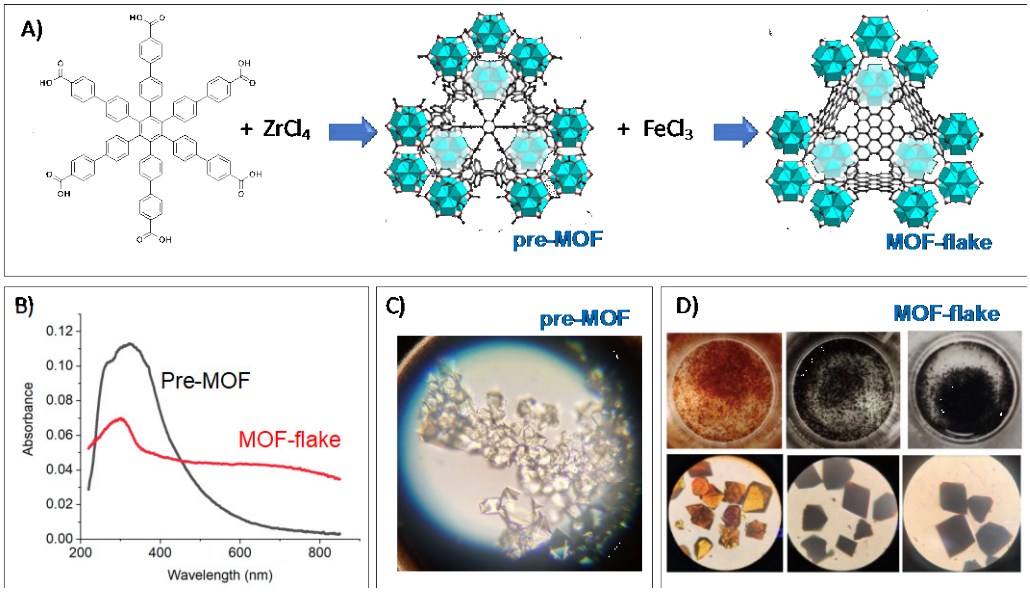

Figure 2. A) Scheme showing the synthesis of nanographene-based MOF using the previously published approach (H-C Zhou, JACS **2019**, 141, 2054); B) UV/Vis reflectance measurements showing high absorptivity of MOF-flake in the visible region; C) microscope image of pre-MOF crystals; D) microscope images of MOF-flake crystals at different degrees of oxidative dehydrogenation reaction using $FeCl_3$.

Publications Acknowledging this Grant: None.

Update on the Reactions and Separations Workshop

Joan Brennecke (UT Austin), Susannah Scott (UCSB), Vassiliki-Alexandra Glezakou (PNNL)

Summary Comments and Updates

Dan Matuszak (DOE Office of Basic Energy Sciences) and Vassiliki-Alexandra Glezakou (PNNL).

2021 Separation Science Research PI Meeting
August 10–12, 2021
Participant List (218)

Nabeel Mujtaba Abbassi
AmesLab/ISU
nma@iastate.edu

Rebeca Abergel
LBNL
rjabergel@lbl.gov

Sara Adelman
LBNL
sadelman@lanl.gov

Hertanto Adidharma
University of Wyoming
adidharm@uwyo.edu

Mueed Ahmad
Stony Brook University
mueed.ahmad@stonybrook.edu

Sarah Allec
PNNL
Sarah.Allec@pnnl.gov

Heather Allen
Ohio State University
allen.697@osu.edu

Jared Anderson
AmesLab/ISU
andersoj@istate.edu

Christopher Arges
Penn State University
cga5126@psu.edu

Brian Arko
LANL
barko@lanl.gov

Polly Arnold
LBNL
pla@lbl.gov

Jason Bara
University of Alabama
jbara@eng.ua.edu

Anastasia Barnes
University of Wyoming
akastl@uwyo.edu

Enrique Batista
Los Alamos National Laboratory
erb@lanl.gov

Bryan Beckingham
Auburn University
bsb0025@auburn.edu

Biki Kumar Behera
UIChicago
behera@uic.edu

Georges Belfort
Rensselaer Polytechnic Institute
belfog@rpi.edu

Brian Benicewicz
University of South Carolina
benice@sc.edu

Ilan Benjamin
UC Santa Cruz
ilan@ucsc.edu

Nabarupa Bhattacharjee
Indiana University
nbhatta@iu.edu

Biswajit Biswas
Ohio State University
biswas.129@osu.edu

Matthew Bogen
UNC-Chapel Hill
mbogen@email.UNC.edu

Paul Bohn
University of Notre Dame
pbohn@nd.edu

Anibal Boscoboinik
Stony Brook University
jorge.boscoboinik@stonybrook.edu

Kristin Bowman-James
University of Kansas
kbjames@ku.edu

Wade Braunecker
NREL
Wade.Braunecker@nrel.gov

Joan Brennecke
UTexas, Austin
jfb@che.utexas.edu

Merlin Bruening
University of Notre Dame
mbruenin@nd.edu

Vyacheslav Bryantsev
ORNL
bryantsevv@ornl.gov

Daniel Burrill
LANL
djburrill@lanl.gov

Louise Cañada
Utexas, Austin
lmcanada19@gmail.com

Riccardo Candeago
UIUC
candeago@illinois.edu

Amanda Carr
ANL
carraj@anl.gov

Moises Carreon Colorado School of Mines
mcarreon@mines.edu

Jesse Carrick
Tennessee Tech University
jcarrick@tntech.edu

Cristopher Chang
NREL
christopher.chang@nrel.gov

Minwei Che
Indiana University
mche@iu.edu

Raylin Chen
UIUC
raylinc2@illinois.edu

Yusheng Chen
Indiana University
chenyush@iu.edu

Tiffany Chen
UC Berkeley
tiffanyklchen@berkeley.edu
Sihoon Choi
GA Tech
schoi420@gatech.edu

Aurora Clark
Washington State University
auclark@wsu.edu

Amanda Coffman
U North Allabama
alhofacker@una.edu

Michael Connolly
LBNL
mdconnolly@lbl.gov

Joseph Cotruvo
Penn State U
juc96@psu.edu

Richard Crooks
University of Texas, Austin
crooks@cm.utexas.edu

Ethan Crumlin
LBNL
ejcrumlin@lbl.gov

Radu Custelcean
Oak Ridge National Laboratory
custelceanr@ornl.gov

Sheng Dai
Oak Ridge National Laboratory
dais@ornl.gov

Morteza Dejam
University of Wyoming
mdejam@uwyo.edu

James Dobscha
Indiana University
jdobscha@indiana.edu

Chi-Linh Do-Thanh
University of Tennessee
cdothanh@utk.edu

Benjamin Doughty
Oak Ridge National Laboratory
doughtybl@ornl.gov

Darren Driscoll
ORNL
driscolldm@ornl.gov

Walter Drisdell
LBNL
WSDrisdell@lbl.gov

Phuoc Duong
University of Wyoming
dphuocho@uwyo.edu

Jeffrey Einkauf
ORNL
einkaufjd@ornl.gov

Kaitlyn Engler
UC Berkeley
kaitlyn.engler@berkeley.edu

Philip Eor
AmesLab/ISU
peor@iastate.edu

Muhammad Qamar Farooq
AmesLab/ISU
mfarooq@iastate.edu

Andrew Ferguson
NREL
andrew.ferguson@nrel.gov

Michael Findlater
UC Merced
Michaelfindlater@ucmerced.edu

David Fiszbein
UC Berkeley
david_fiszbein@berkeley.edu

Amar Flood
Indiana University
aflood@indiana.edu

Benny Freeman
University of Texas, Austin
freeman@che.utexas.edu

Yuqing Fu
UC Riverside
yfu058@ucr.edu

Lena Marie Funke
UC Berekeley
funke@berkeley.edu
Hiroyasu Furukawa
UC Berkeley
furukawa@berkeley.edu

Sophya Garashchuk
U South Carolina
garashch@mailbox.sc.edu

Bruce Garrett
U.S. Department of Energy/BES
bruce.garrett@science.doe.gov

Gregory Girolami
University of Illinois, Urbana-Champaign
girolami@scs.illinois.edu

Vassiliki-Alexandra Glezakou
Pacific Northwest National Laboratory
vanda.glezakou@pnnl.gov

Ksenija Glusac
UI Chicago/ANL
senija.glusac@gmail.com

George Goff
LANL
georgeg@lanl.gov

Subhadip Goswami
Northwestern Univerisity
subhadip.goswami@northwestern.edu

Ruilan Guo
University of Notre Dame
rguo@nd.edu

Joel Harris
University of Utah
harrisj@chem.utah.edu

Shannon Heinrich
UC Santa Barbara
sheinrich@ucsb.edu

David Heldebrant
Pacific Northwest National Laboratory
david.heldebrant@pnnl.gov

Daniel Higgins
Kansas State University
higgins@ksu.edu

Marc Hillmyer
U Minnesota
hillmyer@umn.edu

John Hoberg
U Wyoming
hoberg@uwyo.edu

Holder Aaron
DOE-SC-BES
aaron.holder@science.doe.gov

Joseph Hupp
Northwestern University
j-hupp@northwestern.edu

Kristin Hutchins
Texas Tech U
kristin.hutchins@ttu.edu

Juan Carlos Idrobo
ORNL
idrobojc@ornl.gov

Takashi Ito
Kansas State University
ito@ksu.edu

Alex Ivanov
ORNL
ivanova@ornl.gov

Jacobs Ryan
U Wisconscin Madison
rjacobs3@wisc.edu

Santa Jansone-Popova
Oak Ridge National Laboratory
jansonepopos@ornl.gov

Kevin Jayaatmja
U Wisconscin
kjayaatm@uwyo.edu

Cynthia Jenks
Argonne National Laboratory
cjenks@anl.gov

Mark Jensen
Colorado School of Mines
mjensen@mines.edu

De-en Jiang
UC Riverside
djiang@ucr.edu

Kevin John
LANL
kjohn@lanl.gov

Grant Johnson
PNNL
grant.johnson@pnnl.gov

Katie Johnson
ORNL
johnsonkr@ornl.gov

Jung Min Kim
Auburn University
jzk0090@auburn.edu

Kwiyong Kim
UIUC
kwiyongk@illinois.edu

Abigail Knight
UNC Chapel Hill
aknight@unc.edu

Loukas Kollias
PNNL
loukas.kollias@pnnl.gov

Kommu Anitha
U Wyoming
kommuanitha@gmail.com

William Koros
Georgia Institute of Technology
wjk@chbe.gatech.edu

Stosh Kozimor
Los Alamos Natioinal Laboratory
stosh@lanl.gov

Raju Kumal
ANL
kumalrr@anl.gov

Nitesh Kumar
Washington State U
nitesh.kumar@wsu.edu

Revati Kumar
Louisiana State University
revatik@lsu.edu

Sanat Kumar
Columbia University
sk2794@columbia.edu

Anastasia Kuvayskaya
Colorado School of Mines
kuvayskaya@mymail.mines.edu

Dennis Lee
Johns Hopkins U
dlee237@jhu.edu

Jaeseong Lee
U Texas Austin
dlwotjd11994@utexas.edu

Noemi Leick
NREL
noemi.leick@nrel.gov

Nicholas Leon
GA Tech
nleon6@gatech.edu

Jingzhe Li
ISU
jzli@iastate.edu

Ping Li
ORNL
lip1@ornl.gov

Huina Lin
U South Carolina
huina@mailbox.sc.edu

Yihung Lin
Auburn University
yzl0260@auburn.edu

Lu Lin
ORNL
linl2@ornl.gov
Katie Li-Oakey
University of Wyoming
dli1@uwyo.edu

Jian Liu
Northwestern University
jian.liu@northwestern.edu

Tongyu Liu
UC Riverside
tliu153@ucr.edu

Ryan Lively
Georgia Institute of Technology
ryan.lively@chbe.gatech.edu

Brian Long
University of Tennessee
long@utk.edu

Jeffrey Long
UC Berkeley
jrlong@berkeley.edu

Huimin Luo
ORNL
luoh@ornl.gov

Alketa Lutolli
Indiana University
alutolli@iu.edu

Shannon Mahurin
Oak Ridge National Laboratory
mahurinsm@ornl.gov

Thomas Mallos
Colorado School of Mines
tmallos@mymail.mines.edu

Melissa Manetsch
PNNL
melissa.manetsch@pnnl.gov

George Maracas
DOE SC
george.maracas@science.doe.gov

Maxwell Mattejat
UC Santa Barbara
maxwellmattejat@ucsb.edu

Daniel Matuszak
U.S. Department of Energy/BES
daniel.matuszak@science.doe.gov

Gabriel Menard
UC Santa Barbara
menard@chem.ucsb.edu

Jun Meng
U Wisconscin Madison
jmeng43@wisc.edu

Phillip Milner
Cornell University
pjm347@cornell.edu

Bruce Moyer
ORNL
moyerba@ornl.gov

Karl Mueller
PNNL
karl.mueller@pnnl.gov

Karen Mulfort
ANL
mulfort@anl.gov

Srikanth Nayak
ANL
snayak@anl.gov

Manh-Thuong Nguyen
PNNL
Manhthuong.Nguyen@pnnl.gov

Pravin Aravindhan Parasakthi
Auburn University
pzp0048@auburn.edu

Michele Parrinello
IIT Genoa, Italy
michele.parrinello@iit.it

Roshan Ashokbhai Patel
University of Minnesota
patel658@umn.edu

Danny Perez
LANL
danny_perez@lanl.gov

Colin Peterson
University of Minnesota
pet00842@umn.edu

Jacob Petrich
Ames Laboratory
jwp@iastate.edu

Marek Piechowicz
ANL
mpiechowicz@anl.gov

Ilja Popovs
ORNL
popovsi@ornl.gov

Uvinduni Premadasa
ORNL
up2@ornl.gov

Venkateshkumar Prabhakaran
PNNL
venky@pnnl.gov

Amy Price
LBNL
amyprice@lbl.gov

Krishnan Raghavachari
Indiana University
kraghava@indiana.edu

Pranav Ramesh
ISU
ramesp@rpi.edu

Mario Ramos-Garces
LSU
ramosgarces@lsu.edu

Hamid Rashidi
KSU
rashidi@ksu.edu

Kamal Ray
OSU
ray.727@osu.edu

Steven Regen
Lehigh University
slr0@lehigh.edu

Jeffrey Reimer
UC Berkeley
reimer@berkeley.edu

Julian Richardson
U Texas austin
julianrichardson44@gmail.com
Roger Rousseau
PNNL
roger.rousseau@pnnl.gov

Kevin Ruoff
U Penn
kruoff@sas.upenn.edu

Eric Ruzicka
U South Carolina
eruzicka@email.sc.edu

Eric Schelter
University of Pennsylvania
schelter@sas.upenn.edu

Mark Schlossman
University of Illinois, Chicago
schloss@uic.edu

Daniel Schwartz
University of Colorado, Boulder
daniel.schwartz@colorado.edu

Dodangodage Senadheera Ishara
LSU
dsenad1@lsu.edu

Michael Servis
ANL
mservis@anl.gov

Yusuf Shaidu
UC Berkeley
shaidu@berkeley.edu

Sayali Shaligram
Lehigh University
sas920@lehigh.edu

Edward Sheetz
Indiana University
esheetz@iu.edu

Linda Shimizu
U South Carolina
shimizls@mailbox.sc.edu

David Sholl
Georgia Technical Institute
david.sholl@chbe.gatech.edu

J. Ilja Siepmann
University of Minnesota
siepmann@umn.edu

Varun Singh
UI Chicago
vsingh41@uic.edu

Slowing Igor
DOE BES
Igor.Slowing@science.doe.gov

Emily Smith
AmesLab/ISU
esmith1@ameslab.gov

Zachary Smith
MIT
zpsmith@mit.edu

Randall Snurr
Northwestern University
snurr@northwestern.edu

Lynda Soderholm
Argonne National Laboratory
ls@anl.gov

Xueyu Song
AmesLab/ISU
xsong@iastate.edu

Elliot Springfield
Ohio State University
springfield.7@osu.edu

Mark Steger
NREL
Mark.Steger@NREL.gov

Nicole Stephens
ISU
stephenm@iastate.edu

Xiao Su
UIUC
x2su@illinois.edu

Jingyi Sui
Northwesterns Universtiy
B9t8a7@u.northwestern.edu

Sugata Tan
Planetary Science Institute
stan@psi.edu

Chuanbing Tang
University of South Carolina
TANG4@SC.EDU

Eric Taw
UC Berkeley
tawe141@berkeley.edu

Praveen K Thallapally
PNNL
praveen.thallapally@pnnl.gov

Nikki Thiele
ORNL
thielena@ornl.gov

Jonathan Thompson
University of Texas, Austin
jon.thompson@utexas.edu

Dhileep Nagi Reddy Thummuru
UC Riverside
dhileept@ucr.edu

Michael Tsapatsis
Johns Hopkins University
tsapatsis@jhu.edu

Willliam Tumas
NREL
bill.tumas@nrel.gov

Ahmet Uysal
Argonne National Laboratory
ahmet@anl.gov

Gregory A. Voth
University of Chicago
gavoth@uchicago.edu

Xinyi Wang
University of Tennessee
xwang137@vols.utk.edu

Qi Wang
U South Carolina
qwang@math.sc.edu

Zongheng Wang
UC Santa Barbara
zongheng@ucsb.edu

Gangli Wang
Georgia State University
glwang@gsu.edu

Mufeng Wei
UC Berkeley
mufeng_wei@berkeley.edu

Jay Werber
University of Toronto, CA
jay.werber@utoronto.ca

Kevin West
University of South Alabama
kevinwest@southalabama.edu

Haley White
GATech
white45@gatech.edu

Jennifer Wilcox
US Department of Energy Office of Fossil Energy and Carbon Management
jennifer.wilcox@hq.doe.gov

Philip Wilk
U.S. Department of Energy/BES
philip.wilk@science.doe.gov

Pubudu Wimalasiri
ANL
wimalapn@anl.gov

Ting Xu
LBNL/UC berkeley
tingxu@berkeley.edu

Lianjie Xue
Kansas State University
ljxue@ksu.edu

Weile Yan
UMass Lowell
weile_yan@uml.edu

Zhenzhen Yang
ORNL
zyang17@utk.edu

Ping Yang
Los Alamos National Lab
pyang@lanl

Huan Yang
University of Wyoming
hyang3@uwyo.edu

Young Hee Yoon
GATech
yyoon91@gatecg.edu

Joseph Zadrozny
Colorado State University
joe.zadrozny@colostate.edu

Zapol Peter
ANL
zapol@anl.gov

Difan Zhang
PNNL
difan.zhang@pnnl.gov

Hao Zhuang
UC Berkeley
hao_zhuang@berkeley.edu

U.S. DEPARTMENT OF
ENERGY

Office of
Science